

INFORMATION TO USERS

This manuscript has been reproduced from the microfilm master. UMI films the text directly from the original or copy submitted. Thus, some thesis and dissertation copies are in typewriter face, while others may be from any type of computer printer.

The quality of this reproduction is dependent upon the quality of the copy submitted. Broken or indistinct print, colored or poor quality illustrations and photographs, print bleedthrough, substandard margins, and improper alignment can adversely affect reproduction.

In the unlikely event that the author did not send UMI a complete manuscript and there are missing pages, these will be noted. Also, if unauthorized copyright material had to be removed, a note will indicate the deletion.

Oversize materials (e.g., maps, drawings, charts) are reproduced by sectioning the original, beginning at the upper left-hand corner and continuing from left to right in equal sections with small overlaps. Each original is also photographed in one exposure and is included in reduced form at the back of the book.

Photographs included in the original manuscript have been reproduced xerographically in this copy. Higher quality 6" x 9" black and white photographic prints are available for any photographs or illustrations appearing in this copy for an additional charge. Contact UMI directly to order.

UMI

**A Bell & Howell Information Company
300 North Zeeb Road, Ann Arbor MI 48106-1346 USA
313/761-4700 800/521-0600**

**EPR INVESTIGATIONS OF ANISOTROPIC INTERACTION AND
COLE-DAVIDSON PARAMETERS, NOVEL PHOSPHOLIPIDS,
AND NEWLY SYNTHESIZED BUCKMINSTERFULLERENES
USING NITROXIDE SPIN PROBES**

BY

YAHYA TAQUI AHMED AL-JANABI

**A Dissertation Presented to the
FACULTY OF THE COLLEGE OF GRADUATE STUDIES
KING FAHD UNIVERSITY OF PETROLEUM & MINERALS
DHAHRAN, SAUDI ARABIA**

**In Partial Fulfillment of the
Requirements for the Degree of**

DOCTOR OF PHILOSOPHY
In

C H E M I S T R Y

JUNE 1997

UMI Number: 9806411

UMI Microform 9806411
Copyright 1997, by UMI Company. All rights reserved.

**This microform edition is protected against unauthorized
copying under Title 17, United States Code.**


UMI
300 North Zeeb Road
Ann Arbor, MI 48103

**KING FAHD UNIVERSITY OF PETROLEUM AND MINERALS
DHAHRAN 31261, SAUDI ARABIA**

COLLEGE OF GRADUATE STUDIES

This dissertation, written by **Yahya Taqui A. Al-Janabi** under the direction of his Dissertation Advisor and approved by his Dissertation Committee, has been presented to and accepted by the Dean of the College of Graduate Studies, in partial fulfillment of the requirements for the degree of **DOCTOR OF PHILOSOPHY in Chemistry**.

Dissertation Committee


Prof. J. S. Hwang, *Dissertation Advisor*

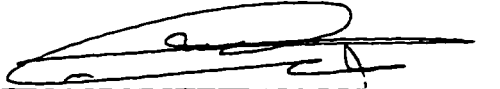

Prof. S. A. Ali, *Member*


Prof. U. K. A. Klein, *Member*


Prof. G. A. Oweimreen, *Member*


Prof. M. I. Wazeer, *Member*


Chairman, Chemistry Department


Dean, College of Graduate Studies

Date: 9-8-97



﴿ بِسْمِ اللّٰهِ الرَّحْمٰنِ الرَّحِیْمِ ﴾

و ما توفیقي إلا بالله

و صل اللهم على محمد و على

آل محمد الطيبين الطاهرين

و على صحبه المنتجبين

To My Family

ACKNOWLEDGMENT

Acknowledgment is due to King Fahd University of Petroleum and Minerals for support of this research and to Saudi ARAMCO for the sponsorship.

I wish to express my sincere appreciation and gratitude to my Major Advisor and Dissertation Committee Chairman Professor Jimmy Shio W. Hwang, who has been a constant source of patient guidance, generous support, and encouragement throughout the course of this study. My thanks and appreciation are extended to the other members of my Dissertation Committee, Professor Shaikh Asrof Ali, Professor Uwe K. A. Klein, Professor Ghassan A. Oweimreen, and Professor Mohammad Ismail Wazeer for their review of my work and for their valuable suggestions and remarks. Special thanks are due to Professor Shaikh Asrof Ali who supervised me in the synthesis of the spin probe adduct, and to Professor Ghassan A. Oweimreen who advised me in my Master's Thesis.

My deep thanks are due to the Chemistry Department, represented by the Chairman Dr. Abdulrahman Ahmed Al-Arfaj, and to the Faculty Members, Colleagues and Staff Members. I would also like to mention the individuals who contributed to this endeavor in one way or another, and these are: Dr. Hamdan (Chem. Dept.), Dr. Perzanowski (Chem. Dept.), Dr. Abu Abdoun (Chem. Dept.), Dr. Hamad (Che. Eng. Dept.), Professor Haque (Chem. Dept.), Professor Hussain (Chem. Dept.), Mr. Al-Mu'Allem (Chem. Dept.), Mr. Al-Hajji (Saudi Aramco), Dr. Morsy (Chem. Dept.), Mr. Pasil (Chem. Dept.), Dr. Hassan (Chem. Dept.), and all of my friends in the Lab R&D Center at Saudi Aramco for their support. I would like to thank the technicians of the Chemistry Department: Mr. Farooqi, who has been very instrumental in preparing some of the glasswares, Mr. Mir Mazhar Hassan, Mr. Baig, Mr. Saleem, Mr. Arab, Mr. Fiyad, Mr. Ismail, and Mr. Al-Ajmi. Finally I would like to thank Mr. Al-'Ubaidan for typing the Arabic abstract.

A word of appreciation and gratitude should go to my family whose support and understanding made this achievement possible.

TABLE OF CONTENTS

	<i>Page</i>
LIST OF TABLES.....	(x)
LIST OF FIGURES	(xiii)
LIST OF SCHEMES	(xxii)
DISSERTATION ABSTRACT (ARABIC).....	(xxiii)
DISSERTATION ABSTRACT (ENGLISH)	(xxv)
 CHAPTER	
I. INTRODUCTION	1
I.1. Anisotropic Interaction and Cole-Davidson Parameters	1
I.2. Phosphatidylcholine-Lanthanide Systems	3
I.3. Buckminsterfullerene Systems	4
II. GENERAL THEORY OF ELECTRON PARAMAGNETIC RESONANCE.....	6
II.1. Introduction.....	6
II.2. Magnetic Interactions.....	9
II.2.1. Zeeman Interaction.....	9
II.2.2. Interaction with the Microwave Field.....	10
II.2.3. Hyperfine Couplings	11
II.2.4. Interactions between Electron Spins.....	12
II.3. Analysis of the EPR Spectra of the Nitroxide Spin Labels	13
II.4. Line Shape Theory	16
II.4.1. Density Matrix.....	16
II.4.2. Relaxation and Line Shapes.....	18
II.4.3. Relaxation Matrix and Correlation Functions.....	19
II.4.4. Linewidth Parameters.....	21
III. ANISOTROPIC INTERACTION AND COLE-DAVIDSON PARAMETERS: PD-TEMPONE IN TOLUENE	24
III.1. Introduction.....	24
III.2. Experimental	26
III.2.1. Materials and Sample Preparation.....	26
III.2.2. Apparatus	31
III.2.2.1. The EPR Spectrometer	31

III.2.2.2.	<i>The Microwave Bridge</i>	34
III.2.2.3.	<i>The EPR Cavity</i>	36
III.2.2.4.	<i>Calibration of Resonators for L- & S-Bands</i>	38
III.2.3.	<u>Measurement and Data Collection</u>	40
III.2.3.1.	<i>Tuning and Coupling for L- and S-Bands</i>	40
III.2.3.2.	<i>Tuning and Coupling for Q-Band</i>	41
III.2.3.3.	<i>Data Collection</i>	43
III.2.3.4.	<i>Selecting a Modulation Amplitude</i>	43
III.2.3.5.	<i>Remote Control and Data Acquisition</i>	47
III.3.	Data Analysis	49
III.3.1.	<u>Computer Programs</u>	49
III.3.1.1.	<i>LWA.FOR</i>	49
III.3.1.2.	<i>EXDEL.FOR</i>	50
III.3.1.3.	<i>GSUMJH.FOR</i>	50
III.3.1.4.	<i>GSUMDP.FOR</i>	51
III.3.1.5.	<i>T22.FOR</i>	52
III.3.1.6.	<i>BCT1.FOR & ABCI.FOR</i>	53
III.4.	Results	56
III.4.1.	<u>L-Band</u>	57
III.4.2.	<u>S-Band</u>	65
III.4.3.	<u>X-Band</u>	71
III.4.4.	<u>Q-Band</u>	76
III.4.5.	<u>The Parameter β</u>	85
III.5.	Discussion	87
IV.	CAPILLARY TRANSLATIONAL DIFFUSION STUDY OF BBTMPO	94
IV.1.	Introduction	94
IV.2.	Experimental	95
IV.2.1.	<u>Materials and Sample Preparation</u>	95
IV.2.1.1.	<i>Capillary Diffusion Cell</i>	96
IV.2.1.2.	<i>Sample Preparation</i>	96
IV.2.2.	<u>Measurement and Data Collection</u>	98
IV.3.	Data Analysis	99
IV.3.1.	<u>Computer Programs</u>	101
IV.3.1.1.	<i>DIFFA.FOR</i>	101
IV.3.1.2.	<i>DIFFYAH.FOR & FITDIF.FOR</i>	102
IV.4.	Results	104
IV.5.	Discussion	107
V.	ANISOTROPIC INTERACTION AND COLE-DAVIDSON PARAMETERS: BBTMPO IN TOLUENE	108
V.1.	Introduction	108

V.2.	Experimental	109
V.2.1.	<u>Materials and Sample Preparation</u>	109
V.2.2.	<u>Modulation Amplitude Selection</u>	110
V.3.	Data Analysis	113
V.3.1.	<u>Computer Programs</u>	113
V.3.1.1.	<i>HGSUMJH.FOR</i>	114
V.3.1.2.	<i>GSUMHP.FOR</i>	116
V.3.1.3.	<i>INTERP.FOR</i>	119
V.4.	Results	122
V.4.1.	<u>X-Band</u>	124
V.4.2.	<u>L-Band</u>	137
V.4.3.	<u>S-Band</u>	145
V.4.4.	<u>Q-Band</u>	153
V.4.5.	<u>The Parameter β</u>	160
V.5.	Discussion	164
VI.	PHOSPHATIDYLCHOLINE-LANTHANIDE SYSTEMS	169
VI.1.	Introduction	169
VI.1.1.	<u>DMPC/DHPC Phosphatidylcholine</u>	172
VI.1.2.	<u>Order Parameters</u>	174
VI.1.3.	<u>EPR Studies of Phosphatidylcholines</u>	180
VI.2.	Experimental	182
VI.2.1.	<u>Materials and Sample Preparation</u>	182
VI.2.1.1.	<i>EPR Sample Preparation</i>	183
VI.2.2.	<u>Measurement and Data Collection</u>	184
VI.2.2.1.	<i>Rigid Limit Experiments</i>	184
VI.2.2.2.	<i>Variable Temperature Experiments</i>	185
VI.3.	Data Analysis	187
VI.4.	Results and Discussion	190
VI.4.1.	<u>Determination of Magnetic Tensor Components - Rigid Limit Simulations</u>	191
VI.4.2.	<u>Variable Temperature Experiments</u>	197
VI.4.2.1.	<i>PD-Tempone in DMPC/DHPC</i>	197
VI.4.2.2.	<i>PD-Tempone in DMPC/DHPC+Yb³⁺</i>	201
VI.4.2.3.	<i>PD-Tempone in DMPC/DHPC+Y³⁺</i>	207
VII.	NITRIC OXIDE AND NITROXIDE SPIN PROBE ADDUCTS OF BUCKMINSTERFULLERENE	216
VII.1.	Introduction	216
VII.1.1.	<u>Buckminsterfullerene</u>	217
VII.1.2.	<u>The Study of Buckminsterfullerene by EPR</u>	219
VII.1.3.	<u>Nitric Oxide (NO)</u>	220
VII.2.	Results and Discussion	222
VII.2.1.	<u>Nitric Oxide and Buckminsterfullerene</u>	222

VII.2.2. <u>Nitroxide Spin Probe Adduct of Buckminsterfullerene</u>	230
VII.3. Experimental	238
VII.3.1. <u>Nitric Oxide and Buckminsterfullerene</u>	238
VII.3.2. <u>Nitroxide Spin Probe Adduct of Buckminsterfullerene</u>	241
VII.3.2.1. <i>Preparation of 2-[(trimethylsilyl)oxy]-1,3-butadiene (2)</i>	242
VII.3.2.2. <i>Preparation of 1,9-(4-hydroxycyclohexano) buckminsterfullerene (6)</i>	243
VII.3.2.3. <i>Synthesis of the Nitroxide Spin Probe-Buckminsterfullerene Adduct</i>	245
VIII. CONCLUSIONS	247
VIII.1. PD-Tempone	247
VIII.2. BBTMPO	249
VIII.3. Lipid	252
VIII.4. Buckminsterfullerene Adducts	256
BIBLIOGRAPHY	261
APPENDIX	281
Appendix A	281
Appendix B	287
Appendix C	289
Appendix D	291

LIST OF TABLES

TABLE	<i>Page</i>
III.1. Observed Line Width as a Function of Peak-to-Peak Modulation Amplitude for PD-Tempone in Toluene at L-Band	44
III.2. Observed Line Width as a Function of Peak-to-Peak Modulation Amplitude for PD-Tempone in Toluene at S-Band.....	46
III.3. Magnetic Parameters of PD-Tempone in Toluene.....	54
III.4. Linewidth Analysis of PD-Tempone in Toluene at L-Band.....	59
III.5. Decay Behavior of PD-Tempone in Toluene at L-Band. The Linewidth , which is Equal to 0.3265 G, is Divided by Four. The Intensities at the Same Quarters from the Center on Both Sides are Averaged. Theoretical Simulation was Carried Out with an a_D of 0.0205 G, and intrinsic width of 0.2820 G.....	60
III.6. Experimental Values of B and C for PD-Tempone in Toluene at L-Band. The Final Six data were Calculated with an a_D of 0.075 G.	63
III.7. Linewidth Analysis of PD-Tempone in Toluene at S-Band.	67
III.8. Experimental Values of B and C for PD-Tempone in Toluene at S-Band.....	70
III.9. Linewidth Analysis of PD-Tempone in Toluene at X-Band.	74
III.10. Decay Behavior of PD-Tempone in Toluene at X-Band. The Linewidth, which is Equal to 0.3015 G, is Divided by Four. The Intensities at the Same Quarters from the Center on Both Sides are Averaged. Theoretical Simulation was Carried Out with an a_D of 0.0205 G, and intrinsic width of 0.2540 G.....	75
III.11. Experimental Values of B and C for PD-Tempone in Toluene at X-Band.....	77
III.12. The Linewidth Analysis of PD-Tempone in Toluene at Q-Band.....	80

III.13. Decay Behavior of PD-Tempone in Toluene at Q-Band. The Linewidth, which is Equal to 1.1730 G, is Divided by Four. The Intensities at the Same Quarters from the Center on Both Sides are Averaged. Theoretical Simulation was Carried Out with an a_D of 0.0205 G, and intrinsic width of 1.160 G.....	81
III.14. Experimental Values of B and C for PD-Tempone in Toluene at Q-Band.....	83
III.15. Summary of the Results for PD-Tempone in Toluene at the Four Microwave Bands: L, S, X, and Q.	90
V.1. Observed Line Width as a Function of Peak-to-Peak Modulation Amplitude for BBTMPO in Toluene at L-Band.	112
V.2. Relative Intensities of Twelve Equivalent Deuterons and Twelve Protons When Each Interact with One Electron.....	115
V.3. Magnetic Parameters of BBTMPO in Toluene.	120
V.4. Linewidth Analysis of BBTMPO in Toluene at X-Band.....	126
V.5. Parameters Determined from the Theoretical Simulation Shown in Fig. V.4 for BBTMPO in Toluene at X-Band.....	129
V.6. Experimental Values of B and C for BBTMPO in Toluene at X-Band.....	135
V.7. Linewidth Analysis of BBTMPO in Toluene at L-Band.....	140
V.8. Parameters Determined from the Theoretical Simulation Shown in Fig. (V.11) for BBTMPO in Toluene at L-Band.....	143
V.9. Experimental Values of B and C for BBTMPO in Toluene at L-Band.....	144
V.10. Linewidth Analysis of BBTMPO in Toluene at S-Band.....	148
V.11. Experimental Values of B and C for BBTMPO in Toluene at S-Band.....	151
V.12. The Linewidth Analysis of BBTMPO in Toluene at Q-Band.....	155

V.13. Experimental Values of B and C for BBTMPO in Toluene at Q-Band.....	158
V.14. Summary of the Results for BBTMPO in Toluene at the Four Microwave Bands: L, S, X, and Q.	166
VI.1. Magnetic Parameters for PD-Tempone in Different Systems.....	193
VII.1. Values in Gauss of the Local Central Fields H_i^{CF} , Peak Widths ΔH_i , and Peak-to-Peak Separations $\Delta H_{i,j}$, for EPR Spectra of NO Interacting with Buckminsterfullerene.	226

LIST OF FIGURES

FIGURE	Page
III.1. Schematic representation of the freeze-pump-thaw setup used to prepare permanent EPR samples.....	29
III.2. A schematic representation of a Bruker EPR spectrometer (adopted from Bruker manual)..	33
III.3. Block diagram of a microwave bridge (adopted from Bruker manual).....	35
III.4. Shape of the reflected microwave power from a resonant cavity (adopted from Bruker manual).....	37
III.5. Coupling of a microwave cavity to waveguide (adopted from Bruker manual).....	37
III.6. The shape of the reflected microwave power at S-Band.....	42
III.7. Observed line width as a function of peak-to-peak modulation amplitude for PD-Tempone in toluene at L-Band. The selected value of modulation amplitude that gave the best compromise between signal intensity and signal distortion was 0.124 Gauss.....	45
III.8. Observed line width as a function of peak-to-peak modulation amplitude for PD-Tempone in toluene at S-Band. The selected value of modulation amplitude that gave the best compromise between signal intensity and signal distortion was 0.125 Gauss.....	48
III.9. Selected experimental spectra of PD-Tempone in toluene at L-Band and at different temperatures.....	58
III.10. Lineshape simulation of the central peak ($M_i=0$) of the EPR spectrum of PD-Tempone in toluene at L-Band and at $T = 165$ K. This simulation was carried out with a deuteron hyperfine coupling constant of 0.0750 G and an intrinsic linewidth of 1.422 G. The observed linewidth is 1.553 G.....	61

III.11. (A): Experimental and theoretical values of B and C for PD-Tempone in toluene at L-Band with a deuteron hyperfine coupling constant of 0.0205 G. The parameters used were $z^*=Y$, $N=1.0$, $\beta=0.55$, $\varepsilon=\varepsilon^*=1.0$. (B): η/T versus reorientational correlation time τ_R for the same system. η is the calculated coefficient of shear viscosity at different toluene temperatures.	64
III.12. Selected experimental spectra of PD-Tempone in toluene at S-Band and at different temperatures.....	66
III.13. Lineshape simulation of the central peak ($M_I=0$) of half of the EPR spectrum of PD-Tempone in toluene at S-Band and at $T = 295$ K. This simulation was carried out with a deuteron hyperfine coupling constant of 0.0205 G and an intrinsic linewidth of 0.372 G. The observed linewidth is 0.409 G.....	68
III.14. Lineshape simulation of the central peak ($M_I=0$) of half of the EPR spectrum of PD-Tempone in toluene at S-Band and at $T = 161.2$ K. This simulation was carried out with a deuteron hyperfine coupling constant of 0.0205 G and an intrinsic linewidth of 2.79 G. The observed linewidth is also 2.79 G.....	69
III.15. (A): Experimental and theoretical values of B and C for PD-Tempone in toluene at S-Band with a deuteron hyperfine coupling constant of 0.0205 G. The parameters used were $z^*=Y$, $N=1.0$, $\beta=1.0$, $\varepsilon=\varepsilon^*=1.0$. (B): η/T versus reorientational correlation time τ_R for the same system. η is the calculated coefficient of shear viscosity at different toluene temperatures..	72
III.16. Selected experimental spectra of PD-Tempone in toluene at X-Band and at different temperatures.....	73
III.17. (A): Experimental and theoretical values of B and C for PD-Tempone in toluene at X-Band with a deuteron hyperfine coupling constant of 0.0205 G. The parameters used were $z^*=Y$, $N=1.5$, $\beta=1.0$, $\varepsilon=\varepsilon^*=1.0$. (B): η/T versus reorientational correlation time τ_R for the same system. η is the calculated coefficient of shear viscosity at different toluene temperatures.	78
III.18. Selected experimental spectra of PD-Tempone in toluene at Q-Band and at different temperatures.....	79
III.19. (A): Experimental and theoretical values of B and C for PD-Tempone in toluene at Q-Band with a deuteron hyperfine coupling	

constant of 0.0205 G. The parameters used were $z' = Y$, $N = 2.0$, $\beta = 1.0$, $\varepsilon = \varepsilon' = 1.0$. B and C values generated by $N = 1.0$ are also shown for comparison. (B): η/T versus reorientational correlation time τ_R for the same system, where η is the coefficient of shear viscosity for toluene.	84
III.20. Experimental values of B versus C for PD-Tempone in toluene determined from the four bands with z' set equal to Y, β equal to 1.0 and N values ranging from 1.0 to 6.0. (A) L-Band; (B) S-Band; (C) X-Band; (D) Q-Band. Experimental values of B and C for the L-Band lay well below the theoretical curves. Setting z' equal to X gave a better fit in this case for the L-Band.	86
III.21. Experimental values of B versus C for PD-Tempone in toluene determined from the four bands with z' set equal to Y, β equal to 0.5 and N values ranging from 1.0 to 6.0. (A) L-Band; (B) S-Band; (C) X-Band; (D) Q-Band. Experimental values of B and C for the S-, X-, and Q-Bands assume higher values of N (>1) for best fits.	88
III.22. Experimental values of B versus C for PD-Tempone in toluene determined from the four bands with z' set equal to Y and N values ranging from 1.0 to 6.0. (A) L-Band with $\beta = 0.55$, and $N = 1.0$ gave best fit; (B) S-Band with $\beta = 1.0$, and $N = 1.0$ gave best fit; (C) X-Band with $\beta = 1.0$, and $N = 1.5$ gave best fit; (D) Q-Band with $\beta = 1.0$, and $N = 2.0$ gave best fit.	89
IV.1. A schematic of the capillary diffusion apparatus used for the translational diffusion study of BBTMPO.	96
IV.2. EPR experimental spectra at different time intervals during the diffusion process of BBTMPO in toluene.	99
IV.3. EPR intensities versus time for BBTMPO in toluene. These are raw data normalized to the spectrum obtained at time zero.	104
IV.4. EPR intensities versus time for BBTMPO in toluene. These are the same data shown in Fig. IV.3 with corrected intensities using Eq. [IV.1]. Best fit for the first 100 data points was obtained with $D = 1.9 \times 10^{-5}$ cm ² /sec and $R = 0.2$; while best fit for the last 192 data points was obtained with $D = 1.0 \times 10^{-5}$ cm ² /sec and $R = 1.0$	105
V.1. Observed line width as a function of peak-to-peak modulation amplitude for BBTMPO in toluene at L-Band. The selected value	

	of modulation amplitude that gave the best compromise between signal intensity and signal distortion was 0.696 Gauss.	111
V.2.	Cubic Spline Interpolation performed by the INTERP-program for single peaks from the X-Band EPR spectra of BBTMPO in toluene at T = 295 K and 185 K.	123
V.3.	Selected experimental EPR spectra of BBTMPO in toluene at X-Band and at different temperatures.	125
V.4.	Theoretical simulation of experimental EPR spectra of BBTMPO in toluene at X-Band and at different experimental temperatures. Simulation was performed by considering both Lorentzian and Gaussian contributions to the shape of the line. Parameters determined from these simulations are listed in Table V.5.	128
V.5.	Parameters determined from the theoretical simulations of the EPR spectra of BBTMPO in toluene at X-Band and at different temperatures. (A) Both hydrogen isotropic hyperfine coupling coefficient and the mixing factor of contributions from Lorentzian and Gaussian lineshape functions versus temperature. (B) Both observed and intrinsic linewidths as a function of temperature.	130
V.6.	Values of B versus C calculated by four different methods for BBTMPO in toluene at X-Band and at different temperatures. The first method is by using experimental linewidths measured from single-peak spectra and different values of the isotropic hydrogen hyperfine coupling coefficient A_{iso}^H and the mixing factor λ , and the results are indicated by (o). The second method is like method one but using the same values of A_{iso}^H and λ , and the results are indicated by (\square). The third method is like the first method but the experimental linewidths were measured from three-peak spectra, and the results are indicated by (∇). Likewise, the fourth method is like the second method with the experimental linewidths measured from three-peak spectra, and the results are indicated by (Δ). Disagreements became pronounced at low temperatures if different or same values of A_{iso}^H and λ were used.	132
V.7.	Coefficient of shear viscosity η over temperature versus rotational correlation time τ_R calculated by four different sets of values of B and C for BBTMPO in toluene at X-Band and at different temperatures. The first set of B and C values was calculated by method one described in the text and in Fig. (V.6), and the results of (η/T) versus τ_R are indicated by (o). The second set of B and C	

values was calculated by method two and the results of (η/T) versus τ_R are indicated by (\square). The third set of B and C values was calculated by method three, and the results of (η/T) versus τ_R are indicated by (∇). The fourth set of B and C values was calculated by method four and the results of (η/T) versus τ_R are indicated by (Δ). Disagreements became pronounced at low values of temperature..... 133

V.8. Shear viscosity η over temperature versus correlation times for BBTMPO in toluene. Correlation times were calculated by fitting either experimental B or C values, $\tau_R(B)$ and $\tau_R(C)$, respectively. Similar results were obtained when either values were used..... 136

V.9. (A): Experimental and theoretical values of B and C for BBTMPO in toluene at X-Band. The parameters used were $z^*=X$, $N=7.0$, $\beta = 1.0$, $\varepsilon = \varepsilon^*=1.0$. (B): η/T versus the reorientational correlation time τ_R for the same system. η is the calculated coefficient of shear viscosity at different toluene temperatures. 138

V.10. Selected experimental EPR spectra of BBTMPO in toluene at L-Band and at different temperatures..... 139

V.11. Theoretical simulation of experimental EPR spectra of BBTMPO in toluene at L-Band and at different experimental temperatures. Simulation was performed by considering both Lorentzian and Gaussian contributions to the shape of the line. Parameters determined from these simulations are listed in Table (V.8). Cubic spline interpolation was performed for the experimental curves..... 141

V.12. (A): Experimental and theoretical values of B and C for BBTMPO in toluene at L-Band. The parameters used were $z^*=X$, $N = 7.0$, $\beta = 0.70$, $\varepsilon = \varepsilon^*=1.0$. (B): η/T versus the reorientational correlation time τ_R for the same system. η is the calculated coefficient of shear viscosity at different toluene temperatures. 146

V.13. Selected experimental EPR spectra of BBTMPO in toluene at S-Band and at different temperatures..... 147

V.14. Theoretical simulation of experimental EPR spectra of BBTMPO in toluene at S-Band and at different experimental temperatures. Simulation was performed by considering both Lorentzian and Gaussian contributions to the shape of the line..... 149

V.15. (A): Experimental and theoretical values of B and C for BBTMPO in toluene at S-Band. The parameters used were $z^*=X$, $N = 7.0$, $\beta =$

0.70, $\varepsilon = \varepsilon' = 1.0$. (B): η/T versus the reorientational correlation time τ_R for the same system. η is the calculated coefficient of shear viscosity at different toluene temperatures.....	152
V.16. Selected experimental EPR spectra of BBTMPO in toluene at Q-Band and at different temperatures.....	154
V.17. Theoretical simulation of experimental EPR spectra of BBTMPO in toluene at Q-Band and at different experimental temperatures. Simulation was performed by considering both Lorentzian and Gaussian contributions to the shape of the line. Cubic spline interpolation was performed for the experimental curves.....	156
V.18. (A): Experimental and theoretical values of B and C for BBTMPO in toluene at Q-Band. The parameters used were $z' = X$, $N = 7.0$, $\beta = 1.0$, $\varepsilon = \varepsilon' = 1.0$. (B): η/T versus the reorientational correlation time τ_R for the same system. η is the calculated coefficient of shear viscosity at different toluene temperatures.....	159
V.19. Experimental values of B versus C of BBTMPO in toluene for the four bands with z' set equal to X, β equal to 1.0 and N values ranging from 5.0 to 11.0. The N values that give the best fit with $\beta = 1.0$ for the L-, S-, X-, and Q-Bands are 12.0, 9.0, 7.0, and 7.0, respectively.....	161
V.20. Experimental values of B versus C of BBTMPO in toluene for the four bands with z' set equal to X, β equal to 0.5 and N values ranging from 5.0 to 11.0. The N values that give the best fit with $\beta = 0.5$ for the L-, S-, X-, and Q-Bands are 5.0, 5.0, 4.0, and 4.0, respectively.....	162
V.21. Experimental values of B versus C of BBTMPO in toluene for the four bands with z' set equal to X and N values ranging from 5.0 to 11.0. The β values that give the best fit with $N = 7.0$ for the L-, S-, X-, and Q-Bands are 0.7, 0.7, 1.0, and 1.0, respectively.....	163
VI.1. (A) Schematic representation of a generalized biomembrane, showing proteins integrated in the continuum of the phospholipid bilayer, together with peripheral proteins which are associated with the surface. (B) Schematic of a model bilayer used to study the membrane lipid properties. (C) Illustration of bilayered discoidal mixed micelles or "bicelles," where the lipid is the long-chain phosphatidylcholine DMPC and the detergent is the short-chain phosphatidylcholine DHPC. (A) and (B) were adopted from Brown	

(1996), whereas (C) was adopted from Sanders and Schwonek (1992).....	171
VI.2. A schematic of the finger dewar with the stabilizer designed and constructed in-house.....	186
VI.3. Rigid limit spectrum for PD-Tempone in the phospholipid system DMPC/DHPC and simulation (dashed line) based on magnetic parameters given in Table VI.1.....	192
VI.4. Rigid limit spectra for PD-Tempone in the phospholipid systems DMPC/DHPC+Yb ³⁺ (A) and DMPC/DHPC+Y ³⁺ (B), and simulations (dashed lines) based on magnetic parameters given in Table VI.1.....	195
VI.5. Selected experimental EPR spectra of PD-Tempone in DMPC/DHPC at different temperatures.	198
VI.6. Parameters calculated are for the system PD-Tempone in DMPC/DHPC. (A) Hyperfine splitting a versus temperature. (B) g -Factor versus temperature. (C) Solute order parameter $\langle D_{00}^2 \rangle$ and solvent order parameter λ versus temperature.....	200
VI.7. Parameters calculated are for the system PD-Tempone in DMPC/DHPC. (A) f -Factor versus temperature. (B) Order parameters S_{11} and S_{22} versus temperature. (C) S_{33} and $-\langle D_{00}^2 \rangle_z$ versus temperature.	202
VI.8. Selected experimental EPR spectra of PD-Tempone in DMPC/DHPC+Yb ³⁺ at different temperatures.	203
VI.9. Parameters calculated are for the system PD-Tempone in DMPC/DHPC+Yb ³⁺ . (A) Hyperfine splitting a versus temperature. (B) g -Factor versus temperature. (C) Solute order parameter $\langle D_{00}^2 \rangle$ and solvent order parameter λ versus temperature.	205
VI.10. Parameters calculated are for the system PD-Tempone in DMPC/DHPC+Yb ³⁺ . (A) f -Factor versus temperature. (B) Order parameters S_{11} and S_{22} versus temperature. (C) S_{33} and $-\langle D_{00}^2 \rangle_z$ versus temperature.	206
VI.11. Selected experimental EPR spectra of PD-Tempone in DMPC/DHPC+Y ³⁺ at different temperatures.	208

VL12. Parameters calculated are for the system PD-Tempone in DMPC/DHPC+Y ³⁺ . (A) Hyperfine splitting α versus temperature. (B) g -Factor versus temperature. (C) Solute order parameter $\langle D_{00}^2 \rangle$ and solvent order parameter λ versus temperature.	209
VL13. Parameters calculated are for the system PD-Tempone in DMPC/DHPC+Y ³⁺ . (A) f -Factor versus temperature. (B) Order parameters S_{11} and S_{22} versus temperature. (C) S_{33} and $-\langle D_{00}^2 \rangle_z$ versus temperature.	210
VL14. The order parameter S_{22} calculated using the g -factor and using the hyperfine splitting a for PD-Tempone in the three phospholipid systems: DMPC/DHPC, DMPC/DHPC+Yb ³⁺ , and DMPC/DHPC+Y ³⁺	212
VL15. Order parameters S_{ii} calculated using the hyperfine splitting α for PD-Tempone as a function of temperature in the three phospholipid systems: DMPC/DHPC, DMPC/DHPC+Yb ³⁺ , and DMPC/DHPC+Y ³⁺	213
VL16. Long-range order for DMPC/DHPC discoidal bicelles for perpendicular alignment (left) and parallel alignment (right) relative to the applied magnetic field B_0 . The flipping is induced by the addition of ytterbium(III). The discs at the left form cylindrical distribution whereas the discs on the right organize into layers representing a smectic mesophase all with their unique axes pointing basically in the same direction. The suggested orientation of PD-Tempone is also depicted. (This sketch was adapted from Prosser et al, 1997.).....	215
VII.1. EPR spectra of interacting NO with buckminsterfullerene. The uppermost spectrum was used to calculate the field intervals ΔH_i 's, in Gauss, for the six doublet-peaks, and the center-to-center field intervals $\Delta H_{i,j}$'s, in Gauss, between the consecutive doublet-peaks. The middle and lowermost spectra have the same sweep width but different peak-to-peak modulation amplitudes. The arrows in the lowermost spectrum indicate the lower extrema of hyperfine doublet structures observed between the larger peaks.	224
VII.2. (A) The field intervals ΔH_i , in Gauss, versus field values, also in Gauss, for the six doublet-peaks observed in the EPR spectrum of interacting NO with buckminsterfullerene. (B) The field intervals $\Delta H_{i,j}$, in Gauss, versus intervals sequence number. Here i refers to	

the preceding peak and j refers to the following peak in the calculation. Both ΔH_i and ΔH_{ij} were explained in Fig. VII.1.....227

VII.3. (A) The rigid limit spectrum of the adduct **8** in toluene obtained at 77 K. (B) The rigid limit spectrum of the nitroxide spin probe **7** in toluene obtained at 77 K.....233

VII.4. (A) The room temperature spectrum of the adduct **8** in toluene. (B) The room temperature spectrum of the nitroxide spin probe **7** in toluene.....234

VII.5. (A) The EPR room temperature spectrum of the adduct **8** in the liquid crystal 5CB. (B) The EPR room temperature spectrum of the nitroxide spin probe **7** in the liquid crystal 5CB.....235

VII.6. The room temperature EPR spectrum of a mixture of the adduct **8** and the nitroxide spin probe **7** in 5CB liquid crystal.....237

VII.7. A schematic of the of the system used to react NO gas with buckminsterfullerene.....239

LIST OF SCHEMES

	<i>Page</i>
Scheme III-I	27
Scheme VI-I.....	173

خلاصة الرسالة

إسم الطالب: يحيى تقي أحمد الجني

عنوان الدراسة: دراسات الطنين الألكتروني البارامغناطيسي لمؤشري "التفاعل المتبادل و المتباين" و "كول-ديفيدسون"، و لفوسفوليبيدات مستحدثه، و لمركبي البكمستر فوليرين حديثي التصنيع باستخدام مجسات النيتروكسايد المغزلية

حقل التخصص: كيمياء فيزيائية

تاريخ الشهادة: صفر ١٤١٨ هجره، الموافق يونيو ١٩٩٧ م

تحتوي هذه الدراسة على ثلاثة أقسام رئيسية. تُرْس في القسم الأول بشكل مكثف الديناميكية الممثلة بمؤشر التفاعل المتبادل و المتباين "K"، و بمقدار تباين إعادة التوجه الدوراني "N" لأثنين من مجسات النيتروكسايد المغزلية في انتوليون باستخدام مطيافية الطنين الألكتروني البارامغناطيسي (EPR) عند أربع نبذيات لموجات ميكرونية هي "L" (~1GHZ)، و "S" (~4GHZ)، و "X" (~9GHZ)، و "Q" (~35GHZ). المجس الصغير نسبياً هو "PD-Tempme" و المجس الكبير نسبياً هو "BBTMPO". بعدها استُعمل "PD-Tempme" في القسم الثاني لدراسة الترتيب الأصطفاقي الممغنط للفوسفوليبيد ثنائي الطبقة في وجود اثنين من أيونات فلزات الأرض النادرة هما يتربيوم (Yb^{3+}) و يتريوم (Y^{3+}) باستخدام مطيافية EPR. يتكون الفوسفوليبيد ثنائي الطبقة من مركب ضويل السلسلة وهو DMPC، وقصير السلسلة وهو DHPC، بالإضافة الى محلول كلوريد البوتاسيوم امثالي. أما في القسم الثالث من هذه الدراسة فقد تم تصنيع ودراسة مركبين إندماجين من البكمستر فوليرين (C_{60}) مع أكسيد النيتروجين (NO) و مع مجس نيتروكسايد مغزلي.

بالنسبة لـ "PD-Tempme" فإن قيم "K" متشابهة عند الأربع نبذيات الميكرونية وهي: ٠,٤٠ عند "L"، و ٠,٤٤ عند كل من "S"، و "X"، و "Q". هذا التشابه متوقع نظرياً حيث أن "PD-Tempme" يمارس حركات جزيئية متناغمة دلت عليها قيم "N" القريبة من واحد والتي تم تحديدها في هذه الدراسة عند الأربع نبذيات. كما و لأول مرة تم بنجاح علاج معامل كول-ديفيدسون " β " في عبارة الكثافة الطيفية. تُبَيَّنَت قيمة " β " في النبذبة "L" على ٠,٥٥ لتوحيد قيم ونتائج "N"، و "K"، و التوجه الأصطفاقي الممغنط لـ "PD-Tempme" في التوليونين. قيمة " β " عند النبذبة "L"، و التي كانت أقل من واحد، دلت على وجود توزيع متباعد لأرمان التراخي المرتبطة بأنواع الحركات الجزيئية المختلفة .

لتحديد قيم "K" لـ "BBTMPO" في التوليونين عند الأربع نبذيات الميكرونية، تم قياس نصف القطر الهيدروديناميكي للمذاب عند درجة حرارة الغرفة باستخدام تجربة الانتشار الأنتقالي الشعري. وقد كانت قيمته

٥,٦ أنجستروم والتي حُصِلَ عليها بأفترض أن الحالة المحيطة إنزلافية. بعد ذلك ولأول مرة تم تحليل منحنى أطياف الـ "EPR" للـ "BBTMPO" حيث أُخذَ بعين الاعتبار التضخم الغير متجانس الناتج عن البروتونات الأثني عشر المجاورة لـ "NO". كما عُثِرَ على أفضل محاكاة للمنحنى باستخدام مزيج من عبارتي التشكل "Lorentzion" و "Gaussian". كفت عبارة التشكل "Lorentzion" في محاكاة منحنيات "PD-Tempme" الطيفية. أما إحتياج نظام الـ "BBTMPO" لعبارة التشكل "Gaussian" فيمكن إرجاعه للأثر "Doppler" والناتج عن إستبدال النيوترونات الثقيلة في "PD-Tempme" بالبروتونات في "BBTMPO". تشابهت قيم κ عند الذبذبات "L"، و "S"، و "X" حيث كانت تساوي على التوالي ٠,٢٣، و ٠,٢٤، و ٠,٢٥. أما قيمة κ عند الذبذبة "Q" فقد كانت صغيره (٠,٠٨) مما دل على إنخفاض في التراوح بين المجس "BBTMPO" المغزلي والمذبذب توليويين. فُسِرَ إنخفاض قيمة κ عند الذبذبة "Q" بالتباين العالي لـ "BBTMPO" والذي دل عليه القيمة المرتفعة لـ "N" وهي ٧ عند الذبذبات الأربع. وقد توجد التوزيع المتباعد لأزمان التراخي في الذبذبتين "L" و "S" حيث كانت قيمة β ٠,٧ عند الذبذبتين المذكورتين للمجس "BBTMPO". فُسِرَ الأمتداد إلى الذبذبة "S" بالحجم الأكبر لـ "BBTMPO" مقارنة بحجم "PD-Tempone".

كانت نتائج المجس "PD-Tempone" عند الذبذبة "X" في "DMPC/DHPC" (I)، و "DMPC/DHPC + Yb³⁺" (II)، و "DMPC/DHPC + Y³⁺" (III) مشابهة لنتائج التركيزه لايوتروبيك سمكتيك، أي أن قيم "g" تزيد بزيادة درجة الحرارة بينما الأقسام الطيفي الدقيق "a" يقل بزيادة درجة الحرارة. حدثت التحولات الطورية على مدى حرارتي عريض وكانت كالتالي: ٥٠-٦٠ م° في (I)، ٣٠-٤٠ م° و ٧٠-٨٠ م° في (II)، وعند تقريباً ٤٥ م° في (III). من الواضح أن إضافة كلاً من Yb³⁺ و Y³⁺ أثرت على أطوار "DMPC/DHPC" بشكلٍ مختلف. لوحظت التحولات الطورية بمتابعة التغيرات في قيم كلٍ من "g" و "a" مع تغيير درجة الحرارة. أشارت القيم الأنظمة "S_{II}" و "S₂₂" إلى إنقلاب قدره ٩٠ درجة لثنائي الطبقة بعد إضافة Yb³⁺ و تعريض النظام إلى حقل مغناطيسي ثابت قدره واحد تسلا. لوحظت هذه الظاهره أيضاً باستخدام الطنين المغناطيسي النووي للديوترونات.

في القسم الثالث من هذه الدراسة، أعطى المركب الأندماجي المكون من "C₆₀" الصلب وغاز "NO" ستة منحنيات عابرة فسرت بالتفاعل المتبادل بين جزيئات "NO" والأثني عشر خماسي الموجودين في "C₆₀". جزيئات "NO₂" المدمصه، والتي أعطت منحنى طيفي واحد ظهر في وسط المنحنيات الستة، خفضت التماثل في "C₆₀" مما أدى إلى ستة مجموعات مختلفة مكونة من خماسيين متكافئين. تم إعداد المركب الأندماجي الثاني بأسترة الكحول 1,9-(4-hydroxycyclohexano)-buckminsterfullerene مع 2,2,5,5-tetramethyl pyrrolidine-1-oxyl-3-carboxylic acid. كما تم التحقق من الناتج بالنظر إلى أطياف المركب الأندماجي والمجس المغزلي الحر في كلٍ من التوليويين والسائل المتبلور 5CB. حيث أن المركب الأندماجي أعطى منحنى طيفي عريض، وهذا من صفات المجسات المغزلية الضخمة والتي تتراقص بمعدلات بطيئة. كما سيُشرع في إنتاج كميات أكبر من هذا المركب لتسهيل عملية التحقيق بأستخدام الطرق التحليلية المعتادة.

DISSERTATION ABSTRACT

NAME OF STUDENT: **Yahya Taqui A. Al-Janabi**
TITLE OF STUDY: **EPR Investigations of Anisotropic Interaction and Cole-Davidson Parameters, Novel Phospholipids, and Newly Synthesized Buckminsterfullerenes Using Nitroxide Spin Probes**
MAJOR FIELD: **Physical Chemistry**
DATE OF DEGREE: **June 1997**

This study can be divided into three major parts. In the first part, the dynamics, represented by the anisotropic interaction parameter κ and the anisotropy of rotational reorientation N , of two nitroxide spin probes in toluene were thoroughly investigated by Electron Paramagnetic Resonance (EPR) spectroscopy at the four microwave bands L (~1 GHz), S (~4 GHz), X (~9.5 GHz), and Q (~35 GHz). The relatively small and large probes are perdeuterated-2,2,6,6-tetramethyl-4-piperidone-N-oxide (abbreviated as PD-Tempone) and 4-*N*(*p*-*n*-butylbenzilidene) amino 2,2,6,6-tetramethylpiperidine 1-oxide (abbreviated as BBTMPO), respectively. PD-Tempone was consequently used in the second part to study the magnetic arrangement of a phospholipid bilayer in the presence of the rare earth metal ions ytterbium(III), Yb^{3+} , and yttrium(III), Y^{3+} by the EPR technique. The phospholipid bilayer consisted of the long chain 1,2-dimyristoyl-*sn*-glycero-3-phosphocholine (DMPC), the short chain 1,2-dihexanoyl-*sn*-glycero-3-phosphocholine (DHPC), and KCl aqueous solution. In the third part, buckminsterfullerene (C_{60}) adducts of nitric oxide (NO) and nitroxide spin probes were synthesized and investigated by EPR spectroscopy.

For PD-Tempone, values of the κ parameter were similar at the four microwave bands: 0.40 at L-Band and 0.44 at S-, X-, and Q-Bands. This similarity is predicted by theory since PD-Tempone undergoes isotropic molecular motions indicated by N values close to one, determined in this study at the four bands. The Cole-Davidson parameter β was introduced successfully to the spectral densities for the first time. A β value of 0.55 was used at L-Band to unify the results of N , κ and the magnetic alignment of PD-Tempone in toluene. A value of $\beta < 1$ at L-Band suggested the existence of a broad distribution of relaxation times associated with different modes of molecular motions.

To determine the κ values for BBTMPO in toluene at the four microwave bands, the solute hydrodynamic radius was determined at room temperature by the capillary translational diffusion experiment. Assuming a slip boundary condition, a value of 5.6 Å was obtained. Lineshape analysis of the EPR spectra of BBTMPO was performed for the first time to account for inhomogeneous broadening resulting from the twelve protons adjacent to the NO-moiety. The lineshape was best fit by utilizing a mixture of both Lorentzian and Gaussian shape functions. The Lorentzian shape function was sufficient for describing the

EPR lines of PD-Tempone. The need for the Gaussian function in the BBTMPO system was attributed to the Doppler effect arising from substituting the heavier deuterons in PD-Tempone with protons in BBTMPO. Values of κ at L-, S-, and X-Bands were similar and were equal to 0.23, 0.24, and 0.25, respectively. The κ value at Q-Band was much smaller (0.08) which indicated reduced coupling between the spin probe BBTMPO and the solvent toluene. The behavior at Q-Band was attributed to the high anisotropy of BBTMPO suggested by a large N value of 7 obtained at the four bands. The broader distribution of relaxation times was present at L- and S-Bands with a β value of 0.7 at both bands for BBTMPO. The extension to S-Band was explained by the larger size of BBTMPO compared to PD-Tempone.

The X-band EPR results of PD-Tempone in DMPC/DHPC (I), DMPC/DHPC + Yb³⁺(II), and DMPC/DHPC + Y³⁺ (III) were typical of lyotropic smectic mesophases, i.e., the g -factor increased with temperature whereas the hyperfine splitting a decreased with temperature. Phase transitions took place at relatively wide temperature ranges: 50-60 °C for I, 30-40 °C and 70-80 °C for II, and at ~45 °C for III. Clearly, addition of Yb³⁺ and Y³⁺ affected the DMPC/DHPC phase differently. Phase transitions were observed by following variations in the g -factor and the a parameter as a function of temperature. Ordering parameters S_{11} and S_{22} indicated 90° flipping of the bilayer after adding Yb³⁺ and exposing the system to a static magnetic field of one Tesla. This phenomena was also observed by ²H NMR.

In the third part of this study, the adduct of C₆₀ and NO gave six transient EPR peaks which were attributed to gaseous NO molecules interacting with the twelve pentagons in the solid C₆₀. Adsorbed NO₂ molecules, which produced a single EPR line at the center of the six peaks, reduced the symmetry of C₆₀ resulting in six different sets of two equivalent pentagons. The second adduct was prepared by the esterification of the alcohol 1,9-(4-hydroxycyclohexano)-buckminsterfullerene with the nitroxide spin probe 2,2,5,5-tetramethyl pyrrolidine-1-oxyl-3-carboxylic acid. The product was verified by comparing the EPR spectra of the adduct and the free spin probe in toluene and in the liquid crystal 5CB. The adduct in the 5CB gave broad EPR lines characteristic of large spin probes tumbling at slow rates. Production of macroquantities will be attempted to allow verification of the adduct by typical analytical techniques.

DOCTOR OF PHILOSOPHY DEGREE

KING FAHD UNIVERSITY OF PETROLEUM AND MINERALS
Dhahran, Saudi Arabia

June 1998

CHAPTER I

INTRODUCTION

This dissertation can be divided into three major parts. In the first part, the dynamics of two relatively small and large nitroxide spin probes in toluene were thoroughly investigated by Electron Paramagnetic Resonance (EPR) spectroscopy at variable temperature and microwave frequency. The small nitroxide spin probe was consequently used in the second part to study the magnetic arrangement of a phospholipid bilayer in the presence and absence of rare earth metals by EPR spectroscopy. In the third part, buckminsterfullerene adducts of nitric oxide (NO) and nitroxide spin probes were synthesized and investigated by EPR spectroscopy.

I.1. Anisotropic Interaction and Cole-Davidson Parameters

The determination of structural information about a system at the molecular level is a very important area of research in chemistry. In the field of electron paramagnetic resonance, this can be achieved by introducing stable

nitroxide radicals into the system and studying their dynamic interactions with the system. The half-width at half-height, or the intrinsic line width w , of the EPR lines and its isotropic hyperfine coupling constant A_{iso} provide information concerning the motion of the probes or their local environments. These two parameters, i.e., w and A_{iso} , are not directly measurable from the EPR spectra. One method to obtain these parameters is to perform a line shape study and resort to computer simulation.

From these calculations a rotational correlation time, τ_R , is obtained at the different temperatures. The correlation time is also given by the Debye expression

$$\tau_R = \left(\frac{4 \pi r_o^3 \eta}{3 kT} \right) \kappa \quad [I-1]$$

where k is the Boltzmann constant, T the absolute temperature in K, η the coefficient of shear viscosity of the solvent, r_o the effective radius of the solute, and κ is the anisotropic interaction parameter. It was found in this laboratory (Rahman 1988) and elsewhere (Hwang et al, 1975) that the κ values for the same spin probe in the same solvent were different at different microwave frequencies.

In this study, we would like to investigate this behavior more deeply and study the possibility of a unified description for the anisotropic interaction parameter at the different microwave frequencies. The introduction of the Cole-

Davidson parameter β to the spectral density will be attempted to achieve this objective.

I.2. Phosphatidylcholine-Lanthanide Systems

Biomembranes consist mainly of lipids and proteins, together with carbohydrates associated with the cellular and organelle surfaces. According to the present knowledge, lipids typically form a bilayer containing proteins. The lipid bilayer is typically a liquid-crystalline material. The dynamical properties associated with the motions of the lipid molecules may be important.

The study of structural and dynamical features of integral membrane and membrane associated proteins by Nuclear Magnetic Resonance has been advanced by the development of magnetically oriented bilayered micelles, or "bicelles." In the presence of a magnetic field, highly oriented bilayers may be readily formed from mixtures of long- and short-chain phosphatidylcholines. Typically these are dimyristoyl phosphatidylcholine (DMPC) and dihexanoyl phosphatidylcholine (DHPC). Recently, it was reported that the combination of a bicelle solution with relatively small amounts of paramagnetic ions (e.g. europium, Eu^{3+} , erbium, Er^{3+} , and ytterbium, Yb^{3+}) results in a fully oriented bilayered system in which the average bilayer normal is parallel to the magnetic field (Posser et al, 1996).

To study the dynamical properties associated with the motions of the lipid molecules, a spin probe could be used as a reporter molecule whose behavior is

observed using EPR spectroscopy. From the magnetic parameters of the spin probe (i.e., the g -factor and the hyperfine coupling constant a) several types of ordering parameters can be determined.

The objective of this part is to study the orientational arrangement of magnetically aligned bilayered micelles in the presence of lanthanide ions using EPR spectroscopy by doping the mixture with a tiny amount of a nitroxide spin probe.

I.3. Buckminsterfullerene Systems

Although a large amount of research has been devoted to buckminsterfullerene since its discovery and preparation in macroquantities, very few adsorption studies of this material have been reported. Buckminsterfullerene has a spherical "soccer ball" structure of 12 pentagon rings and 20 hexagon rings, which contain unsaturated double bonds. Because of the aromaticity of C_{60} , the surface is susceptible to interactions with other molecules. In recent studies (Pace et al, 1992; Pace et al, 1994), surface reactions of C_{60} with gaseous molecules were reported. Although C_{60} is not a free radical, indigenous paramagnetic impurities often occur in C_{60} powders at room temperature. These impurities produce EPR signal which were used to study the interaction of C_{60} with oxygen, nitrogen, and nitrogen dioxide.

The adsorption of nitric oxide, NO, on buckminsterfullerene was studied using IR spectroscopy (Fastow et al, 1992). The study of NO adsorption on

buckminsterfullerene using EPR spectroscopy will hopefully give some insight into the adsorption characteristics of the adduct.

The second part of this study is concerned with chemical modifications of fullerenes by selective bond formation to provide a vital tool in fullerene science and technology. Intensive efforts in the past few years have laid an organic foundation on the C_{60} sphere that includes ring systems of different sizes (An et al, 1993; Yamago et al, 1993).

The next step is to construct useful functionalities on such foundations. A nitroxide spin probe derived from buckminsterfullerene, C_{60} , would be very useful to probe C_{60} using EPR spectroscopy. In this work we will attempt to synthesize a nitroxide spin probe derivitized from C_{60} .

CHAPTER II

GENERAL THEORY OF ELECTRON PARAMAGNETIC RESONANCE[§]

II.1. Introduction

Since the detection of the first electron paramagnetic resonance (or EPR) signal by Zavoisky in 1945, the EPR technique has attained a state of advanced maturity.

Electron paramagnetic resonance spectroscopy studies magnetic dipole transitions between Zeeman levels of a paramagnetic system split by an external magnetic field. The transitions are induced by an oscillating microwave radiation. The permanent magnetic dipole moment μ is related to the electronic angular momentum \mathbf{J} by

$$\mu = -g \beta_e \mathbf{J} \quad [\text{II-1}]$$

with

[§] This chapter is basically a summary of the chapter by Nordio (1976) with reference to Slichter (1992), Poole (1983), Carrington and McLachlan (1980), and Pake and Estle (1973).

- the total angular momentum given by $\mathbf{J} = \mathbf{S} + \mathbf{L}$, here \mathbf{S} and \mathbf{L} are, respectively, the electronic spin and orbital angular momenta, and
- the spectroscopic splitting factor g given by

$$g = 1 + \frac{J(J+1) + S(S+1) - L(L+1)}{2J(J+1)} \quad [\text{II-2}]$$

where β_e is the electronic Bohr magneton, $|e|\hbar/2mc$, and J , S , and L are the quantum numbers corresponding to \mathbf{J} , \mathbf{S} , and \mathbf{L} .

The interaction between the external magnetic field \mathbf{H} and the magnetic dipole moment $\boldsymbol{\mu}$ can be calculated by the Hamiltonian operator

$$\mathcal{H} = -\boldsymbol{\mu} \cdot \mathbf{H} = g \beta_e \mathbf{H} \cdot \mathbf{J} = g \beta_e H_o J_z \quad [\text{II-3}]$$

where the z axis is taken to be the direction of the applied magnetic field \mathbf{H} with a uniform intensity H_o and J_z is the operator of the angular momentum component along the direction of \mathbf{H} . For a single electron, the expectation values M_I of J_z are $\pm 1/2$ and with the selection rule $\Delta M_I = \pm 1$, the resonance condition for the absorption of energy by the unpaired electron is represented by

$$h\nu = g \beta_e H_o \quad [\text{II-4}]$$

where ν is the microwave frequency. In a regular EPR experiment, the microwave frequency is kept constant and the magnetic field is swept until the resonance condition is found.

The phenomenological Bloch equations describe relaxation mechanisms by which the system restores the equilibrium populations after the induced

transitions. The first mechanism is nonradiative thermal relaxation transitions described by

$$dM_z/dt = -(M_z - M_{eq})/T_1 \quad [\text{II-5}]$$

where T_1 is a characteristic time called the spin-lattice or longitudinal relaxation time, M_z is the macroscopic magnetization of the sample and M_{eq} is given by the Curie law

$$M_{eq} = N g_e^2 \beta_e^2 S(S+1)H/3kT \quad [\text{II-6}]$$

where N is the total number of spins, g_e is the free-electron g value, and T is the absolute temperature. Due to the Heisenberg uncertainty principle, the EPR spectral lines are broadened by this relaxation mechanism.

The second type of mechanisms are characterized by a relaxation time T_2 called the transverse relaxation time. These processes, which do not cause any transitions, produce modulation of the magnetic levels and therefore broaden the EPR spectral lines. The corresponding Bloch equation is

$$dM_x/dt = -M_x/T_2 \quad [\text{II-7}]$$

where M_x is the perpendicular component of the magnetization. The peak-to-peak linewidth denoted by δ is given in terms of T_2 by

$$\delta = 2/(\sqrt{3} T_2) \quad [\text{II-8}]$$

for a first derivative EPR curve given by a Lorentzian shape function (*cf.*, subsections III.3.1.4 & V.3.1.2).

II.2. Magnetic Interactions

There are several types of magnetic interactions which take place in a paramagnetic system. Intermolecular magnetic interactions are usually avoided by diluting the paramagnetic sample in a diamagnetic host, the solvent. The remaining common interactions are between the spin of the unpaired electron and the magnetic field (Zeeman interaction), the microwave field, the magnetic moment of the nucleus (hyperfine coupling), and with another unpaired electron in the case of biradicals.

II.2.1. Zeeman Interaction

The electronic Zeeman interaction energy which represents the interaction of the magnetic moment of the unpaired electron with the external magnetic field is given by

$$\mathcal{H}_z = -\mu_e \cdot \mathbf{H} = g_e \beta_e \mathbf{H} \cdot \mathbf{S} = g_e \beta_e H_o S_z \quad [\text{II-9}]$$

where the subscript e refers to the unpaired electron. In the presence of a nucleus possessing a spin, the nuclear Zeeman interaction energy is given by $(-g_N \beta_N H_o I_z)$ which is much smaller than the electronic part; g_N , β_N , and I_z are the g value, the Bohr magneton, and the spin angular momentum for the nucleus.

The g factor is expressed as a second-rank tensor due to spin-orbit coupling:

$$g_{ij} = g_e \delta_{ij} - 2\lambda \sum_l \frac{\langle \psi_o | L_i | \psi_l \rangle \langle \psi_l | L_j | \psi_o \rangle}{E_l - E_o} \quad [\text{II-10}]$$

where δ_{ij} is the Kronecker delta, λ is the spin-orbit coupling, ψ_0 and ψ_i are the wave functions representing, respectively, the ground and the excited states of the system and E_0 and E_i are the corresponding energies, and L_i 's are the components of the angular momentum. The Zeeman Hamiltonian in tensor notation becomes

$$\mathcal{H}_Z = \beta_e \mathbf{H} \cdot \mathbf{g} \cdot \mathbf{S} \quad [\text{II-11}]$$

where now \mathbf{g} can be represented by a 3x3 matrix. The reference system can be selected to be the laboratory or the molecular axis systems. The principal values of the \mathbf{g} tensor can be determined from an analysis of the angular dependence of the \mathbf{g} factor for paramagnetic systems trapped in a glassy environment.

II.2.2. Interaction with the Microwave Field

The EPR transitions are induced by the oscillating microwave field. The microwave field is applied perpendicular to the external magnetic field, and hence the associated oscillating magnetic field has components given by

$$H_{1x} = H_1 \cos \omega t, \quad H_{1y} = H_{1z} = 0 \quad [\text{II-12}]$$

and the corresponding Hamiltonian is given by

$$\mathcal{H}' = g_e \beta_e H_1 S_x \cos \omega t \quad [\text{II-13}]$$

This Hamiltonian is considered as a perturbation and the rate of the transitions between $|\alpha\rangle$ and $|\alpha'\rangle$ of \mathcal{H}_Z of energies E_α and $E_{\alpha'}$ is given by the transition probability

$$w_{\alpha\alpha'} = (2\pi/\hbar) g_e^2 \beta_e^2 H_1^2 |\langle \alpha | S_x | \alpha' \rangle|^2 \delta(E_\alpha - E_{\alpha'} - \hbar\omega) \quad [\text{II-14}]$$

where δ is the Dirac delta function imposing the requirement that $E_\alpha - E_{\alpha'} = \hbar\omega$.

For the matrix elements $\langle \alpha | S_x | \alpha' \rangle$ it is more convenient to express S_x by the "shift" operators S_+ and S_- , where

$$S_\pm = S_x \pm iS_y, \quad S_x = \frac{1}{2} (S_+ + S_-)$$

The eigenvalues for these operators are given by

$$S_\pm | S, m_s \rangle = [S(S+1) - m_s(m_s \pm 1)]^{1/2} | S, m_s \pm 1 \rangle \quad [\text{II-15}]$$

which result in the selection rule $\Delta m_s = \pm 1$.

II.2.3. Hyperfine Couplings

Hyperfine interactions refer to the splitting of the electron spin levels to $2I+1$ sublevels by the magnetic field associated with the spin angular momentum I of the nucleus, which produces a multiplet structure in the EPR spectrum. The Hamiltonian for these interactions is represented by

$$\mathcal{H} = -g_e \beta_e g_N \beta_N \left\{ \frac{(\mathbf{I} \cdot \mathbf{S})r^2 - 3(\mathbf{I} \cdot \mathbf{r})(\mathbf{S} \cdot \mathbf{r})}{r^5} - \frac{8\pi}{3} (\mathbf{I} \cdot \mathbf{S})\delta(\mathbf{r}) \right\} \quad [\text{II-16}]$$

where \mathbf{r} is the distance vector between the electron and the nucleus. The first term in the Hamiltonian describes the electron-nucleus dipolar interaction whereas the second term describes the Fermi contact coupling. The complete hyperfine Hamiltonian can be written in the compact form

$$\mathcal{H}_{\text{hf}} = \mathbf{I} \cdot \mathbf{A} \cdot \mathbf{S} \quad [\text{II-17}]$$

where \mathbf{A} is the hyperfine tensor and it is the summation of a second-rank dipolar interaction tensor and an isotropic coupling constant.

II.2.4. Interactions between Electron Spins

These interactions exist in biradicals and can be represented by a dipolar Hamiltonian similar to the first term in [II-16]

$$\mathcal{H} = g_e^2 \beta_e^2 \left\{ \frac{(\mathbf{S}_1 \cdot \mathbf{S}_2)r^2 - 3(\mathbf{S}_1 \cdot \mathbf{r})(\mathbf{S}_2 \cdot \mathbf{r})}{r^5} \right\} \quad [\text{II-18}]$$

where \mathbf{r} is the distance vector between the two electrons. The dipolar spin Hamiltonian \mathcal{H}_d can then be written as

$$\mathcal{H}_d = \mathbf{S} \cdot \mathbf{D} \cdot \mathbf{S} \quad [\text{II-19}]$$

where $\mathbf{S} = \mathbf{S}_1 + \mathbf{S}_2$ and \mathbf{D} is a second-rank dipolar interaction tensor.

II.3. Analysis of the EPR Spectra of the Nitroxide Spin Labels

The Hamiltonian of the dipole magnetic moments associated with the $2p\pi$ unpaired electron ($S = \frac{1}{2}$) on the nitroxide moiety and the nitrogen nucleus ($I = 1$) can be expressed as

$$\mathcal{H} = \beta_e \mathbf{H} \cdot \mathbf{g} \cdot \mathbf{S} - \beta_N \mathbf{H} \cdot \mathbf{g}_N \cdot \mathbf{I} + \mathbf{I} \cdot \mathbf{A} \cdot \mathbf{S} \quad [\text{II-20}]$$

Since the very fast molecular reorientations of the nitroxide spin label in the solvent toluene average out the anisotropic terms in the Hamiltonian given by Eq. [II-20] due to thermal motions, the isotropic Hamiltonian can then be written as

$$\begin{aligned}\mathcal{H} &= g\beta_e \mathbf{H} \cdot \mathbf{S} - g_N \beta_N \mathbf{H} \cdot \mathbf{I} + a \mathbf{S} \cdot \mathbf{I} \\ &= g\beta_e H_o S_z - g_N \beta_N H_o I_z + a \mathbf{S} \cdot \mathbf{I}\end{aligned}\quad [\text{II-21}]$$

where $g = \frac{1}{3} \text{Tr } g$ and $a = \frac{1}{3} \text{Tr } A$ [\text{II-22}]

An appropriate basis functions for this system can be written as:

$$\begin{aligned}\phi_1 &= |+\frac{1}{2} +1\rangle = |++\rangle \\ \phi_2 &= |+\frac{1}{2} 0\rangle = |+0\rangle \\ \phi_3 &= |+\frac{1}{2} -1\rangle = |+-\rangle \\ \phi_4 &= |-\frac{1}{2} +1\rangle = |-\rangle \\ \phi_5 &= |-\frac{1}{2} 0\rangle = |-0\rangle \\ \phi_6 &= |-\frac{1}{2} -1\rangle = |--\rangle\end{aligned}\quad [\text{II-23}]$$

Treating the hyperfine interactions as a perturbation, the corresponding energies corrected to second order hyperfine couplings are

$$\begin{aligned}E_1 &= \frac{1}{2} g\beta_e H_o - g_N \beta_N H_o + \frac{a}{2} \\ E_2 &= \frac{1}{2} g\beta_e H_o + \frac{a^2}{4(g\beta_e H_o + g_N \beta_N H_o)} \\ E_3 &= \frac{1}{2} g\beta_e H_o + g_N \beta_N H_o - \frac{a}{2} + \frac{a^2}{4(g\beta_e H_o + g_N \beta_N H_o)} \\ E_4 &= -\frac{1}{2} g\beta_e H_o - g_N \beta_N H_o - \frac{a}{2} - \frac{a^2}{4(g\beta_e H_o + g_N \beta_N H_o)} \\ E_5 &= -\frac{1}{2} g\beta_e H_o - \frac{a^2}{4(g\beta_e H_o + g_N \beta_N H_o)}\end{aligned}\quad [\text{II-24}]$$

$$E_6 = -\frac{1}{2} g\beta_e H_o + g_N \beta_N H_o + \frac{a}{2}$$

A schematic of the second-order spin energy levels of a nitroxide spin label and the allowed EPR transitions are depicted in Figure II.1. The EPR transitions follow the selection rules $\Delta m_s = \pm 1$ and $\Delta M_I = 0$. The energies for the three allowed transitions are given by

$$\begin{aligned} \Delta E_1 &= g\beta_e H_o + a + \frac{a^2}{4(g\beta_e H_o + g_N \beta_N H_o)} \\ \Delta E_2 &= g\beta_e H_o + \frac{a^2}{2(g\beta_e H_o + g_N \beta_N H_o)} \\ \Delta E_3 &= g\beta_e H_o - a + \frac{a^2}{4(g\beta_e H_o + g_N \beta_N H_o)} \end{aligned} \quad [\text{II-25}]$$

A sample calculation was performed for PD-Tempone (a nitroxide spin probe) in toluene at room temperature using the following values

$$\begin{aligned} g &= 2.002322, & \beta_e &= 0.92731 \times 10^{-20} \text{ erg/gauss}, \\ g_N &= 5.585486, & \beta_N &= 0.50504 \times 10^{-23} \text{ erg/gauss, and} \\ H_o &= 3245.2678 \text{ gauss.} \end{aligned}$$

The experimental and calculated values for the energies of the three allowed transitions are

	$\Delta E_1 / g\beta_e$ (Gauss)	$\Delta E_2 / g\beta_e$ (Gauss)	$\Delta E_3 / g\beta_e$ (Gauss)
Experimental	3260.1065	3245.6715	3231.2755
Calculated	3259.700	3245.300	3230.868

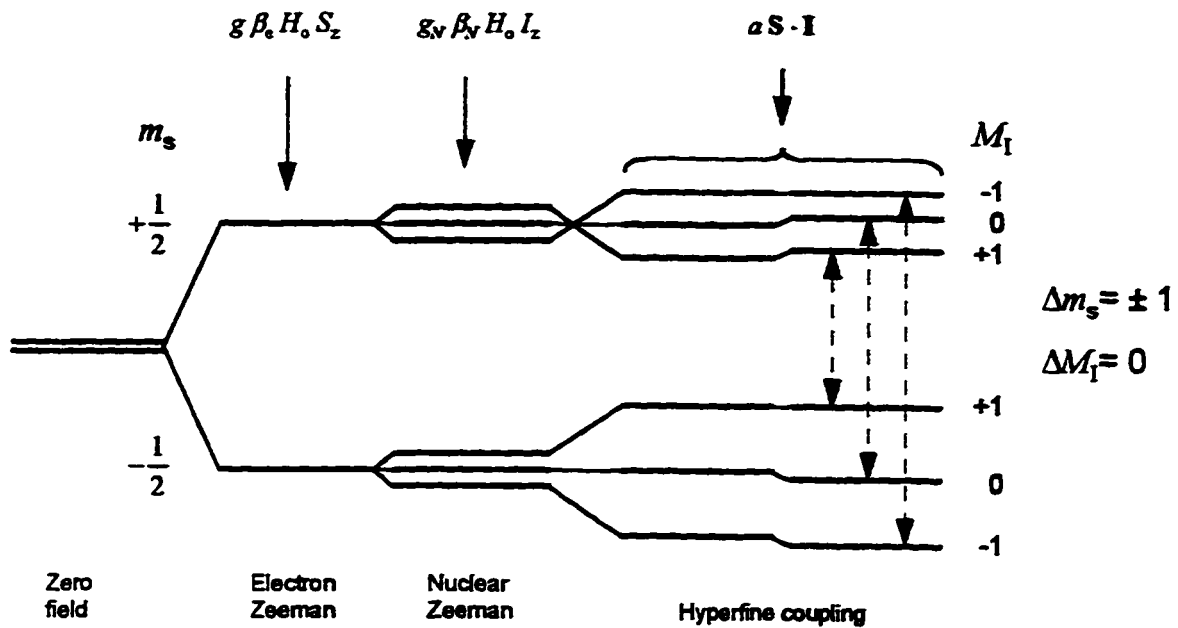


Figure II.1. Second-order energy levels of a nitroxide spin label, and the allowed EPR transitions. The $2p\pi$ unpaired electron is interacting with the nitrogen nucleus of spin 1.

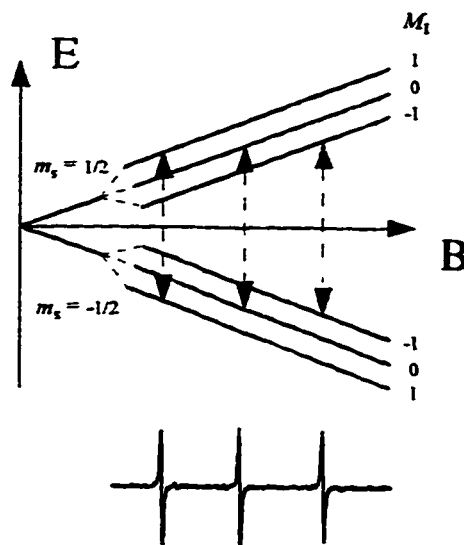


Figure II.2. Dependence of the energy levels on the field strength of Fig. II.1, and the corresponding experimental spectra for PD-Tempone in toluene at room temperature.

Figure II.2 shows the dependence on the magnetic field strength of the energy levels and a typical experimental EPR spectrum of PD-Tempone in toluene at room temperature.

II.4. Line Shape Theory

Line shape analysis is very important in magnetic resonance to obtain information on molecular motions (Abragam 1994; Slichter 1992; Atherton 1973; Freed and Fraenkel 1963; Freed 1964; Kivelson 1972; Hudson and Luckhurst 1969).

II.4.1. Density Matrix

Relaxation theory is described best by density matrix formalism. Using the time-dependent density operator $\rho(t)$, the time variation of the macroscopic observable A can be described by

$$\langle A(t) \rangle = \text{Tr } \rho(t)A \quad [\text{II-26}]$$

here Tr stands for the trace. The explicit form for the density matrix operator in a system at equilibrium is

$$\rho_{\text{eq}} = e^{-\mathcal{H}/kT} / \text{Tr } e^{-\mathcal{H}/kT} \quad [\text{II-27}]$$

The theory of spin relaxation is very much related to the time dependence of the macroscopic magnetization \mathcal{M}_x of the spin system. Referring back to Eq. [II-1] and applying relation [II-26], the following expressions are obtained for the components of the macroscopic magnetization:

$$\mathcal{H}_i(t) = -Ng\beta_e \langle S_i \rangle = -Ng\beta_e \text{Tr } \rho(t) S_i, \quad i = x, y, z \quad [\text{II-28}]$$

where N is the number of spins.

The time evolution of the density matrix is described by the Hamiltonian of the system \mathcal{H} using the equation of motion

$$d\rho(t)/dt = (i/\hbar)[\rho(t), \mathcal{H}] \quad [\text{II-29}]$$

Assuming that the Hamiltonian of the system consists of a time-independent part \mathcal{H}_0 and a part $\mathcal{H}_1(t)$ that varies randomly as a function of time, then Eq. [II-29] will have the form

$$d\rho(t)/dt = (i/\hbar)[\rho(t), \mathcal{H}_0 + \mathcal{H}_1(t)] \quad [\text{II-30}]$$

The Redfield approximation followed by statistical averaging produce the following system of linear differential equations

$$\begin{aligned} d\rho_{\alpha\alpha'}/dt &= (i/\hbar)[\rho, \mathcal{H}_0]_{\alpha\alpha'} + \sum_{\beta\beta'} R_{\alpha\alpha'\beta\beta'} \rho_{\beta\beta'} \\ &= (i/\hbar)(E_{\alpha'} - E_{\alpha}) \rho_{\alpha\alpha'} + \sum_{\beta\beta'} R_{\alpha\alpha'\beta\beta'} \rho_{\beta\beta'} \end{aligned} \quad [\text{II-31}]$$

where the coefficients $R_{\alpha\alpha'\beta\beta'}$ form a matrix known as the *relaxation matrix*, the subscripts denote matrix elements, and the summation is restricted to states with energies satisfying the condition $E_{\alpha} - E_{\alpha'} = E_{\beta} - E_{\beta'}$. The complete Hamiltonian contains the contribution from the interactions with the applied microwave alternating field $\mathcal{H}_2(t)$, and Eq. [II-31] becomes

$$d\rho_{\alpha\alpha'}/dt = (i/\hbar)[\rho, \mathcal{H}_0 + \mathcal{H}_2(t)]_{\alpha\alpha'} + \sum_{\beta\beta'} R_{\alpha\alpha'\beta\beta'} \rho_{\beta\beta'}$$

$$\begin{aligned}
&= (i/\hbar)(E_{\alpha'} - E_{\alpha}) \rho_{\alpha\alpha'} + (i/\hbar) \sum_{\alpha''} [\rho_{\alpha\alpha''} \langle \alpha'' | \mathcal{H}_2(t) | \alpha' \rangle \\
&\quad - \langle \alpha | \mathcal{H}_2(t) | \alpha'' \rangle \rho_{\alpha''\alpha}] + \sum_{\beta\beta'} R_{\alpha\alpha'\beta\beta'} \rho_{\beta\beta'} \quad \text{[II-32]}
\end{aligned}$$

II.4.2. Relaxation and Line Shapes

The shape of the EPR line is determined by the profile of the intensity of the energy absorbed which in turn is a function of the oscillating field $H_x(t)$ given by Eq. [II-12]. The power P absorbed by the sample is given by

$$P = -\mathcal{M} \cdot d\mathbf{H}/dt = -\mathcal{M}_x (dH_x/dt) \quad \text{[II-33]}$$

where \mathcal{M}_x is the induced magnetic moment by the oscillating field $H_x(t)$ in the macroscopic sample. The actual spectrum is given by the average power absorbed per cycle

$$\overline{P(\omega)} = -(\omega / 2\pi) \int_0^{2\pi/\omega} \mathcal{M}_x (dH_x/dt) dt \quad \text{[II-33]}$$

where \mathcal{M}_x is found to be composed of

$$\mathcal{M}_x(t) = H_1 [\chi'(\omega) \cos \omega t + \chi''(\omega) \sin \omega t] \quad \text{[II-34]}$$

and after integration the spectral line shape is given by

$$\overline{P(\omega)} = \frac{1}{2} \omega \chi''(\omega) H_1^2 \quad \text{[II-35]}$$

For a two-level system

$$\chi''(\omega) = \frac{1}{2} \pi \omega_0 \chi_0 f(\omega) \quad \text{[II-36]}$$

where χ_0 is the static susceptibility and $f(\omega)$ is a Lorentzian shape function (Sec. V.3.1.2).

II.4.3. Relaxation Matrix and Correlation Functions

For the theoretical interpretation of the spectral lines, the relaxation matrix must be computed. Since the perturbation $\mathcal{H}_1(t)$ is a random function of time, its effect on the system must be calculated statistically.

The general expression for the relaxation matrix $R_{\alpha\alpha'\beta\beta'}$ is given by

$$\begin{aligned}
 R_{\alpha\alpha'\beta\beta'} &= 2J_{\alpha\beta\alpha'\beta'}(\omega_{\alpha\beta}) - \delta_{\alpha'\beta'} \sum_{\gamma} J_{\alpha\gamma\beta\gamma}(\omega_{\gamma\beta}) \\
 &\quad - \delta_{\alpha\beta} \sum_{\gamma} J_{\gamma\alpha'\gamma\beta'}(\omega_{\beta'\gamma}) \\
 J_{\alpha\alpha'\beta\beta'}(\omega) &= \frac{1}{2} \int_{-\infty}^{+\infty} G_{\alpha\alpha'\beta\beta'}(t) e^{-i\omega t} dt \quad [\text{II-37}]
 \end{aligned}$$

$$G_{\alpha\alpha'\beta\beta'}(t) = \hbar^{-2} \langle \mathcal{H}_1(0)_{\alpha\alpha'} \mathcal{H}_1(t)_{\beta\beta'}^* \rangle$$

where $\mathcal{H}_1(t)_{\alpha\beta}$ is the α, β matrix element of $\mathcal{H}_1(t)$, the brackets indicate statistical average over the spins ensemble, and $\omega_{\alpha\beta} = (E_{\alpha} - E_{\beta})/\hbar$. $G(t)$ is called the correlation function of $\mathcal{H}_1(t)$, and $J(\omega)$ is the corresponding spectral density which is the Fourier transform of the correlation function. The function $G(t)$ provides the information on how the value of \mathcal{H}_1 at any time is correlated to its values at later times. Based on statistical models, $G(t)$ has the general form of an exponential decay:

$$G(t) = \hbar^{-2} \langle |\mathcal{H}_1|^2 \rangle e^{-t/\tau_c} \quad [\text{II-38}]$$

where τ_c is the correlation time for the random motion, e.g., rotational diffusion, which is the chief mechanism responsible for the modulation of the anisotropic interactions of $\mathcal{H}_1(t)$.

A reasonable model for the random process is molecular reorientations subjected to Brownian motion which is described by the generalized Debye (1945) equation for rotational diffusion. If the molecules are axially symmetric, the diffusion equation is formally analogous to the Schrödinger equation for the symmetric rotator whose eigenfunctions are the Wigner functions $D_{lm}^j(\Omega)$ and the corresponding eigenvalues are

$$\lambda_{jm} = - [j(j+1)D_{\perp} + (D_{\parallel} - D_{\perp}) m^2] \quad [\text{II-39}]$$

where D_{\parallel} and D_{\perp} are the principal values of the diffusion tensor. From the general solution of the diffusion equation, the correlation functions of the Wigner matrices are found to be

$$\begin{aligned} \langle D_{l'm'}^{j'}(0) D_{lm}^{j*}(t) \rangle &= \int d\Omega_0 D_{l'm'}^{j'}(\Omega_0) P(\Omega_0) \int d\Omega D_{lm}^j(\Omega) P(\Omega_0 | \Omega t) \\ &= \langle D_{l'm'}^{j'}(\Omega_0) D_{lm}^{j*}(\Omega_0) \rangle \exp(\lambda_{jm} t) \\ &= \delta_{j'j} \delta_{l'l} \delta_{m'm} [1/(2j+1)] \exp(-|t|/\tau_{jm}) \quad [\text{II-40}] \end{aligned}$$

which decay exponentially with a characteristic time $\tau_{jm} = -\lambda_{jm}^{-1}$. Here the orthogonality properties of the Wigner functions were used; $P(\Omega_0) \equiv P(\Omega, 0)$ is the probability of finding the molecule within the solid angle $d\Omega$ at initial time $t = 0$; $P(\Omega_1 t_1 | \Omega_2 t_2)$ is the conditional probability which calculates Ω in the range $(\Omega_2, \Omega_2 + d\Omega_2)$ at time $t = t_2$, given Ω_1 at initial time $t = t_1$.

II.4.4. Linewidth Parameters

Linewidth parameters refer to the coefficients of the polynomial used to fit the linewidths $1/T_2$ versus the nuclear quantum number M specifying the transition. For the case of a nitroxide free radical in a liquid medium the fitting equation has the form

$$[T_2(M)]^{-1} = A + BM + CM^2 \quad [\text{II-41}]$$

The linewidth parameters A , B , and C can be derived from a calculation of the elements $R_{\alpha\alpha'\beta\beta'}$ of the relaxation matrix which are involved in the determination of the x component of the magnetization. The condition $E_\alpha - E_{\alpha'} = E_\beta - E_{\beta'}$ and the EPR selection rules for states connected by the operator S_x result in a diagonal relaxation matrix if there is no degeneracy in the EPR transitions. An example of this case is the nitroxide free radical. Additional assumptions are that the paramagnetic species have an axially symmetric diffusion tensor, and the major mechanisms for spin relaxation are the g factor and hyperfine anisotropies. Therefore, fluctuating solvent interactions and molecular geometry variations, which can modify the instantaneous values of the magnetic parameters, are neglected.

The perturbing Hamiltonian $\mathcal{H}_1(t)$ in spherical basis under these assumptions becomes

$$\mathcal{H}_1(t) = \sum_{\mu} \sum_{m,m'} (-1)^{m'} F_{\mu}^{(-m')} D_{m,m'}^2(t) A_{\mu}^{(m)} \quad [\text{II-42}]$$

and the corresponding correlation function of $\mathcal{H}_1(t)$ is

$$G_{\alpha\alpha'\beta\beta}(t) = \hbar^{-2} \sum_{\mu,\nu} \sum_{m,m'} (-1)^{m+m'} F_{\mu}^{(-m)} F_{\nu}^{(m)} g_{mm}(t) \\ \times \langle \alpha | A_{\mu}^{(m)} | \alpha' \rangle \langle \beta | A_{\nu}^{(-m)} | \beta' \rangle \quad [\text{II-43}]$$

All of the relevant interactions are represented by second-rank tensors, and $g_{mm}(t)$ is the correlation function of the rotation matrix component $D_{mm}^2(\alpha\beta\gamma)$. According to Eq. [II-40], cross terms of the form $\langle D_{mm}^2(0) D_{m'm'}^2(t) \rangle$ vanish from the summation.

The spectral density $j_{mm}(\omega)$, which is the Fourier transform of the correlation function $g_{mm}(t)$, can be calculated from Eq. [II-40],

$$j_{mm}(\omega) = \frac{1}{2} \int_{-\infty}^{\infty} \frac{1}{\tau_m} \exp(-|t|/\tau_m) \exp(-i\omega t) dt = \frac{1}{\tau_m} (1 + \omega^2 \tau_m^2)^{-1} \\ \tau_m = [6D_{\perp} + (D_{\parallel} - D_{\perp}) m^2]^{-1} \quad [\text{II-44}]$$

Finally, the spectral density $J_{\alpha\alpha'\beta\beta}(\omega)$ of Eq. [II-37] can be written as

$$J_{\alpha\alpha'\beta\beta}(\omega) = \hbar^{-2} \sum_{\mu,\nu} \sum_{m,m'} (-1)^{m+m'} F_{\mu}^{(-m)} F_{\nu}^{(m)} j_{mm}(\omega) \\ \times \langle \alpha | A_{\mu}^{(m)} | \alpha' \rangle \langle \beta | A_{\nu}^{(-m)} | \beta' \rangle \quad [\text{II-45}]$$

Contributions to the relaxation matrix $R_{\alpha\alpha'\beta\beta}$ from the Hamiltonian $\mathcal{H}_1(t)$ are divided into three groups of terms: *secular* terms with spin operators of the type $H_0 S_z$ and $I_z S_z$ having only diagonal matrix elements, and for these terms $\omega_{\alpha\beta} = 0$; *nonsecular* terms with spin operators of the type S_{\pm} which connect states with energy difference $\hbar\omega_0$, where ω_0 is the resonance frequency; and *pseudosecular* terms which contain spin operators of the type $I_{\pm} S_z$ and the nonvanishing matrix

elements are between states with energy difference equivalent to the hyperfine coupling constant a .

The linewidth parameters are derived, after calculating all the contributions to the relaxation matrix, and found to be

$$[T_2(M)]^{-1} = -R_{\alpha\alpha'\alpha\alpha'} = A + BM + CM^2 \quad [\text{II-46}]$$

$$A = \frac{1}{6} H_0^2 \hbar^{-2} \sum_m (-1)^m F_g^{(m)} F_g^{(-m)} [4j_{0m}(0) + 3j_{1m}(\omega_0)]$$

$$+ \frac{1}{12} I(I+1) \sum_m (-1)^m F_A^{(m)} F_A^{(-m)} [j_{0m}(\omega_0) + 3j_{1m}(\omega_{hf}) + 6j_{2m}(\omega_0)]$$

$$B = \frac{1}{6} H_0 \hbar^{-2} \sum_m (-1)^m [F_A^{(m)} F_g^{(-m)} + F_A^{(-m)} F_g^{(m)}] [4j_{0m}(0) + 3j_{1m}(\omega_0)]$$

$$C = \frac{1}{6} \hbar^{-2} \sum_m (-1)^m F_A^{(m)} F_A^{(-m)} \{4j_{0m}(0) + 3j_{1m}(\omega_0)$$

$$- \frac{1}{2} [j_{0m}(\omega_0) + 3j_{1m}(\omega_{hf}) + 6j_{2m}(\omega_0)]\} \quad [\text{II-47}]$$

The actual expressions used in this work to calculate the linewidth parameters B and C are given in the sub-section III.3.1.6.

CHAPTER III

ANISOTROPIC INTERACTION AND COLE-DAVIDSON PARAMETERS: PD-TEMPONE IN TOLUENE

III.1. Introduction

EPR provides the means to study rotational and reorientational motions of free radicals. These motions are usually characterized by correlation times. Correlation times, τ_c (*cf.* Eq. III-38), can be determined for the free radical at different temperatures. This can be achieved by reproducing theoretically the experimental B and C values. The variation of τ_c as a function of temperature for linear and spherical molecules was first derived by Debye (1945). Debye generalized the Stokes-Einstein diffusion relationships to describe correlation times in dielectric relaxation. Bloembergen, Purcell, and Pound (BPP) (1948) extended the Debye expression to describe correlation times in spin relaxation. BPP derived the following expression

$$\tau_c = \frac{4 \pi r^3 \eta}{3 k_B T} \quad \text{[III-1]}$$

where r is the radius of the solute molecules, η is the coefficient of shear viscosity of the solvent, T is absolute temperature, and k_B is Boltzmann constant.

The molecular radius r determined by EPR was found to be smaller than the radius of the same molecule determined by other techniques. At the beginning, an empirical parameter was introduced (McClung and Kivelson 1968) such that

$$r = \kappa^{1/3} r_0 \quad \text{[III-2]}$$

where r_0 is the radius of the molecule, r is called the effective radius r_e , and $0 \leq \kappa \leq 1$. Equation [III-1] was modified to the following

$$\tau_c = \frac{4 \pi (\kappa r_0^3) \eta}{3 k_B T} \quad \text{[III-3]}$$

Plotting τ_c versus (η/T) , and if r_0 is determined from an independent study, the parameter κ can be evaluated.

Kivelson et al. (1970) derived an expression for the parameter κ , which is a measure of the anisotropy of intermolecular interactions, and found that it is proportional to the ratio of the mean square intermolecular torques of the solute $\langle \mathcal{T}^2 \rangle$ to the mean square intermolecular forces of the solvent $\langle \mathcal{F}^2 \rangle$.

$$\kappa \approx (3 / 4 r_0^2) \langle \mathcal{T}^2 \rangle / \langle \mathcal{F}^2 \rangle \quad \text{[III-4]}$$

where $\langle \mathcal{T}^2 \rangle$ is related to the fluctuating intermolecular torques associated with the angular momentum of the solute, and $\langle \mathcal{F}^2 \rangle$ is related to the translational

shear forces of the solvent. Hence, κ is actually a measure of the anisotropic interactions between the solute and the solvent molecules.

If the solute-solvent system is kept the same, then based on Eq.'s [III-3] and [III-4] the values of κ obtained at different microwave frequencies would be the same. However, earlier studies showed that values of the anisotropic interaction parameter κ were different at different microwave frequencies (Hwang et al., 1975; Rahman, 1988).

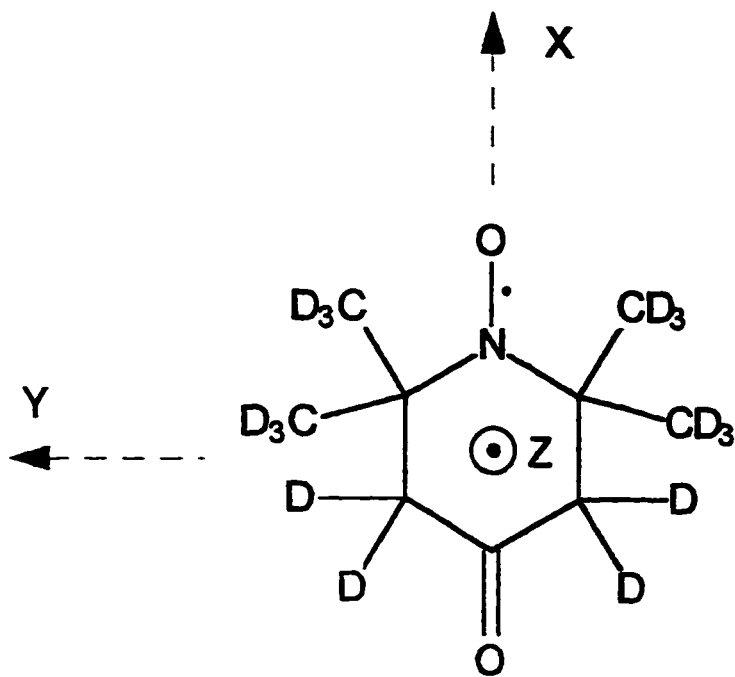
The objective of this study (Chap.'s III and V) was to determine the anisotropic interaction parameter κ for the nitroxide spin probe perdeuterated-2,2,6,6-tetramethyl-4-piperidone-N-oxide (shown in Scheme III-I) in toluene at the microwave frequency Bands: L (~1 GHz), S (~4 GHz), X (~9.5 GHz), and Q (~35 GHz).

III.2. Experimental

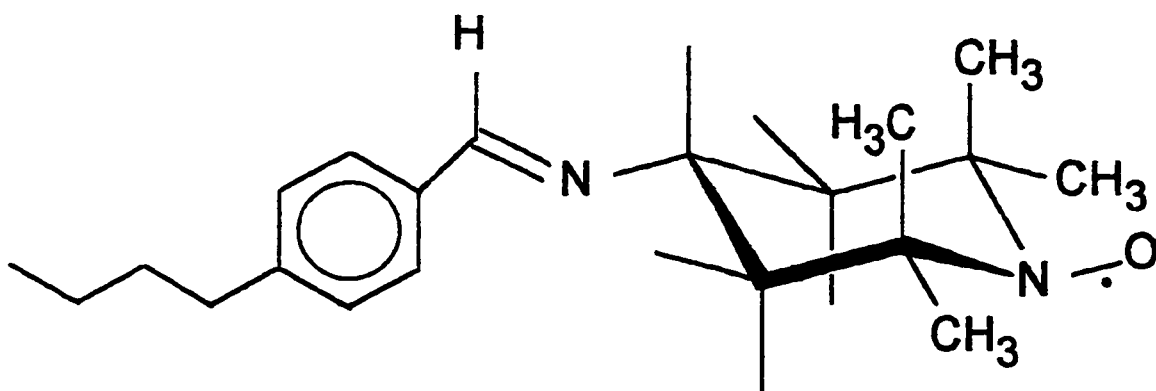
III.2.1. Materials and Sample Preparation

The nitroxide spin probe perdeuterated-2,2,6,6-tetramethyl-4-piperidone-N-oxide (abbreviated as PD-Tempone) was obtained from Stohler Isotope and used without further purification. The solvent toluene was purchased from Fluka AG, Switzerland. Samples of PD-Tempone in toluene for L-, S-, and X-Bands were prepared in 2-mm i.d. × 3-mm o.d. Pyrex sample tubes. These solutions contain oxygen from the atmosphere, and oxygen is paramagnetic and would cause the first derivative EPR lines to be broader. Therefore, dissolved oxygen

PD-Tempone



BBTMPO



Scheme III-I

was removed by several cycles of freeze-pump-thaw. The concentration of the nitroxide free radical in toluene was $1-10 \times 10^{-5}$ M.

To prepare permanent samples of PD-Tempone in toluene for L-, S-, and X-Bands, a modified vacuum system manufactured by Pope Scientific Inc. was used. This vacuum system was utilized to perform the freeze-pump-thaw cycles. The procedure for cycles of freeze-pump-thaw consisted of (refer to Fig. III.1):

1. The vacuum line was evacuated while valves (1) and (2) were open until a stable reading of the pressure was attained. Usually a reading close to $10 \mu\text{Hg}$ was reached.
2. The EPR sample tube filled with the solution was inserted in the port, the tube was immersed in liquid nitrogen, and valve (3) was opened. The setup was left running for 4-5 minutes.
3. Valve (3) was closed, the liquid nitrogen dewar was removed, and the solution was allowed to melt. During the process of melting dissolved oxygen bubbled off. Then, when no more bubbles were observed, the EPR sample tube was immersed in liquid nitrogen and valve (3) was opened. The process was repeated until no more oxygen bubbles were observed.
4. While the EPR sample tube immersed in liquid nitrogen, and with valve (3) opened the tube was sealed with a mini-torch.

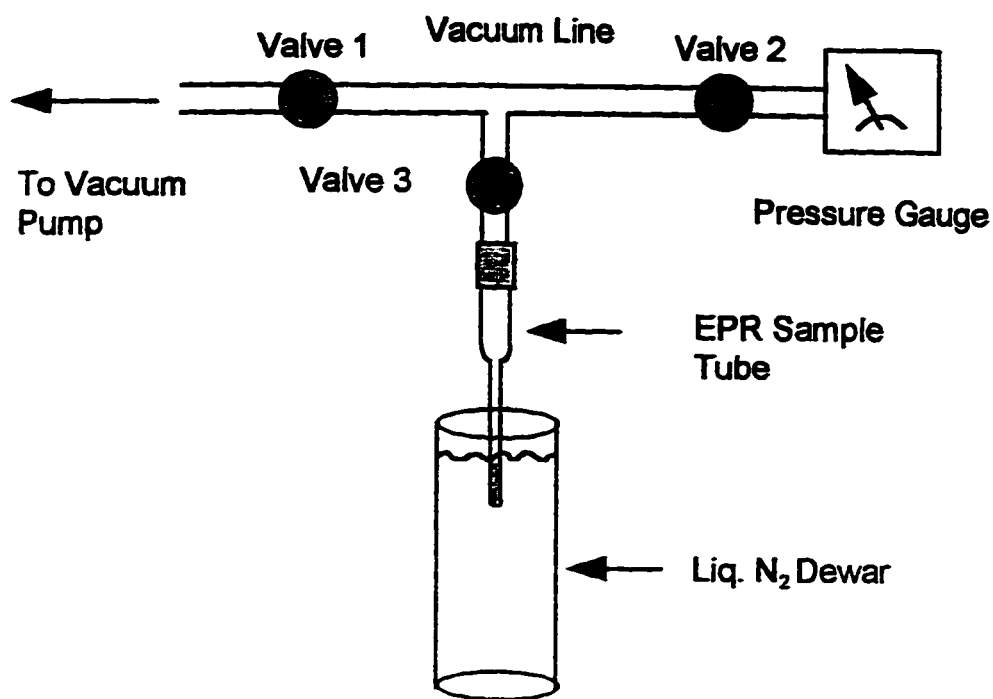


Figure III.1. Schematic representation of the freeze-pump-thaw setup used to prepare permanent EPR samples.

The procedure for the preparation of permanent samples ($1-10 \times 10^5$ M) in small quartz tubes (1 mm i.d. \times 1.5 mm o.d. \times 60 mm height) for studies conducted at the Q-Band was different. The steps involved were:

1. All required glass- and lab-wares and sample solution were placed inside the glove bag model X-27-27 purchased from Instruments for Research and Industry, Pennsylvania, USA. The glove bag was modified by cutting the two hand pieces and attaching a more convenient gloves using elastic rubbers.
2. The solution, which was prepared outside the glove bag, was purged with nitrogen gas for half an hour, while the glove bag was almost completely sealed. Quartz tubes (1-mm i.d. \times 1.5-mm o.d. and 9-cm in length) sealed from one end were also purged with nitrogen. Then, the bag was completely sealed and was inflated until it became like a soft pillow.
3. Using a syringe, a quartz tube was filled with the solution to about 3-cm in height. The quartz tube was then clogged with Critoseal[®] (Lancer Div. of Sherwood Medical, a Brunswick Co., St. Louis Missouri), and finally sealed with epoxy. It was verified experimentally with DPPH (acronym for 1,1-diphenyl-2-picrylhydrazyl) solid sample that the epoxy did not have any effect on the EPR signal. DPPH was used for this purpose because its *g* value is well known. The *g* value of DPPH was determined in the presence and in absence of epoxy and was found to be the same. The sealed tubes were kept inside the glove bag

under nitrogen atmosphere until the epoxy cured (usually the tubes are left overnight).

III.2.2. Apparatus

III.2.2.1. The EPR Spectrometer- The EPR measurements were performed using Bruker Electron Spin Resonance spectrometer model ER 200E/D-SRC along with a micro-station the ESP 300E Software installed on Bruker Data System ESP 3220. The version of the software used was 3.02. To accurately measure the microwave frequency and the field of the magnet a Hewlett Packard 5342A Microwave Frequency Counter and the NMR Gaussmeter ER 035M were used, respectively. The HP 5342A Microwave Frequency Counter gave a stable reading of at least eight digits. The Bruker Variable Temperature Unit ER 4111VT was used to vary the temperature of the cavity containing the sample. The accuracy of this unit is ± 1 degrees K.

The different microwave bridges and cavities for the four bands were:

Band	Microwave Bridge	Cavity
L (~1 GHz)	ER 065 LR	ER 6502 LH
S (~4 GHz)	ER 061 SR	ER 6103 SH
X (~9.5 GHz)	ER 045 MRBDH	ER 4105 DR
Q (~34 GHz)	ER 053 QRD	ER 5102 QT

Other accessories included a Bruker ER 072 Power Supply, a Bruker heat exchanger unit to cool both the magnet and the microwave bridge, a water cooling bath, and a Hewlett Packard 7475A plotter. The plotter is connected to the micro-station which is driven by OS/9 operating system. To manipulate the data, a software developed by Bruker was installed on a PC that was interfaced with the ESP 3220 micro-station. The software is WIN-EPR version 921201. The data can then be printed on a Hewlett Packard Laser Jet 4 Plus.

Figure III.2 depicts a general schematic representation of a Bruker EPR spectrometer. The essential components of any spectrometer are: a source of electromagnetic radiation, a sample, and a detector. The electromagnetic radiation source and the detector are in the microwave bridge. The sample is in a microwave cavity, which is a metal box that assists in amplifying weak signals from the sample. The magnet is to "tune" the electronic spin energy levels of the unpaired electron in the sample. In addition, the control device contains signal processing and control electronics, also called the console, and a computer or a micro-station. The computer is used for analyzing the data as well as coordinating all the units for acquiring a spectrum.

The main components of the console are a field controller ER 032 M, a signal channel ER 023 M, a microwave controller ER 048 H, and an NMR gaussmeter ER 035 M. Each component is built as a separate unit or a module. The ER 032 M field control module is used to control the magnetic field. The sweep width (in Gauss), the central field (in Gauss), and the sweep time (in

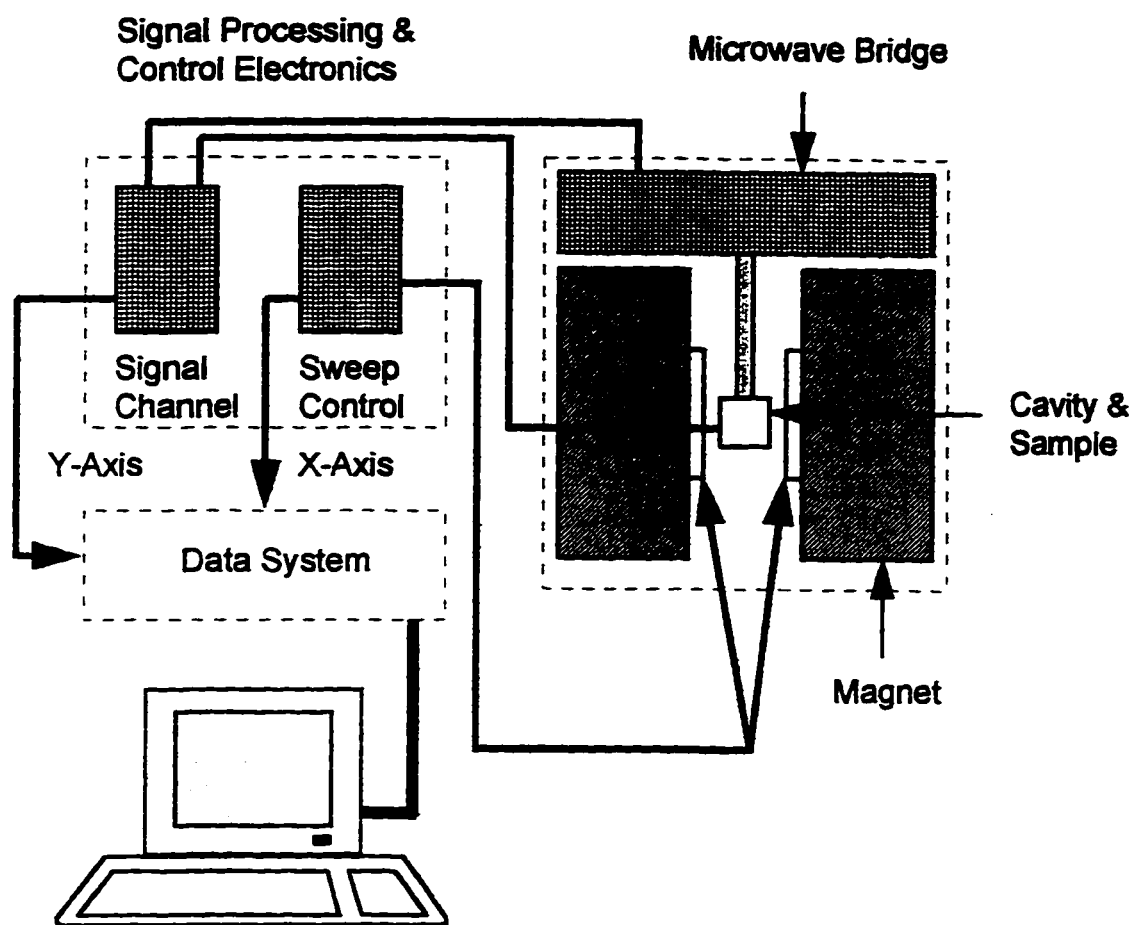


Figure III.2. A schematic representation of a Bruker EPR spectrometer (adopted from Bruker manual).

seconds) are set through this controller. The ER 023 M signal channel module works by phase sensitive detection and applies magnetic field modulation to increase the sensitivity. Optimum settings of modulation amplitude, modulation frequency, and time constant are required to achieve good sensitivity and accurate results. Absolute calibration of field modulation amplitude for Bruker EPR cavities is achieved by a calibrated "tune box" supplied with each cavity type. The ER 048 H microwave controller is used to control the microwave bridge. The radiation output power level can be set in one dB steps and a direct true power reading in mW, μ W, and nW is possible on the ER 048 LED display.

III.2.2.2. *The Microwave Bridge.* In this study four different microwave bridges were used to investigate the behavior at four different microwave frequency regions the L-, S-, X- , and Q-bands mentioned above. A block diagram of the microwave bridge is depicted in Figure III.3. The microwave bridge contains the microwave source and the detector. The microwave source can be Gunn oscillator or a klystron. The microwave source used in the bridges used in this study is a klystron. The variable attenuator, which blocks the flow of the microwave radiation, comes after the microwave source. The attenuator is used to control the amount of microwave power that the sample is exposed to it. The circulator controls the flow of radiation with help of the three ports. The incident microwave radiation passes only through the first and second ports to the sample in the cavity. The reflected microwave radiation is directed to the

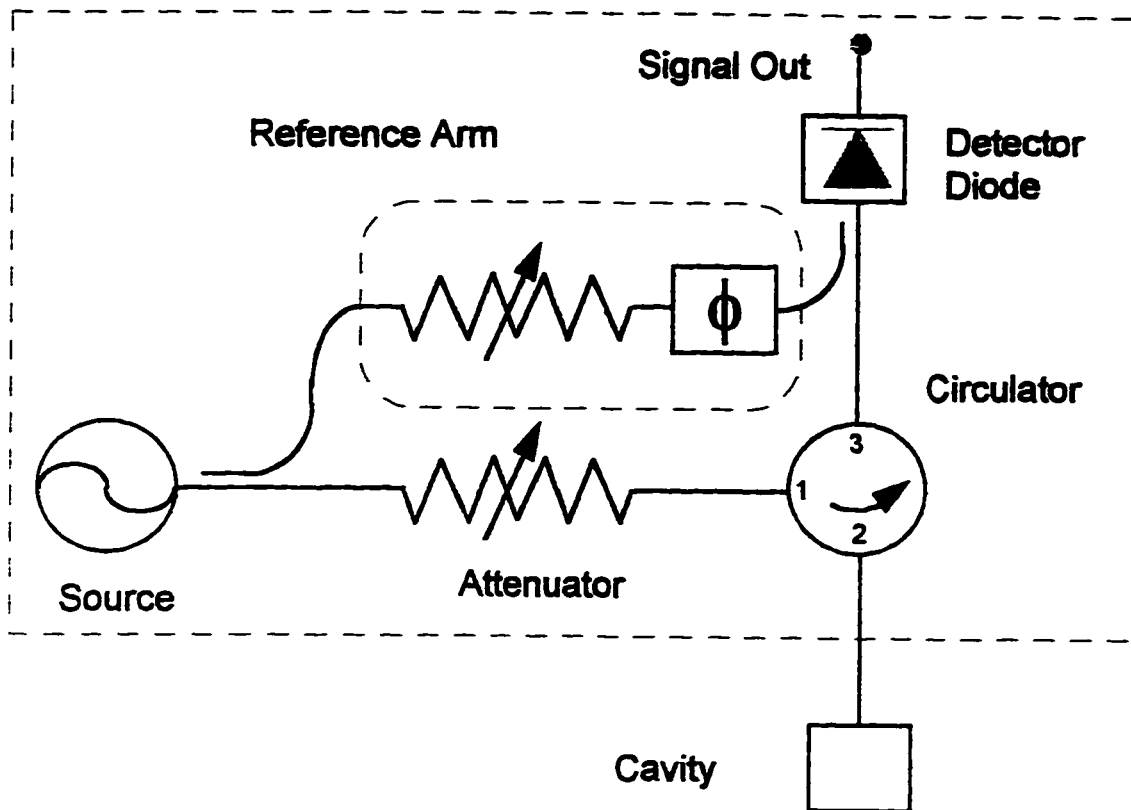


Figure III.3. Block diagram of a microwave bridge (adopted from Bruker manual).

detector only through ports two and three. Therefore, the Bruker EPR spectrometer is a reflection spectrometer which measures the changes (due to absorption) in the amount of radiation reflected back from the microwave cavity containing the sample. The detector is a Schottky barrier diode which converts the microwave power to an electrical current. For the diode to operate in the linear region, the detector current should be approximately 200 micro-amperes. This is for optimal operating conditions. The reference arm supplies the detector with some extra microwave power or "bias". The second attenuator controls the power level so that the detector operates with optimal performance.

III.2.2.3. The EPR Cavity. Microwave EPR cavities are used to amplify weak signals from the sample. The cavity is a metal box that resonates with microwaves. At the resonance frequency of the cavity, the cavity stores the microwave energy and, therefore, no microwaves will be reflected back but will remain inside the cavity. Hence, the shape of the reflected microwave will be as shown in Figure III.4. In the Figure the ν_{res} is the resonant frequency of the cavity. The cavity is coupled to the cavity via a hole called an iris. The iris matches the impedances of the cavity and the waveguide, which is used to transfer microwaves from the microwave bridge to the cavity. The matching is achieved by adjusting the height of the iris screw (see Figure III.5). The EPR signal results when the sample absorbs the microwave energy. Absorption by the sample alters the impedance of the cavity and the matching, or coupling,

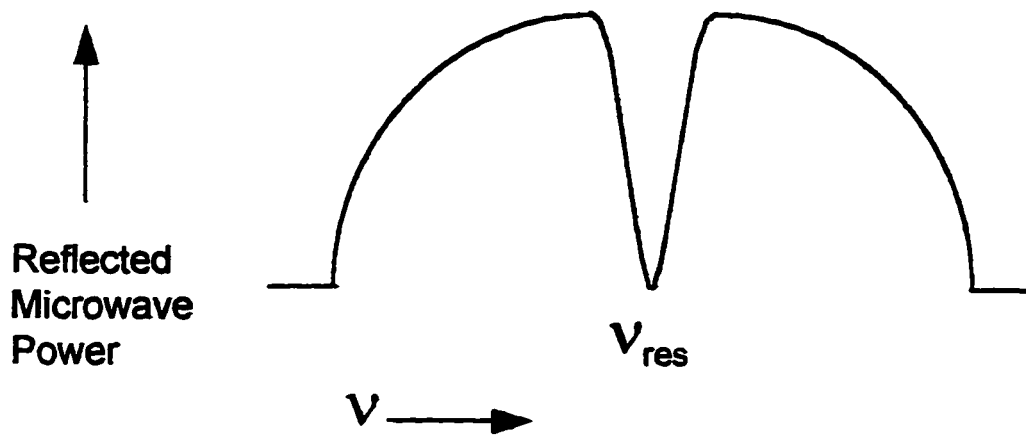


Figure III.4. Shape of the reflected microwave power from a resonant cavity
(adopted from Bruker manual).

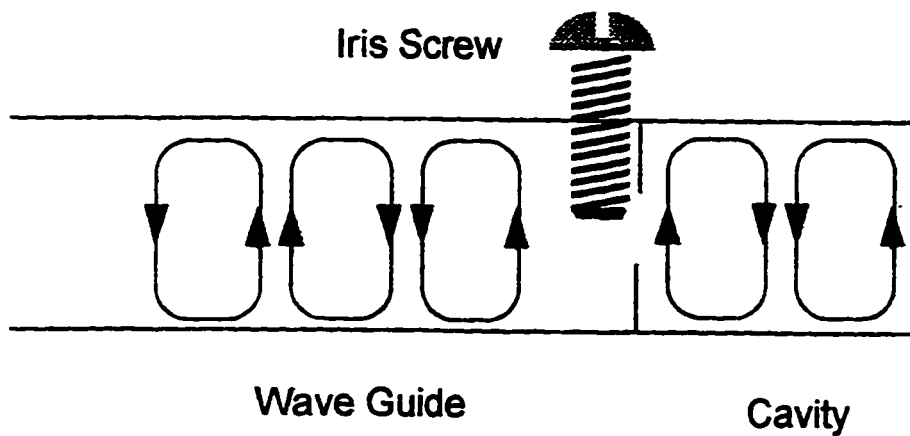


Figure III.5. Coupling of a microwave cavity to waveguide (adopted from Bruker manual).

between the cavity and the waveguide is lost. Thus, the cavity is not critically coupled and the microwave radiation will be reflected back to the bridge. This will give rise to an EPR signal.

III.2.2.4. Calibration of Resonators for L- & S-Bands. A calibration file must be constructed before any resonator type (or cavity) can be used. Calibration files for the L- and S-Bands were constructed because they were not provided by Bruker. The calibration procedures for the microwave bridge ER 065 LR (L-Band) and resonator ER 6502 LH and for the microwave bridge ER 061 SR (S-Band) and resonator ER 6103 SH were performed as follows:

1. The AFC toggle in the rear panel of the microwave bridge was set "ON" at a value of 10. The potential of the modulation frequency (MF) in the rear of the console was set equal to 3.00.
2. A DPPH (acronym for 1,1-diphenyl-2-picryl hydrazyl) solid sample, which is a frequently used reference sample, was placed in the cavity. Both buttons on the ER 048 H bridge controller "OPERATE" and "REF." were pressed. The bridge power was set at 60 dB and, using the "BIAS" screw, the diode current was adjusted to 200 μ A.
3. The ER 048 H was the switched to "TUNE" and the power was increased to 25 dB. If no dip was observed the iris screw would be adjusted, and if still no dip,

the "REF." button might be pressed again and the value of the "REF. PHASE" could be changed.

4. The "REF." button was put "OFF" and the "OPERATE" button was switched "ON". Both the diode current and the AFC pointers were at the center. If this was not the case, the AFC was adjusted by the "FREQUENCY" knob, and the diode current with the iris screw and/or the "REF. PHASE" knob. The power was increased to 15 dB, and the "RAPID" button with the "RECORD" option on the Time Base ER 001 module was switched "ON" and the 200 G was selected on the "RAPID SCAN". A time constant of 40 μ sec was selected on the signal channel.

5. The phase was varied until the first derivative EPR signal was maximum. Then ± 90 degrees were added to that phase angle so that there was a completely flat line. This phase angle was recorded. After that the receiver gain on the signal channel was increased until the signal completely filled the screen of the oscilloscope. Half this receiver gain and the central field were also recorded.

6. The following parameters were entered into the main program ESP300E:

Central Field: the value recorded in step (5)

Sweep Width: 10 Gauss

Phase Angle: the value recorded in step (5)

Conversion Time: 5.12 msec

Time Constant: 1.28 msec

Then "C" for calibration was entered in the main menu followed by "A". The MF potential was adjusted to obtain a value of ~7 Gauss for the modulation amplitude which corresponded to a modulation frequency of 100.00 kHz. Finally, the calibration file was stored in the computer.

III.2.3. Measurement and Data Collection

Although the measurement procedure is well documented for the X-Band, nothing was mentioned for the other three bands, namely the L-, S-, and Q-Bands. Following the basic ideas in the procedure for the X-Band, it was possible to design suitable tuning and coupling procedures for these bands. The tuning and coupling procedures for the L- and S-Bands were similar.

III.2.3.1. *Tuning and Coupling for L- and S-Bands.* The tuning and coupling procedure for the L- and S-Bands was slightly different from the procedure for the X-Band. The procedure consisted of the following steps:

1. The power was increased while on "TUNE" as follows: 55dB → 45dB → 35dB → 25dB. The fluctuating sound of the bands at these microwave ranges was not amplified when this method of stepping-up the power was adapted. The dip, similar to the dip shown in Figure III.4, was centered using the "FREQUENCY" knob.

2. The iris screw was used to produce a dip with maximum sharpness and deepness. Then, the "REF." button was pressed "ON" and the dip was again centered by fine adjustment of the "FREQUENCY" knob. The shape of the resulted dip is depicted in Figure III.6.

3. The whole peak in Fig. III.6 was maximized using the "REF. PHASE" knob. The two peaks on the shoulders of the dip were made at their highest level, although their heights were not equal. Then the "REF." button was switched "OFF" and the "OPERATE" button was switched "ON" followed by the "REF." button.

4. The diode current was set equal to 200 μA by manually adjusting the iris screw on the cavity. The power was increased to 15 dB while maintaining the diode current at 200 μA by adjusting the level of the iris screw. This is called critical coupling.

5. The instrument was then ready for spectrum acquisition.

III.2.3.2. Tuning and Coupling for Q-Band. In this section the differences in the tuning and coupling procedure of the Q-Band from the other Bands will be clarified. These differences are:

1. To be able to see the dip the power was increased to 8 to 12 dB.
2. The microwave frequency was adjusted by two knobs: the "FREQUENCY" knob on the ER 048 H controller and the "+ f -" knob on the Q-Band resonator.

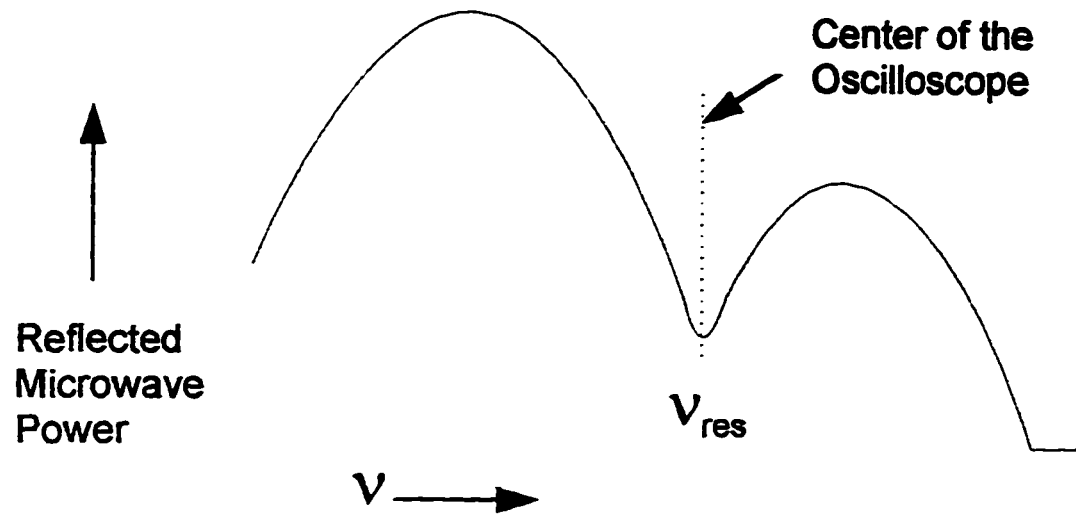


Figure III.6. The shape of the reflected microwave power at S-Band.

3. To obtain the sharpest and deepest possible dip four things could be adjusted. These are the "REF. PHASE" and the "FREQUENCY knobs on the ER 048 H microwave bridge controller and the "f" knob and the iris screw on the Q-Band resonator. The shape of the dip was similar to the dip from the X-Band.

III.2.3.3. Data Collection. The next step is acquiring a spectrum. Before the instrument can be used for spectrum acquisition, good parameter values must be selected and entered into the spectrometer. These parameters are: Modulation Amplitude (mA), Modulation Frequency (MF), Receiver Gain (RG), Conversion Time, Time Constant, Central Field (CF), Sweep Width (SW), and Phase.

III.2.3.4. Selecting a Modulation Amplitude. The intensity of the EPR signal increases as the magnetic field modulation amplitude increases. However, excessive field modulation broadens the EPR signal which then becomes distorted. The variation of observed linewidth as a function of peak-to-peak modulation amplitude is shown in Table III.1 for PD-Tempone in toluene at L-Band. Figure III.7 shows that variation graphically. The value of peak-to-peak modulation amplitude that gave the best compromise between signal intensity and signal distortion for PD-Tempone in toluene at L-Band was 0.124 Gauss. For S-Band the variation of observed linewidth as a function of peak-to-peak modulation amplitude is shown in Table III.2 for PD-Tempone in toluene.

TABLE III.1. Observed Line Width as a Function of Peak-to-Peak Modulation Amplitude for PD-Tempone in Toluene at L-Band.

Modulation Amplitude p-p (Gauss)	Observed Line Width (Gauss)
0.0493	0.309
0.0620	0.314
0.0696	0.299
0.0781	0.317
0.0876	0.319
0.0983	0.314
0.1100	0.309
0.1240	0.309
0.1390	0.306
0.1560	0.332
0.1750	0.332
0.1960	0.327
0.2200	0.335
0.2470	0.327
0.2770	0.342
0.3110	0.363
0.3490	0.358

* The shaded cells in the table represent the selected value of modulation amplitude, i.e. 0.124 Gauss, and the corresponding observed line width.

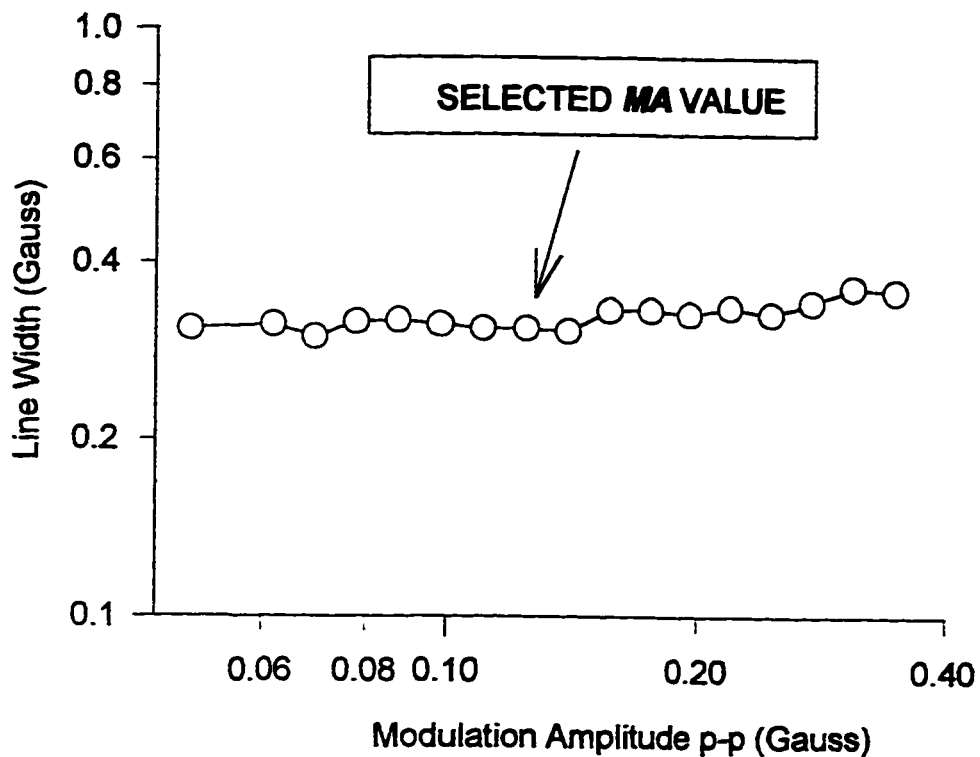


Figure III.7. Observed line width as a function of peak-to-peak modulation amplitude for PD-Tempone in toluene at L-Band. The selected value of modulation amplitude that gave the best compromise between signal intensity and signal distortion was 0.124 Gauss.

TABLE III.2. Observed Line Width as a Function of Peak-to-Peak Modulation Amplitude for PD-Tempone in Toluene at S-Band.

Modulation Amplitude p-p (Gauss)	Observed Line Width (Gauss)
0.0500	0.25739
0.0630	0.25024
0.0800	0.25739
0.1000	0.27169
0.1250	0.25739
0.1600	0.27884
0.2000	0.29314
0.2500	0.31459
0.3200	0.32174
0.4000	0.42184
0.5000	0.50764
0.6300	0.61489
0.8000	0.77218
1.0000	1.00098

* The shaded cells in the table represent the selected value of modulation amplitude, i.e. 0.125 Gauss, and the corresponding observed line width.

Graphical representation of this variation is shown in Figure III.8. In this case the value of peak-to-peak modulation amplitude that gave the best compromise between signal intensity and signal distortion for PD-Tempone in toluene was 0.125 Gauss.

III.2.3.5. Remote Control and Data Acquisition. Remote control of the Bruker EPR spectrometer and acquisition of data can be performed using the ESP 300E software. After booting, this software can be entered by typing "esp300e" at the shell prompt, the dollar sign. The main menu contains such options as File handling, Acquisition, Parameters, Data handling, Calibration, ... etc. Each option in the main menu and in the sub-menus can be entered by selecting it using the arrows in the key board and hitting enter or directly by pressing the designated letter. Measurement parameters and spectra are stored in pages which can then be saved. These pages are numbered respectively.

A brief description of the main options will clarify some of their functions. The option '*File handling*,' as the name implies, is for activities like opening files, saving files, entering operator's name and comment lines, and so forth. Through the '*Acquisition*' option the following activities can be performed: acquisition of spectra with the signal channel, deletion of spectra, transferring of spectrum and/or parameters from the active page to another page, and editing and execution of automation routines. The option '*Parameters*' is for setting the

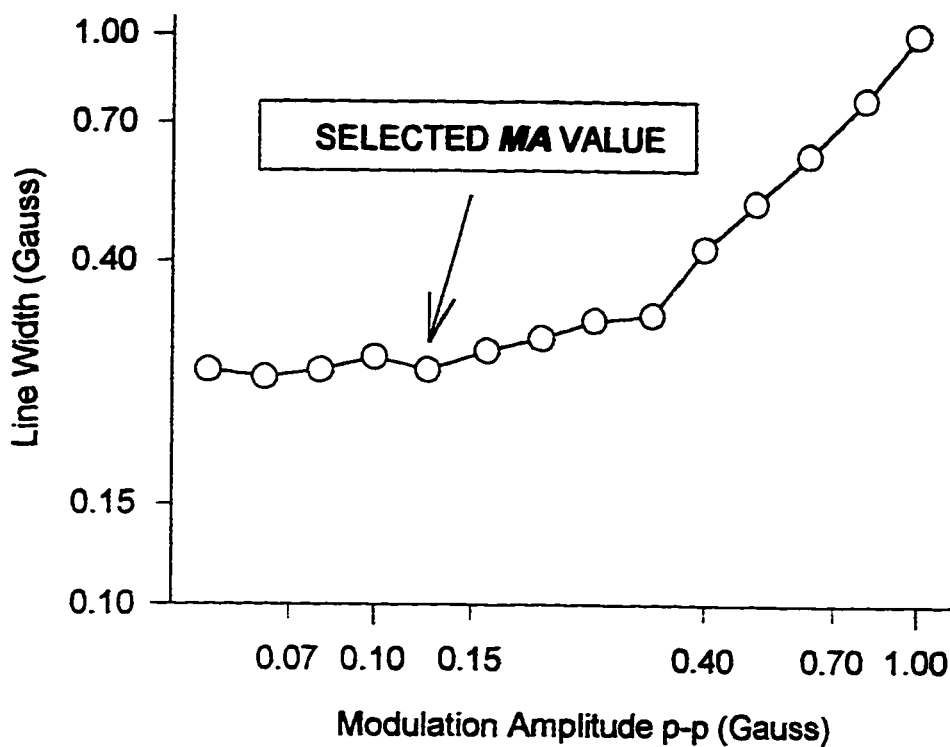


Figure III.8. Observed line width as a function of peak-to-peak modulation amplitude for PD-Tempone in toluene at S-Band. The selected value of modulation amplitude that gave the best compromise between signal intensity and signal distortion was 0.125 Gauss.

parameters of, for example, the field controller, the signal channel, and for downloading and uploading the parameters to and from the instrument.

III.3. Data Analysis

To manipulate the data, files of the resulting spectra were transferred from the Bruker data acquisition system to a PC using the software WIN-EPR which is written by Bruker. Then, using this software the files of the spectra were transformed from binary format to ASCII format. The ASCII format can be read easily by other programs. Computer programs, written in FORTRAN language, were either developed from scratch or modified to assist in the analysis of the results.

III.3.1. Computer Programs

The computer programs, which were used extensively in this study, are described below and are arranged according to the order of their usage. Lists of these programs can be found in Appendix (A) at the end of this dissertation. The accuracy of the first and second programs was checked by performing a sample calculation manually and by using these computer programs. Then, the results were compared, which agreed satisfactorily.

III.3.1.1. LWA.FOR. This program was written to perform linewidth analysis. Given the name of the text file of a three lines , i.e. the three nitroxide

lines corresponding to M_{+1} , M_0 , and M_{-1} , this program will return the linewidths and the peak-to-peak heights for the three lines.

III.3.1.2. EXDEL.FOR. This program calculates the normalized intensities corresponding to quarters of a first derivative EPR single spectrum. This is achieved by first determining the linewidth, which is the difference between the two extrema. The intensities are then calculated at distances from the central field in steps of quarter the linewidth. This was performed to both the positive and negative peaks. The values of intensities at equal distances to the left and right of the central field were averaged and normalized to one. This decay behavior is necessary for the next step.

III.3.1.3. GSUMJH.FOR. This program, which simulates the lineshape of a single Lorentzian peak, was used to determine the isotropic hyperfine coupling constant of deuterium, A_{iso}^D . This was achieved by varying, in the input data file, A_{iso}^D and the intrinsic linewidth. The program returned the theoretical observed linewidth and decay behavior. The results were compared with the experimental linewidth and decay behavior calculated by EXDEL.FOR. This process was iterated until a good match was achieved between experimental and theoretical results. Once a good match was obtained and for a more precise comparison, a theoretical curve was generated and compared graphically with the experimental curve. The computed intensity was normalized

to unity for comparison with the experimentally obtained curve. The mathematical equation used in this program is the same as the equation used in the next program.

III.3.1.4. GSUMDP.FOR. This computer program calculates the Lorentzian half-width -at-half-height (the intrinsic linewidth) using the following equation (Li & Hwang, 1984).

$$Y_j = \sum_{k=-12}^{12} \frac{2D_k}{\sum_{i=-12}^{12} D_i} \cdot \frac{(Q_k \cdot A - H_j)w}{\left[(Q_k \cdot A - H_j)^2 + w^2 \right]^2} \quad [\text{III-5}]$$

where

- H_j is the magnetic field at point j on the simulation;
- Y_j is the intensity at magnetic field H_j ;
- D is the degeneracy;
- Q_k is the quantum number of D_k ;
- w is the intrinsic linewidth;
- A is the isotropic deuteron hyperfine coupling constant.

The first term is a weighting factor which comes from the degeneracy of the twelve equivalent deuterons in PD-Tempone adjacent to the N=O fragment. The rest is a Lorentzian lineshape function. The above Equation sums the intensities of all the twenty five degenerate hyperfine lines and calculates Y_j , the

intensity at magnetic field H_j . Since it is completely symmetrical, only half of the spectrum was simulated. The output of this program is a list of "observed" linewidths and corresponding "intrinsic" linewidths and "peak-to-peak heights." This output is used to generate the input for the next computer program.

III.3.1.5. T22.FOR. The experimental A , B , and C values are obtained using this program. Entered in the input file, along with the generated list from the GSUMDP.FOR, are the experimental linewidth of the sharpest peak and the peak-to-peak heights for all of the three lines corresponding to $M_i = +1, 0$, and -1 . The T22-program interpolates the intrinsic linewidths from the given list. Then the three intrinsic linewidths are fitted to the equation (Hwang et al, 1975)

$$\delta(M) = A + BM + CM^2 \quad \text{[III-6]}$$

where $\delta(M)$ is the intrinsic linewidth corresponding to the spectral index number M . Solving this Equation for $M = +1, 0$, and -1 , one obtains

$$A = \delta(M = 0) \quad \text{[III-7]}$$

$$B = 0.5 \times [\delta(M = +1) - \delta(M = -1)] \quad \text{[III-8]}$$

$$C = 0.5 \times [\delta(M = -1) + \delta(M = +1) - 2 \times \delta(M = 0)] \quad \text{[III-9]}$$

The fractional errors in A , B , and C are also calculated in the computer analysis.

III.3.1.6. BCT1.FOR & ABCI.FOR. These two programs were used to calculate the rotational correlation time τ_R (reorientational correlation times will be referred to as τ_R which is equivalent to τ_C in Section III.1), and the theoretical B and C values. The BCT1.FOR program provides a first look at the behavior of the experimental data. From this program it is possible to find the axes of rotational diffusion (X , Y , or Z), and to limit the range of the anisotropy of molecular reorientation (N) and correlation time τ_R . These information are fed to the ABCI.FOR program along with the microwave frequency and the experimental values of B and C . The ABCI-program then calculates iteratively the correlation times τ_R by matching experimental and theoretical values of either B or C . The narrower the range found with the BCT1-program is, the faster the ABCI-program can find the correlation times τ_R .

The motion narrowing analysis of Freed et al. (Goldman et al, 1972; Goldman et al, 1973; & Hwang et al, 1975) has been adapted. We have also incorporated an experimentally adjustable parameter, β , for a broader range of non-Debye type spectral density. This parameter, suggested by Cole and Davidson, may assume values between zero and one (Davidson & Cole, 1951). Table III.3 gives the magnetic parameters of PD-Tempone in toluene (Hwang et al, 1975) needed for the calculation which was carried out by using Equations [III.10-12] (Li & Hwang, 1985).

$$C_0 = \frac{8}{3} - \frac{1}{\left[1 + (\omega_\alpha \tau_0)^2 \varepsilon'\right]^\beta} - \frac{1}{3\left[1 + (\omega_0 \tau_0)^2 \varepsilon\right]^\beta} \quad \text{[III-10]}$$

**TABLE III.3. Magnetic Parameters of PD-
Tempone in Toluene.[§]**

$$g_e = 2.00232$$

$$g_x = 2.0096 \pm 0.0002$$

$$g_y = 2.0063 \pm 0.0002$$

$$g_z = 2.0022 \pm 0.0001$$

$$A_x = 4.1 \pm 0.5 \text{ G}$$

$$A_y = 6.1 \pm 0.5 \text{ G}$$

$$A_z = 33.4_5 \pm 0.2 \text{ G}$$

[§]From Hwang, *et al.*, 1975.

$$C_2 = \frac{8}{3} - \frac{1}{\left[1 + (\omega_a \tau_2)^2 \varepsilon'\right]^\beta} - \frac{1}{3\left[1 + (\omega_0 \tau_2)^2 \varepsilon\right]^\beta}$$

$$C = \left(\frac{2}{3^{1/2} \gamma}\right) (0.8\pi^2) (D_0^2 \tau_0 C_0 + 2D_2^2 \tau_2 C_2) \quad \text{[III-11]}$$

$$B_0 = \frac{16}{3} + \frac{4}{\left[1 + (\omega_0 \tau_0)^2 \varepsilon\right]^\beta}$$

$$B_2 = \frac{16}{3} + \frac{4}{\left[1 + (\omega_0 \tau_2)^2 \varepsilon\right]^\beta}$$

$$B = \left(\frac{-2}{3^{1/2} \gamma}\right) (0.1\pi\omega_0) (g_0 D_0 \tau_0 B_0 + 2g_2 D_2 \tau_2 B_2) \quad \text{[III-12]}$$

with

$$g_N = (g_x + g_y + g_z)/3$$

$$g_0 = (g_z - g_N)(3/2)^{1/2}$$

$$g_2 = (g_x - g_y)/2$$

$$A_N = (A_x + A_y + A_z)/3$$

$$\gamma = 1.764097 \times 10^7 \text{ rad s}^{-1} \text{ G}^{-1}$$

$$\gamma_P = \gamma g_N / g_e$$

$$D_0 = (A_x - A_N)(|\gamma_P|/2\pi)(3/8)^{1/2} \text{ MHz}$$

$$D_2 = (A_x - A_y)|\gamma_P|/(8\pi) \text{ MHz}$$

$$\tau_0 = \tau_R N^{1/2}$$

$$\tau_2 = 3\tau_0 / (1+2N)$$

$$\omega_0 = 2\pi\nu$$

$$\omega_a = A_N \gamma_P / 2$$

III.4. Results

In this section the results obtained for PD-Tempone in toluene at the different microwave frequency bands, i.e., L-, S-, X-, and Q-Bands will be presented. Then, at the end of this section, a comparison of these results will be cited. The objective is to look at the behavior of the anisotropic interaction parameter κ at the different microwave frequencies for the same system PD-Tempone in toluene.

Once correlation times, τ_R , are calculated (using the ABCI-program) for the system at different temperatures, the anisotropic interaction parameter κ can be calculated. For spherical top or linear molecules, the correlation time τ_R is related to the anisotropic interaction parameter κ as (Kivelson, 1972 and Eq. III-3, rewritten here for convenience)

$$\tau_R = \kappa \left[\frac{4\pi}{3} \frac{r_0^3}{k_B} \left(\frac{\eta}{T} \right) \right] \quad \text{[III-14]}$$

The coefficient of shear viscosity η for the solvent toluene at different temperatures can be calculated using the following equation (Barlow, 1966).

$$\ln \eta = -7.266 + \frac{409.6^\circ \text{K}}{T - 103.1^\circ \text{K}} \quad \text{[III-15]}$$

This equation is valid in the temperature range 288-155 K.

III.4.1. L-Band

The study of PD-Tempone in toluene at L-Band (~1 GHz), with 100-KHz field modulation, was performed over a range of temperatures from 145 to 295 K and selected spectra are shown in Figure III.9.

The results of the linewidth analysis, which was performed by the LWA-program, are given in Table III.4. The first column of this Table contains values of temperature in K. The second, third, and fourth columns contain, respectively, observed linewidths (in Gauss), peak-to-peak heights, and central fields (in Gauss) for $M_I = +1$. The same pattern is repeated for $M_I = 0$ and $M_I = -1$.

The decay behavior, which is an average of three runs, of the second peak at $T = 295.2$ K is given in Table III.5. This calculation was done with the EXDEL-program. The results of the simulation, which were calculated using the GSUMJH-program, are given in the same Table. Clearly, the match between experimental and theoretical values is acceptable which validate the use of an a_D of 0.0205 G. The results of this analysis, for an observed linewidth of 0.3265 ± 0.0001 G, are a deuteron hyperfine coupling constant, a_D , of 0.0205 G and an intrinsic linewidth equals to 0.2820 G. Since a_D varies with temperature (Eaton, et al, 1980), the decay behavior at $T = 165.0$ K was also checked. The results are shown graphically in Figure III.10 where only half of each spectrum is shown. As mentioned earlier the first derivative EPR spectrum is symmetrical

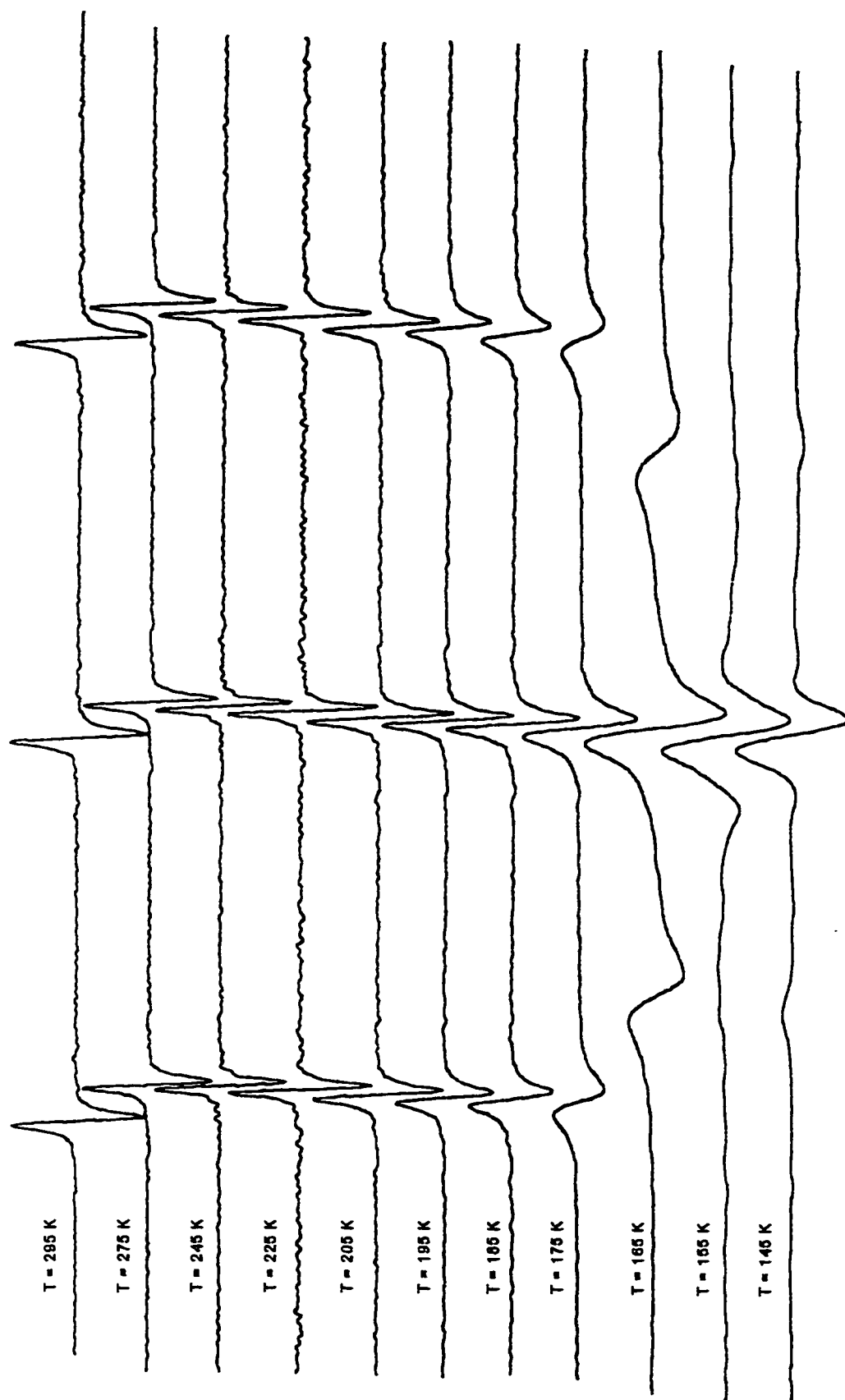


Figure III.9. Selected experimental spectra of PD-Tempone in toluene at L-Band and at different temperatures.

TABLE III.4. Linewidth Analysis of PD-Tempone in Toluene at L-Band.

Temp. (K)	$M_I = +1$				$M_I = 0$				$M_I = -1$			
	OLW (GAUSS)	PTPI	CFLD (GAUSS)	OLW (GAUSS)	PTPI	CFLD (GAUSS)	OLW (GAUSS)	PTPI	CFLD (GAUSS)	OLW (GAUSS)	PTPI	CFLD (GAUSS)
295.2	.3421	.3074E+005	382.6228	.3421	.3173E+005	396.9434	.3421	.3047E+005	411.7528			
275.0	.3422	.4019E+005	382.6716	.3421	.4123E+005	396.9434	.2932	.3994E+005	411.7283			
265.0	.3422	.4432E+005	382.6716	.2933	.4646E+005	396.9190	.3421	.4340E+005	411.7039			
255.0	.2933	.4828E+005	382.6472	.2933	.4984E+005	396.9190	.2933	.4729E+005	411.6795			
245.0	.2933	.5172E+005	382.6472	.2933	.5364E+005	396.8701	.2932	.5077E+005	411.5817			
235.0	.2932	.5427E+005	382.5983	.2933	.5618E+005	396.8212	.2932	.5255E+005	411.5328			
225.0	.2932	.7530E+005	382.4977	.2932	.7749E+005	396.7206	.2932	.7323E+005	411.4322			
215.0	.2933	.8033E+005	382.4489	.2933	.8598E+005	396.6229	.2933	.7654E+005	411.3345			
205.0	.2933	.6965E+005	382.4000	.2933	.7866E+005	396.5740	.3421	.6457E+005	411.2612			
195.0	.3910	.5363E+005	382.3511	.3421	.6623E+005	396.5007	.3910	.4711E+005	411.1878			
185.0	.5376	.3169E+005	382.2778	.4887	.4828E+005	396.3785	.5865	.2651E+005	411.0413			
175.0	.8309	.1864E+005	382.1801	.6354	.3733E+005	396.3051	.9286	.1482E+005	410.9190			
165.0	2.3655	.1634E+005	382.3041	1.5591	.4109E+005	396.3095	2.9033	.1252E+005	410.8525			
165.0	2.2581	.8312E+004	382.3041	1.4516	.2191E+005	396.3094	2.9570	.6330E+004	410.8256			

TABLE III.5. Decay Behavior of PD-Tempone in Toluene at L-Band. The Linewidth , which is Equal to 0.3265 G, is Divided by Four. The Intensities at the Same Quarters from the Center on Both Sides are Averaged. Theoretical Simulation was Carried Out with an α_D of 0.0205 G, and intrinsic width of 0.2820 G.

	Experimental		Theoretical
Multiples of 1/4 from Center	Relative Amplitude	Standard Deviation	Relative Amplitude
0.0	0.0101	0.0093	0.0147
1.0	0.7454	0.0042	0.7592
2.0	0.9943	0.0033	0.9978
3.0	0.8509	0.0050	0.8474
4.0	0.6124	0.0052	0.6081
5.0	0.4114	0.0025	0.4154
6.0	0.2791	0.0001	0.2844
7.0	0.1935	0.0018	0.1989
8.0	0.1342	0.0025	0.1428
9.0	0.0936	0.0011	0.1053
10.0	0.0618	0.0037	0.0795

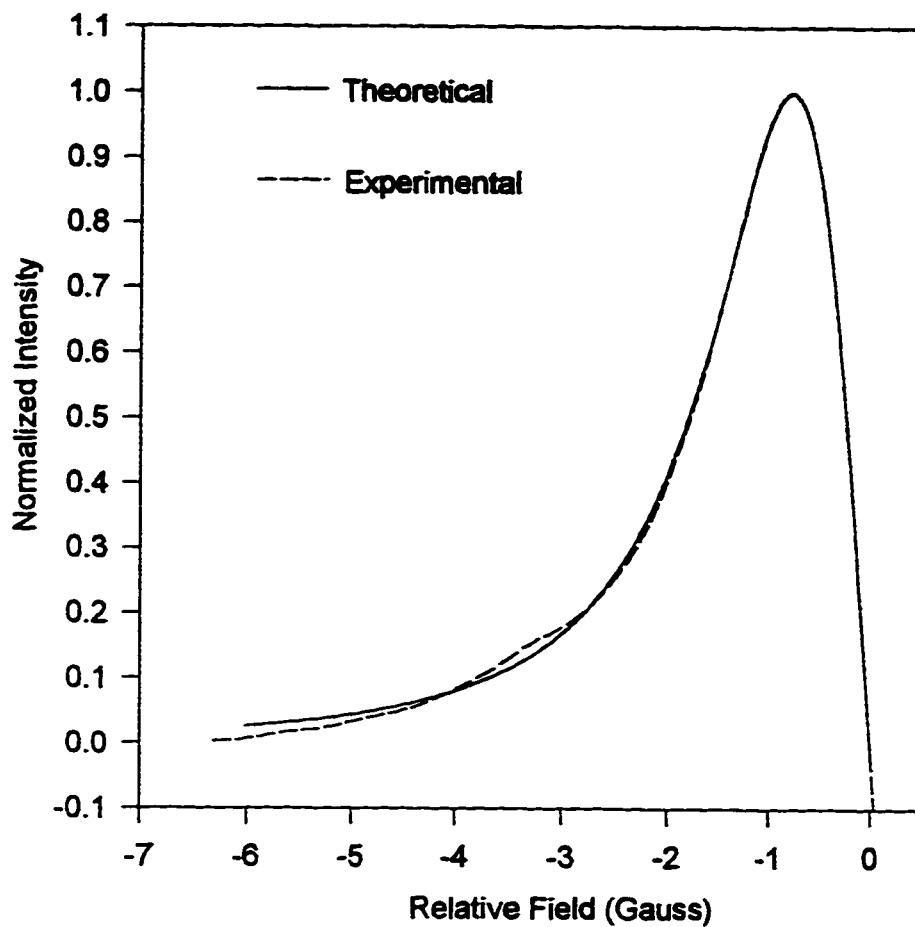


Figure III.10. Lineshape simulation of the central peak ($M_I=0$) of the EPR spectrum of PD-Tempone in toluene at L-Band and at $T = 165$ K. This simulation was carried out with a deuteron hyperfine coupling constant of 0.0750 G and an intrinsic linewidth of 1.422 G. The observed linewidth is 1.553 G.

about the central field. Although the best simulation was obtained with an a_D of 0.0750 G, the difference in the results of B and C due to this variation was small compared with experimental errors. As will be shown later that a_D assumes higher values as the temperature decreases. Hence, the a_D would vary from 0.0205 G to 0.0750 G. But since the effect on the final results is relatively small (as given in Table III.6), an a_D of 0.0205 G was used for all temperatures to generate the intrinsic linewidths by the GSUMDP-program.

The generated list was used in the T22-program to obtain the B and C values which are presented in Table III.6. Based on these experimental C values, the reorientational correlation times τ_R for the spectra at different temperatures, and the corresponding theoretical B and C values were calculated using the BCT1- and the ABCI-programs. The parameters used in these calculations (after experimenting with $z' = X, Y, \text{ or } Z; N = 1 \text{ to } 20; \beta = 0.1 \text{ to } 4.0, \varepsilon = 1 \text{ to } 20; \text{ and } \varepsilon' = 1 \text{ to } 20$) are $z' = Y, N = 1.0, \beta = 0.55, \text{ and } \varepsilon = \varepsilon' = 1.0$. Curves of the experimental and theoretical results of B and C, and of τ_R values versus η/T are shown in Figure III.11. The slope of the τ_R versus (η/T) curve is $0.40 \times 10^{-6} \text{ s.K.P}^{-1}$, which is equal to $\left(\frac{4 \pi r_0^3}{3 k_B} \kappa \right)$, and with r_0 equal to 3.2 Å (Hwang et al, 1975), the value of the anisotropic interaction parameter κ came out to be 0.40 ± 0.11 .

TABLE III.6. Experimental Values of B and C for PD-Tempone in Toluene at L-Band. The Final Six data were Calculated with an a_D of 0.075 G.

TEMP. (K)	M_I	B (Gauss)	C (Gauss)	C/B
295.2	+1	.00072379	.00584652	8.07759
295.2	0	.00074093	.00600277	8.10166
295.2	-1	.00070880	.00585414	8.25919
275.0	+1	.00051188	.00463289	9.05065
275.0	0	.00052215	.00475474	9.10605
275.0	-1	.00043669	.00398623	9.12837
265.0	+1	.00173698	.00938477	5.40291
265.0	0	.00150807	.00818741	5.42906
265.0	-1	.00169048	.00940368	5.56273
255.0	+1	.00145876	.00588471	4.03406
255.0	0	.00147929	.00596841	4.03465
255.0	-1	.00144558	.00583108	4.03374
245.0	+1	.00130480	.00637306	4.88432
245.0	0	.00132617	.00647621	4.88338
245.0	-1	.00129364	.00631914	4.88476
235.0	+1	.00227243	.00708264	3.11677
235.0	0	.00230836	.00719403	3.11651
235.0	-1	.00224041	.00698247	3.11660
225.0	+1	.00196496	.00595669	3.03146
225.0	0	.00199000	.00603237	3.03134
225.0	-1	.00194105	.00588434	3.03153
215.0	+1	.00342364	.01280967	3.74154
215.0	0	.00352824	.01320051	3.74139
215.0	-1	.00335138	.01254156	3.74221
205.0	+1	.00539761	.02200197	4.07624
205.0	0	.00569777	.02321714	4.07478
205.0	-1	.00615470	.02504621	4.06944
195.0	+1	.01271042	.05093598	4.00742
195.0	0	.01216334	.04875404	4.00828
195.0	-1	.01196057	.04788187	4.00331
185.0	+1	.02466008	.12549330	5.08893
185.0	0	.02740350	.13928600	5.08278
185.0	-1	.02472109	.12586910	5.09157
175.0	+1	.05004555	.29266510	5.84797
175.0	0	.05358928	.31323470	5.84510
175.0	-1	.05001011	.29244800	5.84778
165.0	+1	.16812930	1.04072000	6.19000
165.0	0	.17529210	1.08526900	6.19120
165.0	-1	.18068250	1.11899900	6.19318
165.0	+1	.16455510	1.03048200	6.26223
165.0	0	.17110220	1.07221700	6.26653
165.0	-1	.18793340	1.17838300	6.27021
165.0	+1	.16616820	1.03574600	6.23312
165.0	0	.16856050	1.05057600	6.23263
165.0	-1	.17963020	1.11835600	6.22588
165.0	+1	.16229360	1.02564400	6.31969
165.0	0	.16358130	1.03308200	6.31540
165.0	-1	.18692860	1.17829000	6.30342

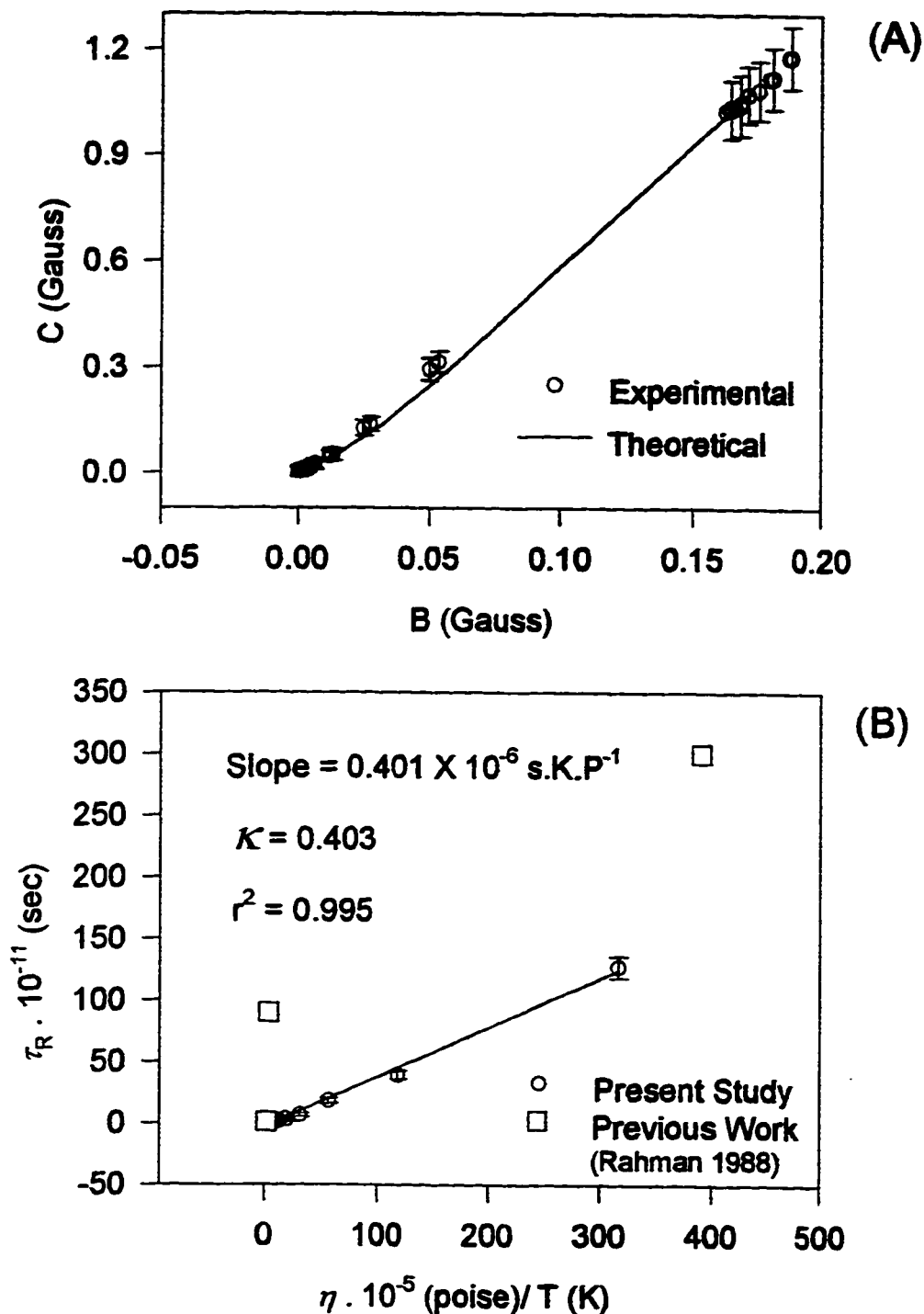


Figure III.11. (A): Experimental and theoretical values of B and C for PD-Tempone in toluene at L-Band with a deuteron hyperfine coupling constant of 0.0205 G. The parameters used were $z^*=Y$, $N=1.0$, $\beta = 0.55$, $\varepsilon = \varepsilon^* = 1.0$. (B): η/T versus reorientational correlation time τ_R for the same system. η is the calculated coefficient of shear viscosity at different toluene temperatures.

III.4.2. S-Band

Figure III.12 shows representative spectra of PD-Tempone in toluene at S-Band (~4 GHz), with 100-KHz field modulation, which was studied over a range of temperatures from 107 to 295 K. The results of the linewidth analysis, which was performed by the LWA-program, are given in Table III.7.

Lineshape simulations of half of the second peak ($M_l = 0$) for the spectra at the two temperatures 295.0 and 161.2 K are shown in Figures III.13 and III.14, respectively. Both simulations were performed with a deuteron hyperfine coupling constant, a_D , of 0.0205 G. At $T = 295.0$ K the observed linewidth was 0.409 G, which corresponded to an intrinsic linewidth of 0.372 G, while at $T = 161.1$ K both observed and intrinsic linewidths were equal to 2.79 G. These two Figures show an acceptable match between experimental and theoretical results, which support the a_D of 0.0205 G. The simulations were calculated using the GSUMJH-program. An a_D of 0.0205 G was used for all temperatures to generate the intrinsic linewidths by the GSUMDP-program.

The generated list was, then, used in the T22-program to obtain the B and C values which are presented in Table III.8. Based on the experimental C values, the reorientational correlation times τ_R for the spectra at different temperatures, and the corresponding theoretical B and C values were calculated using the BCT1- and the ABCI-programs. The parameters used in these calculations (after experimenting with $z' = X, Y, \text{ or } Z; N = 1 \text{ to } 20; \beta = 0.1 \text{ to } 4.0, \varepsilon = 1 \text{ to } 20; \text{ and } \varepsilon' = 1 \text{ to } 20$) are $z' = Y, N = 1.0, \beta = 1.0, \text{ and } \varepsilon = \varepsilon' = 1.0$. Curves of

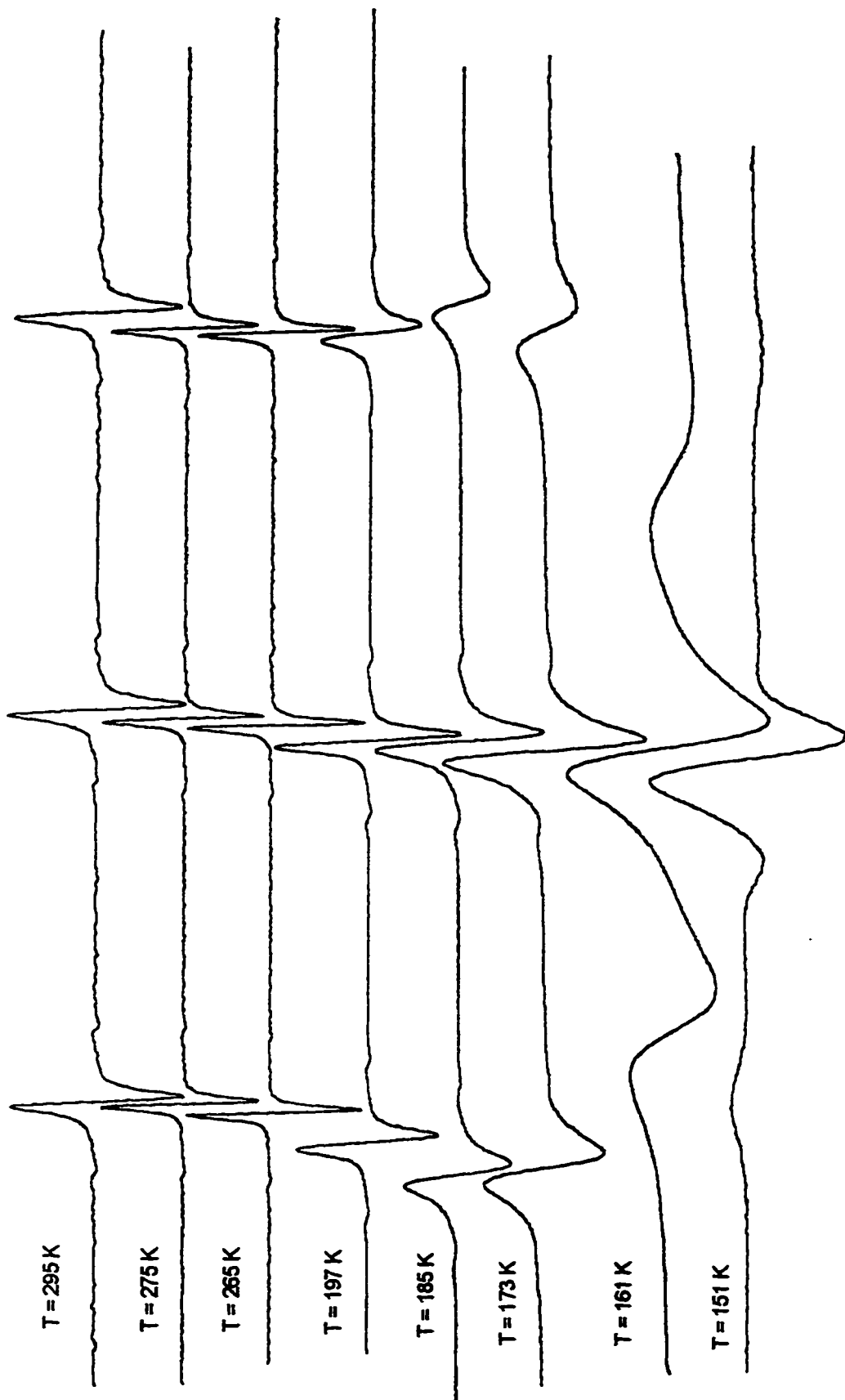


Figure III.12. Selected experimental spectra of PD-Tempone in toluene at S-Band and at different temperatures.

TABLE III.7. Linewidth Analysis of PD-Tempone in Toluene at S-Band.

TEMP. (K)	$M_I = +1$				$M_I = 0$				$M_I = -1$			
	OLW (GAUSS)	PTPI	CFLD (GAUSS)	OLW (GAUSS)	PTPI	CFLD (GAUSS)	OLW (GAUSS)	PTPI	CFLD (GAUSS)	OLW (GAUSS)	PTPI	CFLD (GAUSS)
295.0	.3910	.1100E+005	1400.1023	.3910	.1132E+005	1414.5696	.4399	.1063E+005	1429.2079			
295.0	.2933	.6323E+005	1396.4591	.2932	.6513E+005	1410.9263	.2932	.6052E+005	1425.5402			
275.0	.2932	.3705E+005	1396.7523	.2444	.3812E+005	1411.1951	.2933	.3473E+005	1425.7846			
265.0	.2444	.4176E+005	1395.6037	.2444	.4209E+005	1410.0221	.2933	.3700E+005	1424.6116			
197.2	.5619	.3433E+005	1405.2794	.5150	.4499E+005	1419.5838	.6087	.2442E+005	1434.0990			
185.4	.7492	.1323E+005	1405.1389	.6556	.2073E+005	1419.4199	.9365	.7059E+004	1433.8883			
172.6	1.1237	.5860E+004	1405.1389	.8896	.9944E+004	1419.3965	1.5920	.2850E+004	1433.8414			
161.2	4.1642	.5606E+004	1406.2552	2.7566	.1334E+005	1420.2141	6.9795	.2737E+004	1434.4077			
150.6	*****	.1587E+004	1382.5115	3.9101	.1610E+005	1420.7324	*****	.1030E+004	1461.2994			
150.6	*****	.7198E+003	1382.7070	4.0078	.7618E+004	1420.4880	*****	.4648E+003	1460.4685			
138.8	7.5269	.3439E+004	1394.2906	4.6921	.2596E+005	1420.8302	*****	.2121E+004	1460.5662			
124.2	*****	.3783E+004	1397.8096	5.2786	.2693E+005	1420.4391	*****	.1985E+004	1460.8595			
107.4	*****	.3824E+004	1398.1029	5.4741	.2736E+005	1420.8302	*****	.2120E+004	1460.7617			

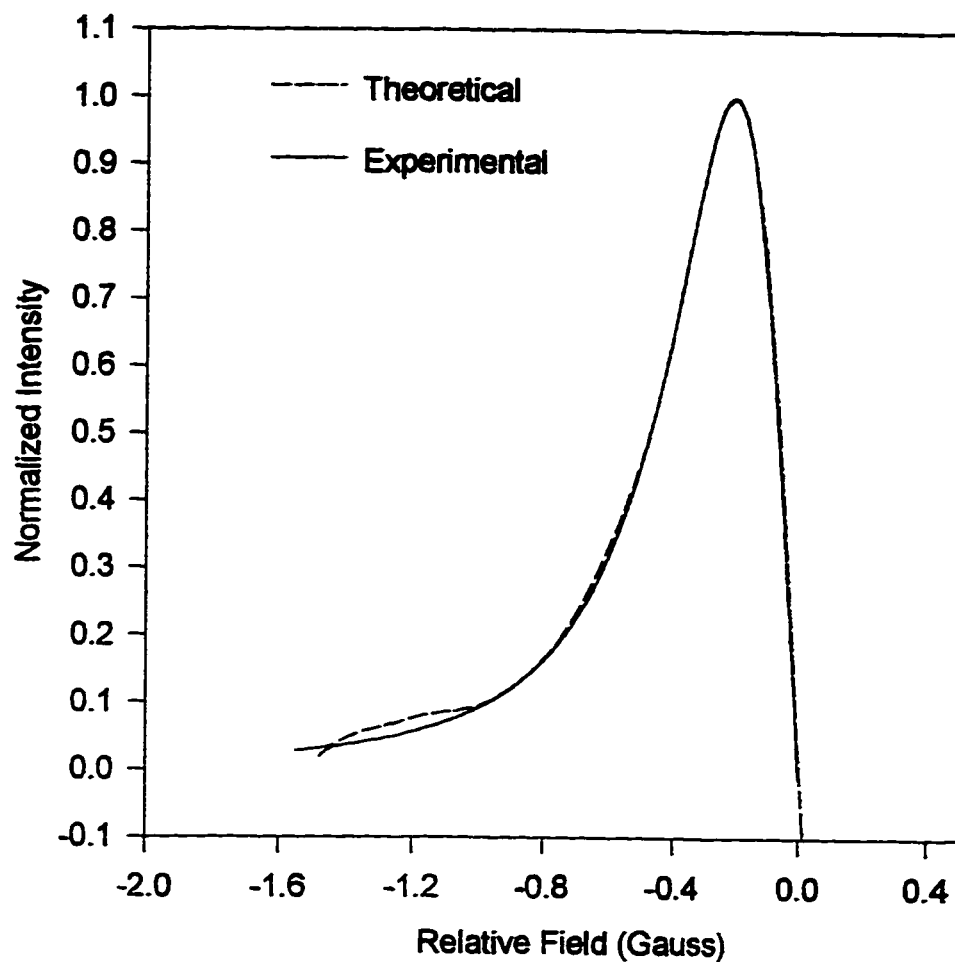


Figure III.13. Lineshape simulation of the central peak ($M_I=0$) of half of the EPR spectrum of PD-Tempone in toluene at S-Band and at $T = 295$ K. This simulation was carried out with a deuteron hyperfine coupling constant of 0.0205 G and an intrinsic linewidth of 0.372 G. The observed linewidth is 0.409 G.

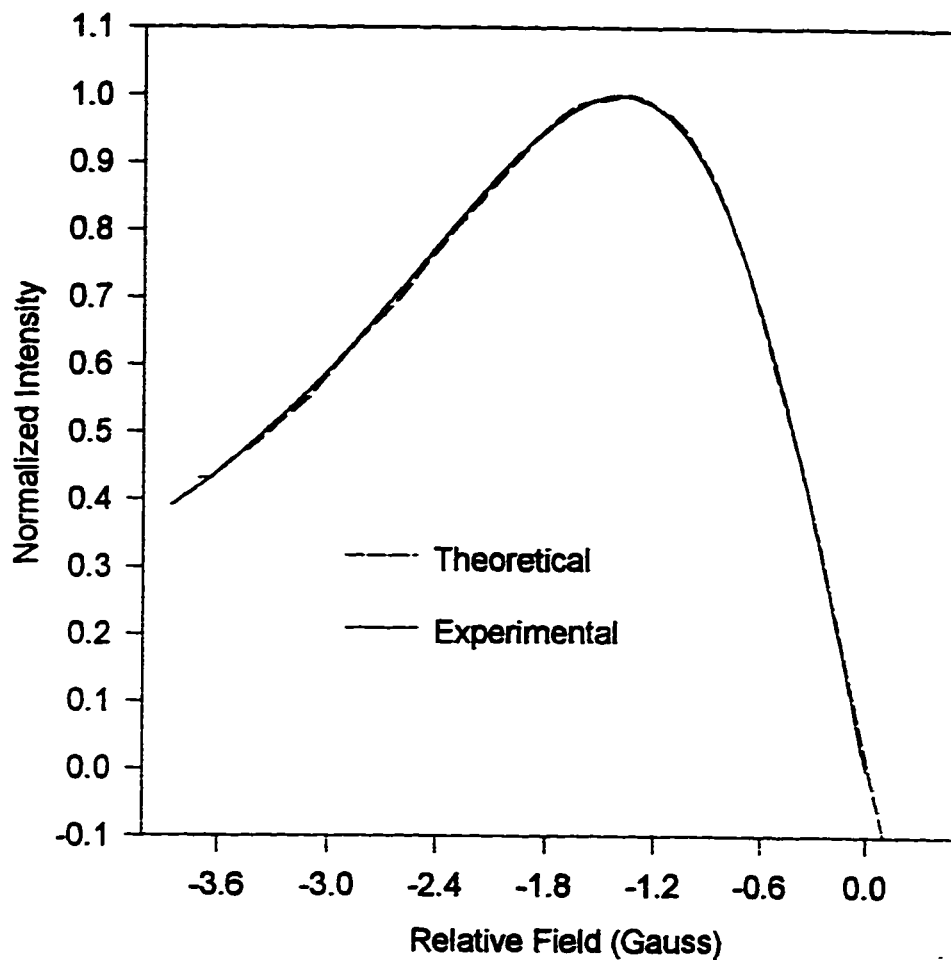


Figure III.14. Lineshape simulation of the central peak ($M_I=0$) of half of the EPR spectrum of PD-Tempone in toluene at S-Band and at $T = 161.2$ K. This simulation was carried out with a deuteron hyperfine coupling constant of 0.0205 G and an intrinsic linewidth of 2.79 G. The observed linewidth is also 2.79 G.

TABLE III.8. Experimental Values of B and C for PD-Tempone in Toluene at S-Band.

TEMP. (K)	M_r	B (Gauss)	C (Gauss)	C/B
295.0	+1	.00328043	.00869730	2.65127
295.0	0	.00332549	.00881925	2.65201
295.0	-1	.00365132	.00967157	2.64879
295.0	+1	.00309975	.00722242	2.33000
295.0	0	.00313970	.00731483	2.32978
295.0	-1	.00303945	.00708234	2.33014
275.0	+1	.00459535	.00855972	1.86269
275.0	0	.00381213	.00710510	1.86382
275.0	-1	.00446820	.00832316	1.86275
265.0	+1	.00713541	.00803853	1.12657
265.0	0	.00715915	.00806517	1.12655
265.0	-1	.00826019	.00930484	1.12647
197.2	+1	.05125120	.12141600	2.36904
197.2	0	.05343306	.12649940	2.36744
197.2	-1	.04717864	.11179740	2.36966
185.4	+1	.13663570	.28627650	2.09518
185.4	0	.14873170	.31150960	2.09444
185.4	-1	.12566970	.26343490	2.09625
172.6	+1	.24242260	.50256810	2.07311
172.6	0	.24888970	.51586560	2.07267
172.6	-1	.24053820	.49854190	2.07261
161.2	+1	.02080870	1.48460900	71.34559
161.2	0	-.06298375	1.43049100	-22.71206

the experimental and theoretical results of B and C, and of τ_R values versus η/T are shown in Figure III.15. The slope of the τ_R versus (η/T) curve is 0.44×10^{-6} s.K.P⁻¹ and the value of the anisotropic interaction parameter κ came out to be 0.44 ± 0.14 .

III.4.3. X-Band

The study of PD-Tempone in toluene at X-Band (~9.5 GHz), with 100-KHz field modulation, was conducted over a range of temperatures from 104 to 295 K and representative spectra are shown in Figure III.16. The results of the linewidth analysis, which was performed by the LWA-program, are given in Table III.9.

Table III.10 gives the decay behavior, which is an average of three runs, of the first peak ($M_i = +1$) at T = 295.0 K. This calculation was done with the EXDEL-program. The results of the simulation, which were calculated using the GSUMJH-program, are given in the same Table. Clearly, the match between experimental and theoretical values is acceptable which validate the use of an a_D of 0.0205 G. The results of this analysis, for an observed linewidth of 0.3015 ± 0.0050 G, are a deuteron hyperfine coupling constant, a_D , of 0.0205 G and an intrinsic linewidth equals to 0.2540 G. Based on what was learned from the results of the L- and S-Bands, the difference in the values of B and C due to the variation in a_D with temperature was small compared with experimental errors.

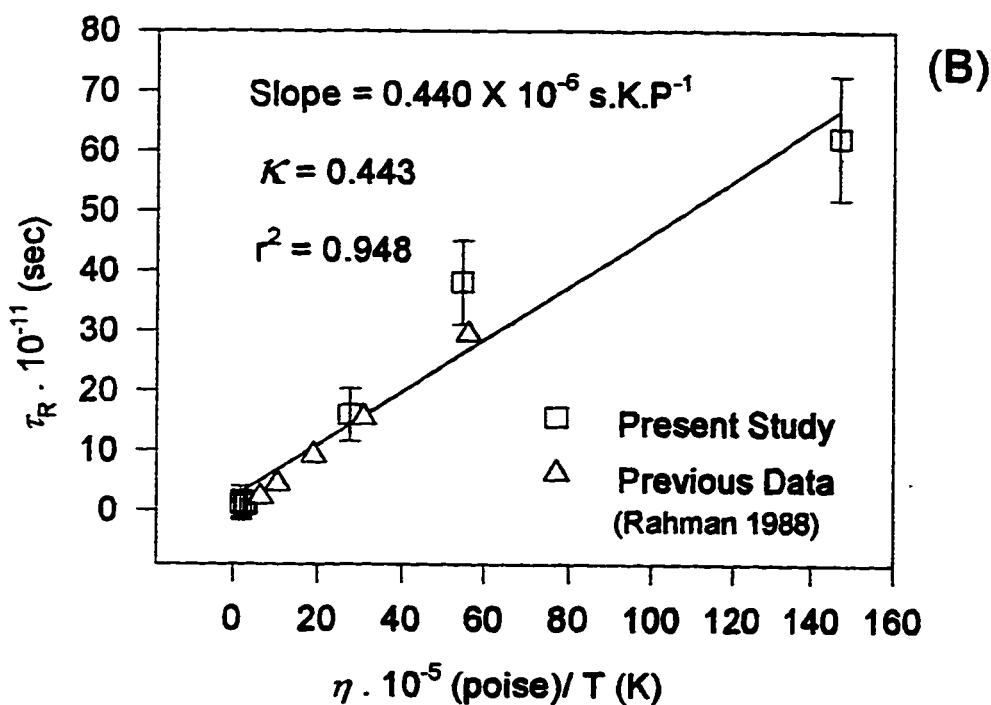
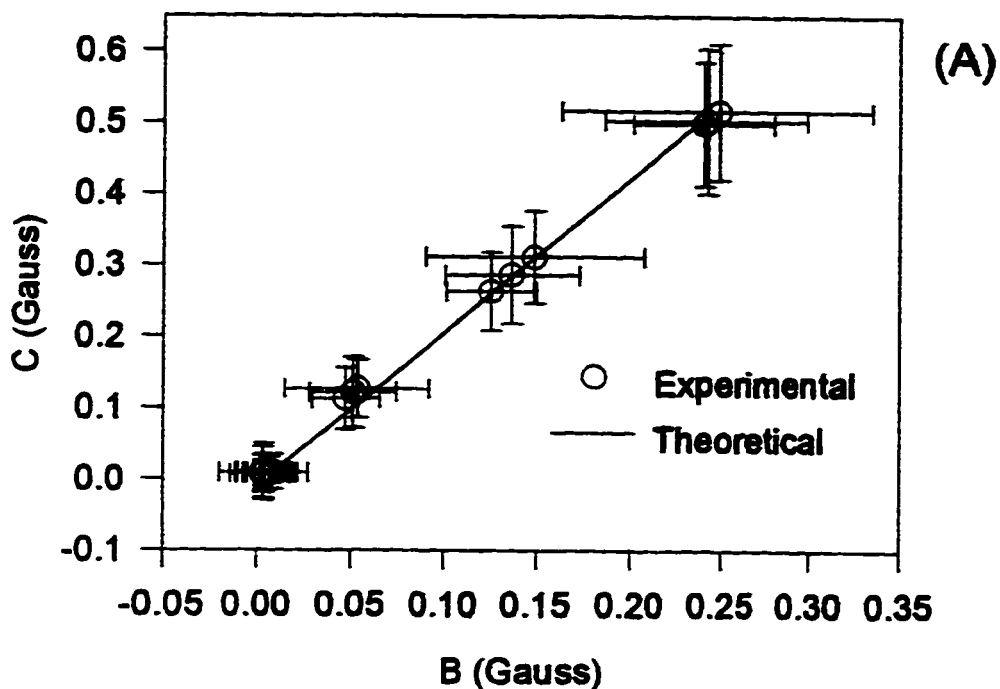


Figure III.15.. (A): Experimental and theoretical values of B and C for PD-Tempone in toluene at S-Band with a deuteron hyperfine coupling constant of 0.0205 G. The parameters used were $z=Y$, $N=1.0$, $\beta = 1.0$, $\epsilon = \epsilon' = 1.0$. (B): η/T versus reorientational correlation time τ_R for the same system. η is the calculated coefficient of shear viscosity at different toluene temperatures.

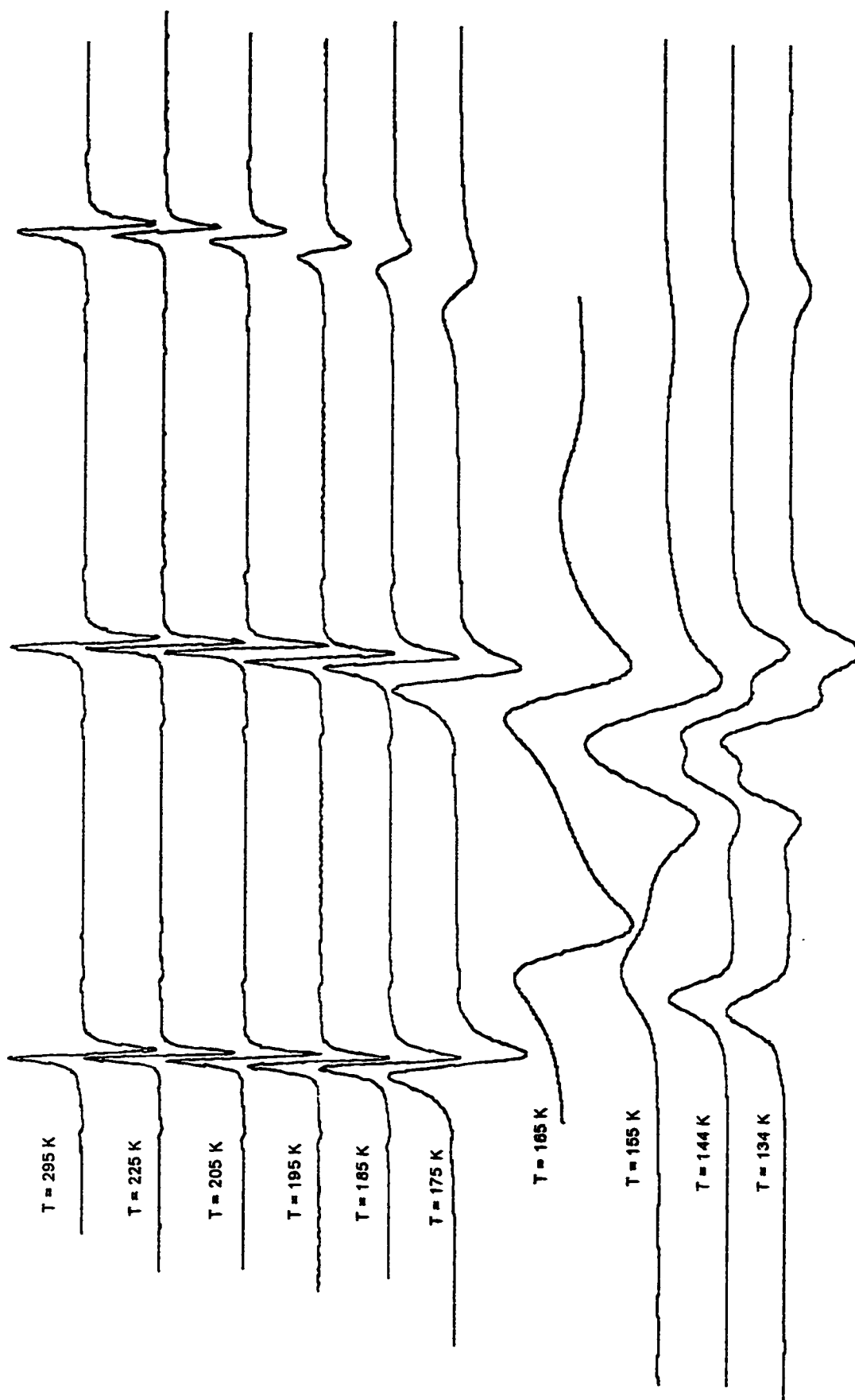


Figure III.16. Selected experimental spectra of PD-Tempone in toluene at X-Band and at different temperatures.

TABLE III.9. Linewidth Analysis of PD-Tempone in Toluene at X-Band.

TEMP. (K)	$M_I = +1$				$M_I = 0$				$M_I = -1$			
	OLW (GAUSS)	PTPI	CFLD (GAUSS)	OLW (GAUSS)	PTPI	CFLD (GAUSS)	OLW (GAUSS)	PTPI	CFLD (GAUSS)	OLW (GAUSS)	PTPI	CFLD (GAUSS)
295.1	.3284	.2402E+005	3383.2997	.2874	.2399E+005	3397.8129	.3284	.2232E+005	3412.4082			
295.0	.3285	.2399E+005	3383.2587	.3284	.2402E+005	3397.7513	.3284	.2236E+005	3412.3261			
275.0	.2737	.2958E+005	3380.4766	.2737	.2955E+005	3394.9829	.3421	.2601E+005	3409.5235			
265.0	.2737	.3496E+005	3380.5450	.2737	.3464E+005	3394.9829	.2737	.3000E+005	3409.5577			
255.0	.2737	.4015E+005	3380.6134	.2737	.3867E+005	3395.0514	.2737	.3252E+005	3409.6261			
255.0	.2737	.8030E+005	3380.6134	.2737	.7742E+005	3395.0514	.2737	.6533E+005	3409.6261			
245.0	.2737	.4433E+005	3380.7503	.2737	.4431E+005	3395.1882	.2737	.3613E+005	3409.6946			
245.0	.2737	.8774E+005	3380.7503	.2737	.8772E+005	3395.1882	.2737	.7188E+005	3409.6946			
235.0	.2737	.1504E+006	3380.8187	.2737	.1568E+006	3395.2566	.3421	.1301E+006	3409.7288			
225.0	.2737	.9540E+005	3381.0924	.2053	.1009E+006	3395.4961	.2737	.6864E+005	3409.9683			
215.0	.2052	.9180E+005	3381.1950	.2737	.9944E+005	3395.5988	.2737	.5718E+005	3410.0367			
205.0	.2737	.1645E+006	3381.2977	.2737	.1730E+006	3395.6672	.3422	.8026E+005	3410.1393			
195.0	.2737	.6148E+005	3381.3661	.3422	.6503E+005	3395.7698	.4790	.2217E+005	3410.2077			
185.0	.4106	.3144E+005	3381.4345	.4106	.2997E+005	3395.8040	.8896	.7617E+004	3410.2077			
175.0	.8895	.9292E+004	3381.6056	.9579	.8644E+004	3395.9409	1.7107	.2162E+004	3410.2762			
165.0	3.0108	.1949E+005	3381.6398	3.0107	.2081E+005	3395.9409	6.8426	.3477E+004	3409.4208			

TABLE III.10. Decay Behavior of PD-Tempone in Toluene at X-Band. The Linewidth, which is Equal to 0.3015 G, is Divided by Four. The Intensities at the Same Quarters from the Center on Both Sides are Averaged. Theoretical Simulation was Carried Out with an a_D of 0.0205 G, and intrinsic width of 0.2540 G.

	Experimental		Theoretical
Multiples of 1/4 from Center	Relative Amplitude	Standard Deviation	Relative Amplitude
0.0	0.0125	0.0216	0.0163
1.0	0.7384	0.0082	0.7598
2.0	0.9935	0.0012	0.9972
3.0	0.8539	0.0110	0.8429
4.0	0.6095	0.0147	0.5998
5.0	0.4089	0.0123	0.4059
6.0	0.2735	0.0109	0.2757
7.0	0.1890	0.0078	0.1917
8.0	0.1336	0.0063	0.1370
9.0	0.0991	0.0047	0.1006
10.0	0.0747	0.0040	0.0757

Hence, an a_0 of 0.0205 G was used for all temperatures to generate the intrinsic linewidths by the GSUMDP-program.

The generated list was used in the T22-program to obtain the B and C values which are presented in Table III.11. Based on these experimental C values, the reorientational correlation times τ_R for the spectra at different temperatures, and the corresponding theoretical B and C values were calculated using the BCT1- and the ABCI-programs. The parameters used in these calculations (after experimenting with $z' = X, Y, \text{ or } Z; N = 1 \text{ to } 20; \beta = 0.1 \text{ to } 4.0, \varepsilon = 1 \text{ to } 20; \text{ and } \varepsilon' = 1 \text{ to } 20$) are $z' = Y, N = 1.5, \beta = 1.0, \text{ and } \varepsilon = \varepsilon' = 1.0$. Curves of the experimental and theoretical results of B and C, and of τ_R values versus η/T are shown in Figure III.17. The slope of the τ_R versus (η/T) curve is 0.44×10^{-6} s.K.P⁻¹ and the value of the anisotropic interaction parameter κ came out to be 0.44 ± 0.05 .

III.4.4. Q-Band

The spectra of PD-Tempone in toluene at Q-Band (~34 GHz), with 12.5-KHz field modulation, were taken over a range of temperatures from 109 to 295 K and representative spectra are shown in Figure III.18. The results of the linewidth analysis, which was performed by the LWA-program, are given in Table III.12.

The decay behavior, which is an average of three runs, of the second peak ($M_l = 0$) at T = 295.0 K is given in Table III.13. This calculation was done

TABLE III.11. Experimental Values of B and C for PD-Tempone in Toluene at X-Band.

TEMP (K)	M_T	B(Gauss)	C(Gauss)	C/B
295.1	+1	.00594418	.00574614	.96668
295.1	0	.00511196	.00494105	.96657
295.1	-1	.00571039	.00551948	.96657
295.0	+1	.00569893	.00589700	1.03475
295.0	0	.00569995	.00589798	1.03474
295.0	-1	.00547764	.00566956	1.03504
275.0	+1	.00860293	.00847119	.98469
275.0	0	.00859922	.00846742	.98467
275.0	-1	.01032497	.01016672	.98467
265.0	+1	.01028984	.00909180	.88357
265.0	0	.01024830	.00905474	.88354
265.0	-1	.00963138	.00850894	.88346
255.0	+1	.01435725	.00943176	.65693
255.0	0	.01412371	.00927727	.65686
255.0	-1	.01310728	.00860708	.65666
255.0	+1	.01404011	.00925119	.65891
255.0	0	.01381849	.00910410	.65883
255.0	-1	.01284295	.00845774	.65855
245.0	+1	.01391361	.01385500	.99579
245.0	0	.01391082	.01385222	.99579
245.0	-1	.01273658	.01268270	.99577
245.0	+1	.01354697	.01351737	.99782
245.0	0	.01354563	.01351604	.99782
245.0	-1	.01242895	.01240183	.99782
235.0	+1	.00973368	.01510577	1.55191
235.0	0	.00991237	.01538210	1.55181
235.0	-1	.01159601	.01798256	1.55075
225.0	+1	.02303021	.03023364	1.31278
225.0	0	.01701975	.02238730	1.31537
225.0	-1	.01997678	.02624699	1.31388
215.0	+1	.02464515	.03210208	1.30257
215.0	0	.03547290	.04605392	1.29828
215.0	-1	.02790002	.03629246	1.30080
205.0	+1	.05496204	.06144480	1.11795
205.0	0	.05622340	.06284892	1.11784
205.0	-1	.05073716	.05674217	1.11836
195.0	+1	.08410054	.09131478	1.08578
195.0	0	.11088080	.12026800	1.08466
195.0	-1	.09519368	.10330850	1.08525
185.0	+1	.20324920	.19355350	.95230
185.0	0	.19859430	.18912290	.95231
185.0	-1	.22576720	.21502590	.95242
175.0	+1	.47254290	.44002940	.93119
175.0	0	.49146720	.45767170	.93124
175.0	-1	.44243910	.41198460	.93117

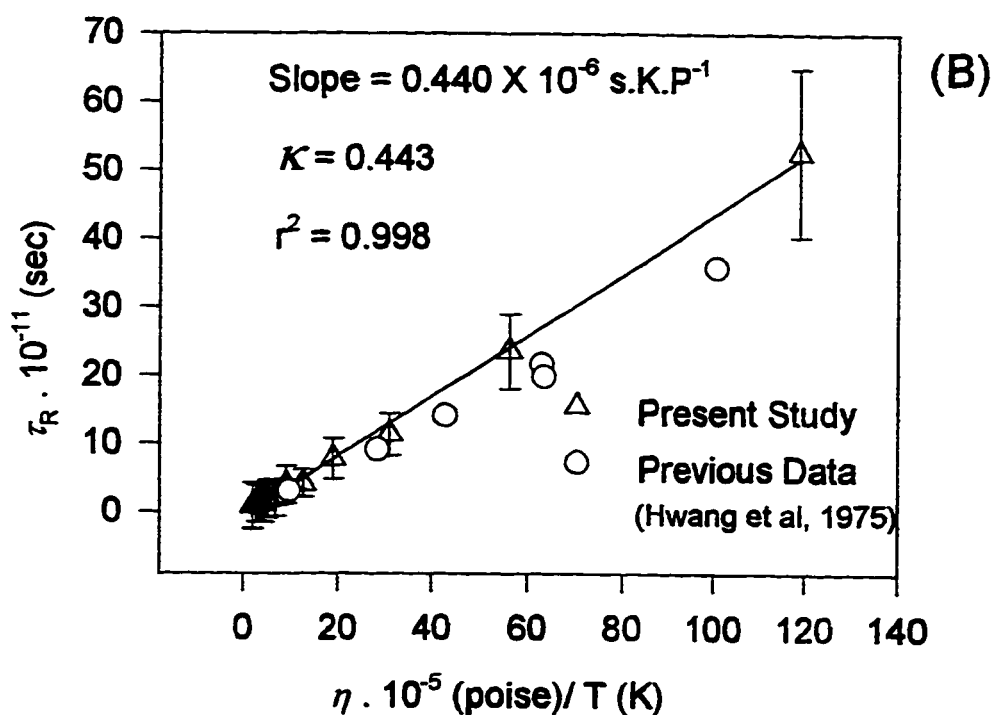
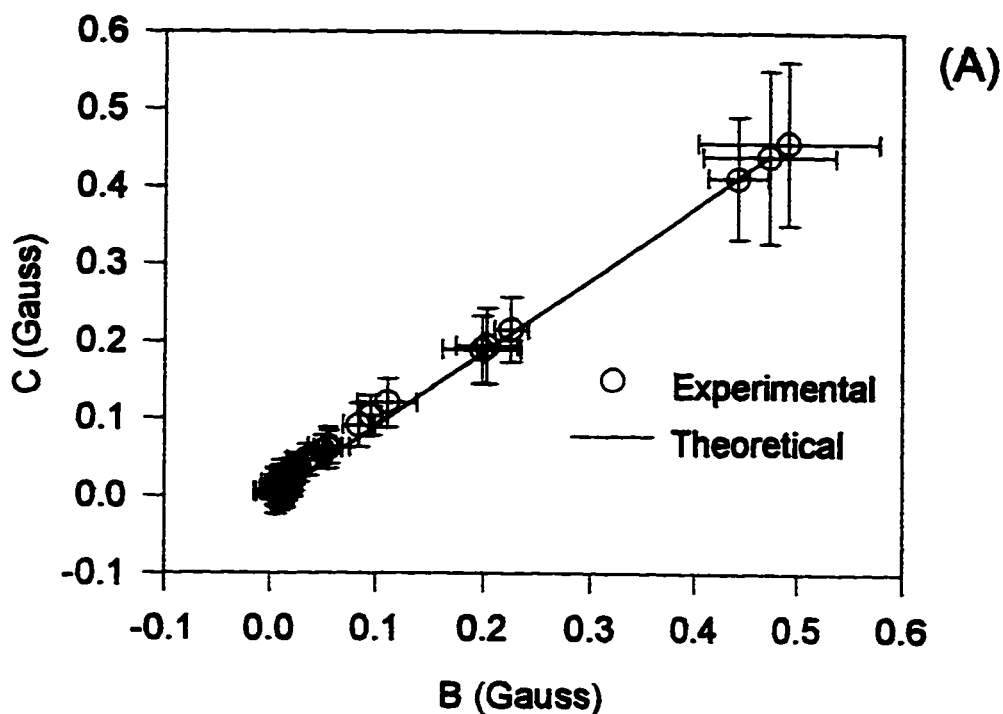


Figure III.17. (A): Experimental and theoretical values of B and C for PD-Tempone in toluene at X-Band with a deuteron hyperfine coupling constant of 0.0205 G. The parameters used were $z'=Y$, $N=1.5$, $\beta = 1.0$, $\epsilon = \epsilon' = 1.0$. (B): η/T versus reorientational correlation time τ_R for the same system. η is the calculated coefficient of shear viscosity at different toluene temperatures.

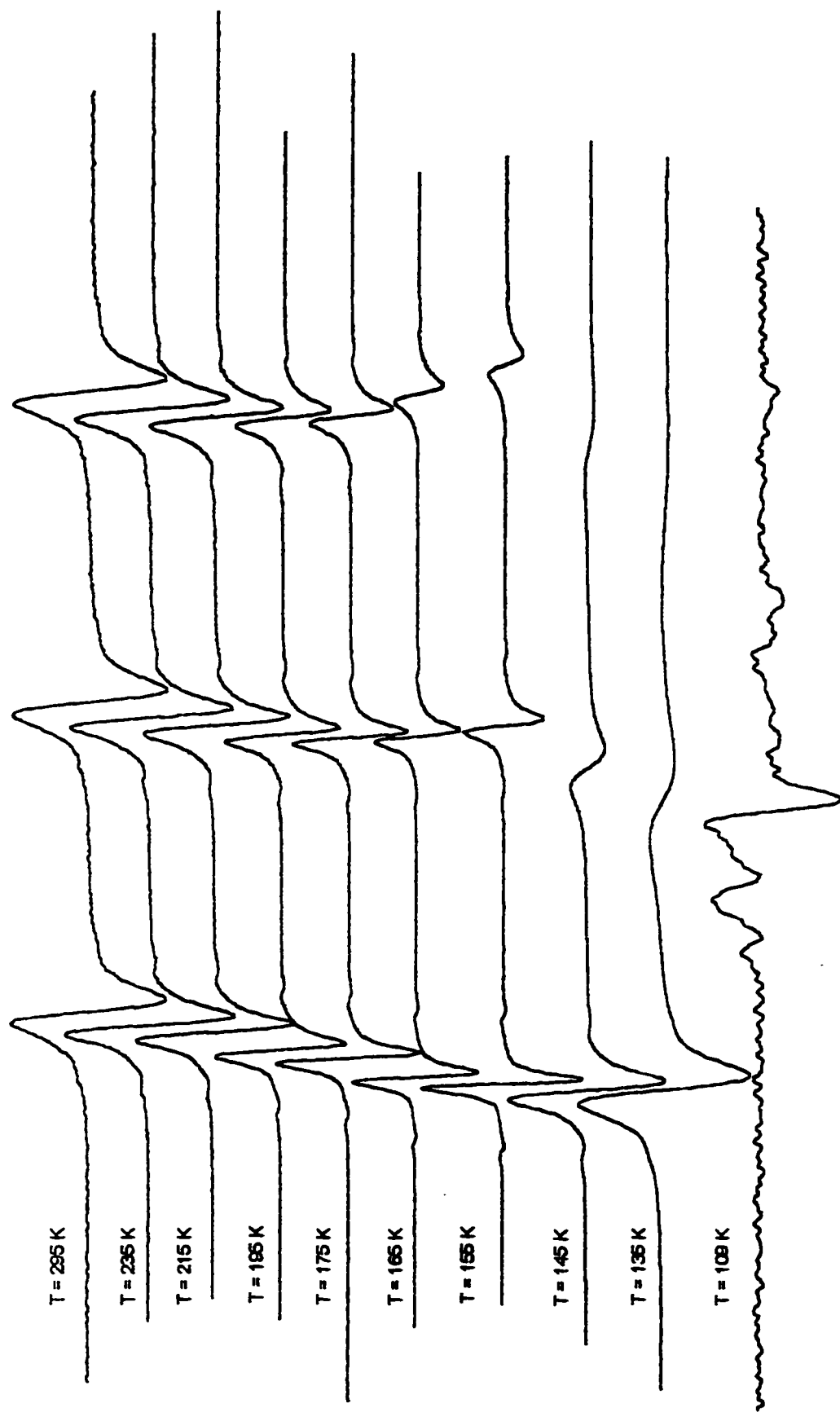


Figure III.18. Selected experimental spectra of PD-Tempone in toluene at Q-Band and at different temperatures.

TABLE III.12. The Linewidth Analysis of PD-Tempone in Toluene at Q-Band.

TEMP. (K)	$M_I = +1$				$M_I = 0$				$M_I = -1$			
	OLW (GAUSS)	PTPI	CFLD (GAUSS)	OLW (GAUSS)	PTPI	CFLD (GAUSS)	OLW (GAUSS)	PTPI	CFLD (GAUSS)	OLW (GAUSS)	PTPI	CFLD (GAUSS)
295.0	1.1292	.9348E+004	12232.1930	1.1887	.9297E+004	12246.7839	1.2481	.9168E+004	12261.4341			
275.0	1.1292	.1078E+005	12231.4204	1.0698	.1056E+005	12246.0112	1.1887	.1038E+005	12260.6318			
265.0	1.0103	.1177E+005	12231.5393	1.0698	.1140E+005	12246.0706	1.1293	.1113E+005	12260.6615			
255.0	1.0104	.1361E+005	12230.8846	1.0698	.1325E+005	12245.4160	1.1292	.1263E+005	12259.9473			
245.0	.9509	.1515E+005	12230.3200	.9509	.1448E+005	12244.8811	1.0103	.1391E+005	12259.4125			
235.0	.9510	.1682E+005	12229.6662	.8915	.1618E+005	12244.1976	1.0104	.1532E+005	12258.7587			
225.0	.8915	.1932E+005	12229.3988	.8915	.1826E+005	12243.9599	.9509	.1712E+005	12258.4913			
215.0	.7726	.2351E+005	12228.2695	.8320	.2181E+005	12242.8009	.8915	.1981E+005	12257.3323			
205.0	.7726	.2506E+005	12227.6752	.7727	.2282E+005	12242.1769	.8321	.2028E+005	12256.7083			
195.0	.6538	.3904E+005	12228.0912	.6538	.3430E+005	12242.6523	.7726	.2880E+005	12257.2134			
185.0	.5943	.4461E+005	12228.0021	.6538	.3852E+005	12242.4740	.7132	.3113E+005	12257.0054			
175.0	.5349	.2908E+005	12227.6318	.5944	.2319E+005	12242.1037	.6538	.1684E+005	12256.5756			
235.0	.8914	.8716E+004	12229.3553	.9509	.8200E+004	12243.8867	.9509	.7588E+004	12258.4478			
225.0	.8321	.8486E+004	12229.9794	.9509	.7985E+004	12244.5405	.9509	.7270E+004	12259.1016			
215.0	.8320	.9128E+004	12231.1275	.8915	.8473E+004	12245.5995	.9509	.7540E+004	12260.1903			
205.0	.7726	.1248E+005	12230.9195	.7726	.1130E+005	12245.4806	.8321	.9744E+004	12260.0714			
195.0	.6538	.1726E+005	12231.2761	.7131	.1514E+005	12245.8075	.7727	.1241E+005	12260.3983			
185.0	.6538	.2114E+005	12231.1572	.6538	.1792E+005	12245.7183	.7726	.1400E+005	12260.2794			
175.0	.4754	.3019E+005	12231.3058	.5943	.2303E+005	12245.8669	.7132	.1559E+005	12260.4280			
165.0	.4754	.3781E+005	12231.4841	.5943	.2538E+005	12245.9858	.7132	.1475E+005	12260.5468			
155.0	.4160	.3657E+005	12231.2761	.5943	.1826E+005	12245.6886	.8915	.7917E+004	12260.2200			
145.0	.8915	.1604E+005	12230.6818	1.7235	.3456E+004	12245.0646	3.2093	.9090E+003	12259.4771			

TABLE III.13. Decay Behavior of PD-Tempone in Toluene at Q-Band. The Linewidth, which is Equal to 1.1730 G, is Divided by Four. The Intensities at the Same Quarters from the Center on Both Sides are Averaged. Theoretical Simulation was Carried Out with an a_D of 0.0205 G, and intrinsic width of 1.160 G.

	Experimental		Theoretical
Multiples of 1/4 from Center	Relative Amplitude	Standard Deviation	Relative Amplitude
0.0	0.0012	0.0011	0.0036
1.0	0.7535	0.0032	0.7596
2.0	0.9973	0.0007	1.0000
3.0	0.8749	0.0049	0.8677
4.0	0.6666	0.0058	0.6480
5.0	0.4809	0.0076	0.4621
6.0	0.3342	0.0064	0.3284
7.0	0.2322	0.0056	0.2366
8.0	0.1781	0.0063	0.1739
9.0	0.1423	0.0047	0.1304
10.0	0.1299	0.0040	0.0998

with the EXDEL-program. The results of the simulation, which were calculated using the GSUMJH-program, are given in the same Table. Clearly, the match between experimental and theoretical values is acceptable which validate the use of an a_D of 0.0205 G. The results of this analysis, for an observed linewidth of 1.1730 ± 0.0092 G, are a deuteron hyperfine coupling constant, a_D , of 0.0205 G and an intrinsic linewidth equals to 1.1600 G. As was mentioned in the section for the X-Band, the difference in the values of B and C due to the variation in a_D with temperature would be small compared with experimental errors. Hence, an a_D of 0.0205 G was used for all temperatures to generate the intrinsic linewidths by the GSUMDP-program.

The generated list was used in the T22-program to obtain the B and C values which are presented in Table III.14. Based on these experimental C values, the reorientational correlation times τ_R for the spectra at different temperatures, and the corresponding theoretical B and C values were calculated using the BCT1- and the ABCI-programs. The parameters used in these calculations (after experimenting with $z' = X, Y, \text{ or } Z; N = 1 \text{ to } 20; \beta = 0.1 \text{ to } 4.0, \varepsilon = 1 \text{ to } 20; \text{ and } \varepsilon' = 1 \text{ to } 20$) are $z' = Y, N = 2.0, \beta = 1.0, \text{ and } \varepsilon = \varepsilon' = 1.0$. Curves of the experimental and theoretical results of B and C, and of τ_R values versus η/T are shown in Figure III.19. The slope of the τ_R versus (η/T) curve is 0.44×10^{-6} s.K.P⁻¹ and the value of the anisotropic interaction parameter κ came out to be 0.44 ± 0.04 . The axes for the τ_R versus (η/T) curve are in the common logarithmic scale. This is because, unlike in the L-, S-, and X-Bands, the data

TABLE III.14. Experimental Values of B and C for PD-Tempone in Toluene at Q-Band.

TEMP. (K)	M_r	B (Gauss)	C (Gauss)	C/B
295.0	+1	.00548875	.00241840	.44061
295.0	0	.00576806	.00252628	.43798
295.0	-1	.00597465	.00260079	.43530
275.0	+1	.01072276	-.00092065	-.08586
275.0	0	.01005197	-.00086534	-.08609
275.0	-1	.01108491	-.00095487	-.08614
265.0	+1	.01423562	-.00191760	-.13470
265.0	0	.01484746	-.00202340	-.13628
265.0	-1	.01549405	-.00209385	-.13514
255.0	+1	.01911920	.00557345	.29151
255.0	0	.01998842	.00580013	.29017
255.0	-1	.02061206	.00600821	.29149
245.0	+1	.02060503	-.00100631	-.04884
245.0	0	.02014965	-.00098717	-.04899
245.0	-1	.02100149	-.00102910	-.04900
235.0	+1	.03174293	.00433451	.13655
235.0	0	.03287634	.00447318	.13606
235.0	-1	.03165314	.00431320	.13626
225.0	+1	.03316078	.00767490	.23145
225.0	0	.03683418	.00851041	.23105
225.0	-1	.03517574	.00815117	.23173
215.0	+1	.04136491	.01005530	.24309
215.0	0	.04276460	.01038980	.24295
215.0	-1	.04308987	.01049048	.24346
205.0	+1	.05038998	.01141927	.22662
205.0	0	.04797724	.01086339	.22643
205.0	-1	.04809570	.01088428	.22630
195.0	+1	.05785576	.01409534	.24363
195.0	0	.05926913	.01447129	.24416
195.0	-1	.05831951	.01425517	.24443
185.0	+1	.07378447	.01814514	.24592
185.0	0	.06806040	.01675200	.24613
185.0	-1	.07145590	.01756406	.24580
175.0	+1	.09065585	.02332439	.25728
175.0	0	.10017110	.02582687	.25783
175.0	-1	.09972565	.02567197	.25743
165.0	+1	.13884650	.03649290	.26283
165.0	0	.14420400	.03795071	.26317
165.0	-1	.13333730	.03497380	.26230
155.0	+1	.22941030	.06239477	.27198
155.0	0	.23782420	.06479342	.27244
155.0	-1	.23841550	.06497049	.27251
145.0	+1	1.40997800	.39134010	.27755
145.0	0	1.27713200	.35403760	.27721
145.0	-1	1.22324300	.33899640	.27713

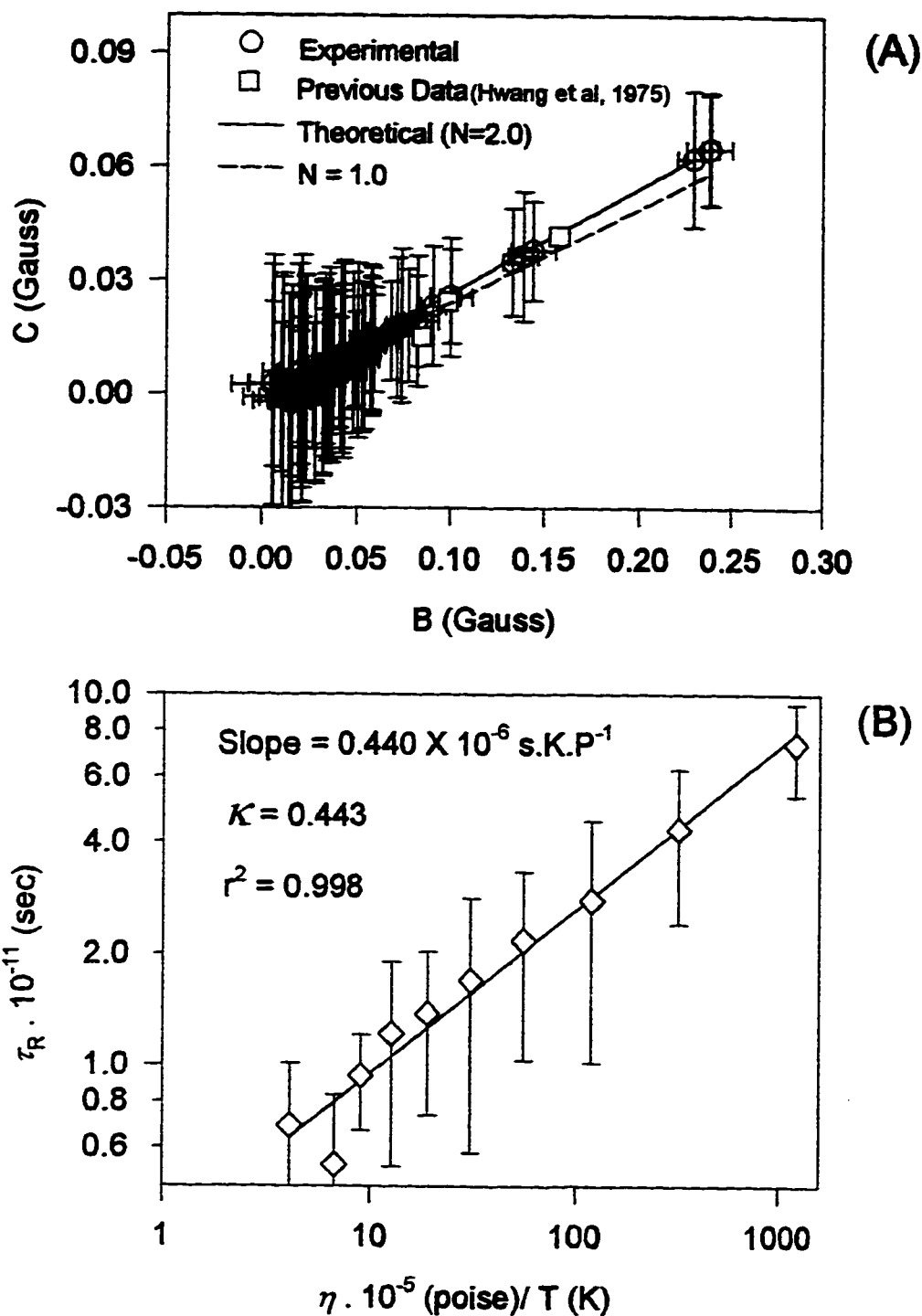


Figure III.19.. (A): Experimental and theoretical values of B and C for PD-Tempone in toluene at Q-Band with a deuteron hyperfine coupling constant of 0.0205 G. The parameters used were $z'=Y$, $N=2.0$, $\beta = 1.0$, $\varepsilon = \varepsilon' = 1.0$. B and C values generated by $N=1.0$ are also shown for comparison. (B): η/T versus reorientational correlation time τ_R for the same system, where η is the coefficient of shear viscosity for toluene.

points in the rapid rotational region contribute significantly to the nonsecular terms, i.e., $\omega^2 \cdot \tau_R^2 > 1$. For these points to have more weight in determining the slope of the curve a logarithmic scale was adapted. If a linear scale was selected, only the points in the slow rotational region would dominate the calculation of the slope of the curve. The slope in the latter case is 0.0047×10^{-6} s.K.P⁻¹ and the value of the anisotropic interaction parameter κ would be 0.0048.

III.4.5. The Parameter β

The parameter β which was introduced to the spectral density function by Cole and Davidson (Davidson & Cole, 1951) proved to be useful in the calculation of B and C coefficients. The experimental values of B and C for the L-Band were fit theoretically, when β equals to 1.0, with the parameters $z' = X$ and $N = 4.0$. $z' = X$ is physically not plausible since for all other bands z' equals Y, i.e. best fit of experimental B and C values was obtained when z' was set equal to Y. The experimental values of B and C were well below the theoretical values when $z' = Y$ was used for fitting (Fig. III.20-A). On the contrary, for the other three bands best fits of experimental values were obtained with this setting (Fig. III.20-B,C,&D). The "best fit" N values for the S-, X-, and Q-Bands were, respectively, 1.0, 1.5, and 2.0. These observations are presented graphically in Figure III.20 for values of N ranging from 1.0 to 6.0.

Setting β equal to 0.5, on the other hand, made possible the fitting of the experimental values of B and C for the L-Band with $z' = Y$ and N close to 1.0,

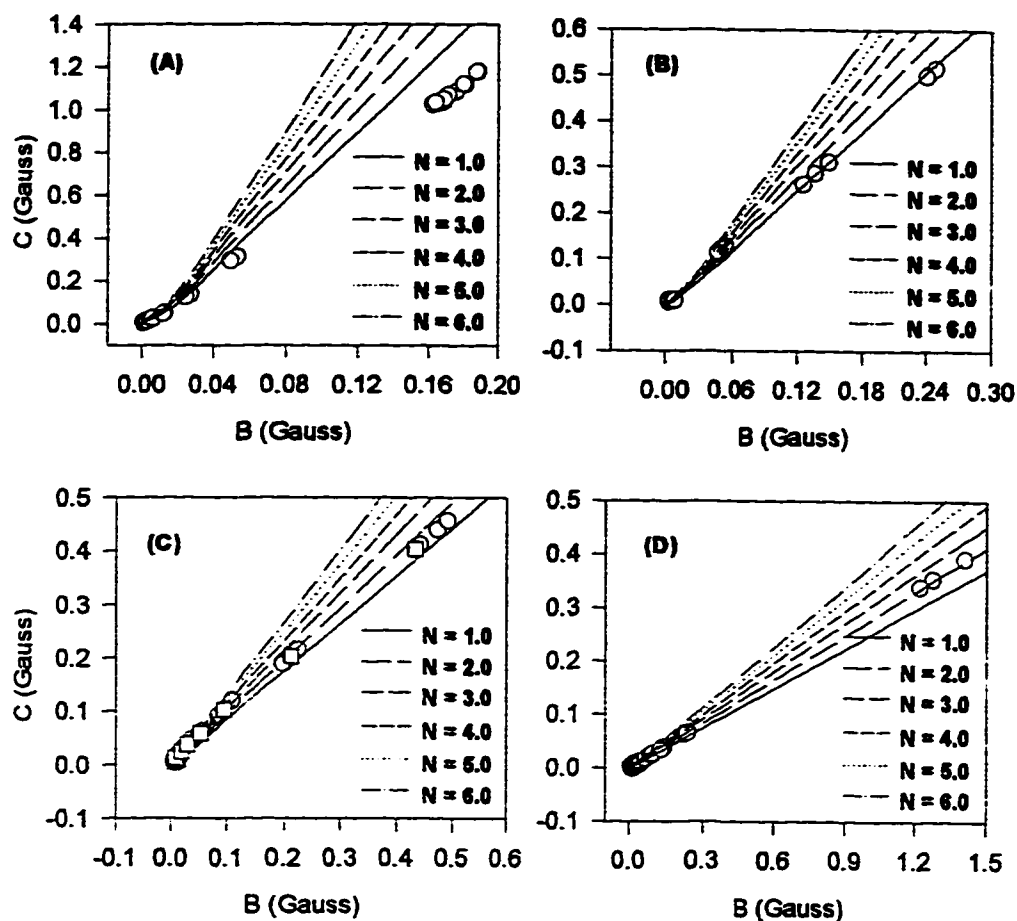


Figure III.20.. Experimental values of B versus C for PD-Tempone in toluene determined from the four bands with z' set equal to Y, β equal to 1.0 and N values ranging from 1.0 to 6.0. (A) L-Band; (B) S-Band; (C) X-Band; (D) Q-Band. Experimental values of B and C for the L-Band lay well below the theoretical curves. Setting z' equal to X gave a better fit in this case for the L-Band.

which are the theoretically conceivable results. However, the N values for the S-, X-, and Q-Bands would be higher than one. Figure III.21 shows plots of B versus C for the four bands with $z' = Y$, $\beta = 0.5$, and $N = 1.0$ to 6.0 . Best fits are shown in Figure III.22, where for the L-Band $\beta = 0.55$, and for the other three bands $\beta = 1.0$, and in all z' was set equal to Y . The N values, as can be seen from the figure, are 1.0, 1.0, 1.5, and 2.0 for the L-, S-, X-, and Q-Bands, respectively. The effects of these variations on the values of τ_R were minimal.

III.5. Discussion

A summary of the results obtained for PD-Tempone in toluene at the four microwave bands L, S, X, and Q is given in Table III.15. Molecules of PD-Tempone in toluene at the four bands align under the applied magnetic field such that the molecular Y axis corresponds to the z' axis in the laboratory frame, which is taken to be the direction of the applied magnetic field. This is also in accordance with the previous work on the same system (Hwang et al., 1975; Rahman, 1988).

Values of the anisotropic rotational reorientation N are close to one. N is the ratio of $R_{||}/R_{\perp}$, where $R_{||}$ is the rotational diffusion constant along the longer molecular axis and R_{\perp} is the rotational diffusion constant perpendicular to the longer molecular axis (Goldman et al, 1972; Goldman et al, 1973; & Hwang et al, 1975). In PD-Tempone, $R_{||} = R_x$ and $R_{\perp} = R_y = R_z$. The shape of PD-Tempone

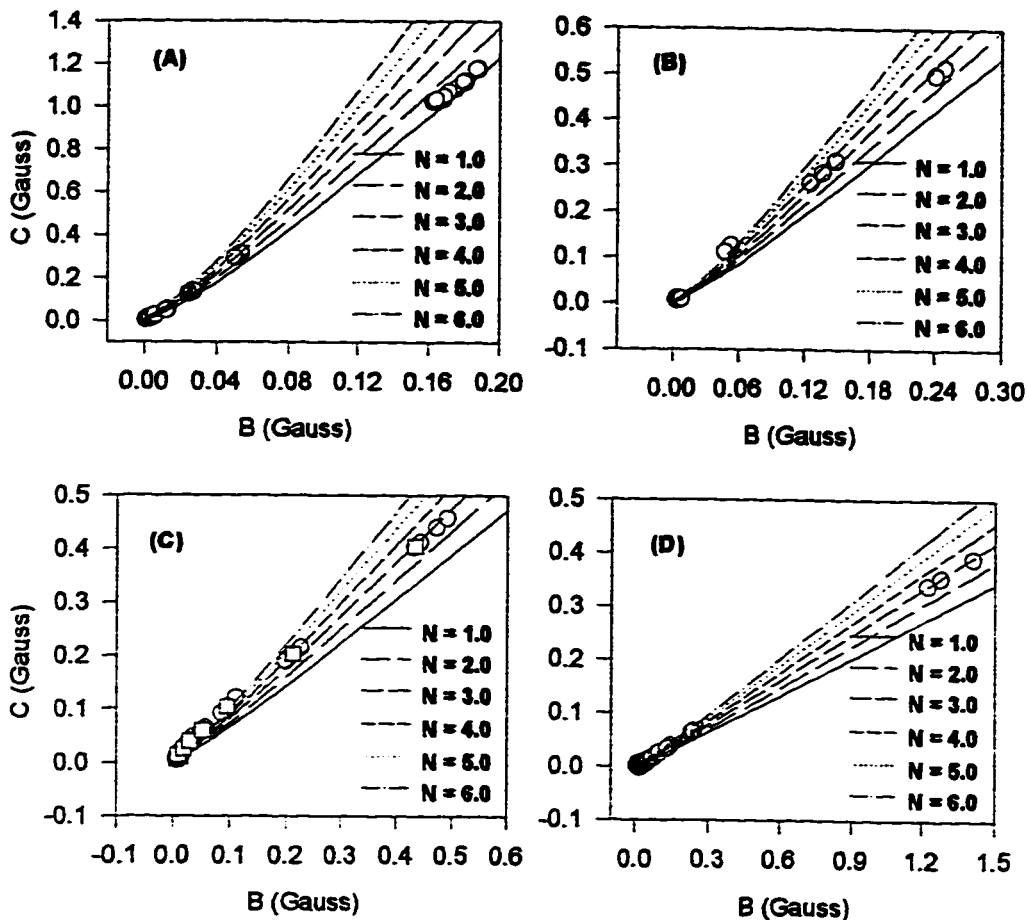


Figure III.21. Experimental values of B versus C for PD-Tempone in toluene determined from the four bands with z' set equal to Y, β equal to 0.5 and N values ranging from 1.0 to 6.0. (A) L-Band; (B) S-Band; (C) X-Band; (D) Q-Band. Experimental values of B and C for the S-, X-, and Q-Bands assume higher values of N (>1) for best fits.

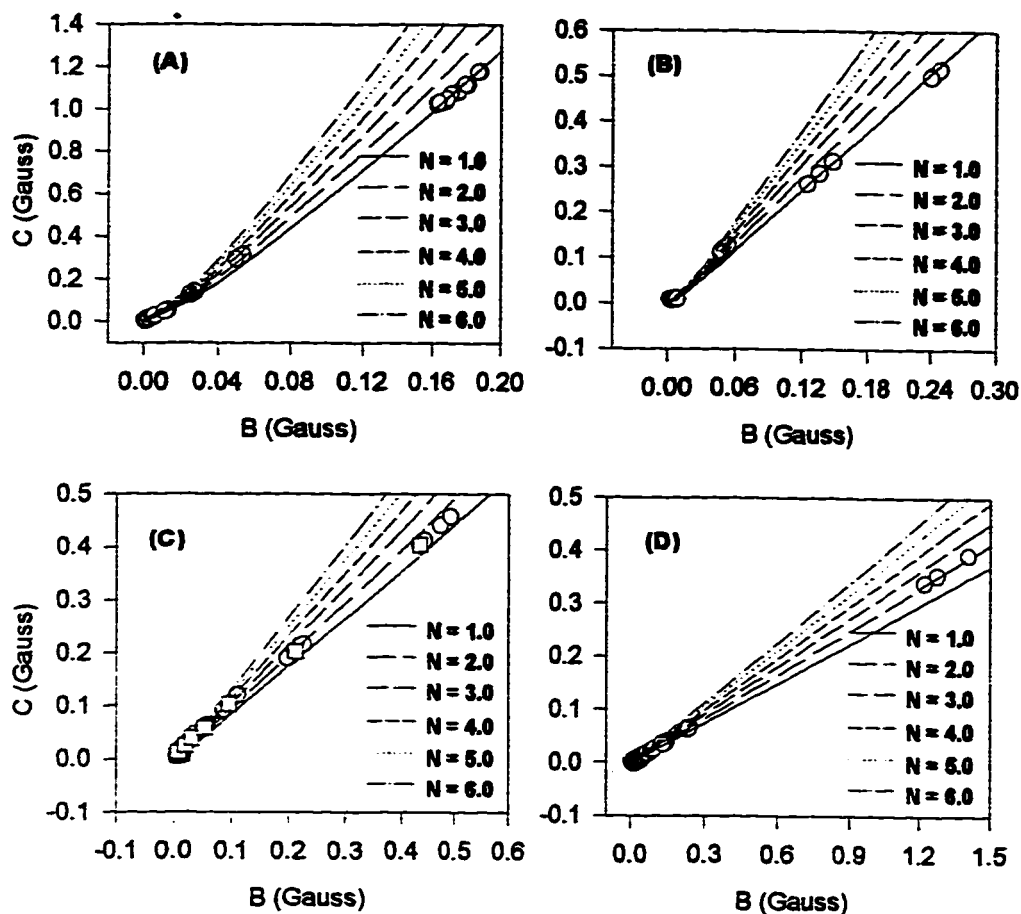


Figure III.22.. Experimental values of B versus C for PD-Tempone in toluene determined from the four bands with z' set equal to Y and N values ranging from 1.0 to 6.0. (A) L-Band with $\beta = 0.55$, and $N = 1.0$ gave best fit; (B) S-Band with $\beta = 1.0$, and $N = 1.0$ gave best fit; (C) X-Band with $\beta = 1.0$, and $N = 1.5$ gave best fit; (D) Q-Band with $\beta = 1.0$, and $N = 2.0$ gave best fit.

TABLE III.15. Summary of the Results for PD-Tempone in Toluene at the Four Microwave Bands: L, S, X, and Q.

Band	z'	N	β	Present Study κ	Previous Work κ
L	Y	1.0 ± 0.5	0.55 ± 0.05	0.40 ± 0.11	0.747^\dagger
S	Y	1.0 ± 0.5	1.0	0.44 ± 0.14	0.552^\dagger
X	Y	1.5 ± 0.5	1.0	0.44 ± 0.05	0.405^\ddagger
Q	Y	2.0 ± 0.5	1.0	0.44 ± 0.04	0.266^\ddagger

[†] Rahman, 1988.

[‡] Hwang et al., 1975.

is nearly a prolate axially symmetric ellipsoid with $a_{\parallel} = a_x = 4.2 \text{ \AA}$ and $a_{\perp} \cong 2.85 \text{ \AA}$ (Hwang et al., 1975), which gives an r_g of 3.2 \AA . At $\sim 1 \text{ GHz}$ and $\sim 4 \text{ GHz}$, PD-Tempone undergoes isotropic rotational diffusion, whereas at $\sim 9.5 \text{ GHz}$ and $\sim 35 \text{ GHz}$ its rotational diffusion becomes slightly anisotropic. The slow tumbling region started at a lower temperature in the Q-Band than in the other three bands. This suggests that the strength of the applied magnetic field has a clear effect on the molecular motion of PD-Tempone, and consequently on the anisotropy of the rotational diffusion represented by the N values.

Values of the anisotropic interaction parameter κ determined in this study for PD-Tempone in toluene were similar at the four microwave bands. This similarity is predicted by theory for linear or spherical molecules undergoing isotropic molecular motion (McClung & Kivelson, 1968). Values of the anisotropy of molecular reorientation (N) which are close to one indicates isotropic molecular motions.

To unify the results for the alignment of PD-Tempone in toluene, the anisotropic rotational reorientation N , and for the anisotropic interaction parameter κ determined at the four microwave bands, a β value of 0.55 was used at L-Band so that $z' = Y$. The Cole-Davidson parameter can assume values in the range $0 < \beta \leq 1$, where the Debye-type spectral densities are recovered by setting β equal to 1 (Davidson & Cole, 1951). A β value of less

than one indicates the existence of multiple intermolecular motions, or equivalently a broader distribution of relaxation times associated with different types of motions (Davidson & Cole, 1951; Davidson, 1961; Beckmann, 1988). At least there are two types of correlation times: the correlation time for angular momentum which is a characteristic time for "free rotations" of the molecules in the liquid, and the correlation time for molecular reorientation (McClung & Kivelson, 1968). Most probably, the distinction between these types of motions becomes clear in the L-Band range for PD-Tempone in toluene, which necessitated setting β equal to < 1 .

The value of the anisotropic interaction parameter κ determined for PD-Tempone in toluene at the Q-Band depended significantly on whether the scale of the axes used for plotting τ_R versus (η/T) is logarithmic or linear. Axes with a logarithmic scale gave a κ value which is similar to the values obtained at the other microwave bands. In this case, the slope of the line is determined mainly by data points at temperatures close to room temperature, whereas the effect of data points at relatively lower temperatures will predominate when the slope is obtained using axes with a linear scale. The κ values obtained using axes with logarithmic and linear scales (0.44 and 0.0048, respectively) show that at high temperatures (close to room temperature) the coupling between the spin probe and the solvent is higher than at lower temperatures. At low temperatures, the solvent becomes viscous while the spin probe is precessing at high rates, due to

the high magnetic fields applied at Q-Band, resulting in a weak coupling of the rotational motion of the spin probe to the translational modes of the solvent. The result from the plot with linear scale axes is closer to the X-Band results for PD-Tempone in jojoba oil (Li & Hwang, 1985) and in liquid crystals (Polnaszek & Freed, 1975) which have κ values of 0.018 and 0.044, respectively.

CHAPTER IV

CAPILLARY TRANSLATIONAL DIFFUSION STUDY OF BBTMPO

IV.1. Introduction

In order to calculate the anisotropic interaction parameter κ for BBTMPO (*vide infra*), its molecular volume must be determined. The molecular volume of the paramagnetic species has been determined in the past using the Dreiding model (Hwang et al., 1986) and experimentally using such techniques as the porous disk method (McClung & Killelson, 1968), the electron spin resonance/spin exchange method (Lang & Freed, 1972), the constant volume tracer diaphragm technique (Ahn & Derlacki, 1978), and the capillary diffusion method (Ahn, 1976; Ahn & Ormond, 1978; Hwang & Balkhoyor, 1995). In this study, the translational diffusion coefficient of 4-*N*(*p*-*n*-butylbenzilidene)amino 2,2,6,6-tetramethylpiperidine 1-oxide (abbreviated as BBTMPO and shown in Scheme III-I) was measured in toluene at room temperature (22 ± 1 °C) by the capillary diffusion method. From the measurement of the translational diffusion

coefficient one can determine the hydrodynamic radius of solvated BBTMPO molecules in solution.

The translational diffusion coefficient under the slip boundary condition is given by the Stokes-Einstein expression

$$D = \frac{k_B T}{4\pi \eta r_0} \quad \text{[IV-1]}$$

where r_0 is the hydrodynamic radius of the solvated molecules, k_B is the Boltzmann constant, T is the absolute temperature, and η is the coefficient of shear viscosity. The molecular hydrodynamic volume was determined assuming a hard sphere geometry of BBTMPO.

The intensity was monitored as a function of time with EPR spectroscopy because of the high sensitivity of the EPR spectrometer. The EPR capillary diffusion experiment measurement technique is advantageous since it allows simultaneous measurement of translational and reorientational diffusion coefficients (this chapter and next chapter, respectively) for a given sample.

IV.2. Experimental

IV.2.1. Materials and Sample Preparation

The nitroxide spin probe BBTMPO was synthesized by the condensation of *p-n*-butylbenzaldehyde and 4-amino 2,2,6,6-tetramethylpiperidine *N*-oxide (4-tempamine) (Hwang et al, 1986). Purification of the crude material was performed by adsorption column chromatography. A one gram portion of the crude material was filtered through a 15×1 cm column filled with activated

neutral alumina with 100 ml of hexane as an eluant (Baker Analyzed Reagent). The sample was further purified by several recrystallizations from hexane. The translational diffusion experiment of BBTMPO was performed using a capillary diffusion cell, which is described in the following section.

IV.2.1.1. Capillary Diffusion Cell. The capillary diffusion apparatus is depicted schematically in Figure IV.1 (Ahn, 1976). The capillary diffusion cell was made of 1 mm i.d. heavy wall Pyrex tubing which was closed from one end and the other end was ground flat. The capillary was joined to a 11 mm o.d. tubing (A). A small distortion of the capillary at the joining spot is unavoidable. The total length of the capillary, l , was 3.50 cm. The chamber (C) is a 10 ml graduated cylinder, and (E) is a male ground joint that fits into the vacuum system described in the experimental section of PD-Tempone.

IV.2.1.2. Sample Preparation. The procedure followed here is slightly different from the procedure described in the literature. A weighed amount of the solid BBTMPO, dissolved in a small amount of vacuum distilled toluene, which was purchased from Fluka AG, was introduced into the chamber (C) through a side arm (D). The side arm was then sealed with a torch. Dissolved oxygen in the solution was removed by several cycles of freeze-pump-thaw. The cell was connected to the vacuum system through the male ground joint (E). After that, the entire cell was evacuated, the solvent toluene was vacuum distilled into

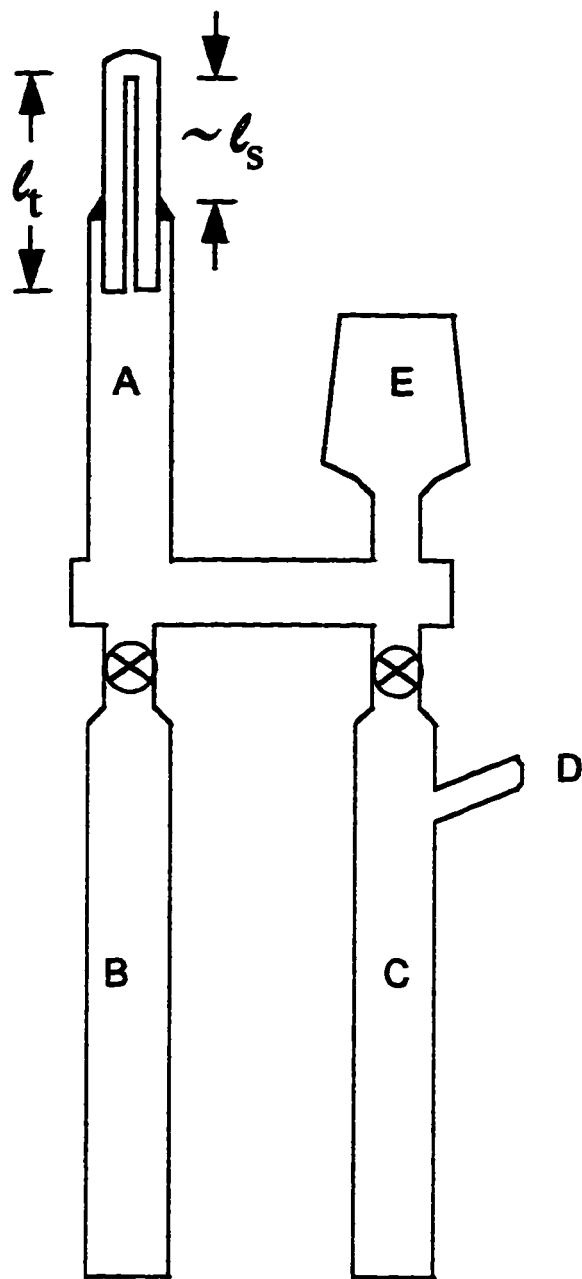


Figure IV.1. A schematic of the capillary diffusion apparatus used for the translational diffusion study of BBTMPO.

reservoirs (B) and (C) and the constriction below E was sealed under vacuum. Vacuum distillation consisted of two steps: after attaching the diffusion cell and another chamber that contains toluene into the vacuum system, both of them were immersed in liquid nitrogen and were entirely evacuated; then, liquid nitrogen was removed away from the solvent chamber, toluene was allowed to vaporize under vacuum, and due to liquid nitrogen, toluene condensed in the diffusion cell. This process was repeated until enough toluene was collected in the diffusion cell (Balkhoyor, 1993).

The concentration of the solution prepared in C was 2.0×10^{-3} M. A small amount of the sample solution in C was transferred into the capillary, the excess solution was poured back into C, and A was washed with a small amount of pure toluene from B and the washed solution was poured back into C. Then, the pure solvent in C was introduced into the 11 mm o.d. tubing (A) above the open end of the capillary. Simultaneously, a portion of the capillary at the closed end was placed into the microwave cavity of the EPR spectrometer, and at this instant the time zero was recorded. The height of the cell in the cavity was also noted to assist in the estimation of ζ .

IV.2.2. Measurement and Data Collection

The measurements were performed at X-band with the EPR Bruker system described in the experimental section of PD-Tempone. At the beginning, the settings of the spectrometer were optimized and kept fixed throughout the

diffusion experiment. The microwave frequency was 9.663 GHz; the microwave power and the modulation amplitude were 6.3 mW and 0.121 G, respectively. The receiver gain was set at 8.0×10^4 . Spectra were, then, acquired automatically by the computer at selected time intervals. This was achieved by writing an automation routine which is a program consisting of a set of commands that control the acquisition process. In the first hour spectra were recorded every 10 minutes. In the second, third, and fourth hours spectra were recorded every 15 minutes. After that and for the next four days spectra were recorded every 30 minutes. In the following days time intervals were increased from one hour to two and four hours during the last days. The experiment took about 15 days, from which 292 spectra were collected. The cell was left in the cavity undisturbed and the spectrometer was kept operating for the whole duration of the room-temperature experiments.

IV.3. Data Analysis

To manipulate the data, spectra files of the translational diffusion experiment of BBTMPO were processed as described in the 'Data Analysis' section of PD-Tempone. Selected spectra obtained at different time intervals in the translational diffusion experiment of BBTMPO in toluene are shown in Figure IV.2. Computer programs, written in FORTRAN language, were either developed from scratch or modified to assist in the analysis of the results.

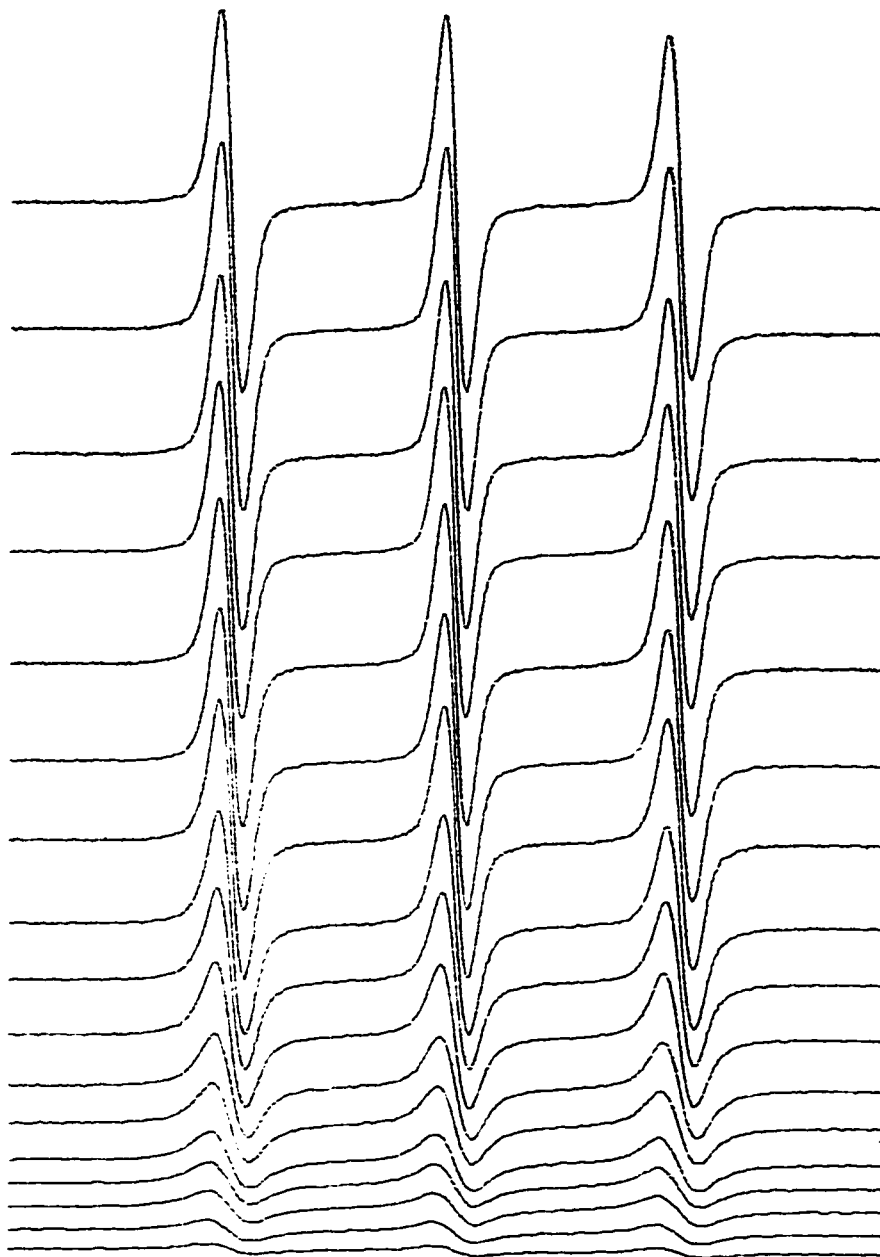


Figure IV.2. EPR experimental spectra at different time intervals during the diffusion process of BBTMPO in toluene.

IV.3.1. Computer Programs

The computer programs, which were used extensively in this study, are described below and are arranged according to the order of their usage. Lists of these programs can be found in Appendix (B) at the end of this dissertation. The accuracy of the first program was checked by performing a sample calculation manually and by using this computer program. Then, the results were compared, which agreed satisfactorily.

IV.3.1.1. *DIFFA.FOR*. This program was written to perform linewidth analysis on a time basis. Given the name of the text file of an EPR spectrum with three lines and the day and time it was acquired, this program will return the total corrected peak-to-peak height for the three lines and the time in seconds. Corrections to the total intensity were necessary since linewidth changes were observed during the diffusion process (Ahn, 1976). The amount of free radicals in the solution is represented by the total area under the first-derivative EPR line. For accurate measurements, the total area under the line of the first derivative EPR absorption spectra should be used in the calculation instead of the peak-to-peak heights. To measure the area under the curve, double integration of all spectra files must be performed. To overcome this cumbersome task (this process would be performed for 292 spectra!), all linewidths are normalized to the linewidth of the EPR signal corresponding to M_{+1} of the spectrum acquired at time zero. In this manner, the intensities would

represent variations in the area under the curve. The normalization was performed using the following equation which is valid for an EPR line with a simple Lorentzian shape (Ahn and Johnson, 1969).

$$I_1 / I_2 = (\delta_2 / \delta_1)^2 \quad \text{[IV-2]}$$

where the I are the first-derivative intensities and δ are the linewidths.

IV.3.1.2. DIFFYAH.FOR & FITDIF.FOR. These programs calculate translational diffusion constants, D . The basic logic behind these programs is to fit the intensity versus time data by a polynomial regression. A data point is located at which the best match is achieved between theoretically generated data and experimental data. This data point is then used to calculate a translational diffusion constant where the following equation is applied (Ahn, 1976; Wang, 1951; Witherspoon and Saraf, 1965).

$$\frac{I(t)}{I_0} = \frac{8}{\pi^2} \frac{1}{R} \sum_{n=0}^{\infty} (-1)^n f_n(t) \sin \frac{(2n+1) \pi R}{2}, \quad \text{[IV-3]}$$

with

$$f_n(t) = \exp \left\{ -(2n+1)^2 \pi^2 \frac{Dt}{4l_c^2} \right\} / (2n+1)^2, \quad \text{[IV-4]}$$

where I_0 is the intensity at time zero, $I(t)$ is the intensity at time t , R is equal to the ratio l/l_c , l_c is the length of the capillary seen by the spectrometer, l is the total length of the capillary, and D is the translational diffusion constant. (A list of the DIFFYAH-program can be found in Balkhoyor, 1993.)

This value of the translational diffusion constant is then used in the above two Equations to calculate a theoretical curve which is compared with the experimental curve. In this calculation, the series in Eq. [IV-3] is truncated at the n th term for which the value of the expression $f_n(t)$ becomes less than 10^{-4} .

Applying Eq.'s [IV-3] & [IV-4], the computer program FITDIFF searches for the D value in increments ranging from 0.00001×10^{-5} to 0.01×10^{-5} cm^2/sec and for the R value in increments of 0.1, where the results from DIFYAH are used as a guidance. This program iterates until minimum variance is obtained between experimental and theoretical data. The searched D and R values are returned along with theoretical time and intensity data. These results are again compared with the experimental data. This process was repeated until a good match was achieved between experimental and theoretical results. Once a good match was obtained, and for a more precise comparison, a theoretical curve was generated and compared graphically with the experimental curve.

Moreover, a range of the experimental data can be sampled for calculation. Usually, slightly different values of D are obtained which give rise to slightly different theoretical curves. For example, with the first 100 data points the calculated D and R values were 1.9×10^{-5} cm^2/sec and 0.2, respectively; while with the last 192 data points the calculated D and R values were 1.0×10^{-5} cm^2/sec and 1.0, respectively. From the measurement of the translational diffusion coefficient, the hydrodynamic radius of the solvated molecules, i.e., BBTMPO, in the solution can be determined using Eq. [IV-1].

IV.4. Results

The EPR technique and the capillary cell made possible the determination of the translational diffusion coefficient of BBTMPO in toluene. The raw results of the translational diffusion experiment of BBTMPO in toluene are shown in Figure IV.3, where the intensities of the spectra were normalized with respect to the intensity of the spectrum acquired at time zero. These data were obtained without intensity corrections. Figure IV.4 shows intensities which were corrected using Eq.[IV-2]. For the first 100 data points the calculated D and R values were $1.9 \times 10^{-5} \text{ cm}^2 / \text{sec}$ and 0.2, respectively. The last 192 data points were best fitted when the calculated D and R values were $1.0 \times 10^{-5} \text{ cm}^2 / \text{sec}$ and 1.0, respectively.

The D value of $1.0 \times 10^{-5} \text{ cm}^2 / \text{sec}$ was selected for further calculations of the anisotropic interaction parameter κ of BBTMPO in toluene at the four microwave bands. The flat portion at small values of t in Fig.'s IV.3 and IV.4 is due to the inequality $I_s < I_t$. The calculated ratio (I_s / I_t) or R is 0.2 at the beginning of the diffusion experiment. R , however, assumes a value of 1.0 towards the more steady diffusion of the nitroxide free radicals. The diffusion coefficient would be more representative when I_s theoretically equals I_t and when the diffusion process becomes more steady. Hence, a D value of $1.0 \times 10^{-5} \text{ cm}^2 / \text{sec}$ was selected. The hydrodynamic radius calculated using the Stokes-Einstein equation was found to be 5.6 Å, and the corresponding hydrodynamic volume was 735.6 Å³. The coefficient of shear viscosity η was calculated by

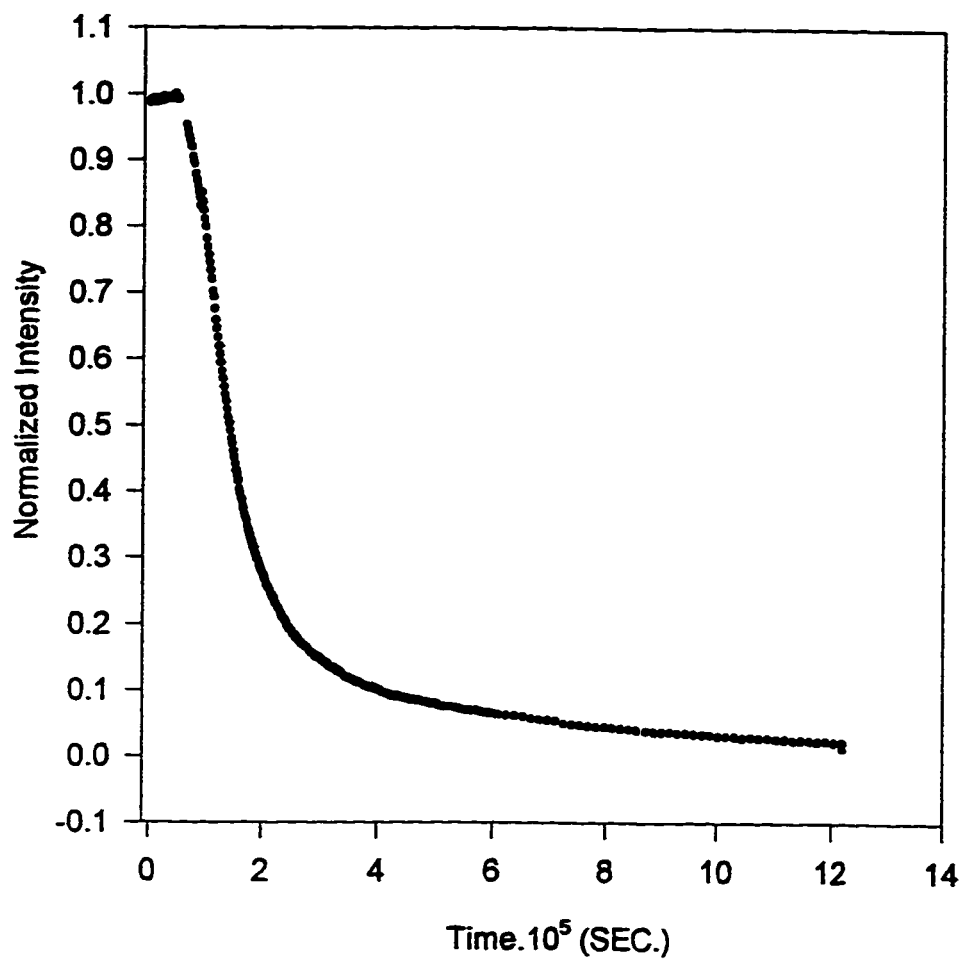


Figure IV.3. EPR intensities versus time for BBTMPO in toluene. These are raw data normalized to the spectrum obtained at time zero.

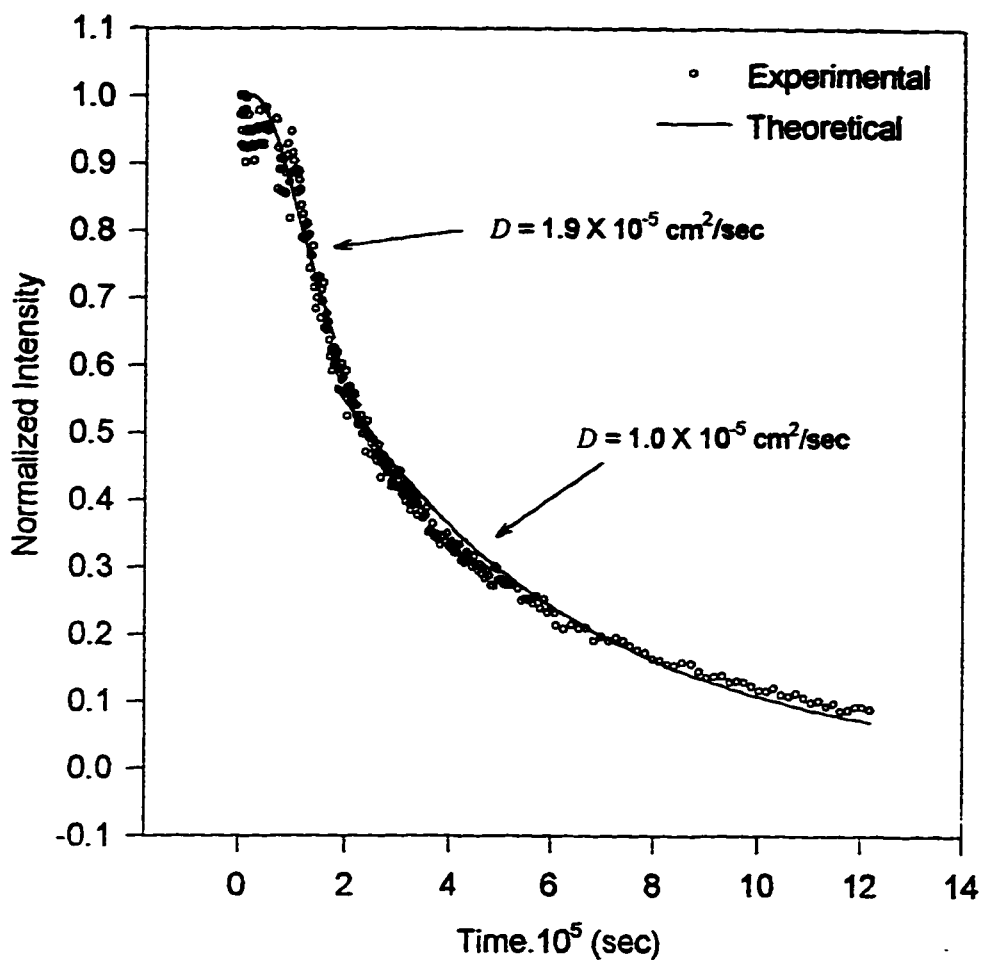


Figure IV.4. EPR intensities versus time for BBTMPO in toluene. These are the same data shown in Fig. IV.3 with corrected intensities using Eq. [IV.1]. Best fit for the first 100 data points was obtained with $D = 1.9 \times 10^{-5} \text{ cm}^2/\text{sec}$ and $R = 0.2$; while best fit for the last 192 data points was obtained with $D = 1.0 \times 10^{-5} \text{ cm}^2/\text{sec}$ and $R = 1.0$.

interpolation of the data given on page F-42 of the "Handbook of Chemistry and Physics," 64th Ed., 1983-1984, and at 22 °C it was found to be 5.78×10^{-3} poise.

IV.5. Discussion

Based on a D value of 1.0×10^{-5} cm² / sec, the hydrodynamic radius calculated using the Stokes-Einstein equation in the slip limit was found to be 5.6 Å. The Stokes-Einstein formula, Eq. IV-1, is derived with the boundary condition assumption that the solvent slips perfectly over the surface of the solute which is assumed to be a sphere of radius r_0 . In this case, the friction coefficient is equal to $4\pi\eta r_0$. If, on the other hand, the boundary condition assumption was that the solvent sticks perfectly to the surface of the spherical solute, then the calculated hydrodynamic radius would be 3.7 Å. In this other case, the friction coefficient is equal to $6\pi\eta r_0$. The corresponding hydrodynamic volumes for the slip and the stick boundary conditions, assuming a hard sphere solute molecule, are 735.6 Å³ and 217.4 Å³, respectively. The molecular volume of BBTMPO was estimated using Dreiding models to be equal to 333 Å³ (Hwang et al, 1986). Therefore, the assumption of a slip boundary condition seems to be more plausible. The difference between the experimental results and the values obtained using models is most probably due to the anisotropic BBTMPO, thermal rotations of BBTMPO and solvation of BBTMPO by toluene.

CHAPTER V

ANISOTROPIC INTERACTION AND COLE-DAVIDSON PARAMETERS: BBTMPO IN TOLUENE

V.1. Introduction

The reorientational motion of the spin probe PD-Tempone has been found to be isotropic in the solvent toluene. This is anticipated since PD-Tempone has an isotropic overall shape. In this chapter, the effect of solute size on the reorientational motion of the probe will be studied by examining the anisotropic interaction parameter, κ . The solute chosen in this study, BBTMPO, is about twice the length of PD-Tempone and has a molecular mass (315.5) of about twice that of PD-Tempone (178.3). BBTMPO is about three times heavier and longer than the solvent molecules (toluene). It would be possible, using BBTMPO, to study the effect of doubling the solute size and mass on the anisotropic interaction parameter, κ . As a result of BBTMPO having a rod-like structure and being rigid, its rotational motion is expected to be anisotropic.

Earlier studies showed that values of the anisotropic interaction parameter κ for BBTMPO in toluene were different at different microwave frequencies (Hwang et al., 1985; Rahman, 1988). The objective of this study was to determine the anisotropic interaction parameter κ for the nitroxide spin probe BBTMPO (shown in Scheme III-I) in toluene at the microwave frequency Bands: L (~1 GHz), S (~4 GHz), X (~9.5 GHz), and Q (~35 GHz). For the first time, lineshape analysis using the ABC-method (Chapt. III) will be performed for the EPR spectra of BBTMPO. This procedure was used to analyze the EPR spectra of PD-Tempone (Chapt. III), whereas the EPR spectra of BBTMPO were analyzed in the past by simulation using computer programs (Hwang et al., 1985; Rahman, 1988).

V.2 Experimental

V.2.1. Materials and Sample Preparation

The solute 4-*N*(*p*-*n*-butylbenzilidene)amino 2,2,6,6-tetramethylpiperidine 1-oxide (abbreviated as BBTMPO), which is a nitroxide spin probe, was synthesized and purified as described in the previous chapter. The solvent toluene was purchased from Fluka.AG, Switzerland. Samples of BBTMPO in toluene for L-, S-, and X-Bands were prepared in 2-mm i.d. × 3-mm o.d. Pyrex sample tubes. These solutions contain oxygen from the atmosphere, and oxygen is paramagnetic and would cause the first derivative EPR lines to be

broader. Therefore, dissolved oxygen was removed by several cycles of freeze-pump-thaw. The concentration of BBTMPO in toluene was 5.2×10^{-4} M.

To prepare permanent samples of BBTMPO in toluene for L-, S-, and X-Bands, a modified vacuum system manufactured by Pope Scientific Inc. was used. This vacuum system was utilized to perform the freeze-pump-thaw cycles. The procedure for cycles of freeze-pump-thaw was described in the experimental section of PD-Tempone. The procedure for the preparation of permanent samples (5.2×10^{-4} M) in small quartz tubes (1 mm i.d. \times 1.5 mm o.d. \times 60 mm height) for studies conducted at the Q-Band was also described in the experimental section of PD-Tempone.

The same apparatus and measurement and data collection procedures that were described in the experimental section of PD-Tempone were also applied for BBTMPO.

V.2.2. Modulation Amplitude Selection

The modulation amplitude must be selected carefully to avoid the introduction of instrumental artifacts in the EPR spectra. The observed linewidth of the first-derivative EPR signals for BBTMPO are broader than the signals for PD-Tempone. This allowed the use of higher modulation amplitudes. Figure V.1 shows the variation of the observed linewidth as a function of the level of the peak-to-peak modulation amplitude. The same data is also listed in Table V.1. The value of peak-to-peak modulation amplitude that gave the best compromise

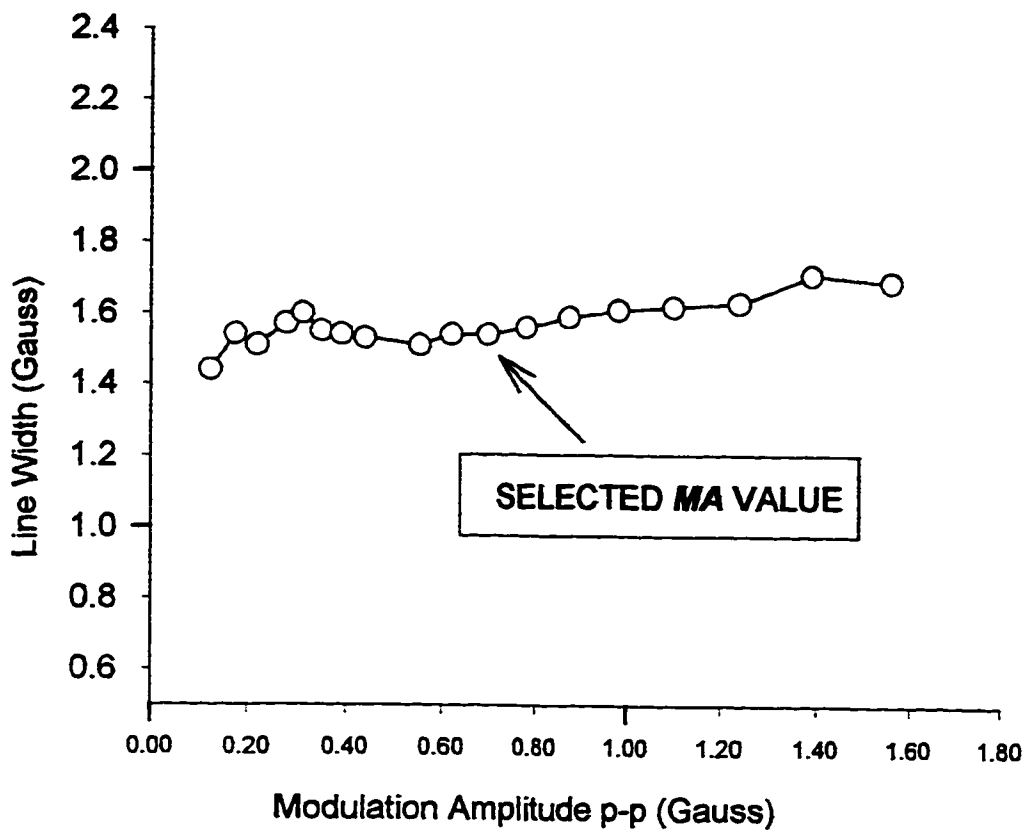


Figure V.1. Observed line width as a function of peak-to-peak modulation amplitude for BBTMPO in toluene at L-Band. The selected value of modulation amplitude that gave the best compromise between signal intensity and signal distortion was 0.696 Gauss.

TABLE V.1. Observed Line Width as a Function of Peak-to-Peak Modulation

Amplitude for BBTMPO in Toluene at L-Band.

Modulation Amplitude p-p (Gauss)	Observed Line Width (Gauss)
0.124	1.44
0.175	1.54
0.220	1.51
0.277	1.57
0.311	1.60
0.349	1.55
0.391	1.54
0.439	1.53
0.553	1.51
0.620	1.54
0.696	1.54
0.781	1.56
0.876	1.59
0.983	1.61
1.100	1.62
1.240	1.63
1.390	1.71
1.560	1.69

* The shaded cells in the table represent the selected value of modulation amplitude, i.e. 0.696 Gauss, and the corresponding observed line width.

between signal intensity and signal distortion for BBTMPO in toluene at L-Band was 0.696 Gauss. This value can be contrasted with the value of modulation amplitude for PD-Tempone in toluene at L-Band, which is 0.124 Gauss. The observed linewidths for BBTMPO and PD-Tempone corresponding to these values of modulation amplitudes were 1.54 and 0.309, respectively.

V.3. Data Analysis

The data files of the resulting spectra for BBTMPO in toluene were manipulated in the same manner as described in the 'Data Analysis' section of PD-Tempone. Mainly, the same computer programs which were used in the analysis of the results for PD-Tempone were also used in the results analysis of BBTMPO.

V.3.1. Computer Programs

The computer programs, which were used in this study, are basically the same programs that were used for the analysis of the results from the PD-Tempone study. However, due to the presence of protons in BBTMPO instead of the deuterons in PD-Tempone, substantial modifications to the programs 'GSUMJH' and 'GSUMDP' were made. Moreover, due to the fact that BBTMPO exhibited larger linewidths relative to PD-Tempone, a program, 'INTERP', was written to perform interpolation between the subsequent data points. This gave an enhanced resolution of the spectra. These three programs will be described

below. Lists of these programs can be found in Appendix (C) at the end of this Dissertation.

V.3.1.1. HGSUMJH.FOR. This program, which simulates the lineshape of a single first-derivative EPR peak, was used to determine the isotropic hyperfine coupling coefficient for hydrogen, A_{iso}^H . This was achieved by varying, in the input data file, A_{iso}^H and the intrinsic linewidth. The program returned the theoretical observed linewidth and decay behavior. Fitting the lineshape of a single first-derivative spectrum of BBTMPO was not possible when only Lorentzian contributions to the shape of the line were considered. In addition to the Lorentzian contributions, Gaussian contributions to the lineshape had to be considered. Moreover, the relative intensity distribution due to the twelve equivalent protons is different from the intensity distribution for the twelve equivalent deuterons. Table V.2 gives the relative intensities distributions for 12 deuterons (spin = 1) and 12 protons (spin = $\frac{1}{2}$). Interaction of the odd electron on the N[•]-O fragment with twelve equivalent protons results in 12+1 lines whose relative intensities are proportional to the coefficients of the binomial expansion of $(1+x)^{12}$ (Carrington and McLachlan, 1980). The coefficients of a binomial expansion of degree N is given by the following expression.

$$\binom{N}{j} = \sum_{j=0}^N \frac{N!}{(N-j)! j!} \quad [V-1]$$

TABLE V.2. Relative Intensities of Twelve.Equivalent Deuterons and Twelve Protons When Each Interact with One Electron.

Twelve Deuterons		Twelve Protons	
Quantum No.	Degeneracy	Quantum No.	Degeneracy
-12	1	-6	1
-11	12		
-10	78	-5	12
-9	352		
-8	1221	-4	66
-7	3432		
-6	8074	-3	220
-5	16236		
-4	28314	-2	495
-3	43252		
-2	58278	-1	792
-1	69576		
0	73789	0	924
1	69576		
2	58278	1	792
3	43252		
4	28314	2	495
5	16236		
6	8074	3	220
7	3432		
8	1221	4	66
9	352		
10	78	5	12
11	12		
12	1	6	1

More generally, when N nuclei of spin I produce identical hyperfine splittings, the first-order spectrum will consist of $2NI+1$ equally spaced lines with intensities given by (Pake and Estle, 1973)

$$I \propto p_N(M_I) = \frac{1}{(2I+1)^N} \sum_{j=0}^k (-1)^j \binom{N}{j} \binom{NI - M_I - j(2I+1) + N - 1}{N-1}, \text{ [V-2]}$$

where

$$M_I = \sum_{i=1}^N m_i, \quad k \text{ is the largest integer less than or equal to } (NI - M_I)/(2I+1), \text{ and}$$

$$\binom{a}{b}$$

is the binomial coefficient given by Eq. [V-1]. The leading factor $(2I+1)^N$ in Eq. [V-2] can be neglected in the calculation since it is the same for the different M_I states.

The results were treated in the same manner as was described previously for the program 'GSUMJH' in the 'Results and Discussion' section of PD-Tempone. The mathematical equation used in this program is the same as the equation used in the next program.

V.3.1.2. GSUMHP.FOR. This computer program calculates the intrinsic linewidth by considering both Lorentzian and Gaussian contributions to the lineshape (Bales, 1993). Following is a derivation of the equation which was used to accomplish this task.

Lorentzian line is usually described by the shape function $g(\omega)$ which on an angular frequency scale is given by (Carrington and McLachlan, 1980)

$$g(\omega) = \frac{T_2}{\pi} \frac{1}{1 + T_2^2(\omega - \omega_0)^2} \quad [\text{V-3}]$$

where T_2 is the transverse relaxation time or the spin-spin relaxation time, ω is the microwave angular frequency ($= 2\pi\nu$), and ω_0 is the resonance frequency.

Dividing the numerator and the denominator of the r.h.s. of Eq. [V-3] by T_2^2 and setting $1/T_2$ equal to w

$$\Rightarrow g(\omega) = \frac{1}{\pi} \frac{w}{(\omega - \omega_0)^2 + w^2}$$

differentiating w.r.t. ω

$$\Rightarrow Y^L = \frac{dg}{d\omega} = \frac{1}{\pi} \frac{-2(\omega - \omega_0)w}{[(\omega - \omega_0)^2 + w^2]^2}$$

and for simulation purposes, the substitutions $\omega \rightarrow Q_k \cdot A$ and $\omega_0 \rightarrow H_j$, give

$$Y^L = -\frac{2}{\pi} \frac{(Q_k \cdot A - H_j)w}{[(Q_k \cdot A - H_j)^2 + w^2]^2} \quad [\text{V-4}]$$

A Gaussian curve is described by the function (Carrington and McLachlan, 1980)

$$g(\omega) = \frac{T_2}{\sqrt{2\pi}} e^{-\frac{1}{2}T_2^2(\omega - \omega_0)^2} \quad [\text{V-5}]$$

making the substitution $1/T_2 = w$ or $T_2 = 1/w$

$$\Rightarrow g(\omega) = \frac{1}{\sqrt{2\pi}} \frac{1}{w} e^{-\frac{1}{2}(\omega-\omega_0)^2/w^2}$$

differentiating w.r.t. ω

$$\Rightarrow Y^G = \frac{dg}{d\omega} = \frac{-1}{\sqrt{2\pi}} \frac{1}{w^3} (\omega - \omega_0) e^{-\frac{1}{2}(\omega-\omega_0)^2/w^2}$$

and for simulation purposes, the substitutions $\omega \rightarrow Q_k \cdot A$ and $\omega_0 \rightarrow H_j$, give

$$\Rightarrow Y^G = -\frac{1}{\sqrt{2\pi}} \frac{(Q_k \cdot A - H_j)}{w^3} e^{-\frac{1}{2}(Q_k \cdot A - H_j)^2/w^2} \quad [\text{V-6}]$$

Finally, combining Eq.'s [V-4] and [V-6] \Rightarrow

$$I_j = \sum_{k=-6}^6 \frac{D_k}{\sum_{i=-6}^6 D_i} (-1)^k \left\{ \lambda \frac{2}{\pi} \frac{(Q_k \cdot A - H_j)w}{[(Q_k \cdot A - H_j)^2 + w^2]^2} + (1-\lambda) \frac{1}{\sqrt{2\pi}} \frac{(Q_k \cdot A - H_j)}{w^3} \exp\left[-\frac{1}{2}(Q_k \cdot A - H_j)^2/w^2\right] \right\} \quad [\text{V-7}]$$

where

I_j is the intensity at magnetic field H_j ;

Q_k is the quantum number of D_k ;

D is the degeneracy;

A is the isotropic deuteron hyperfine coupling constant;

H_j is the magnetic field at point j on the simulation;

w is equal to $1/T_2$;

λ is the mixing factor, i.e., when $\lambda = 1$ the line is completely Lorentzian and when $\lambda = 0$ the line is completely Gaussian.

The intrinsic linewidth of a Lorentzian curve is equal to $\frac{2}{T_2\sqrt{3}}$ and the intrinsic linewidth of a Gaussian curve is equal to $2 / T_2$. The first term is a weighting factor which comes from the degeneracy of the twelve equivalent protons in BBTMPO adjacent to the N=O fragment. The above Equation sums the intensities of all the thirteen degenerate hyperfine lines and calculates I_j , the intensity at magnetic field H_j . Since it is completely symmetrical, only half of the spectrum was simulated. The output of this program is a list of "observed" linewidths and corresponding "intrinsic" linewidths and "peak-to-peak heights." The next steps are exactly the same as was described for the treatment of the PD-Tempone results. The only modification is to use the magnetic parameters of BBTMPO in the 'BCT1' and 'ABC1' programs. Table V.3 gives the magnetic parameters of BBTMPO in toluene (Hwang, *et al.*, 1986).

V.3.1.3. INTERP.FOR. This program was written to obtain a higher resolution of the experimental data by generating more points between subsequent experimental data points. The spectra are stored as x-y data points. Due to the broader linewidths in BBTMPO, the extrema in the spectrum could lay between two points. The program for linewidth analysis search for data points with maximum (or minimum) values. Therefore, the program will not recognize the correct maxima (or minima). The method of Cubic Spline Interpolation

**TABLE V.3. Magnetic Parameters of
BBTMPO in Toluene.[§]**

$$g_x = 2.0097$$

$$g_y = 2.0060$$

$$g_z = 2.0023$$

$$\langle g \rangle = 2.0060$$

$$A_x = 7.0 \text{ G}$$

$$A_y = 5.3 \text{ G}$$

$$A_z = 34.20 \text{ G}$$

[§]From Hwang et al, 1986.

(Press, *et al.*, 1987) allows the interpolation between two experimental data points and generates more data points.

The basis for the method of Cubic Spline Interpolation comes from linear interpolation. Assuming $y=y(x_i)$, $i=1, \dots, N$, $y=y(x)$ could be found for x which lies between x_j and x_{j+1}

$$\frac{y - y_j}{y_{j+1} - y_j} = \frac{x - x_j}{x_{j+1} - x_j}$$

rearranging \Rightarrow

$$y - y_j = \frac{x - x_j}{x_{j+1} - x_j} y_{j+1} - \frac{x - x_j}{x_{j+1} - x_j} y_j$$

further rearrangement gives \Rightarrow

$$\begin{aligned} y &= \left(1 - \frac{x - x_j}{x_{j+1} - x_j}\right) y_j + \frac{x - x_j}{x_{j+1} - x_j} y_{j+1} \\ &= \frac{x_{j+1} - x}{x_{j+1} - x_j} y_j + \frac{x - x_j}{x_{j+1} - x_j} y_{j+1} \end{aligned}$$

or $y = A y_j + B y_{j+1}$

where

$$\begin{aligned} A &= \frac{x_{j+1} - x}{x_{j+1} - x_j}, \quad \text{and} \\ B &= (1 - A) = \frac{x - x_j}{x_{j+1} - x_j} \end{aligned}$$

and for a cubic linear polynomial function (Press, *et al.*, 1987)

$$y = Ay_j + By_{j+1} + Cy_j'' + Dy_{j+1}''$$

where

$$C \equiv \frac{1}{6}(A^3 - A)(x_{j+1} - x_j)^2, \quad \text{and}$$

$$D \equiv \frac{1}{6}(B^3 - B)(x_{j+1} - x_j)^2$$

The precision of this method is presented graphically in Figure V.2 for single peaks from the EPR spectra of BBTMPO in toluene at T = 295 K and 185 K.

V.4. Results

In this section the results obtained for BBTMPO in toluene at the different microwave frequency bands, i.e., L-, S-, X-, and Q-Bands, will be presented. Then, at the end of this section, results showing the effect of the Cole-Davidson parameter will be cited. The objective is to look at the behavior of the anisotropic interaction parameter κ at the different microwave frequencies for the same system BBTMPO in toluene, similar to what was done to PD-Tempone in toluene.

The main steps involved to arrive at the final results for each microwave frequency band are, first, to simulate the sharpest peak of the spectra obtained at the different temperatures. The isotropic hyperfine coupling coefficient for hydrogen, A_{iso}^H and the mixing factor λ , along with the intrinsic linewidth, are determined for each temperature by theoretical simulation using the HGSUMJH-program. Lists of intrinsic linewidths are then generated with the GSUMHP-program using the predetermined isotropic hyperfine coupling coefficient for

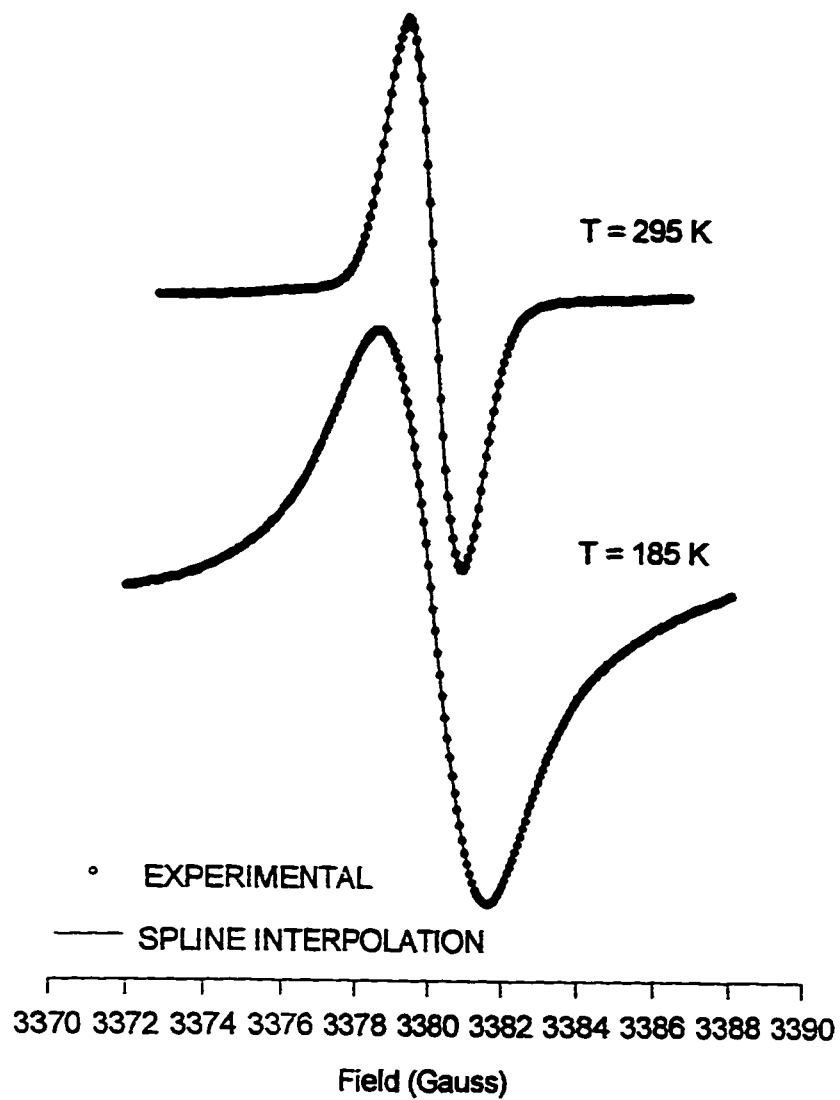


Figure V.2. Cubic Spline Interpolation performed by the INTERP-program for single peaks from the X-Band EPR spectra of BBTMPO in toluene at $T = 295$ K and 185 K.

hydrogen, A_{iso}^H and the mixing factor λ . After that, experimental B and C values are calculated using the T22-program. From the B and C values, correlation times, τ_R , are calculated using the BCT1- and the ABCI-program. Once correlation times τ_R are calculated (using the ABCI-program) for the system at different temperatures, the anisotropic interaction parameter κ can be calculated following the same procedure which was outlined for the treatment of the PD-Tempone results.

V.4.1. X-Band

The study of BBTMPO in toluene at X-Band (~9.5 GHz), with 100-KHz field modulation, was conducted over a range of temperatures from 105 to 295 K and representative spectra are shown in Figure V.3. The well-resolved first-derivative three-peak spectra were observed up to a temperature of ~185.0 K. The first-derivative peak corresponding to $M_I = +1$ was the sharpest as this temperature was approached.

The results of the linewidth analysis, which was performed by the LWA-program, are given in Table V.4. The first column of this Table contains values of temperature in K. The second, third, and fourth columns contain, respectively, observed linewidths (in Gauss), peak-to-peak heights, and central fields (in Gauss) for $M_I = +1$. The same pattern is repeated for $M_I = 0$ and $M_I = -1$.

The decay behaviors of the experimental spectra at the different temperatures were calculated with the EXDEL-program. The results of the

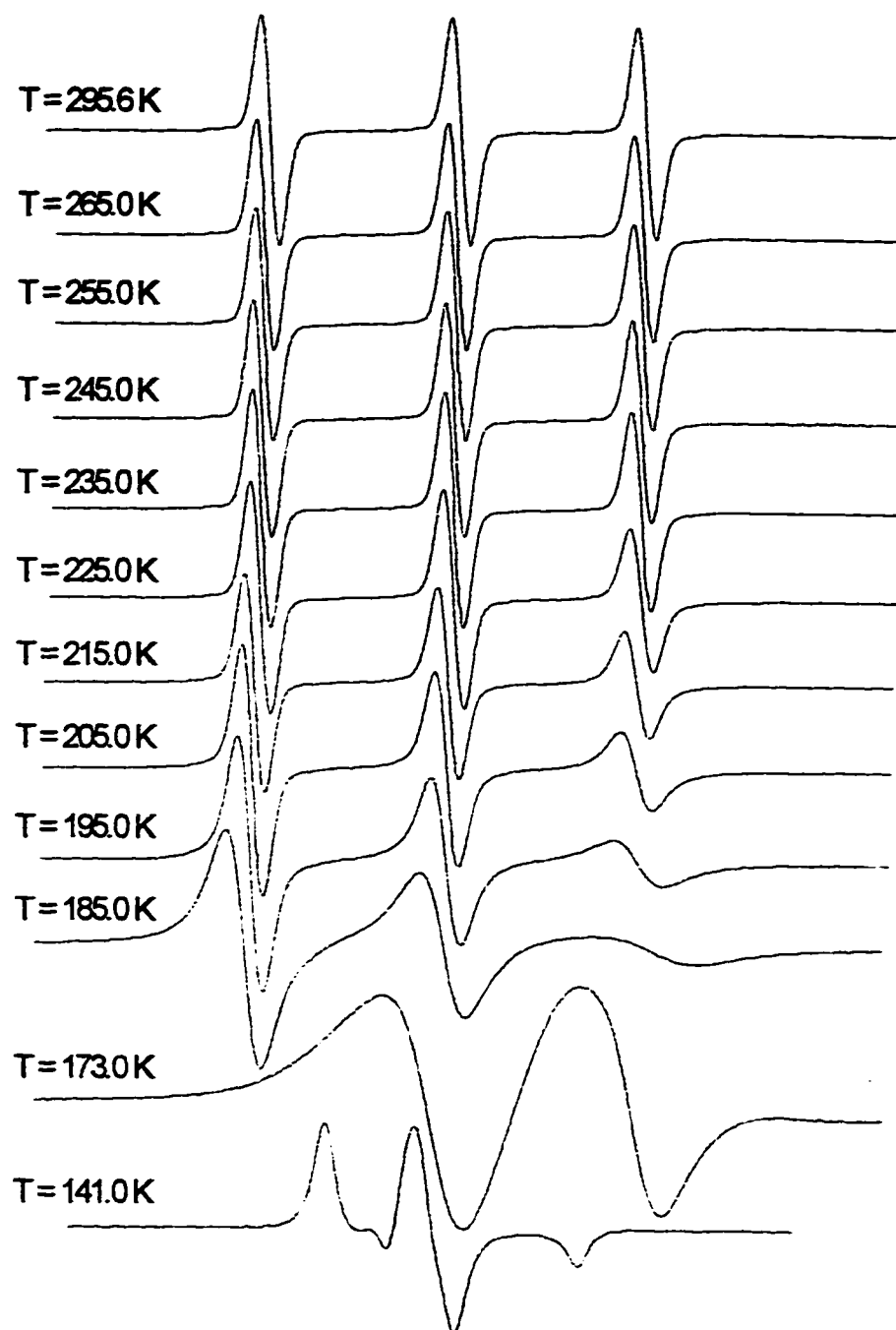


Figure V.3. Selected experimental EPR spectra of BBTMPO in toluene at X-Band and at different temperatures.

TABLE V.4. Linewidth Analysis of BBTMPO in Toluene at X-Band.

TEMP. (K)	$M_I = +1$			$M_I = 0$			$M_I = -1$		
	OLW (GAUSS)	PTPI	CFLD (GAUSS)	OLW (GAUSS)	PTPI	CFLD (GAUSS)	OLW (GAUSS)	PTPI	CFLD (GAUSS)
295.6	1.5738	.4413E+005	3381.3003	1.5054	.4350E+005	3396.7304	1.5738	.4056E+005	3412.2289
275.0	1.5054	.4398E+005	3380.2397	1.5738	.4325E+005	3395.7382	1.5738	.3936E+005	3411.2710
265.0	1.5054	.4429E+005	3380.2397	1.5738	.4360E+005	3395.7382	1.6422	.3946E+005	3411.3052
255.0	1.5738	.8923E+005	3380.2055	1.5054	.8794E+005	3395.7040	1.6422	.7885E+005	3411.3052
245.0	1.5738	.4544E+005	3380.2055	1.6422	.4488E+005	3395.7040	1.7106	.3867E+005	3411.3394
235.0	1.5738	.4567E+005	3380.2055	1.5738	.4512E+005	3395.7382	1.7106	.3811E+005	3411.3394
225.0	1.6422	.8913E+005	3380.2397	1.7107	.8373E+005	3395.8067	1.9843	.5484E+005	3411.5447
215.0	1.7791	.4186E+005	3380.2397	1.8475	.3679E+005	3395.8751	2.1212	.2051E+005	3411.6131
205.0	1.9159	.3634E+005	3380.2397	2.0528	.2798E+005	3395.9093	2.6687	.1132E+005	3411.7500
195.0	2.1897	.2459E+005	3380.1713	2.4634	.1602E+005	3395.9777	4.2424	.4404E+004	3411.9894
185.0	3.0107	.4580E+005	3380.1029	3.6266	.2772E+005	3396.1488	7.4584	.5148E+004	3413.4606
165.0	3.0108	.1949E+005	3381.6398	3.0107	.2081E+005	3395.9409	6.8426	.3477E+004	3409.4208

simulation, which were performed using the HGSUMJH-program, and the corresponding experimental spectra are given in Fig. V.4. Half of each spectrum is shown, since as was mentioned earlier the first derivative EPR spectrum is symmetrical about the central field. Clearly, the match between experimental and theoretical curves is satisfactory. The parameters determined from these theoretical simulations, namely the isotropic hyperfine coupling coefficient for hydrogen, A_{iso}^H , the mixing factor λ , the intrinsic linewidth, and the theoretically calculated observed linewidth, are listed in Table V.5 and are presented graphically in Fig. V.5.

The experimental B and C values for this system were calculated by four different routes for comparison purposes. The first one was by determining the experimental linewidths from single-peak spectra, i.e., sweeping the magnetic field so that only the sharpest peak from the three peaks (corresponding to $M_I = +1, 0, -1$) was scanned. This would give a spectrum of high resolution for linewidth measurements. Then B and C values were determined from linewidths measured from these single-peak spectra and by using different values of the isotropic hyperfine coupling coefficient for hydrogen, A_{iso}^H , and the mixing factor λ . The second method was to use the linewidths from the single-peak spectra, like in method one, but with the a single set of values for A_{iso}^H and λ determined from the spectrum acquired at room temperature. The third and fourth methods differed from the former methods in that here linewidths were measured from spectra containing the three peaks corresponding to $M_I = +1, 0, -1$.

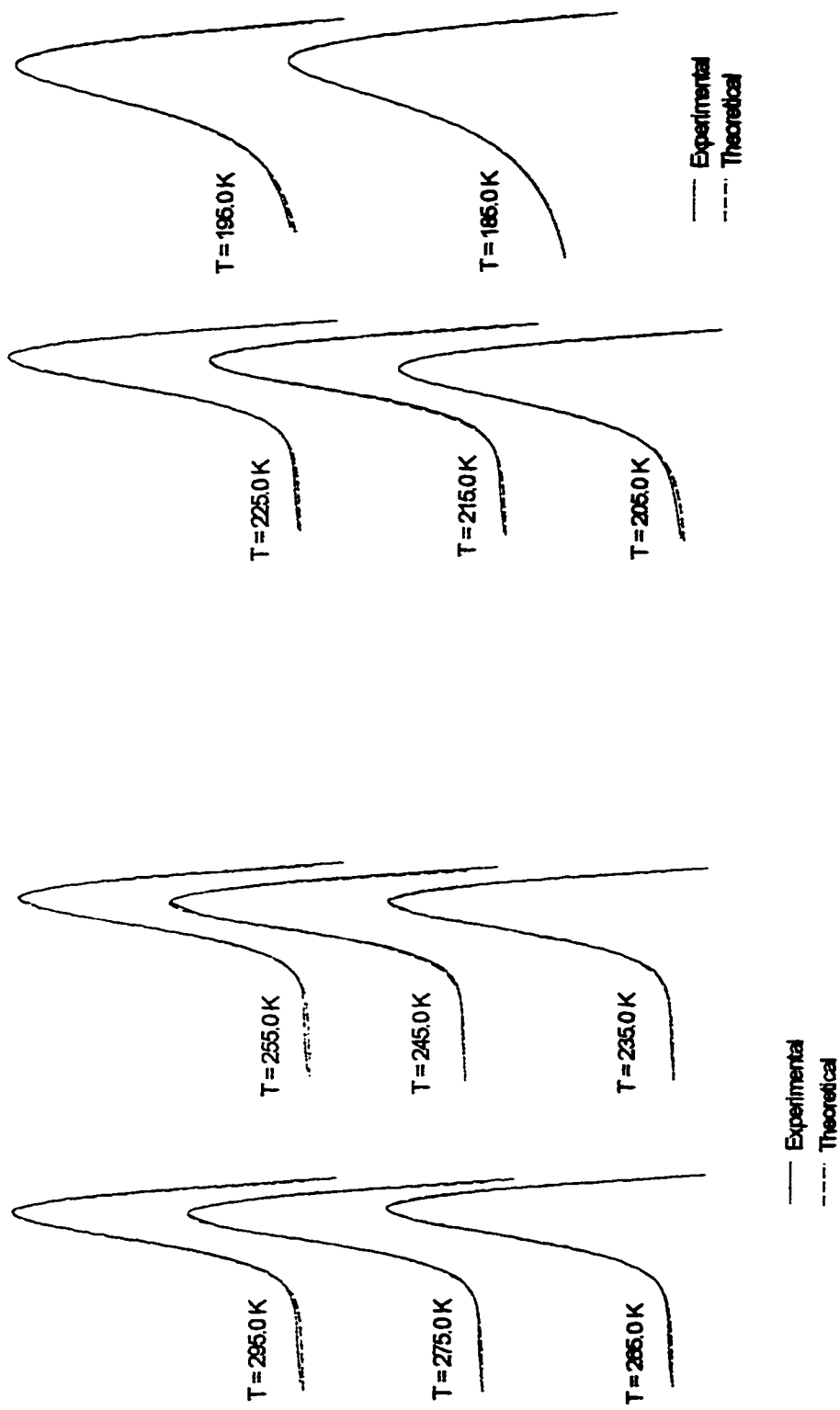


Figure V.4. Theoretical simulation of experimental EPR spectra of BBTMPO in toluene at X-Band and at different experimental temperatures. Simulation was performed by considering both Lorentzian and Gaussian contributions to the shape of the line. Parameters determined from these simulations are listed in Table V.5.

Table V.5. Parameters Determined from the Theoretical Simulation Shown in Fig. V.4 for BBTMPO in Toluene at X-Band.

T (K)	$\$ A_{iso}^H$ (G)	Mixing Factor λ	Experimentally Observed Linewidth (G)	Theoretical Observed Linewidth (G)	Intrinsic Linewidth (G)
295.0	0.26 ± 0.02	0.47 ± 0.02	1.5151 ± 0.0057	1.5199 ± 0.0010	1.170 ± 0.010
275.0	0.28 ± 0.02	0.43 ± 0.02	1.5282 ± 0.0113	1.5299 ± 0.0010	1.120 ± 0.010
265.0	0.28 ± 0.02	0.40 ± 0.02	1.5542 ± 0.0200	1.5599 ± 0.0010	1.160 ± 0.010
255.0	0.28 ± 0.02	0.40 ± 0.02	1.5575 ± 0.0149	1.5599 ± 0.0010	1.160 ± 0.010
245.0	0.28 ± 0.02	0.40 ± 0.02	1.5510 ± 0.0149	1.5599 ± 0.0010	1.160 ± 0.010
235.0	0.28 ± 0.02	0.40 ± 0.02	1.5705 ± 0.0057	1.5699 ± 0.0010	1.180 ± 0.010
225.0	0.28 ± 0.02	0.40 ± 0.02	1.6781 ± 0.0203	1.6699 ± 0.0010	1.310 ± 0.010
215.0	0.28 ± 0.02	0.42 ± 0.02	1.7172 ± 0.0204	1.7199 ± 0.0010	1.370 ± 0.010
205.0	0.28 ± 0.02	0.58 ± 0.02	1.8573 ± 0.0001	1.8599 ± 0.0010	1.520 ± 0.010
195.0	0.28 ± 0.02	0.77 ± 0.02	2.1114 ± 0.0258	2.1099 ± 0.0030	1.770 ± 0.030
185.0	0.30 ± 0.01	0.96 ± 0.02	2.8983 ± 0.0170	2.9099 ± 0.0020	2.560 ± 0.030

$\$ A_{iso}^H$ is the hydrogen isotropic hyperfine coupling coefficient.

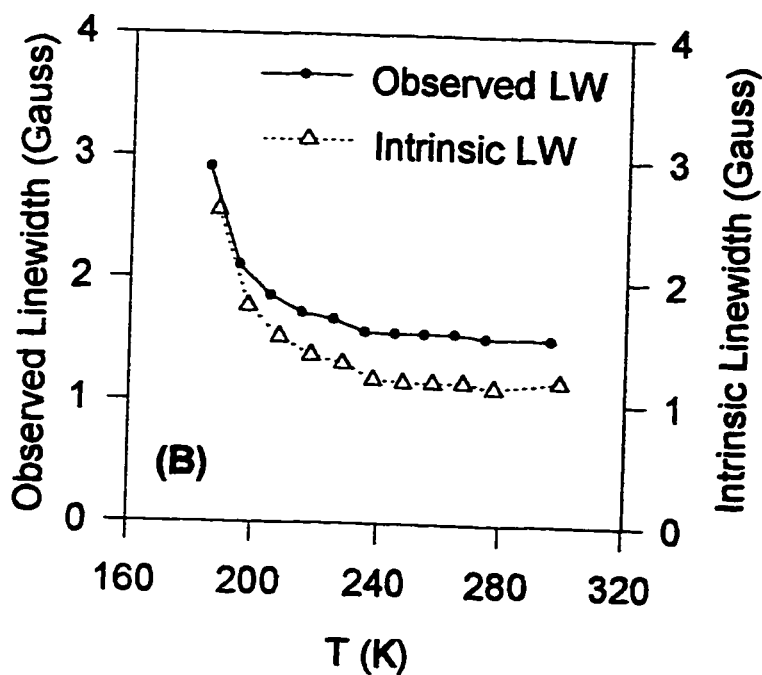
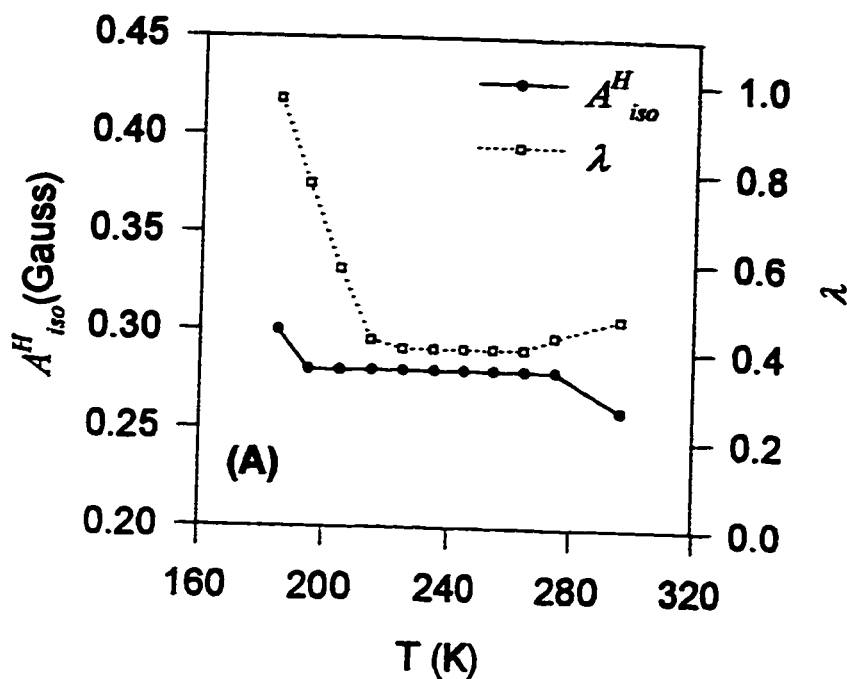


Figure V.5. Parameters determined from the theoretical simulations of the EPR spectra of BBTMPO in toluene at X-Band and at different temperatures. (A) Both hydrogen isotropic hyperfine coupling coefficient and the mixing factor of contributions from Lorentzian and Gaussian lineshape functions versus temperature. (B) Both observed and intrinsic linewidths as a function of temperature.

The calculated B and C values were close when the experimental linewidth was either measured from single-peak or three-peak spectra. However, the calculated B and C values disagreed at low temperatures when either different or the same values of A_{iso}^H and λ were used. These findings can be seen clearly from Figure V.6 which plots values of B versus C calculated by the four different methods. The disagreements are indicated in the Figure. The effects of these four methods on the calculations of the correlation time τ_R are presented in Figure V.7. The same observations from the calculations of B and C were carried over to the calculations of τ_R .

The results of the coefficient of shear viscosity η over absolute temperature T versus correlation time τ_R obtained by the four different methods show that if different values of A_{iso}^H and λ were used, the anisotropic interaction parameter κ would exhibit temperature dependency. Usually, curves of η/T versus τ_R are linear resulting in a temperature independent value of the anisotropic interaction parameter κ . The slope of the (η/T) versus τ_R curve is

equal to $\left(\frac{4}{3} \pi r_0^3 \frac{\kappa}{k_B} \right)$. Assuming the molecular radius r_0 to be constant with

temperature, the only parameter that could show variation as a function of temperature is κ . Since the main objective of this study is to compare the κ values obtained at the different microwave frequencies, less dependence of κ on temperature was desired. Hence, although values of A_{iso}^H and λ were calculated at different temperatures, selected values of A_{iso}^H and λ obtained at different

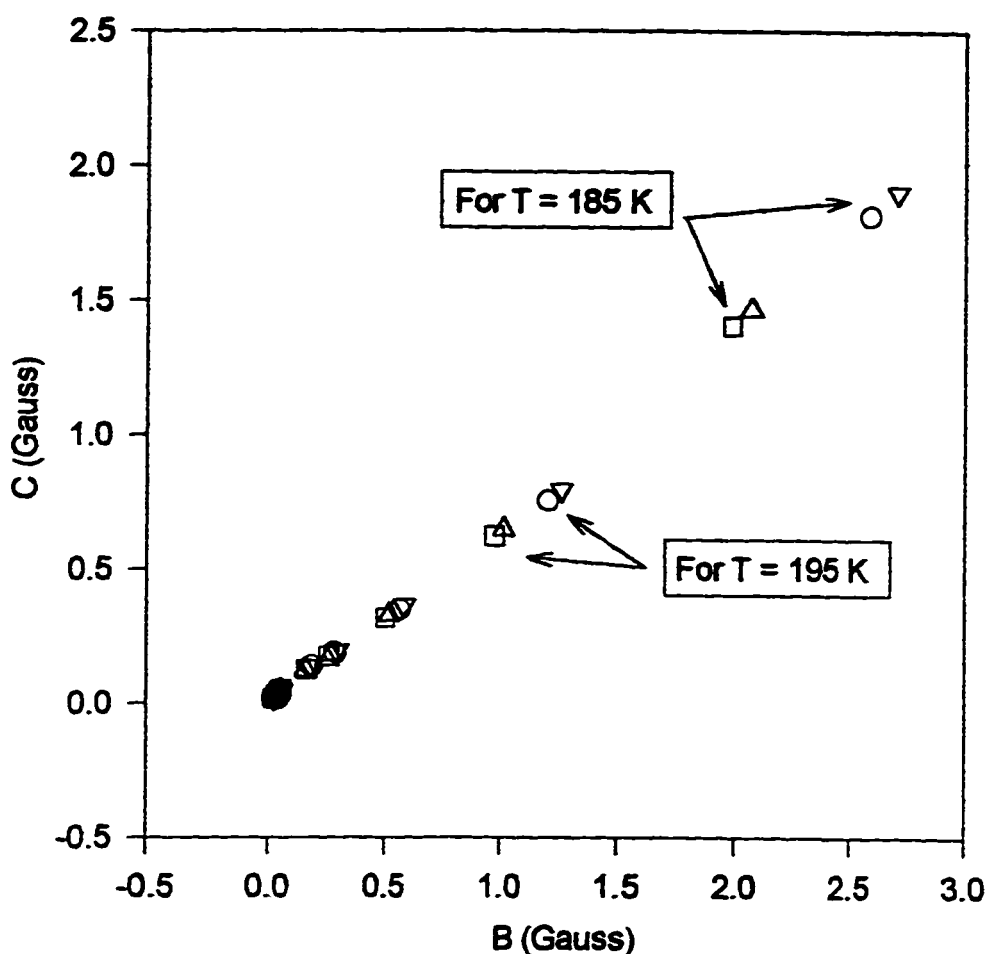


Figure V.6. Values of B versus C calculated by four different methods for BBTMPO in toluene at X-Band and at different temperatures. The first method is by using experimental linewidths measured from single-peak spectra and different values of the isotropic hydrogen hyperfine coupling coefficient A_{iso}^H and the mixing factor λ , and the results are indicated by (○). The second method is like method one but using the same values of A_{iso}^H and λ , and the results are indicated by (□). The third method is like the first method but the experimental linewidths were measured from three-peak spectra, and the results are indicated by (▽). Likewise, the fourth method is like the second method with the experimental linewidths measured from three-peak spectra, and the results are indicated by (Δ). Disagreements became pronounced at low temperatures if different or same values of A_{iso}^H and λ were used.

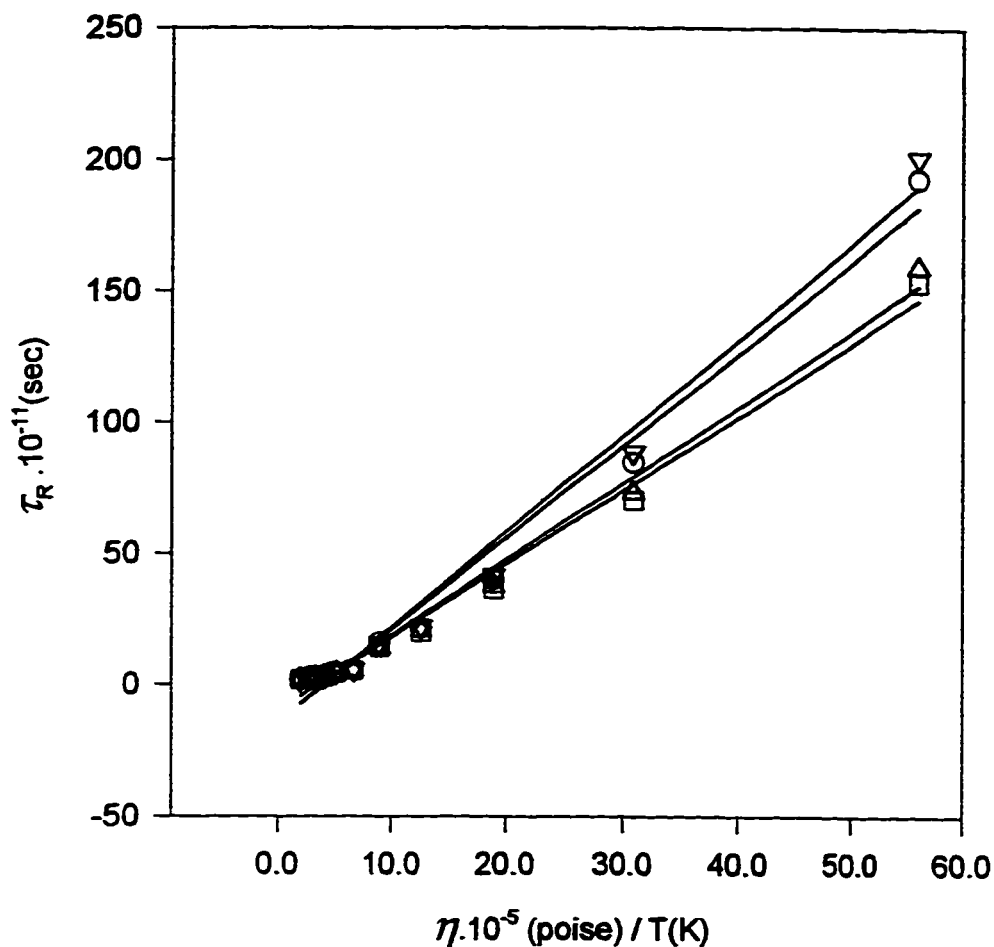


Figure V.7. Coefficient of shear viscosity η over temperature versus rotational correlation time τ_R calculated by four different sets of values of B and C for BBTMPO in toluene at X-Band and at different temperatures. The first set of B and C values was calculated by method one described in the text and in Fig. (V.6), and the results of (η/T) versus τ_R are indicated by (o). The second set of B and C values was calculated by method two and the results of (η/T) versus τ_R are indicated by (□). The third set of B and C values was calculated by method three, and the results of (η/T) versus τ_R are indicated by (▽). The fourth set of B and C values was calculated by method four and the results of (η/T) versus τ_R are indicated by (Δ). Disagreements became pronounced at low values of temperature.

temperature ranges were used for subsequent calculations. The values of A_{iso}^H and λ used in the different temperature ranges were

Temperature Range (K)	A_{iso}^H (Gauss)	λ
295→235	0.26	0.47
225→215	0.28	0.42
205	0.28	0.58
195	0.28	0.77
185	0.30	0.96

These values were used to generate a list of intrinsic linewidths by the GSUMHP-program.

The generated list was used in the T22-program to obtain the B and C values which are presented in Table V.6. Based on these experimental C values, the reorientational correlation times τ_R for the spectra at different temperatures, and the corresponding theoretical B and C values were calculated using the BCT1- and the ABCI-programs. The same calculations could be based upon the values of B rather than C values (when the calculation was based on C values, reasonable agreement with the values of B was maintained, and vice versa). Correlation times fitted by either reproducing experimental B or C values are shown in Figure V.8. Similar results were obtained when either B or C values were used. Correlation times calculated hereafter were fitted by reproducing experimental C values.

**TABLE V.6. Experimental Values of B and C for
BBTMPO in Toluene at X-Band.**

TEMP (K)	M_I	B(Gauss)	C(Gauss)	C/B
295.6	+1	.03862554	.02560240	.66284
295.6	0	.03832108	.02540368	.66292
295.6	-1	.03860146	.02558941	.66291
275.0	+1	.05123150	.03600633	.70282
275.0	0	.05178601	.03642088	.70330
275.0	-1	.05058050	.03554213	.70268
265.0	+1	.05378139	.03928697	.73049
265.0	0	.05392390	.03951353	.73276
265.0	-1	.05383104	.03936595	.73129
255.0	+1	.05772036	.04430467	.76757
255.0	0	.05635625	.04327410	.76787
255.0	-1	.05763006	.04415560	.76619
245.0	+1	.07551152	.06402975	.84795
245.0	0	.07810193	.06629246	.84879
245.0	-1	.07665485	.06498069	.84770
235.0	+1	.08552986	.07446188	.87060
235.0	0	.08533490	.07422531	.86981
235.0	-1	.08566916	.07462204	.87105
225.0	+1	.26045010	.19770010	.75907
225.0	0	.25879870	.19633360	.75863
225.0	-1	.25041600	.18963680	.75729
215.0	+1	.40586870	.27339450	.67360
215.0	0	.40983870	.27594540	.67330
215.0	-1	.37203170	.24776480	.66598
205.0	+1	.76552230	.48163280	.62916
205.0	0	.75186440	.47237830	.62828
205.0	-1	.65699810	.40600220	.61797
195.0	+1	1.42030300	.90125410	.63455
195.0	0	1.36491100	.86401340	.63302
195.0	-1	1.27831200	.80597060	.63050
185.0	+1	2.73121900	1.92535100	.70494
185.0	0	2.72807900	1.92313200	.70494
185.0	-1	2.51012800	1.76620900	.70363

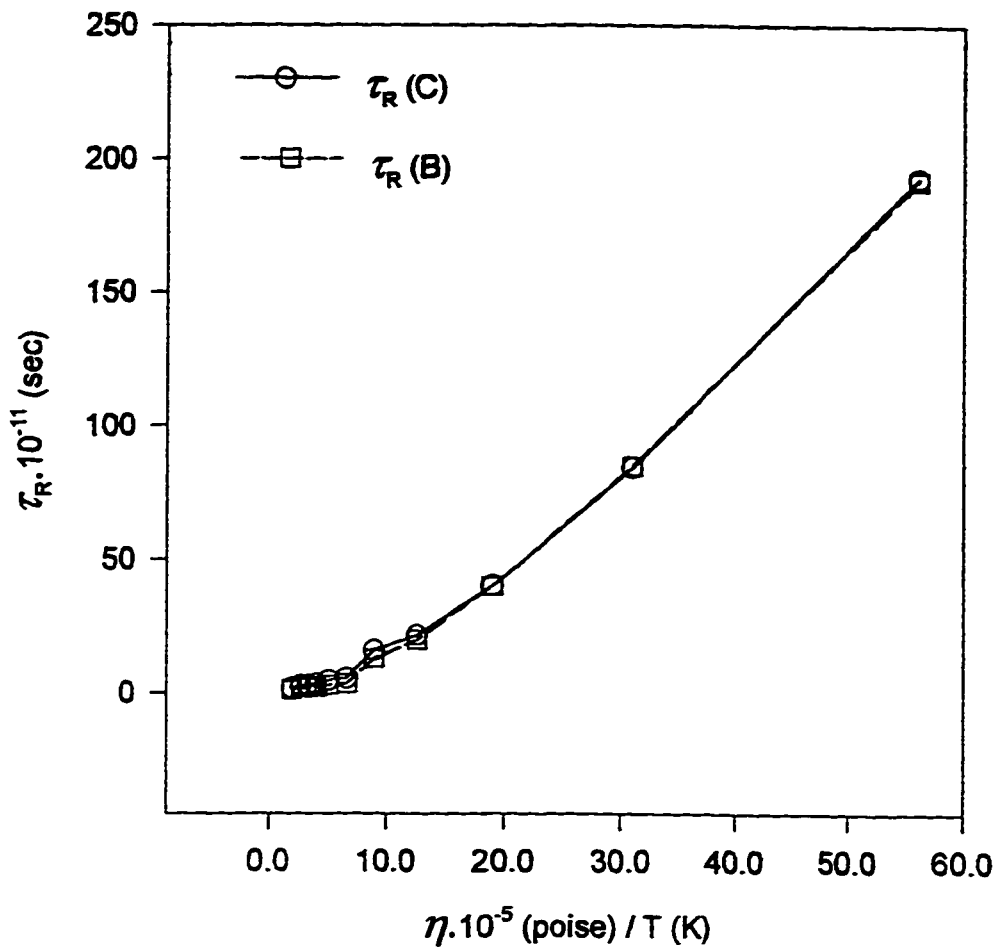


Figure V.8. Shear viscosity η over temperature versus correlation times for BBTMPO in toluene. Correlation times were calculated by fitting either experimental B or C values, $\tau_R(B)$ and $\tau_R(C)$, respectively. Similar results were obtained when either values were used.

The parameters used in the calculations of τ_R for BBTMPO in toluene at X-band (after experimenting with $z' = X, Y, \text{ or } Z$; $N = 1$ to 20 ; $\beta = 0.10$ to 4.0 , $\varepsilon = 1$ to 20 ; and $\varepsilon' = 1$ to 20) were $z' = X$, $N = 7.0$, $\beta = 1.0$, and $\varepsilon = \varepsilon' = 1.0$. Curves of the experimental and theoretical results of B versus C , and of η/T versus τ_R values are shown in Figure V.9. The slope of the (η/T) versus τ_R curve is $(1.31 \pm 0.20) \times 10^{-6} \text{ s.K.P}^{-1}$, and with r_0 equal to 5.6 \AA , the value of the anisotropic interaction parameter κ came out to be 0.25 ± 0.04 .

V.4.2. L-Band

BBTMPO in toluene was studied at L-Band ($\sim 1 \text{ GHz}$), with 100-kHz field modulation, over a range of temperatures from 155 to 295 K and selected experimental spectra are presented in Figure V.10. The well-resolved first-derivative three-peak spectra were observed up to a temperature of $\sim 175.0 \text{ K}$. The first-derivative peak corresponding to $M_I = 0$ was the sharpest as this temperature was approached. The results of the linewidth analysis, which was performed by the LWA-program, are given in Table V.7.

The decay behaviors of the experimental spectra at the different temperatures were calculated using the EXDEL-program. The results of the simulation, which were performed using the HGSUMJH-program, and the corresponding experimental spectra are given in Fig. V.11. Half of each spectrum is shown, since as was mentioned earlier the first derivative EPR spectrum is symmetrical about the central field. Clearly, the match between

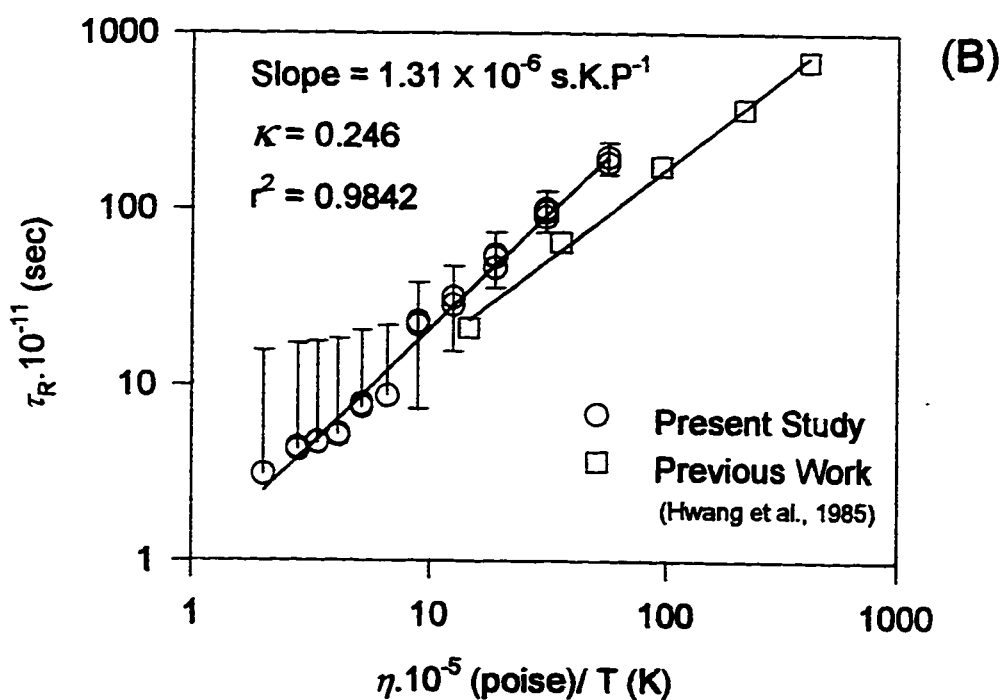
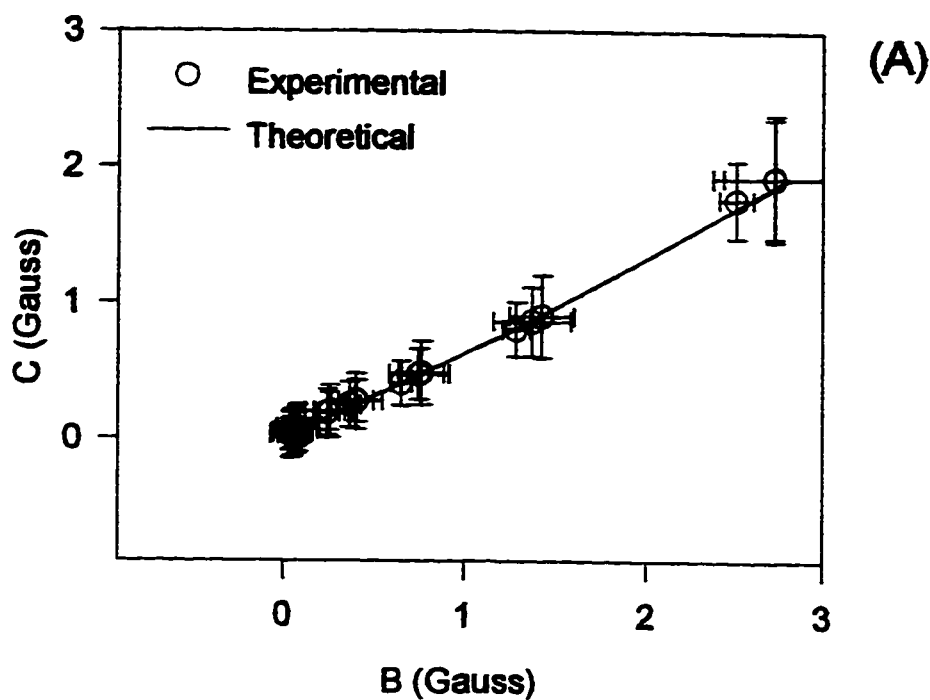


Figure V.9. (A): Experimental and theoretical values of B and C for BBTMPO in toluene at X-Band. The parameters used were $z'=X$, $N=7.0$, $\beta = 1.0$, $\varepsilon = \varepsilon' = 1.0$. (B): η/T versus the reorientational correlation time τ_R for the same system. η is the calculated coefficient of shear viscosity at different toluene temperatures.

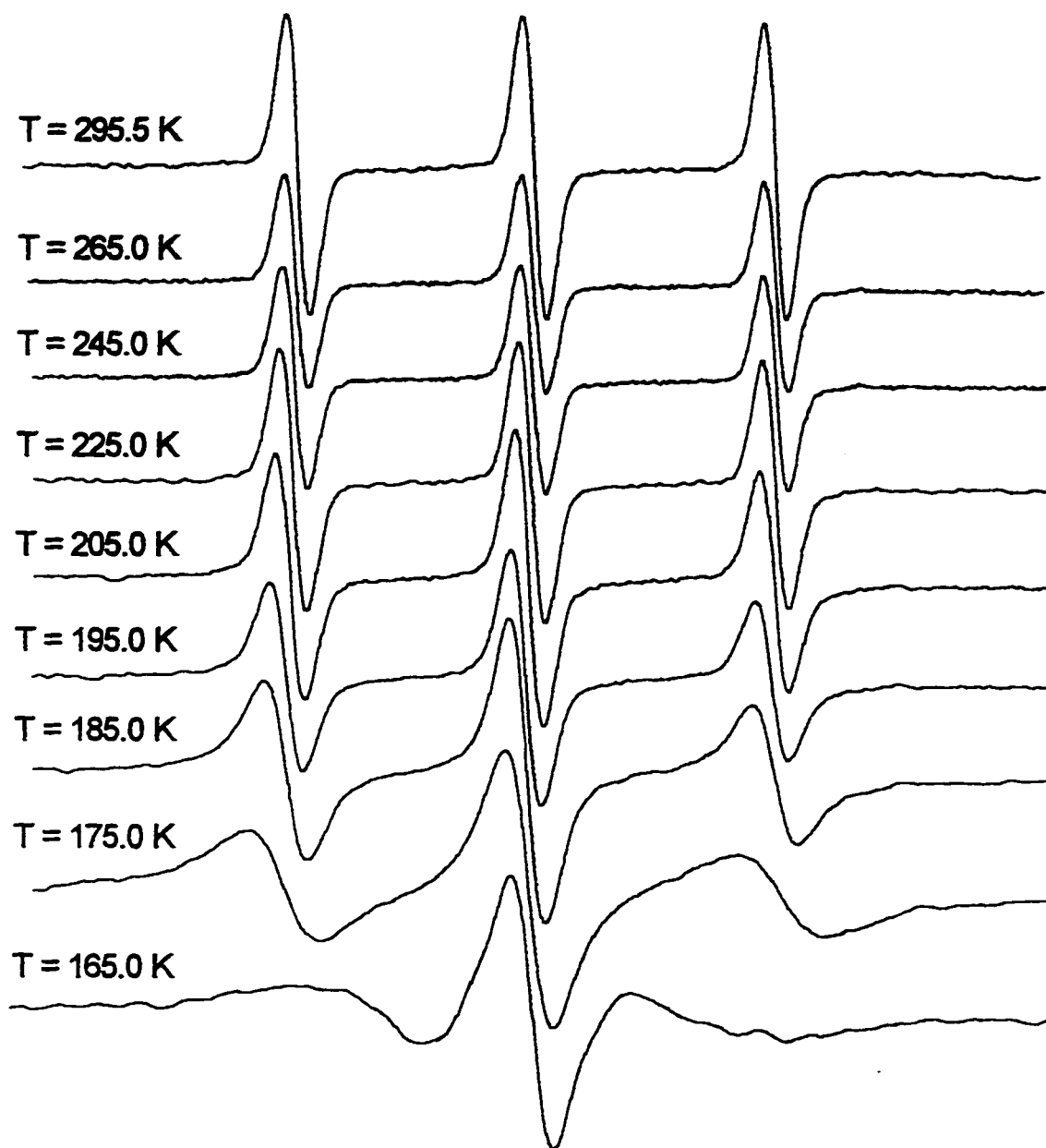


Figure V.10. Selected experimental EPR spectra of BBTMPO in toluene at L-Band and at different temperatures.

TABLE V.7. Linewidth Analysis of BBTMPO in Toluene at L-Band.

TEMP. (K)	$M_I = +1$				$M_I = 0$				$M_I = -1$			
	OLW (GAUSS)	PTPI	CFLD (GAUSS)	OLW (GAUSS)	PTPI	CFLD (GAUSS)	OLW (GAUSS)	PTPI	CFLD (GAUSS)	OLW (GAUSS)	PTPI	CFLD (GAUSS)
295.5	1.5885	.3515E+005	381.4564	1.5884	.3528E+005	396.6421	1.5884	.3455E+005	412.4632			
275.0	1.5249	.3606E+005	381.2340	1.5884	.3643E+005	396.4515	1.6520	.3576E+005	412.3044			
265.0	1.5885	.3721E+005	381.0752	1.5249	.3799E+005	396.3562	1.7155	.3665E+005	412.2091			
255.0	1.7155	.3760E+005	380.9481	1.6520	.3820E+005	396.2291	1.7156	.3704E+005	412.0820			
245.0	1.5885	.9536E+004	380.7574	1.7156	.9838E+004	396.0067	1.7156	.9341E+004	411.9549			
245.0	1.6520	.3890E+005	380.7892	1.6520	.3988E+005	396.0385	1.7791	.3759E+005	411.9232			
235.0	1.7791	.9891E+004	380.6622	1.7791	.1009E+005	395.9750	1.7790	.9345E+004	411.8596			
235.0	1.7155	.3978E+005	380.6304	1.6520	.4082E+005	395.9749	1.7155	.3805E+005	411.8914			
225.0	1.7791	.9182E+004	380.5351	1.7155	.9829E+004	395.8797	1.8426	.8706E+004	411.8278			
225.0	1.8426	.3774E+005	380.5668	1.7155	.4043E+005	395.8797	1.8426	.3556E+005	411.8278			
215.0	1.9062	.8536E+004	380.4715	1.7791	.9554E+004	395.7844	1.9061	.7791E+004	411.7961			
215.0	1.7791	.3483E+005	380.4716	1.7791	.3927E+005	395.7844	1.8426	.3280E+005	411.8278			
205.0	1.9697	.7174E+004	380.3127	1.9062	.8576E+004	395.7208	2.0332	.6322E+004	411.7325			
205.0	1.9061	.2867E+005	380.3445	1.8427	.3471E+005	395.7526	2.0332	.2571E+005	411.7325			
195.0	2.1603	.5444E+004	380.2810	2.0333	.7398E+004	395.6573	2.3509	.4463E+004	411.7008			
195.0	2.1603	.2203E+005	380.2810	2.0333	.2997E+005	395.6573	2.2239	.1853E+005	411.7008			
185.0	2.9228	.3894E+004	380.0903	2.4145	.6397E+004	395.6573	3.1770	.3006E+004	411.8596			
185.0	2.8593	.1574E+005	380.1221	2.4145	.2668E+005	395.6573	3.0499	.1220E+005	411.7961			
175.0	4.2570	.1817E+004	379.8679	2.9863	.4589E+004	395.7526	4.8925	.1292E+004	412.0820			
175.0	4.5747	.1436E+005	380.0268	3.1134	.3648E+005	395.7526	5.7820	.1056E+005	412.1455			

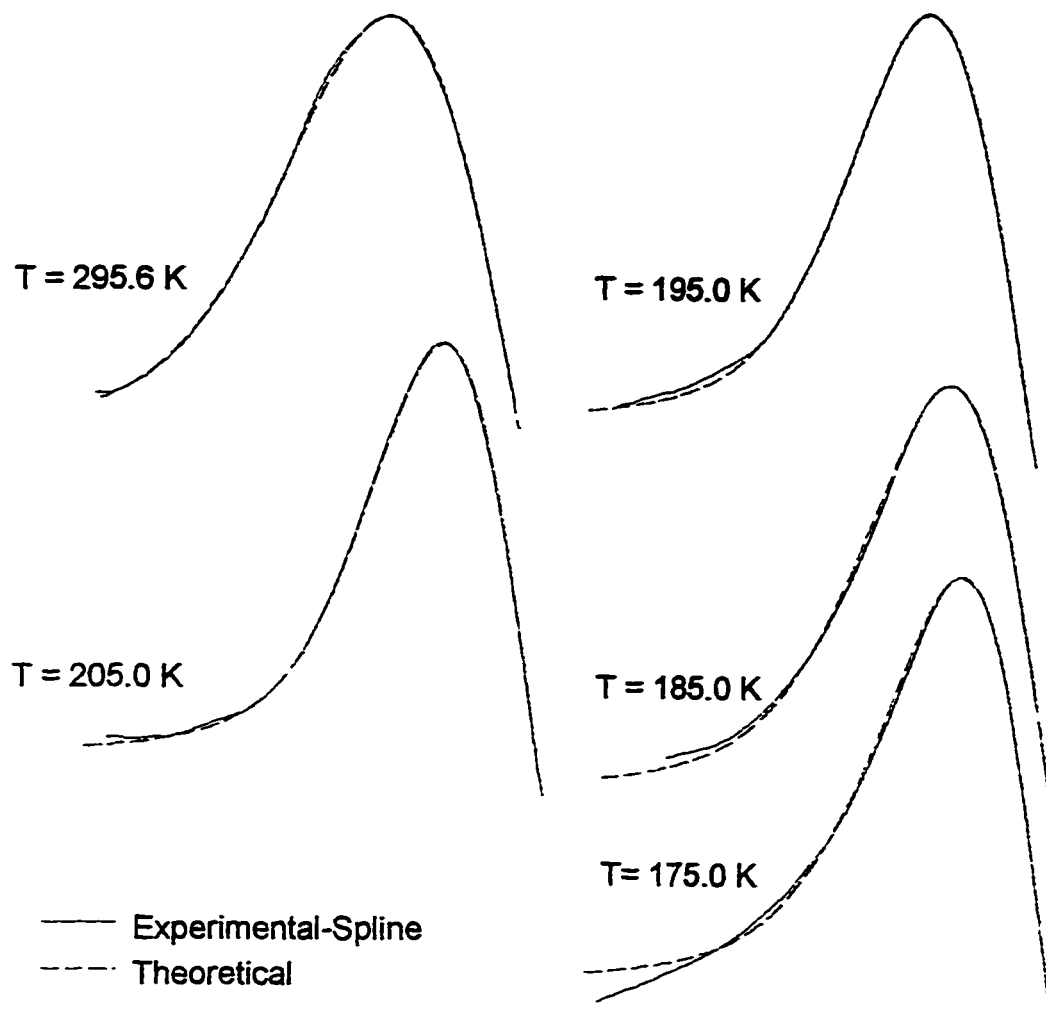


Figure V.11. Theoretical simulation of experimental EPR spectra of BBTMPO in toluene at L-Band and at different experimental temperatures. Simulation was performed by considering both Lorentzian and Gaussian contributions to the shape of the line. Parameters determined from these simulations are listed in Table (V.8). Cubic spline interpolation was performed for the experimental curves.

experimental and theoretical curves is satisfactory. Experimental curves were processed by the INTERP-program to obtain spectra of higher resolution. The parameters determined from these theoretical simulations, namely the isotropic hyperfine coupling coefficient for hydrogen, A_{iso}^H , the mixing factor λ , the intrinsic linewidth, and the theoretically calculated observed linewidth, are listed in Table V.8. The values of A_{iso}^H and λ used in calculating the intrinsic linewidths for the different temperature ranges were

Temperature Range (K)	A_{iso}^H (Gauss)	λ
295→225	0.28	0.44
215→205	0.28	0.58
195→175	0.28	0.68

These values were used to generate a list of intrinsic linewidths by the GSUMHP-program.

This list was used by the T22-program to obtain the experimental B and C values which are presented in Table V.9. Based on the experimental C values calculated by using the different values of A_{iso}^H and λ , the reorientational correlation times τ_R for the spectra at different temperatures, and the corresponding theoretical B and C values were calculated using the BCT1- and the ABCI-programs. The parameters used in these calculations (after experimenting with $z' = X, Y, \text{ or } Z$; $N = 1 \text{ to } 20$; $\beta = 0.1 \text{ to } 4.0$, $\varepsilon = 1 \text{ to } 20$; and $\varepsilon' = 1 \text{ to } 20$) are $z' = X$, $N = 7.0$, $\beta = 0.70$, and $\varepsilon = \varepsilon' = 1.0$. Curves of the experimental

TABLE V.8. Parameters Determined from the Theoretical Simulation Shown in Fig. (V.11) for BBTMPO in Toluene at L-Band.

T (K)	$\$ A_{120}^H$ (G)	Mixing Factor λ	Experimentally Observed Linewidth (G)	Theoretical Observed Linewidth (G)	Intrinsic Linewidth (G)
295.6	0.28 ± 0.01	0.44 ± 0.02	1.5805	1.5841 ± 0.0010	1.190 ± 0.001
205.0	0.28 ± 0.01	0.58 ± 0.02	1.8533	1.8514 ± 0.0010	1.510 ± 0.001
195.0	0.28 ± 0.01	0.68 ± 0.04	2.0015	2.0240 ± 0.0030	1.700 ± 0.001

$\$ A_{120}^H$ is the hydrogen isotropic hyperfine coupling coefficient.

**TABLE V.9. Experimental Values of B and C for
BBTMPO in Toluene at L-Band.**

TEMP. (K)	M_I	B (Gauss)	C (Gauss)	C/B
295.6	+1	.00840867	.01196516	1.42296
295.6	0	.00835848	.01190388	1.42417
295.6	-1	.00828731	.01182711	1.42713
265.0	+1	.00740635	.02736485	3.69478
265.0	0	.00739485	.02734643	3.69804
265.0	-1	.00766981	.02819979	3.67673
255.0	+1	.00759041	.02358699	3.10747
255.0	0	.00745809	.02331734	3.12645
255.0	-1	.00759369	.02323920	3.06033
245.0	+1	.01691449	.04144049	2.45000
245.0	0	.01679713	.04128712	2.45799
245.0	-1	.01753509	.04266620	2.43319
235.0	+1	.02246481	.04831094	2.15052
235.0	0	.02202326	.04744476	2.15430
235.0	-1	.02219844	.04784739	2.15544
225.0	+1	.02755558	.09678411	3.51232
225.0	0	.02781034	.09778821	3.51625
225.0	-1	.02779531	.09766948	3.51388
215.0	+1	.03052515	.14940760	4.89457
215.0	0	.03156197	.15435360	4.89049
215.0	-1	.03061533	.14985840	4.89488
205.0	+1	.05869639	.25475080	4.34015
205.0	0	.06156379	.26639670	4.32717
205.0	-1	.05945730	.25745400	4.33007
195.0	+1	.10313590	.43768960	4.24381
195.0	0	.10909440	.46202470	4.23509
195.0	-1	.09874064	.42043180	4.25794
185.0	+1	.19938610	.89740200	4.50082
185.0	0	.21265040	.95414650	4.48693
185.0	-1	.18900310	.85317030	4.51405
175.0	+1	.38334230	2.13072300	5.55828
175.0	0	.41037270	2.27701400	5.54865
175.0	-1	.41579600	2.30607500	5.54617

and theoretical results of B and C, and of τ_R values versus η/T are shown in Figure V.12. The slope of the (η/T) versus τ_R curve is $(1.23 \pm 0.08) \times 10^{-6}$ s.K.P⁻¹ and the value of the anisotropic interaction parameter κ was calculated and found to be equal to 0.23 ± 0.02 .

V.4.3. S-Band

Figure V.13 shows representative spectra of BBTMPO in toluene at S-Band (~4 GHz), with 12.5-KHz field modulation, which was studied over a range of temperatures from 111 to 295 K. The well-resolved first-derivative three-peak spectra were observed up to a temperature of ~180 K. The first-derivative peak corresponding to $M_I = 0$ was the sharpest as this temperature was approached. The results of the linewidth analysis, which was performed by the LWA-program, are given in Table V.10.

Lineshape simulations of half of the first peak ($M_I = +1$) for the spectra at the three temperatures 295.0, 210, and 190 K are shown in Figure V.14. At 295.0 K, the simulation was performed with an A_{iso}^H of 0.26 G and a mixing factor λ of 0.47. The theoretically calculated observed linewidth was 1.5201 G, which corresponded to an intrinsic linewidth of 1.170 G. At T = 210 K, the values of A_{iso}^H and λ were, respectively, 0.28 G and 0.72, while at T = 190 K, the values of A_{iso}^H and λ were 0.30 G and 0.94, respectively. The theoretically calculated observed linewidths for T=210 and 190 K were 1.9261 G and 2.6392 G, respectively, and the intrinsic linewidths were 1.754 G and 2.260 G,

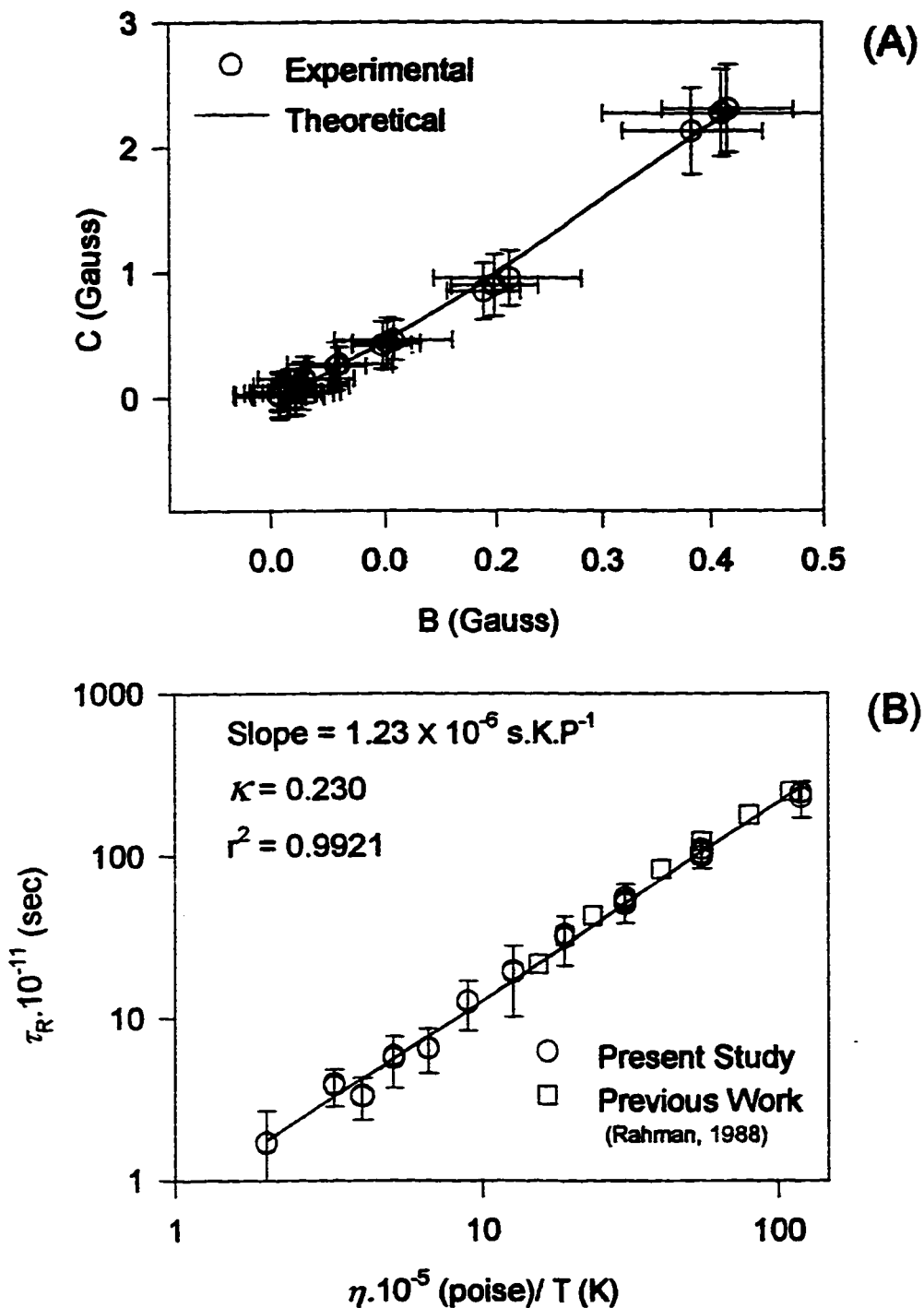


Figure V.12. (A): Experimental and theoretical values of B and C for BBTMPO in toluene at L-Band. The parameters used were $z^*=X$, $N = 7.0$, $\beta = 0.70$, $\varepsilon = \varepsilon^* = 1.0$. (B): η/T versus the reorientational correlation time τ_R for the same system. η is the calculated coefficient of shear viscosity at different toluene temperatures.

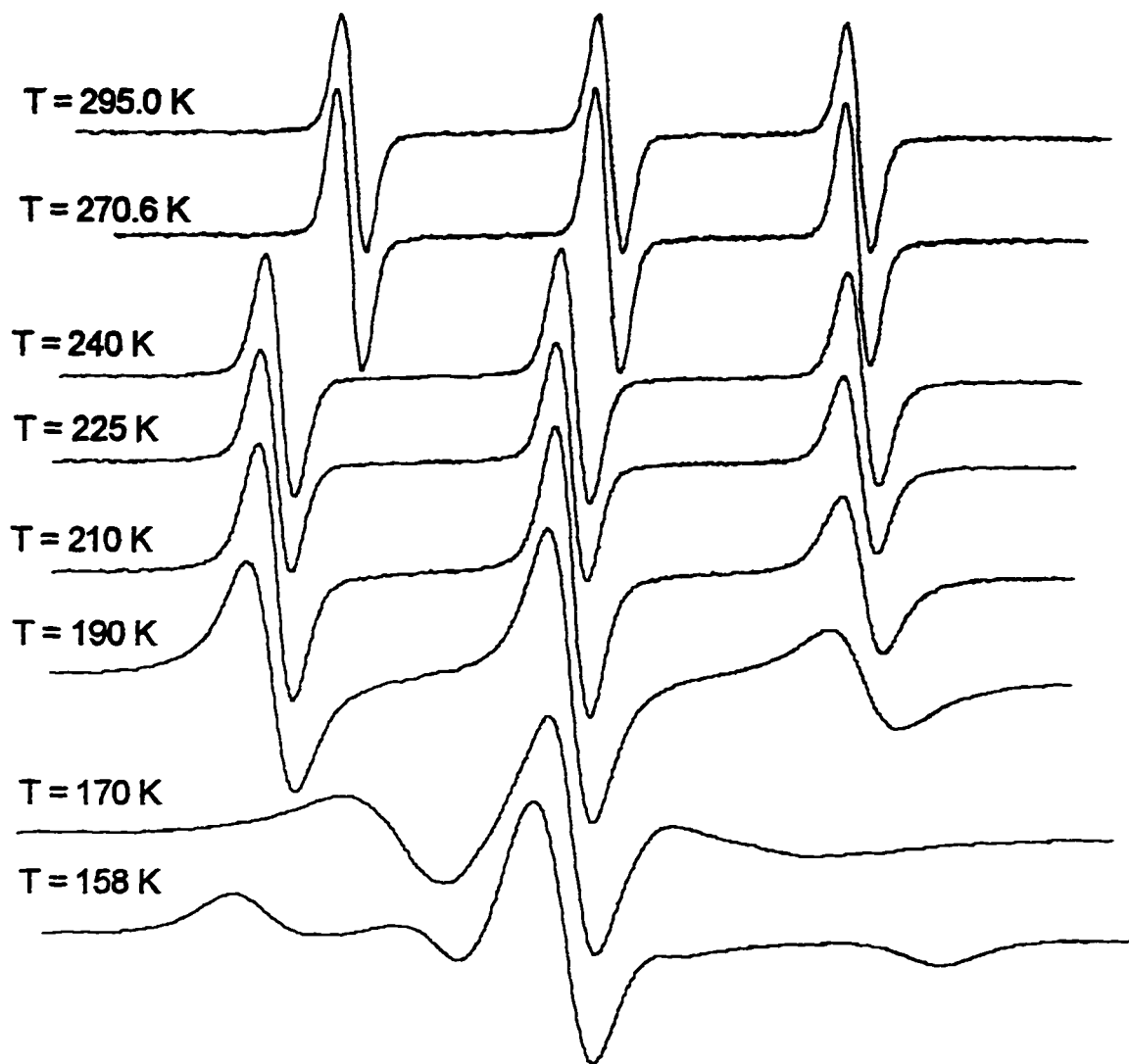


Figure V.13. Selected experimental EPR spectra of BBTMPO in toluene at S-Band and at different temperatures.

TABLE V.10. Linewidth Analysis of BBTMPO in Toluene at S-Band.

TEMP. (K)	$M_I = +1$				$M_I = 0$				$M_I = -1$			
	OLW (GAUSS)	PTPI	CFLD (GAUSS)	OLW (GAUSS)	PTPI	CFLD (GAUSS)	OLW (GAUSS)	PTPI	CFLD (GAUSS)	OLW (GAUSS)	PTPI	CFLD (GAUSS)
295.0	1.5660	.1155E+005	1407.7061	1.4876	.1158E+005	1423.0919	1.5660	.1111E+005	1438.6343			
278.9	1.4877	.1465E+005	1402.5776	1.4877	.1465E+005	1418.0025	1.5660	.1386E+005	1433.6231			
272.4	1.5660	.6530E+004	1402.0686	1.4877	.6487E+004	1417.5327	1.5659	.6113E+004	1433.1534			
270.6	1.4876	.1029E+005	1405.4746	1.5660	.1040E+005	1420.9387	1.6443	.9619E+004	1436.5594			
250	1.6442	.1186E+005	1406.1010	1.5660	.1219E+005	1421.5651	1.6443	.1091E+005	1437.1858			
240	1.6485	.1186E+005	1406.1654	1.5953	.1240E+005	1421.6665	1.8080	.1033E+005	1437.4068			
225	1.7548	.1084E+005	1406.2185	1.7548	.1162E+005	1421.7462	1.9143	.8588E+004	1437.5132			
210	1.9144	.1571E+005	1406.2451	1.9144	.1779E+005	1421.8791	2.3929	.9573E+004	1437.6993			
190	2.7121	.1411E+005	1406.1122	2.4994	.1799E+005	1421.9057	3.6692	.6007E+004	1437.9651			
170	6.1614	.1929E+004	1404.3875	4.4966	.1175E+005	1421.7369	*****	.9272E+003	1457.7584			

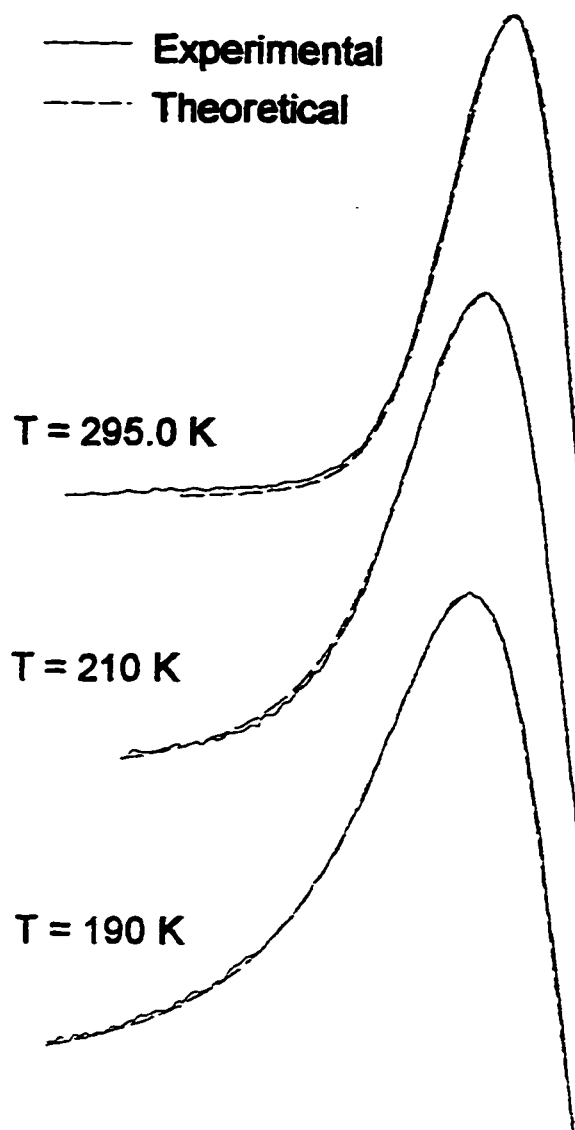


Figure V.14. Theoretical simulation of experimental EPR spectra of BBTMPO in toluene at S-Band and at different experimental temperatures. Simulation was performed by considering both Lorentzian and Gaussian contributions to the shape of the line.

respectively. The experimentally observed linewidths for T=295.0, 210 and 190 K were 1.5132, 1.9266 G and 2.6432 G, respectively. The Figure shows acceptable match between experimental and theoretical results. The simulations were calculated using the HGSUMJH-program. The values of A_{∞}^H and λ used in calculating the intrinsic linewidths for the different temperature ranges were

Temperature Range (K)	A_{∞}^H (Gauss)	λ
295→240	0.26	0.47
225→210	0.28	0.72
190→170	0.30	0.94

These values were used to generate a list of intrinsic linewidths by the GSUMHP-program.

The generated list was, then, used in the T22-program to obtain the experimental B and C values which are presented in Table V.11. Based on the experimental C values, the reorientational correlation times τ_R for the spectra at different temperatures, and the corresponding theoretical B and C values were calculated using the BCT1- and the ABCI-programs. The parameters used in these calculations (after experimenting with $z' = X, Y, \text{ or } Z$; $N = 1 \text{ to } 20$; $\beta = 0.1 \text{ to } 4.0$, $\varepsilon = 1 \text{ to } 20$; and $\varepsilon' = 1 \text{ to } 20$) are $z' = X$, $N = 7.0$, $\beta = 0.70$, and $\varepsilon = \varepsilon' = 1.0$. Curves of the experimental and theoretical results of B and C, and of η/T versus τ_R values are shown in Figure V.15. The slope of the (η/T) versus τ_R curve is

**TABLE V.11. Experimental Values of B and C for
BBTMPO in Toluene at S-Band.**

TEMP (K)	M_r	B (Gauss)	C (Gauss)	C/B
295.0	+1	.01758885	.01993227	1.13323
295.0	0	.01746166	.01978195	1.13288
295.0	-1	.01790792	.02026731	1.13175
279.0	+1	.02548027	.02548027	1.00000
279.0	0	.02496040	.02496040	1.00000
279.0	-1	.02544570	.02544570	1.00000
272.4	+1	.03024399	.02425528	.80199
272.4	0	.02970546	.02379459	.80102
272.4	-1	.03022581	.02424783	.80222
270.4	+1	.03130817	.04106736	1.31171
270.4	0	.03131717	.04106492	1.31126
270.4	-1	.03169721	.04172164	1.31626
259.4	+1	.03868783	.06403244	1.65511
259.4	0	.03927809	.06440252	1.63966
259.4	-1	.03921431	.06433147	1.64051
250.6	+1	.06794989	.11055060	1.62694
250.6	0	.06651682	.10810580	1.62524
250.6	-1	.06835395	.11122700	1.62722
241.8	+1	.11702410	.18328650	1.56623
241.8	0	.11983640	.18787680	1.56778
241.8	-1	.11557690	.18137090	1.56927
229.8	+1	.28172460	.40734180	1.44589
229.8	0	.29738100	.42924800	1.44343
229.8	-1	.28136840	.40676460	1.44567
241.8	+1	.11729060	.18405390	1.56921
241.8	0	.11982420	.18786270	1.56782
241.8	-1	.11557690	.18137090	1.56927
230.2	+1	.28509980	.41230350	1.44617
230.2	0	.29587660	.42748760	1.44482
230.2	-1	.28136840	.40676460	1.44567
215.2	+1	.70074010	1.01083000	1.44252
215.2	0	.72105720	1.03975300	1.44198
215.2	-1	.64526960	.93243220	1.44503
194.2	+1	1.35484400	5.07325100	3.74453
194.2	0	-1.44117100	3.72620700	-2.58554

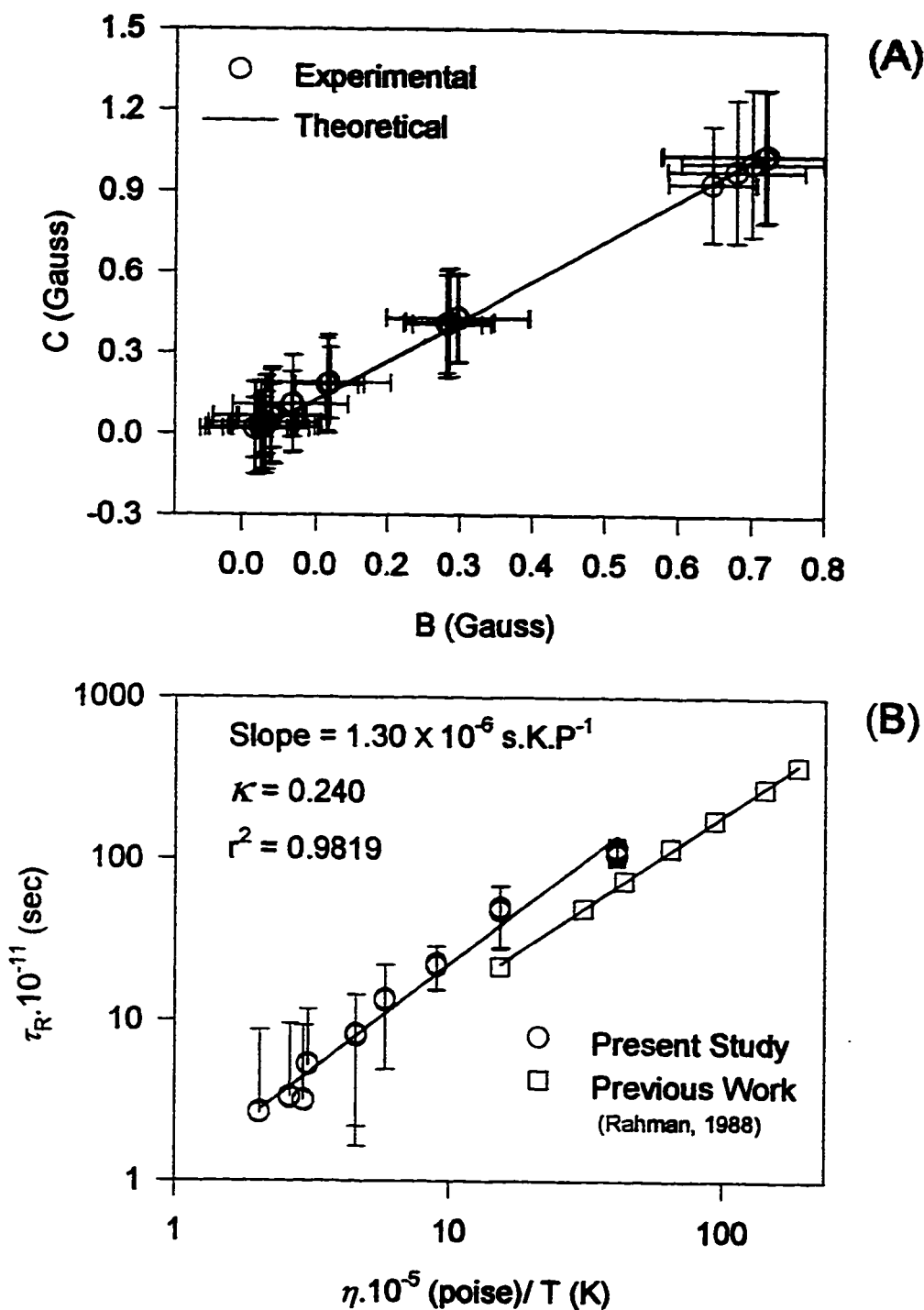


Figure V.15. (A): Experimental and theoretical values of B and C for BBTMPO in toluene at S-Band. The parameters used were $z'=X$, $N = 7.0$, $\beta = 0.70$, $\varepsilon = \varepsilon' = 1.0$. (B): η/T versus the reorientational correlation time τ_R for the same system. η is the calculated coefficient of shear viscosity at different toluene temperatures.

$(1.3 \pm 0.4) \times 10^{-6} \text{ s.K.P}^{-1}$ and the value of the anisotropic interaction parameter κ was calculated and came out to be equal to 0.24 ± 0.08 .

V.4.4. Q-Band

The spectra of BBTMPO in toluene at Q-Band (~34 GHz), with 12.5-KHz field modulation, were taken over a range of temperatures from 126 to 295 K and representative spectra are shown in Figure V.16. The well-resolved first-derivative three-peak spectra were observed up to a temperature of ~145.0 K. The first-derivative peak corresponding to $M_I = +1$ was the sharpest as this temperature was approached. The results of the linewidth analysis, which was performed by the LWA-program, are given in Table V.12.

Lineshape simulations of half of the first peak ($M_I = +1$) for the spectra at the temperatures 295.0, and 215.0 K are shown in Figure V.17. At 295.0 K, the peak from a three-peak spectrum was processed by the INTERP-program. The parameters for simulation for this spectrum were an A_{iso}^H of 0.26 G and a mixing factor λ of 0.68. The theoretically calculated observed linewidth was 1.7399 G, which corresponded to an intrinsic linewidth of 1.410 G. The experimentally observed linewidth was 1.7400 G. At $T = 215.0$ K, the values of A_{iso}^H and λ were 0.392 G and 1.00, respectively. The theoretically calculated observed linewidth for the spectrum at $T = 215.0$ K was 1.800 G, and the intrinsic linewidth was 0.60 G. The experimentally observed linewidth for $T = 215.0$ K was 1.8000 G. In addition, at $T = 165.0$ K, the values of A_{iso}^H and λ were 0.26 G and 0.84,

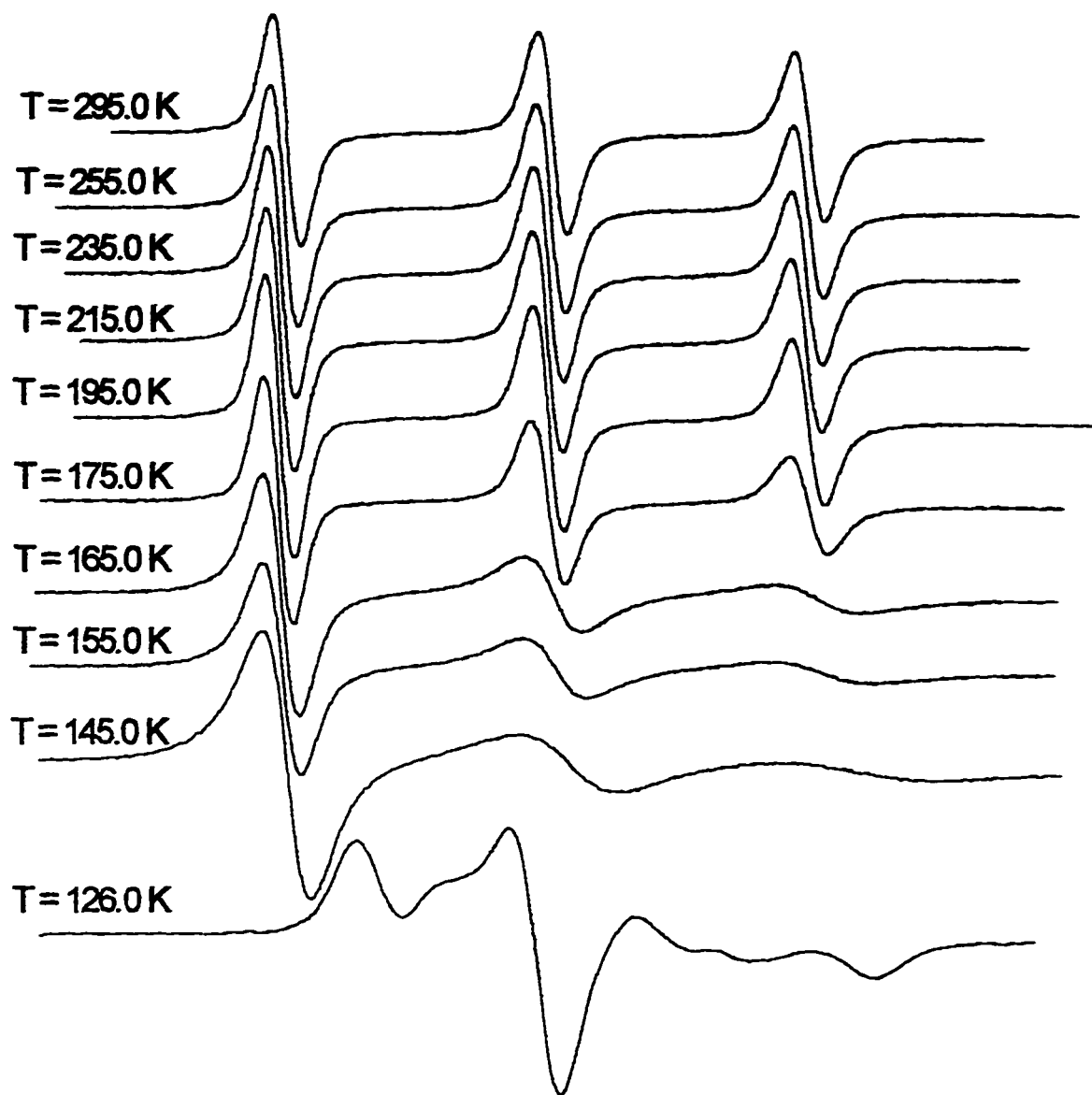


Figure V.16. Selected experimental EPR spectra of BBTMPO in toluene at Q-Band and at different temperatures.

TABLE V.12. The Linewidth Analysis of BBTMPO in Toluene at Q-Band.

TEMP. (K)	$M_I = +1$				$M_I = 0$				$M_I = -1$			
	OLW (GAUSS)	PTPI	CFLD (GAUSS)	OLW (GAUSS)	PTPI	CFLD (GAUSS)	OLW (GAUSS)	PTPI	CFLD (GAUSS)	OLW (GAUSS)	PTPI	CFLD (GAUSS)
295.0	1.7552	.4040E+005	12231.0947	1.8053	.3542E+005	12246.5650	1.8554	.2953E+005	12262.0853			
275.0	1.7551	.4097E+005	12230.0918	1.8053	.3573E+005	12245.7125	1.8555	.2978E+005	12261.2830			
265.0	1.7008	.4176E+005	12229.8158	1.7595	.3624E+005	12245.2704	1.8768	.2988E+005	12260.8715			
255.0	1.7009	.4220E+005	12229.7572	1.8769	.3644E+005	12245.2704	1.9354	.3015E+005	12260.8422			
245.0	1.6422	.4294E+005	12229.3759	1.7595	.3698E+005	12244.9185	1.8768	.3013E+005	12260.4023			
235.0	1.7595	.4386E+005	12229.0827	1.8182	.3750E+005	12244.6545	1.9941	.3030E+005	12260.2264			
225.0	1.7595	.4473E+005	12228.9068	1.8182	.3790E+005	12244.4786	1.9355	.3032E+005	12260.0211			
215.0	1.8182	.4606E+005	12228.1149	1.8768	.3862E+005	12243.6868	1.9355	.3021E+005	12259.2587			
205.0	1.7595	.4838E+005	12228.6135	1.8768	.3928E+005	12244.2146	1.8768	.2965E+005	12259.8158			
195.0	1.7595	.4954E+005	12228.4962	1.8768	.3940E+005	12244.1560	1.9942	.2904E+005	12259.8158			
185.0	1.8182	.4252E+005	12228.2369	1.8768	.3082E+005	12243.8674	2.2288	.2041E+005	12259.5859			
175.0	1.8769	.4318E+005	12227.9144	1.9941	.2861E+005	12243.5742	2.4047	.1709E+005	12259.3220			
165.0	2.1701	.4258E+005	12231.2216	3.1085	.1324E+005	12246.9987	5.3372	.4860E+004	12262.8931			
155.0	2.2288	.3706E+005	12231.4268	3.8710	.1042E+005	12247.3212	6.5689	.3678E+004	12263.3917			
145.0	2.8152	.3137E+005	12231.3095	5.8064	.6590E+004	12247.7611	9.0909	.2077E+004	12265.2392			
126.0	*****	.6984E+004	12200.8292	5.0831	.1950E+005	12234.3092	8.4150	.2923E+004	12264.9012			

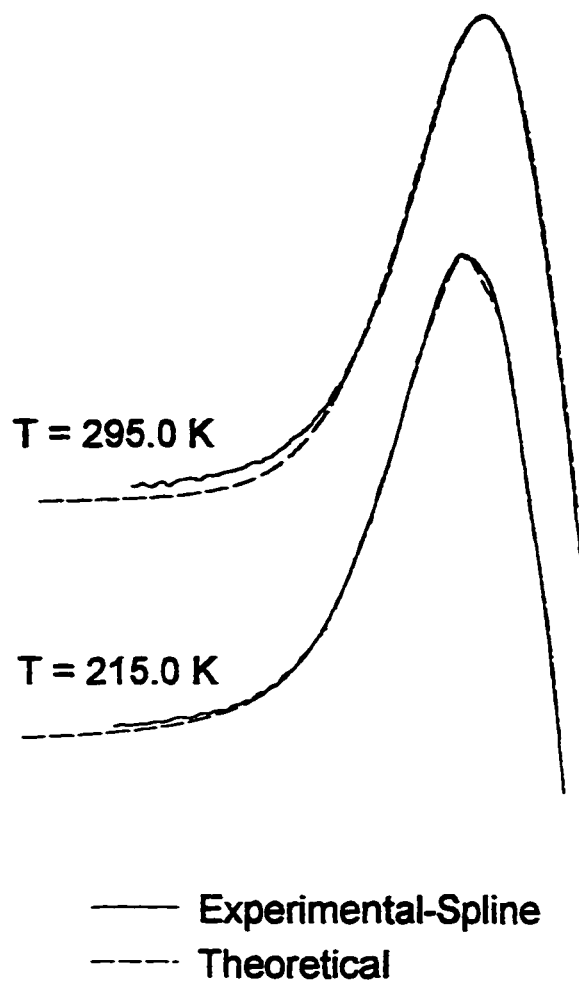


Figure V.17. Theoretical simulation of experimental EPR spectra of BBTMPO in toluene at Q-Band and at different experimental temperatures. Simulation was performed by considering both Lorentzian and Gaussian contributions to the shape of the line. Cubic spline interpolation was performed for the experimental curves.

respectively. The theoretically calculated observed linewidth for the spectrum at $T = 165.0$ K was 2.1500 G, while the experimentally observed linewidth was 2.1421 G. The intrinsic linewidth was 1.8474 G. The Figure shows acceptable match between experimental and theoretical results. The simulations were calculated using the HGSUMJH-program. The values of A_{iso}^H and λ used in calculating the intrinsic linewidths for the different temperature ranges were

Temperature Range (K)	A_{iso}^H (Gauss)	λ
295→225	0.26	0.68
215→145	0.26	0.84

These values were used to generate a list of intrinsic linewidths by the GSUMHP-program.

The generated list was used in the T22-program to obtain the B and C values which are presented in Table V.13. Based on these experimental C values, the reorientational correlation times τ_R for the spectra at different temperatures, and the corresponding theoretical B and C values were calculated using the BCT1- and the ABCI-programs. The parameters used in these calculations (after experimenting with $z' = X, Y, \text{ or } Z$; $N = 1$ to 20; $\beta = 0.1$ to 4.0, $\varepsilon = 1$ to 20; and $\varepsilon' = 1$ to 20) are $z' = X$, $N = 7.0$, $\beta = 1.0$, and $\varepsilon = \varepsilon' = 1.0$. Curves of the experimental and theoretical results of B and C, and of η/T versus τ_R values are shown in Figure V.18.

**TABLE V.13. Experimental Values of B and C for
BBTMPO in Toluene at Q-Band.**

TEMP (K)	M_r	B (Gauss)	C (Gauss)	C/B
295.0	+1	.10544310	.01984075	.18817
295.0	+1	.15809380	.02975905	.18824
295.0	0	.15525030	.02917856	.18795
295.0	-1	.14876600	.02750778	.18491
275.0	+1	.15936150	.02708745	.16997
275.0	0	.15791510	.02681220	.16979
275.0	-1	.15123240	.02531391	.16738
265.0	+1	.16784390	.03065258	.18263
265.0	0	.16256980	.02939343	.18081
265.0	-1	.15977940	.02880830	.18030
255.0	+1	.16775140	.02635330	.15710
255.0	0	.17164150	.02707601	.15775
255.0	-1	.16415890	.02581239	.15724
245.0	+1	.18168210	.03419501	.18821
245.0	0	.17212340	.03206986	.18632
245.0	-1	.16846930	.03128624	.18571
235.0	+1	.19029820	.03551233	.18661
235.0	0	.18462590	.03432637	.18592
235.0	-1	.18384370	.03408545	.18540
225.0	+1	.20083540	.03697568	.18411
225.0	0	.19411380	.03547460	.18275
225.0	-1	.18816880	.03397667	.18056
215.0	+1	.21456100	.04418415	.20593
215.0	0	.20818480	.04246503	.20398
215.0	-1	.19478080	.03932130	.20187
205.0	+1	.25401710	.04998082	.19676
205.0	0	.24192170	.04718405	.19504
205.0	-1	.21784400	.04156435	.19080
195.0	+1	.27531490	.05336875	.19385
195.0	0	.26419100	.05090958	.19270
195.0	-1	.24826600	.04717284	.19001
185.0	+1	.40581800	.08014685	.19749
185.0	0	.36501290	.07036805	.19278
185.0	-1	.36225740	.06983912	.19279
175.0	+1	.55002260	.11448130	.20814
175.0	0	.49044620	.09959662	.20307
175.0	-1	.47228660	.09479415	.20071
165.0	+1	2.04071000	.35725890	.17507
165.0	0	1.72108900	.28978160	.16837
165.0	-1	1.81637400	.31020890	.17078
155.0	+1	2.47123600	.42659590	.17262
155.0	0	2.25101200	.38238480	.16987
155.0	-1	2.29455400	.39120710	.17049
145.0	+1	3.42067200	.12071560	.03529
145.0	0	3.63729300	.44543950	.12246
145.0	-1	3.42075900	.58311010	.17046

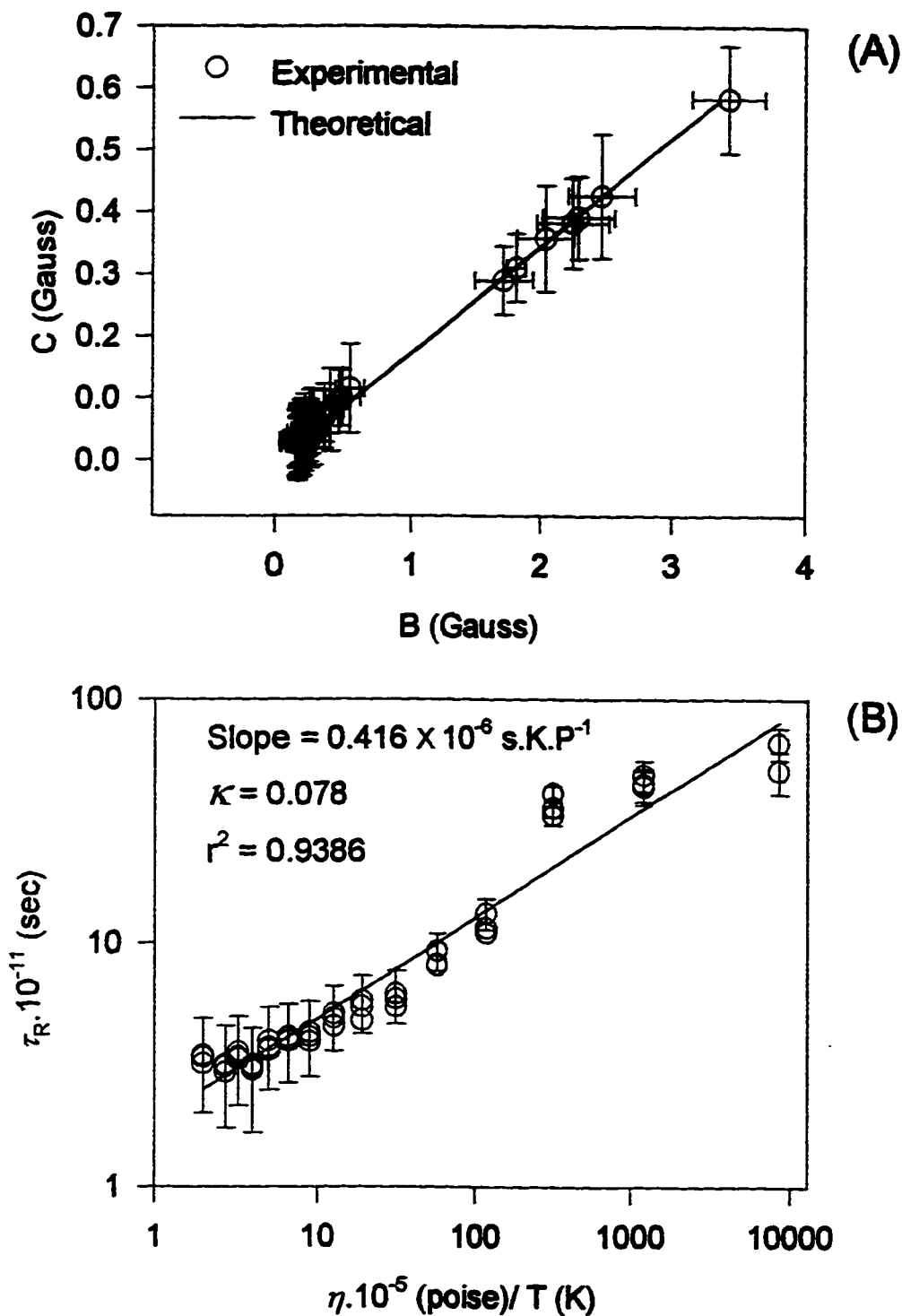


Figure V.18. (A): Experimental and theoretical values of B and C for BBTMPO in toluene at Q-Band. The parameters used were $z'=X$, $N = 7.0$, $\beta = 1.0$, $\varepsilon = \varepsilon' = 1.0$. (B): η/T versus the reorientational correlation time τ_R for the same system. η is the calculated coefficient of shear viscosity at different toluene temperatures.

The slope of the (η/T) versus τ_R curve is $(0.42 \pm 0.02) \times 10^6 \text{ s.K.P}^{-1}$ and the value of the anisotropic interaction parameter κ came out to be equal to 0.08 ± 0.01 .

V.4.5. The Parameter β

As in the analysis of the results of PD-Tempone in toluene (Chapt. III), the Cole-Davidson parameter β proved to be useful in the calculation of B and C coefficients. Figures V.19 and V.20 are plots of B versus C for β values of 1.0 and 0.5, respectively. Figure V.21 is a plot of B versus C for different β values that gave the best fit of the experimental values and with an N value of 7.0. The experimental values of B and C for the L-Band were fit theoretically, when β equals 0.7, with the parameters $z=X$ and $N = 7.0$ (Fig. V.21). However, with $\beta = 1.0$, the best fit of the experimental values of B and C was possible with $N = 12.0$ (Fig. V.19). At S-Band, with $\beta = 1.0$, the best fit of the experimental values of B and C was possible with $N = 9.0$ (Fig. V.19). For an N value of 7.0 and $z=X$, the best fit of the experimental values of B and C at the S-Band was achieved with β equals 0.70 (Fig. V.21). At X-Band, the best fit of the experimental values of B and C was possible when β was set equal to 1.0, z equal to X and N equal to 7.0 (Fig.'s V.19 & V.21). At Q-Band it was not possible to fit the experimental values of B and C with β set equal to 0.5 and N ranging from 5.0 to 11.0 (Fig. V.20). However, when β was set equal to 1.0 an N value of 7.0 gave the best fit

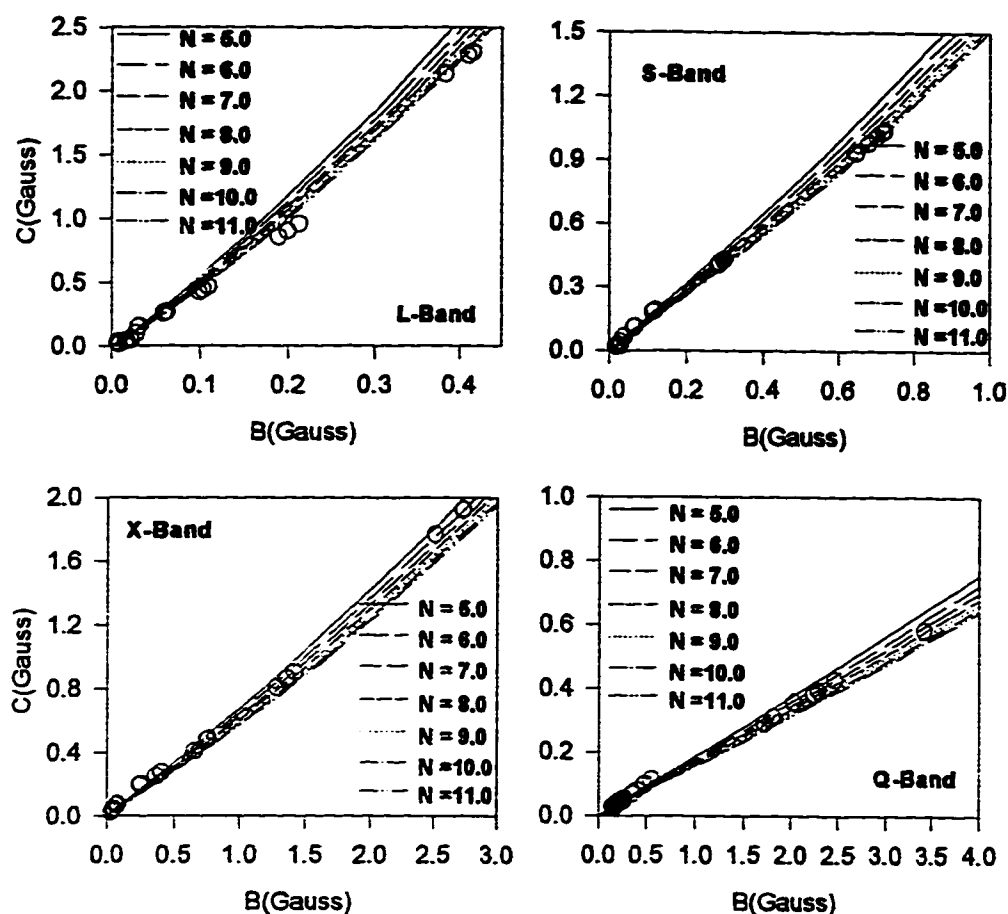


Figure V.19. Experimental values of B versus C of BBTMPO in toluene for the four bands with z' set equal to X , β equal to 1.0 and N values ranging from 5.0 to 11.0. The N values that give the best fit with $\beta=1.0$ for the L-, S-, X-, and Q-Bands are 12.0, 9.0, 7.0, and 7.0, respectively.

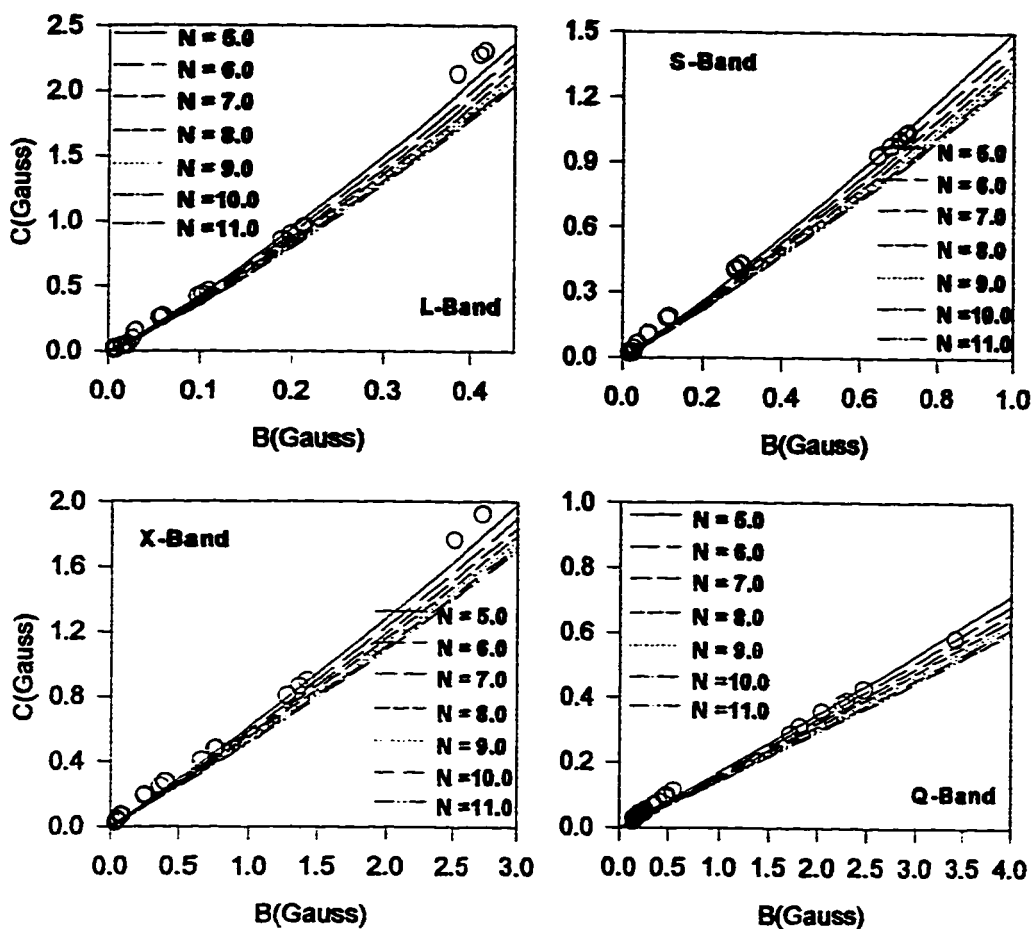


Figure V.20. Experimental values of B versus C of BBTMPO in toluene for the four bands with z' set equal to X, β equal to 0.5 and N values ranging from 5.0 to 11.0. The N values that give the best fit with $\beta=0.5$ for the L-, S-, X-, and Q-Bands are 5.0, 5.0, 4.0, and 4.0, respectively.

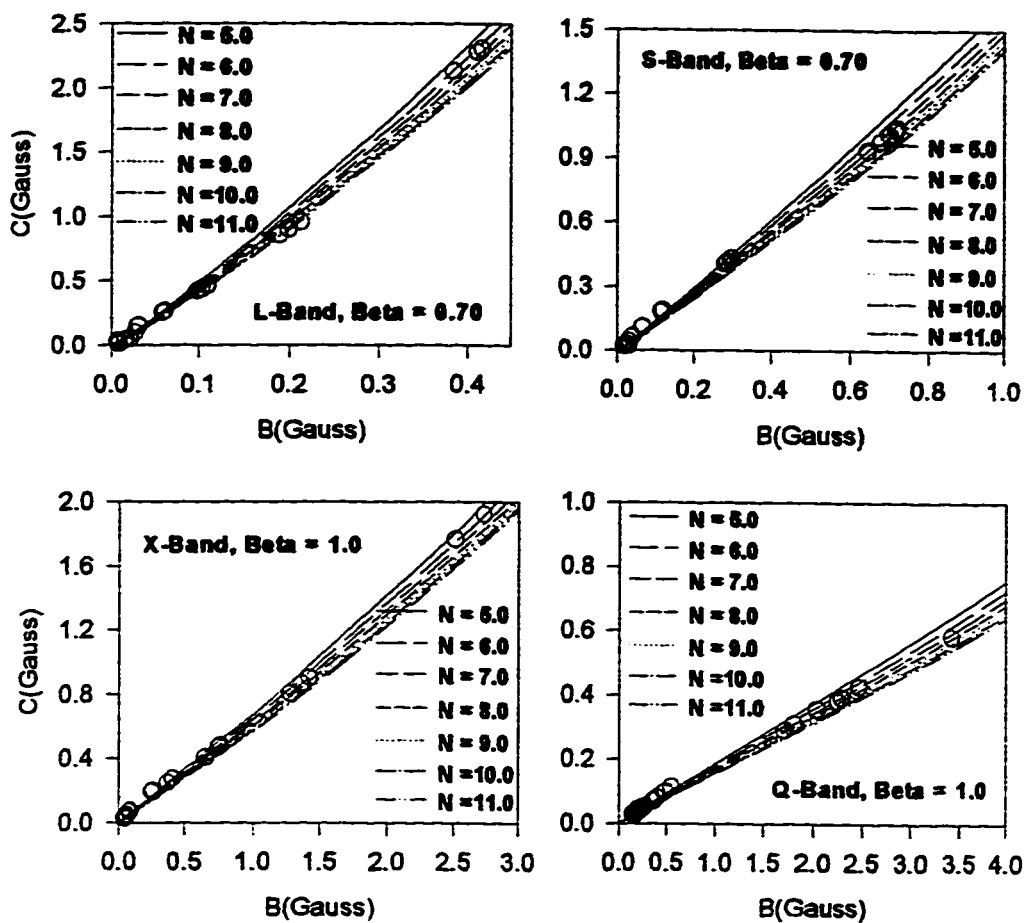


Figure V.21. Experimental values of B versus C of BBTMPO in toluene for the four bands with z' set equal to X and N values ranging from 5.0 to 11.0. The β values that give the best fit with $N = 7.0$ for the L-, S-, X-, and Q-Bands are 0.7, 0.7, 1.0, and 1.0, respectively.

of the experimental values of B and C (Fig.'s V.19 & V.21). The effects of these variations on the values of τ_R were minimal.

V.5. Discussion

For the first time, lineshape analysis was performed for the EPR spectra of BBTMPO to determine intrinsic linewidths from experimentally observed linewidths. The peaks in the EPR spectra of BBTMPO, like in PD-Tempone, are inhomogeneously broadened. An EPR spectral line is inhomogeneously broadened, when it consists of a spectral distribution of individual resonant lines assimilated into one envelope. Sources of inhomogeneous broadening include unresolved fine and hyperfine structures (Poole, 1983).

In the EPR spectra of PD-Tempone, the source of inhomogeneous broadening is the unresolved hyperfine structures resulting from the interaction of the spin magnetic moments of the unpaired electron and the twelve deuterons, whereas in BBTMPO the twelve deuterons are substituted by the twelve protons. This was reflected in the type of lineshape function used to fit the experimental EPR lines. For PD-Tempone, a Lorentzian lineshape function was sufficient to fit all of the experimental EPR lines, however for BBTMPO, a mixture of Lorentzian and Gaussian lineshape functions was necessary for the fitting.

A Gaussian lineshape function was required possibly due to Doppler effect which arises from mass differences between deuterons and protons. The

spectral distribution of the lighter protons assumes a mixture of Gaussian and Lorentzian lines, whereas the heavier deuterons assume a Lorentzian distribution. Moreover, as the temperature is lowered for the BBTMPO system at the four microwave bands, the lineshape function becomes more Lorentzian (*cf.*, Table V.5).

A summary of the results obtained for BBTMPO in toluene at the four microwave bands L, S, X, and Q is given in Table V.14. Molecules of BBTMPO in toluene at the four bands align under the applied magnetic field such that the molecular X axis corresponds to the axis z' in the laboratory frame, which is taken to be the direction of the applied magnetic field. This is also in accordance with the previous work on the same system (Hwang et al., 1986; Rahman, 1988).

Values of the anisotropic rotational reorientation N are equal to 7, which are relatively much higher than the N values for PD-Tempone ($N \equiv 1$). Therefore, at the four bands, BBTMPO undergoes anisotropic rotational diffusion. A value of 7 for the anisotropic rotational reorientation N for BBTMPO in toluene at X-Band was also obtained in the past (Hwang et al., 1986).

Values of the anisotropic interaction parameter κ determined in this study for BBTMPO in toluene were similar at the three microwave bands L, S, and X, whereas at Q-Band the value of the anisotropic interaction parameter κ was much smaller. The values of κ at L, S, and X bands are also similar to previously obtained values at the same bands (Hwang et al., 1986; Rahman,

TABLE V.14. Summary of the Results for BBTMPO in Toluene at the Four Microwave Bands: L, S, X, and Q.

Band	z'	N	β	Present Study κ	Previous Work* κ
L	X	7. \pm 2.	0.7 \pm 0.1	0.23 \pm 0.02	0.23 [†]
S	X	7. \pm 3.	0.7 \pm 0.1	0.24 \pm 0.08	0.21 [†]
X	X	7. \pm 2.	1.0	0.25 \pm 0.04	0.20 [‡]
Q	X	7. \pm 2.	1.0	0.08 \pm 0.01	

* The κ values were calculated by plotting the data and, for comparison purposes, the hydrodynamic volume 745.3 Å³ was used instead of 333 Å³ determined by the Dreding models.

† Rahman, 1988.

‡ Hwang et al., 1986.

1988). Apparently, variations among the three bands are not significant enough to be reflected in the value of the anisotropic interaction parameter κ . However, at Q-Band the difference becomes clear. Similarity among the κ values for PD-Tempone at the four microwave bands was achieved using the Cole-Davidson parameter β and using logarithmic scale for the axes of the τ_R versus η/T plot at Q-Band. In the case of BBTMPO, logarithmic scale was used for the axes of the τ_R versus η/T plots at the four bands, and the value obtained for κ at Q-band was only slightly improved.

To unify the results for the alignment of BBTMPO in toluene, the anisotropic rotational reorientation N , and for the anisotropic interaction parameter κ determined at the four microwave bands, a β value of 0.7 was used at both L- and S-Bands. Unlike PD-Tempone, the existence of multiple intermolecular motions, or equivalently a broader distribution of relaxation times associated with different types of motions, extended from L-Band only for PD-Tempone to both L- and S-Bands for BBTMPO. This can be attributed to the larger size of the BBTMPO molecules. The distinction between the two types of motions, i.e. free rotations and molecular reorientation (McClung & Kivelson, 1968), becomes clear in the L- and S-Bands for BBTMPO, which necessitated setting β equal to < 1 .

The smaller value of the anisotropic interaction parameter κ determined for BBTMPO in toluene at the Q-Band show that at these temperatures the coupling between the spin probe and the solvent is minimal. Due to the high

magnetic fields applied at Q-Band, the spin probe precesses at higher rates and since its motion is highly anisotropic, a weak coupling results between the rotational motion of the spin probe and the translational modes of the solvent.

The previous notions are that the value of the anisotropic interaction parameter κ depends on the type of solvent being used, and that κ would increase as the anisotropy of the paramagnetic species increases (Kivelson, 1972). Excluding the Q-Band result, these conclusions are generally valid if axes with linear scale were used to plot the τ_R versus η/T plots for both PD-Tempone and BBTMPO. Then, for BBTMPO the values of κ from L-, S-, and X-Bands are, respectively, 0.40, 0.53, and 0.66, which are generally higher than the 0.40 to 0.44 values for PD-Tempone. Applying a logarithmic scale to the axes of the τ_R versus η/T plots, minimizes the effect of anisotropy which becomes amplified at lower temperatures. However, from this study, it is highly recommended that comparing the values of κ for two different systems has to be performed with great caution.

CHAPTER VI

PHOSPHATIDYLCHOLINE-LANTHANIDE SYSTEMS

VI.1. Introduction

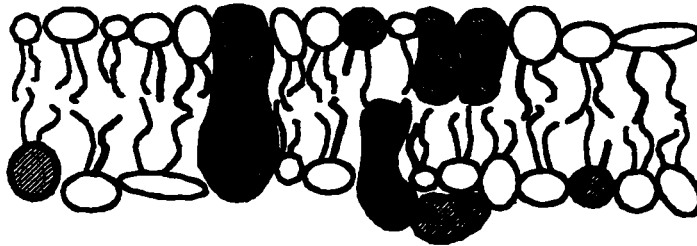
In this chapter, we would like to discuss *preliminary* investigations of the effects of some rare earth metal ions on the magnetic alignment of phospholipids using EPR spectroscopy. Lipids (predominantly phospholipids) are a major constituent of biomembranes, together with proteins and carbohydrates. Typically, lipids form a bilayer containing proteins that are integrated within the membrane or attached to its surface. The lipid moiety is amphiphilic, i.e., part of the molecule is polar and hydrophilic, while part is nonpolar and hydrophobic. Self-assembly of the lipids into biological membranes is governed by their hydrophobicity. The phospholipids are organized into bilayers with the polar head groups of the phospholipids on the exterior of the bilayer, whereas the nonpolar hydrocarbon chains are directed away from the aqueous phase.

The lipid bilayer represents the primary mediator for the passage of ions and polar molecules into and out of a cell. Other major functions of the lipid

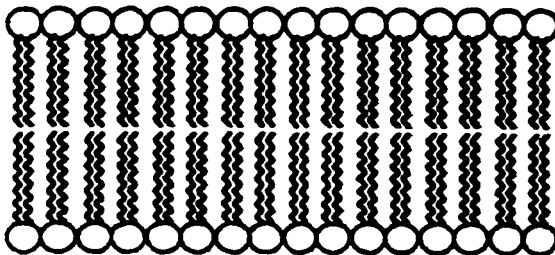
bilayer include its participation in the vectorial organization of membrane components and influencing distinctive functions of biological membranes, which are mainly due to proteins, through lipid-protein interactions. The foregoing discussion is based on two articles by Brown (1996) and Griffith and Jost (1976).

The lipid bilayer is typically a liquid-crystalline material. Liquid crystals can be divided, based on the chemical composition, into two classes: *thermotropic* and *lyotropic* liquid crystals (Seelig, 1976). Thermotropic liquid crystals consist of one component, whereas lyotropic liquid crystals consist of two or more components, for example, amphiphilic molecules treated with a controlled amount of water or other solvent. Lyotropic liquid crystals can have various structures (mesophases). *Lamellar* and *hexagonal* mesophases are two main categories. The lamellar or *smectic* mesophase is composed of molecules that are arranged in coherent double layers of molecules separated by layers of water. In the hexagonal phase molecules are arranged in a rodlike cylindrical shape with a lipophilic core in water. In short, phospholipid bilayers are a *lyotropic smectic* liquid crystals. A general model for a biomembrane showing a phospholipid bilayer with integral (imbedded) and peripheral (associated with the surface) proteins is depicted in Fig. VI.1(A); also shown is a model bilayer used to study the membrane lipid properties, Fig. VI.1(B). These models are based on latest knowledge and are only hypothesized since until now direct proofs are not possible.

A) Biomembrane



B) Lipid bilayer



C) Lipid:detergent bilayer

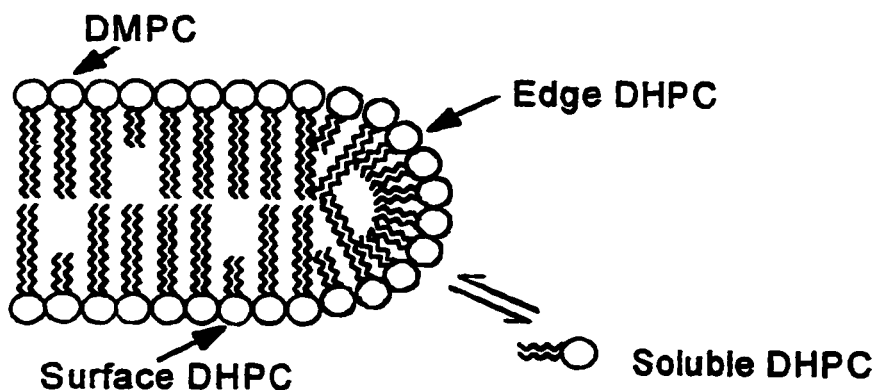
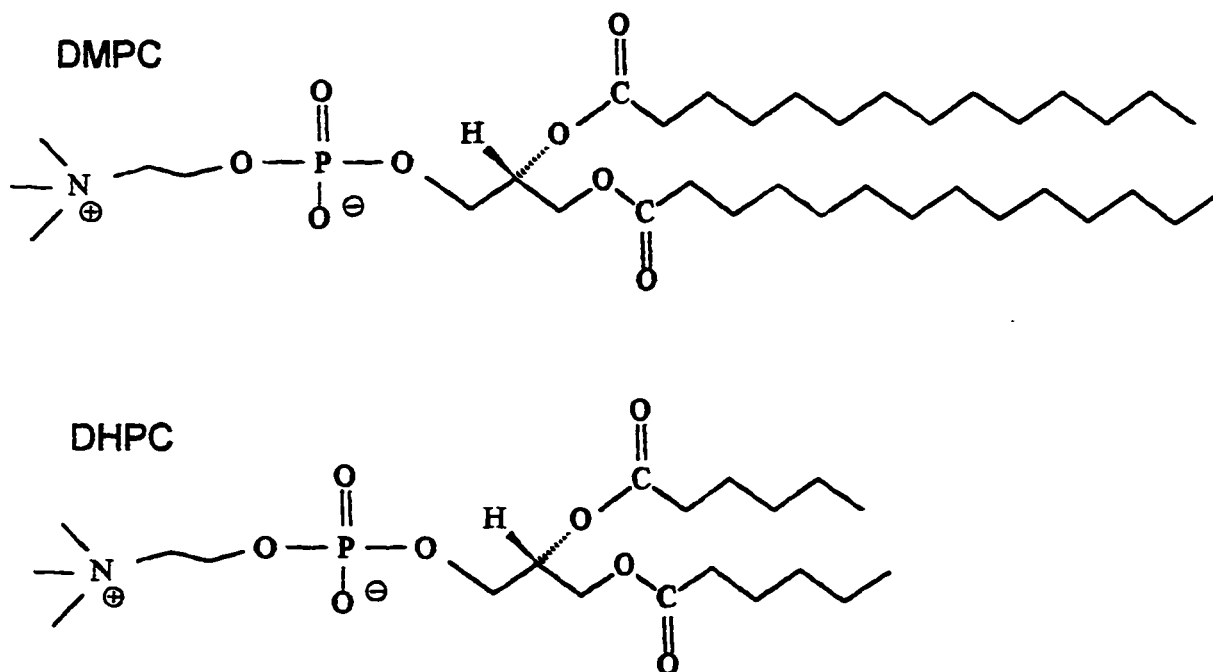


Figure VI.1. (A) Schematic representation of a generalized biomembrane, showing proteins integrated in the continuum of the phospholipid bilayer, together with peripheral proteins which are associated with the surface. (B) Schematic of a model bilayer used to study the membrane lipid properties. (C) Illustration of bilayered discoidal mixed micelles or "bicelles," where the lipid is the long-chain phosphatidylcholine DMPC and the detergent is the short-chain phosphatidylcholine DHPC. (A) and (B) were adopted from Brown (1996), whereas (C) was adopted from Sanders and Schwonek (1992).

VI.1.1. DMPC/DHPC Phosphatidylcholine

Highly oriented, bilayer-like assemblies were formed of mixtures of long-chain and short-chain phosphatidylcholine (PC), where the long-chain PC is dimyristoylphosphatidylcholine (DMPC) and the short-chain PC is dihexanoylphosphatidylcholine (DHPC) (Sanders & Schwonek, 1992). Mixtures of DMPC and DHPC having molar ratios in the range from approximately 1:3.5 to 1:2 (DHPC:DMPC) were found to possess these properties over a wide range of lipid concentrations and at temperatures above T_m , where T_m is the gel to liquid crystalline phase transition temperature. The chemical structures of DMPC and DHPC are given in Scheme VI-I.



Scheme VI-I

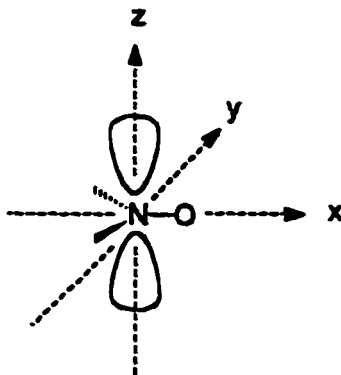
In their study, Sanders and Schwonek (1992) employed multinuclear (^{13}C , ^{31}P , ^2H) solid-state nuclear magnetic resonance. The NMR spectra of pure DMPC show the powder pattern which is usually broad. As a result, it would be difficult to observe minimal variations in these spectra due to structural changes. Upon addition of DHPC, the mixture of DMPC and DHPC gave a solid state NMR spectra of higher resolution, which reflected an increase in the orientation of the phosphatidylcholine bilayer. The detergent usually employed, namely DHPC, has the added advantage of being nearly isostructural with the long-chain lipid component, and therefore experimental artifacts would be minimized. The suggested morphology of the highly oriented DMPC-DHPC assemblies is "discoidal micelles," in which DMPC orients like in a bilayer with some interdispersed DHPC, whereas the edges of the bilayer discs are stabilized by a second population of DHPC. The bilayered discoidal mixed micelles, depicted in Fig. VI.1(C), were named "bicelles" by Sanders and Landis (1995).

This highly ordered bilayer mixture (or bicelles) has a disadvantage which becomes clear when studying large, slowly reorienting intrinsic proteins which would exhibit unresolved powder pattern. Addition of lanthanides was found to flip the normal of phospholipid bicelles from being perpendicular to the magnetic field to being parallel to it (Prosser et al, 1996). The order parameter used to describe these orientations, S_{zz} , is defined by $S_{zz} \equiv \left\langle \frac{1}{2}(3 \cos^2 \beta_{nl} - 1) \right\rangle$, where $\beta_{nl} = 90^\circ$ for the perpendicular orientation yielding a value of $-1/2$ for S_{zz} . The parallel orientation, $S_{zz} \approx 1$, was argued to be resulting from the binding of the

paramagnetic lanthanide ions to the phospholipid headgroups (Prosser et al, 1996; Akutsu & Seelig, 1981).

VI.1.2. Order Parameters

The long axes of the phospholipid molecules in the bilayer tend to orient parallel to each other. The average orientation of the bilayer can then be approximated by a director z' . The motion of the molecules have cylindrical symmetry about z' . In this section the order parameters of the solute (i.e., the nitroxide spin probe) will be introduced first followed by the order parameters of the solvent. Before discussing order parameters, a coordinate system must be defined. Following the discussion of Seelig (1976), an appropriate choice of a Cartesian coordinate system x, y, z is one that would make the hyperfine tensor A and the g tensor diagonal in the molecular frame. These requirements are fulfilled by selecting the x axis to be parallel to the N–O bond in the nitroxide moiety, the z axis to be parallel to the $2p\pi$ orbital of the nitrogen, and the y axis to be defined by a right-handed coordinate system. This choice of coordinate system is shown below.



The hyperfine tensor \mathbf{A} and the \mathbf{g} tensor are then given by:

$$\mathbf{A} = \begin{pmatrix} A_{xx} & 0 & 0 \\ 0 & A_{yy} & 0 \\ 0 & 0 & A_{zz} \end{pmatrix} \quad [\text{VI.1}]$$

$$\mathbf{g} = \begin{pmatrix} g_{xx} & 0 & 0 \\ 0 & g_{yy} & 0 \\ 0 & 0 & g_{zz} \end{pmatrix} \quad [\text{VI.2}]$$

The transformation from the molecule-fixed coordinates x, y, z to the space-fixed coordinates x', y', z' is achieved by using the matrix \mathbf{D} , which is orthogonal,

$$\begin{pmatrix} x' \\ y' \\ z' \end{pmatrix} = \mathbf{D} \begin{pmatrix} x \\ y \\ z \end{pmatrix} \quad [\text{VI.3}]$$

where

$$\mathbf{D} = \begin{pmatrix} \cos \eta_1 & \cos \eta_2 & \cos \eta_3 \\ \cos \xi_1 & \cos \xi_2 & \cos \xi_3 \\ \cos \theta_1 & \cos \theta_2 & \cos \theta_3 \end{pmatrix} \quad [\text{VI.4}]$$

The direction cosines between the molecular axes x, y, z and the director z' are only relevant here, and therefore can be written explicitly as:

$$\mathbf{x} \cdot \mathbf{z}' = \cos \theta_1, \quad \mathbf{y} \cdot \mathbf{z}' = \cos \theta_2, \quad \mathbf{z} \cdot \mathbf{z}' = \cos \theta_3 \quad [\text{VI.5}]$$

where $\mathbf{x}, \mathbf{y}, \mathbf{z}$, and \mathbf{z}' are unit vectors along the respective axes.

Transformation to the space-fixed coordinate system by applying \mathbf{D} leads to the new tensors \mathbf{A}' and \mathbf{g}' :

$$\mathbf{A}' = \mathbf{D} \mathbf{A} \mathbf{D}^{-1}, \quad \mathbf{g}' = \mathbf{D} \mathbf{g} \mathbf{D}^{-1} \quad [\text{VI.6}]$$

The invariance property of the time-averaged \mathbf{A}' and \mathbf{g}' tensors against rotations around z' implies that these new tensors must have axial symmetry:

$$\langle \mathbf{A}' \rangle = \begin{pmatrix} A_{\perp} & 0 & 0 \\ 0 & A_{\perp} & 0 \\ 0 & 0 & A_{\parallel} \end{pmatrix}, \quad \langle \mathbf{g}' \rangle = \begin{pmatrix} g_{\perp} & 0 & 0 \\ 0 & g_{\perp} & 0 \\ 0 & 0 & g_{\parallel} \end{pmatrix} \quad [\text{VI.7}]$$

Performing the transformation given in Eq. [VI.6] and using the orthogonality properties of the matrix \mathbf{D} , the time-averaged components of the \mathbf{g}' tensor are found to be

$$g_{\perp} = \frac{1}{2}(1 - \langle \cos^2 \theta_1 \rangle)(g_{xx} - g_{yy}) + \frac{1}{2}(1 - \langle \cos^2 \theta_3 \rangle)(g_{zz} - g_{yy}) + g_{yy} \quad [\text{VI.8}]$$

$$g_{\parallel} = \langle \cos^2 \theta_1 \rangle(g_{xx} - g_{yy}) + \langle \cos^2 \theta_3 \rangle(g_{zz} - g_{yy}) + g_{yy} \quad [\text{VI.9}]$$

Similar results can be derived for A_{\perp} and A_{\parallel} , but with the approximation $A_{xx} \approx A_{yy}$ simpler formulas are obtained

$$A_{\perp} = \frac{1}{2}(1 - \langle \cos^2 \theta_3 \rangle)(A_{zz} - A_{xx}) + A_{xx} \quad [\text{VI.10}]$$

$$A_{\parallel} = \langle \cos^2 \theta_3 \rangle(A_{zz} - A_{xx}) + A_{xx} \quad [\text{VI.11}]$$

The mean angular fluctuations $\langle \cos^2 \theta_i \rangle$ in liquid crystals is represented by the order parameters S_{ii} , which are defined as follows (Saupe, 1968):

$$S_{ii} = \frac{1}{2}(3\langle \cos^2 \theta_i \rangle - 1), \quad i = 1, 2, 3 \quad [\text{VI.12}]$$

The order parameter S_{ii} is a second-rank tensor, but actually only three order parameters are left corresponding to the fluctuations of the x , y , and z axes of the NO group. The orthogonality relation of the cosines, namely

$$\cos^2 \theta_1 + \cos^2 \theta_2 + \cos^2 \theta_3 = 1 \quad [\text{VI.13}]$$

reduces the number of independent order parameters to two, where the third parameter is fixed by the relation

$$S_{11} + S_{22} + S_{33} = 0 \quad \text{[VI.14]}$$

Combining Eq.'s [VI.9]-[VI.11] with Eq. [VI.12] gives the following expressions:

$$S_{33} = (A_{\parallel} - A_{\perp}) / (A_{zz} - A_{xx}) \quad \text{[VI.15]}$$

$$S_{11} = [3g_{\parallel} - (g_{xx} + g_{yy} + g_{zz}) - 2S_{33}(g_{zz} - g_{yy})] / 2(g_{xx} - g_{yy}) \quad \text{[VI.16]}$$

The ordering tensor S could also be related to the mean restoring potential, $U(\Omega)$, of the probe in the field of the molecules of the anisotropic solvent via the equilibrium distribution of the probe, $P_o(\Omega) = P_o(\theta, \phi)$, by the following expressions (Freed, 1977):

$$S = \int d\Omega P_o(\Omega) \frac{1}{2} (3 \cos^2 \theta - 1) \quad \text{[VI.17]}$$

with

$$P_o(\Omega) = \exp[-U(\Omega) / kT] / \int d\Omega \exp[-U(\Omega) / kT] \quad \text{[VI.18]}$$

and, assuming uniaxial symmetry in the liquid crystals and keeping only the lowest order terms which are spherical harmonics of rank 2, $U(\Omega)$ can be expanded as

$$U(\theta, \phi) / kT = -\lambda \cos^2 \theta - \rho \sin^2 \theta \cos 2\phi \quad \text{[VI.19]}$$

where, in Eq.'s [VI.17]-[VI.19], θ has its previous definition, ϕ is the azimuthal angle for the projection of the director in the molecular x-y plane, λ and ρ are potential parameters, and k and T have their usual meaning.

The restoring potential, $U(\Omega)$, for liquid crystals can generally be expanded as (Polnaszek & Freed, 1975):

$$U(\Omega) = \sum_{L,K,M} \epsilon_{KM}^L D_{KM}^L(\theta, \phi, \psi) \quad [\text{VI.20}]$$

where θ, ϕ, ψ are the Euler angles (Goldstein, 1980), and $D_{KM}^L(\Omega)$ is the ordering tensor. The following assumptions were made in the paper of Polnaszek and Freed (1975) to reach at an operational expression for the order parameter $D_{KM}^L(\Omega)$:

1. The liquid crystalline solvent has cylindrical symmetry about the director axis, \hat{n} . This resulted in fixing the value of M to zero, since otherwise all averages taken over the angle ψ would vanish. Choosing $M = 0$ eliminates the dependency on the angle ψ which, therefore, would be assumed to be constant.
2. The liquid crystalline solvent possesses a uniaxial property, i.e., $\hat{n} \equiv -\hat{n}$. This implied that L must have even values which would eliminate the dependency on the angle ϕ and, as with ψ , the angle ϕ would be assumed to be constant.
3. A Maier-Saupe potential applies, which means that only the leading term $\epsilon_0^2 D_{00}^2(\Omega)$ is considered.

The ordering tensor was then defined by

$$\langle D_{KM}^L(\Omega) \rangle = \int d\Omega P_0(\Omega) D_{KM}^L(\Omega) \quad [\text{VI.21}]$$

where $L = 2$ and $M = 0$, and for calculating the ordering parameters of the solute from experiment, the following equation resulted

$$\langle D_{00}^2 \rangle = \frac{(\langle a \rangle - a)(g_x - g_y) - (\langle g \rangle - g)(a_x - a_y)}{(a_z - a)(g_x - g_y) - (g_x - g)(a_x - a_y)} \quad [\text{VI.22}]$$

where the subscripts x , y , and z refer to the principal axes of the a - and g -tensors, $\langle a \rangle$ and $\langle g \rangle$ are their respective averages, and in this case a and g are, respectively, the hyperfine coupling coefficient and the g -value calculated at each temperature.

The ordering parameter $\langle D_{00}^2 \rangle_x$ was associated with the solute molecules, whereas the potential expansion coefficient λ introduced in Eq. [VI.19] was related to the ordering of the solvent molecules as well as the radical (Polnaszek & Freed, 1975).

Ferruti et al (1969) used another approach to reach at the ordering parameter S (which they referred to as a *micro-ordering* parameter). The EPR of a nitroxide radical in a nematic solvent under a static magnetic field H_0 applied in the z direction of the laboratory frame was described by the spin Hamiltonian

$$\mathcal{H} = (g + \Delta g) \beta H_0 S_z + h (A + \Delta A) I_z S_z \quad [\text{VI.23}]$$

where,

g and A are, respectively, the isotropic invariants of the g tensor and of the hyperfine tensor of the electron in the ^{14}N nucleus, and are given by

$$A = \frac{1}{3} (A_x + A_y + A_z), \quad g = \frac{1}{3} (g_x + g_y + g_z) \quad [\text{VI.24}]$$

Δg and ΔA are deviations from isotropy, and are given by

$$\Delta g = \frac{2}{3} (S_{11} g_{xx} + S_{22} g_{yy} + S_{33} g_{zz}) \quad [\text{VI.25}]$$

$$\Delta A = \frac{2}{3} (S_{11} A_{xx} + S_{22} A_{yy} + S_{33} A_{zz}) \quad [\text{VI.26}]$$

S_z and I_z are, respectively, the projections of the spin and nuclear magnetic moments on the z axis; β is Bohr magneton and h is Plank's constant.

Utilizing the zero-trace property of S_{ii} (Eq. [VI.14]) and the equality of $A_{xx} \approx A_{yy} = A_{\perp}$ in the nitroxide radical, Eq.'s [VI.25] and [VI.26] can, respectively, be rewritten as

$$\Delta g = \frac{1}{3} (2g_{xx} - g_{yy} - g_{zz}) S_{11} + \frac{1}{3} (g_{zz} - g_{yy})(S_{33} - S_{22}) \quad [\text{VI.27}]$$

$$\Delta A = \frac{2}{3} (A_{zz} - A_{\perp}) S_{33} \quad [\text{VI.28}]$$

The treatment of Ferruti et al was extended by Morsy et al (1997) through the introduction of a factor f relating the three ordering parameters of S_{ii} . The operational expressions for S_{ii} derived by the latter group will be described in the "Data Analysis" section.

VI.1.3. EPR Studies of Phosphatidylcholines

Several studies of phosphatidylcholines were conducted by observing variations in the EPR spectra of weakly ordered nitroxide spin probes as a function of temperature. Shimshick and McConnell (1973) and Wu and McConnell (1975) used spin-labels to derive phase diagrams for several lipid systems. Wu and McConnell (1975) studied the partitioning of 2,2,6,6-tetramethylpiperidine-1-oxyl (TEMPO) at X-band (~9.5 GHz) between the

hydrocarbon and aqueous phases of many membrane systems. Smirnov et al (1995) also applied EPR spectroscopy, but at high microwave frequency (94.3 GHz), to study the partitioning and molecular dynamics of TEMPO in liposomes formed by dipalmitoylphosphatidylcholine. The higher resolution of the EPR spectra at this high microwave frequency made the analysis of partitioning between the hydrocarbon and aqueous phases to be more accurate. EPR studies of spin-labeled phosphatidylcholines mixed in hydrated mixtures of the phospholipids were also conducted (e.g., Schorn & Marsh, 1996). To probe the different regions of the bilayer, the phosphatidylcholines are usually labeled with the nitroxide radical at different positions. Using the same approach, spin labels bonded to stearic acid were also observed using EPR spectroscopy to study motion and orientation in the lecithin lipid bilayers (Jost et al, 1971).

The effects of the rare earth metal ions ytterbium(III), Yb^{3+} , and yttrium(III), Y^{3+} , on the structural orientation of the DMPC-DHPC bicelles will be studied using EPR spectroscopy by doping the mixture with a tiny amount of the nitroxide spin probe PD-Tempone. The following experiments will be performed with the abovementioned phospholipid system:

- 1) Variable temperature studies of PD-Tempone + DMPC/DHPC,
- 2) Variable temperature studies of PD-Tempone + DMPC/DHPC + Yb^{3+} , and
- 3) Variable temperature studies of PD-Tempone + DMPC/DHPC + Y^{3+} .

VI.2. Experimental

VII.2.1. Materials and Sample Preparation

1,2-dimyristoyl-*sn*-glycero-3-phosphocholine (DMPC) and 1,2-dihexanoyl-*sn*-glycero-3-phosphocholine (DHPC) were purchased from Avanti Polar Lipids (Birmingham, Alabama). Lipids were used as purchased without further purification. Ytterbium(III) chloride hexahydrate (Yb³⁺) and yttrium(III) chloride hexahydrate(Y³⁺) (both with purity of 99.99 - 99.999%) were purchased from Aldrich Chemicals (Milwaukee, Wisconsin). The nitroxide spin probe perdeuterated-2,2,6,6-tetramethyl-4-piperidone-N-oxide (abbreviated as PD-Tempone) was obtained from Stohler Isotope, and used without further purification. The EPR sample tubes made from clear fused quartz (4mm O.D. × 241 mm length) were purchased from Wilmad (Buena, New Jersey).

A stock solution was supplied by Dr. Hwang and it consisted of DMPC/DHPC with a molar ratio of 3.2:1 in 0.15 M KCl. The solution was prepared as follows. An amount of 140.0 mg of DHPC was added to 667.6 mg of DMPC. A solution with 25% w/v total lipid in 0.15 M KCl was prepared by adding 2.42 ml of a 0.15 M KCl solution to the mixture. The electrolyte added, i.e. KCl, has several functions. It stabilizes the phospholipids DMPC and DHPC and increases the binding efficiency of the paramagnetics to the phospholipids (Hauser et al, 1977; Grasdalen et al, 1977; Chapman et al, 1977). The stock solution was mixed by a combination of heating in an oven at 45 °C for 30 minutes, centrifugation for 10-15 minutes, vortexing for 15 minutes, cooling in a

freezer for 15 minutes. The process was repeated 2-3 times until the solution appeared viscous in the oven and fluid in the freezer.

VL2.1.1. EPR Sample Preparation- The phospholipids were doped with tiny amounts of PD-Tempone to prepare EPR samples. To a small glass vial, 0.6 ml of the DMPC/DHPC stock solution was transferred using a 1cc glass syringe. After that, PD-Tempone was added to this solution using a glass capillary tube by covering the tip of the capillary with PD-Tempone. The same capillary was also used to thoroughly mix the PD-Tempone and the phospholipid solution, which was then heated in the oven at 50 °C for 30 minutes, centrifuged for 10 minutes, and cooled in the freezer for 15 minutes. The process of heating, centrifugation, and cooling was repeated 2-3 times. The mixture was purged with nitrogen gas and placed in an quartz EPR sample tube, while in a glove bag, using a glass syringe so that the height of the sample in the tube is about 2 cm (~ 0.2 ml). Care must be exercised when purging with nitrogen so that water in the solution will not be evaporated. Unless removal of oxygen from the sample is necessary, purging with nitrogen should be avoided. Finally, while in the glove bag, the quartz EPR sample tubes were sealed with Teflon[®] tape and capped. EPR samples containing Yb³⁺ and Y³⁺ were prepared in a similar manner with the mole ratio of DMPC to the lanthanides maintained at 10:1. Proper amounts of the lanthanide salts, which are hygroscopic, were added to the stock solution in the glass vial prior to purging with nitrogen gas. Hence, the

three systems studied were: DMPC/DHPC + PD-Tempone, DMPC/DHPC + PD-Tempone + Yb³⁺, and DMPC/DHPC + PD-Tempone + Y³⁺.

VI.2.2. Measurement and Data Collection

The measurements were performed at X-band with the EPR Bruker system described in the experimental section of PD-Tempone. At the beginning, the EPR sample tube of a phospholipid system was placed in the cavity and was exposed to a magnetic field of 10,000 Gauss (one Tesla) for one hour. Rigid limit and variable temperature experiments of the three systems were conducted following this exposure.

VI.2.2.1. Rigid Limit Experiments- The rigid limit experiment is conducted at the boiling temperature of liquid nitrogen, which is 77 K, using a glass dewar made of fused quartz called the finger dewar. The finger dewar is available from either Bruker (Silberstreifen, Rheinstetten, Germany) or Wilmad (Buena, New Jersey). Following were the main steps involved in a rigid limit experiment.

1. A thin filter paper (~1 cm wide) was placed in the finger dewar just above the region which is observed by the spectrometer. This would help in reducing the vigorousness of the bubbling liquid nitrogen. The EPR sample tube placed in the finger dewar would become more stable and therefore the EPR spectrum would become less noisy.

2. The EPR sample tube was placed in the finger dewar and good quality liquid nitrogen (dry) was poured into the finger dewar.
3. A stabilizer was designed and constructed to partially seal the finger dewar and hold the EPR sample tube in position. The stabilizer consisted of a cover made of polystyrene foam, with a hole in the center. A Teflon[®] rod was inserted in the hole. The rod was to press gently against the EPR sample tube. Figure VI.2 is a schematic of the finger dewar with the stabilizer.
4. The finger dewar filled with liquid nitrogen and the EPR sample tube along with the stabilizer were immediately placed in the cavity to prevent water condensation on the outer wall of the dewar. To slow down water condensation inside the EPR cavity, the cavity was continuously purged with dry nitrogen gas via the waveguide. Tissue papers were also placed around the finger dewar on top of the cavity.
5. The automatic frequency control (AFC) toggle in the rear panel of the microwave bridge was placed in the "ON" position and the module level was set at a value of 10 (this is suggested in the Bruker manual). An EPR spectrum could then be acquired with low microwave power (e.g., 1.2 mW) to prevent sample saturation.

VI.2.2.2. Variable Temperature Experiments- In the variable temperature experiments, the settings of the spectrometer for the three systems of the phospholipids were:

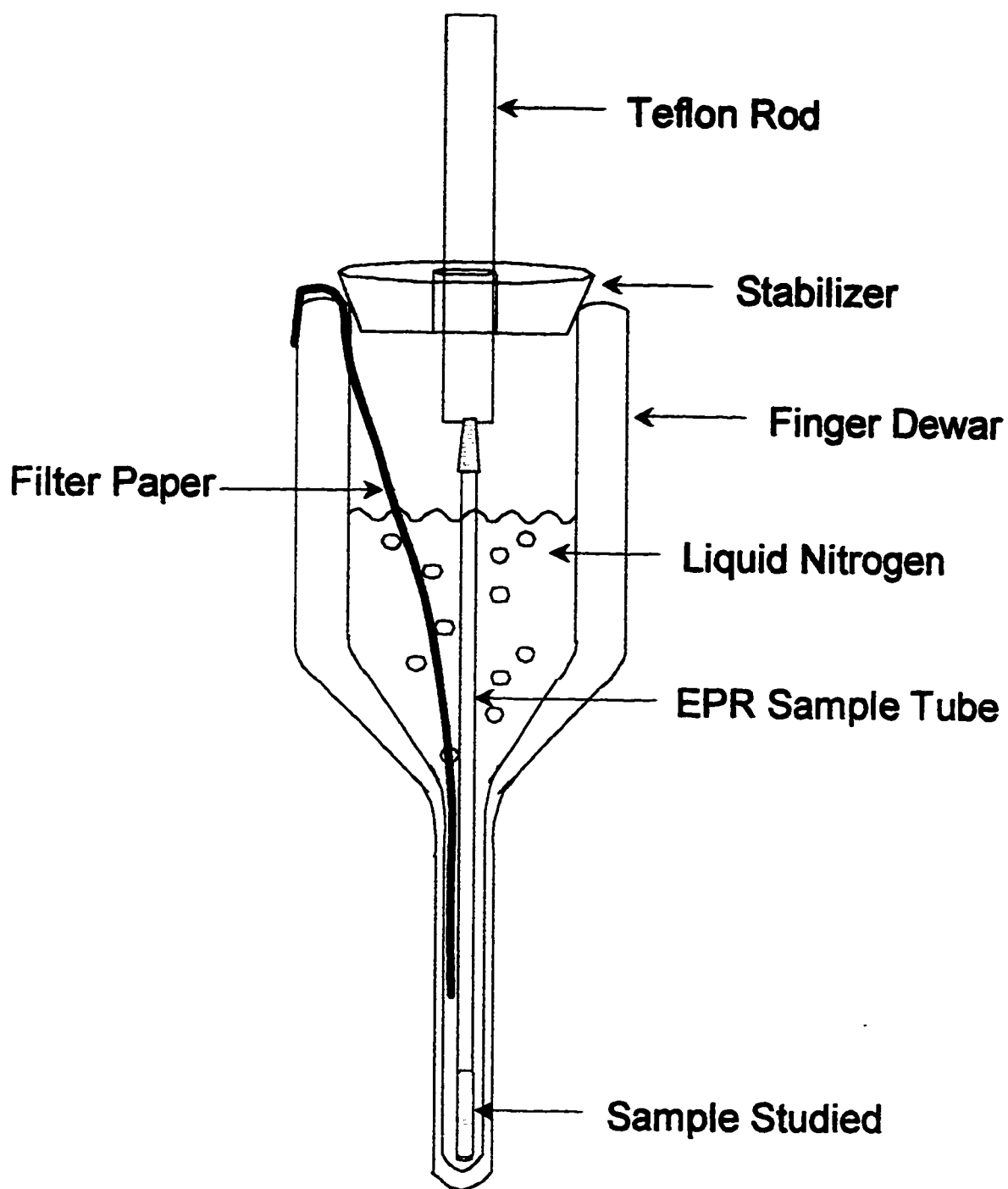


Figure VI.2. A schematic of the finger dewar with the stabilizer designed and constructed in-house.

Receiver Gain = 2.00×10^4 ,

Modulation Frequency = 100.00 kHz,

Microwave Frequency = 9.54 GHz, and

Microwave Power = 6.4 mW.

The temperature ranges that were probed for the three systems of the phospholipids were:

Phospholipid System	Temperature Range (K)
DMPC/DHPC + PD-Tempone	296 - 350
DMPC/DHPC + PD-Tempone + Yb³⁺	296 - 355
DMPC/DHPC + PD-Tempone + Y³⁺	260 - 350

The spectra were plotted and stored in diskettes for further analysis.

VI.3. Data Analysis

To manipulate the data, spectra files of the rigid limit and variable temperature experiments of the three phospholipids systems were processed as described in the 'Data Analysis' section of PD-Tempone. Computer programs, written in FORTRAN language, were modified to assist in the analysis of the results for the variable temperature experiments.

The most important requirement in analyzing variable temperature spectra is to have accurate values of magnetic tensors **A** and **g** determined from the rigid

limit spectrum. These values could be obtained by theoretical simulation of the rigid limit spectrum. The rigid limit simulation was performed using the general methods of Lefebre and Maruani (Lefebre and Maruani, 1965) adapted to nitroxides by Polnaszek (Polnaszek, 1975). The simulation employs Simpson's numerical integration over θ in 45 intervals and over φ in 25 intervals. The values of magnetic tensors **A** and **g** were fed into the program until an acceptable match was obtained between the experimental and the theoretical rigid limit spectra.

The principal components of the **A** and **g** tensors (Eq.'s [VI.1] & [VI.2]) will only contribute to the spin Hamiltonian, which, for brevity, will hereafter be written as A_x, A_y, A_z and g_x, g_y, g_z . Some of these values could be obtained directly from the experimental rigid limit spectrum. The parameters A_z and g_z correspond to the midpoint of the two extrema which is $2A_z$, while g_z correspond to the midpoint of the extrema. The magnetic parameters g_x, g_y, A_x , and A_y and the linewidth were varied to fit the experimental spectrum until the line shape of the central portion was simulated. Two additional conditions that should be always satisfied while adjusting the fitting values are

$$A_{iso} = \frac{1}{3} (A_x + A_y + A_z) \text{ and } g_{iso} = \frac{1}{3} (g_x + g_y + g_z)$$

where A_{iso} and g_{iso} could be measured from an isotropic spectrum which is usually the three-peak spectrum obtained at room temperature.

The nitroxide spin probe PD-Tempone (Rao et al, 1976) was added to the phospholipids to study their orientational arrangement. Spectra from the

variable temperature experiments of the three phospholipids systems, i.e., DMPC/DHPC + PD-Tempone, DMPC/DHPC + PD-Tempone + Yb³⁺, and DMPC/DHPC + PD-Tempone + Y³⁺, were analyzed for ordering characteristics. Ordering was studied by measuring several parameters. The values of the hyperfine spacings **A** and the **g**-factors varied as a function of temperature and these were utilized as indicators to the variation in order as a function of temperature. The order parameter $\langle D_{00}^2 \rangle_z$ and the potential expansion coefficient λ were also calculated for the different spectra obtained at different temperatures. The nominal ordering parameter $\langle D_{00}^2 \rangle_z$ was calculated according to the equation (Polnaszek and Freed, 1975) (same as Eq. [VI.22] written here for easy reference)

$$\langle D_{00}^2 \rangle_z = \frac{(\langle a \rangle - a)(g_x - g_y) - (\langle g \rangle - g)(a_x - a_y)}{(a_z - a)(g_x - g_y) - (g_z - g)(a_x - a_y)} \quad [\text{VI.29}]$$

where the subscripts *x*, *y*, and *z* refer to the principal axes of the *a*- and *g*-tensors determined in the rigid limit at 77 K and $\langle a \rangle$ and $\langle g \rangle$ are their respective averages. Using Dawson's integral (Abramowitz and Stegun, 1964), the solute order parameter $\langle D_{00}^2 \rangle_z$ was transformed into the potential expansion coefficient or the solvent order parameter λ (Hwang, *et al.*, 1994). This transformation was performed using the two programs "D200.FOR" and "LAMBDA.FOR." Lists of these two programs can be found in "Appendix D." Moreover, the principal ordering matrix tensors S_{11} , S_{22} , and S_{33} (Ferruti, *et al.*, 1969) were determined.

The subscripts in S_{ii} denote Cartesian axes in the probe molecule. These were calculated from the following expressions (Morsy, *et al.*, 1997)

$$S_{11} = -f_y S_{22} \quad [\text{VI.30}]$$

$$S_{33} = -(1 - f_y) S_{22} \quad [\text{VI.31}]$$

$$S_{22} = \frac{\Delta a}{\frac{2}{3}[(a_y - a_z) + f_y(a_z - a_x)]} \quad [\text{VI.32}]$$

$$f_y = \frac{\Delta g(a_z - a_y) + \Delta a(g_y - g_z)}{\Delta g(a_z - a_x) + \Delta a(g_x - g_z)} \quad [\text{VI.33}]$$

where

$$\Delta a = a - \langle a \rangle$$

$$\Delta g = g - \langle g \rangle$$

The EPR spectrum at each temperature would have different values of the hyperfine splittings a and the g -factor.

VI.4. Results and Discussion

The interaction of metal cations with phosphatidylcholine bilayers has been investigated extensively using ^1H , ^2H , ^{13}C , and ^{31}P NMR (cf. Prosser *et al.*, 1997; Prosser *et al.*, 1996; Akutsu & Seelig, 1981; Hauser *et al.*, 1977; Chapman *et al.*, 1977; Grasdalen *et al.*, 1977). The advantages of ^2H NMR of deuterons covalently bound to the phospholipid molecules over NMR studies using shift reagents are: the spectra obtained are of higher resolution and hence higher sensitivity can be achieved; the magnetic properties of the ions employed are

immaterial; and experiments can be performed with coarse phospholipid dispersions (Akutsu & Seelig, 1981).

To the best of our knowledge, this is the first time a bilayer system with rare earth metal ions are studied by observing the EPR spectra of weakly ordered nitroxide spin probe. Studying coarse phospholipid dispersions and adding ions of different magnetic properties do not seem to form serious limitations. Moreover, EPR spectroscopy of the nitroxide spin probe is very sensitive to variations in the host environment.

In order to calculate the different ordering indicators mentioned in the previous section, the g and A tensors for the three phospholipids systems must be known. The values of the g and A tensors were obtained by the simulation of the rigid limit spectra. These values were then used to calculate the ordering parameters associated with the each spectrum obtained at a different temperature for the three phospholipids systems.

VI.4.1. Determination of Magnetic Tensor Components - Rigid Limit Simulations

The rigid limit spectrum of PD-Tempone in DMPC/DHPC at 77 K is shown in Figure VI.3. The magnetic parameters which gave the best fit are given in Table VI.1. The fit was obtained with a Lorentzian line width of 3.3 G. The simulation of this spectrum was not straightforward. The experimental spectrum possessed contradicting features. Both the positive and negative intensities of

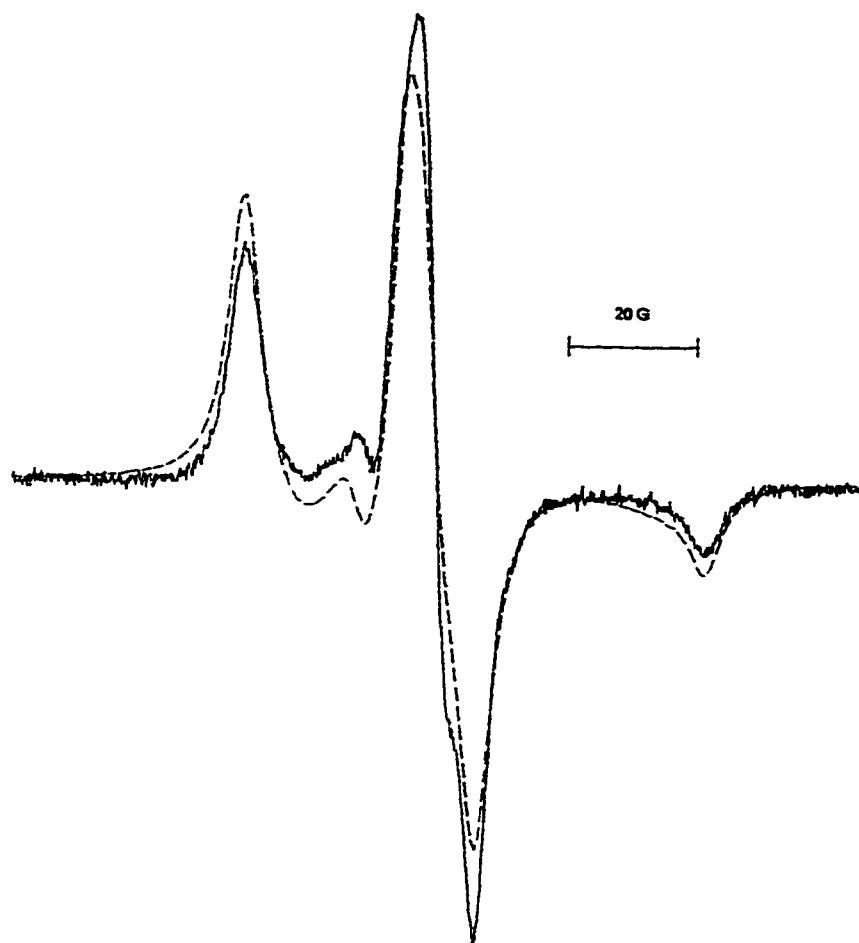


Figure VI.3. Rigid limit spectrum for PD-Tempone in the phospholipid system DMPC/DHPC and simulation (dashed line) based on magnetic parameters given in Table VI.1.

TABLE VI.1. Magnetic Parameters for PD-Tempone in Different Systems.

	PD-Tempone in liquid crystals ^a	PD-Tempone in DMPC/DHPC	PD-Tempone in DMPC/DHPC + Yb ³⁺	PD-Tempone in DMPC/DHPC + Y ³⁺
g_x	2.0097 ± 0.0002	2.00920 ± 0.00020	2.00924 ± 0.00006	2.00914 ± 0.00020
g_y	2.0062 ± 0.0002	2.00660 ± 0.00020	2.00604 ± 0.00006	2.00630 ± 0.00020
g_z	2.00215 ± 0.0001	2.00235 ± 0.00010	2.00191 ± 0.00006	2.00201 ± 0.00020
$\langle g \rangle$	2.0060 ± 0.00017	2.00605 ± 0.00020	2.00573 ± 0.00020	2.00582 ± 0.00020
g_{iso}	2.00601 ± 0.00005	2.00603 ± 0.00005	2.00573 ± 0.00005	2.00582 ± 0.00006
A_x	5.61 ± 0.2	6.50 ± 0.30	6.68 ± 0.10	6.00 ± 0.10
A_y	5.01 ± 0.2	6.00 ± 0.30	6.18 ± 0.10	5.50 ± 0.10
A_z	33.7 ± 0.3	35.45 ± 0.05	35.45 ± 0.10	35.90 ± 0.10
$\langle A \rangle$	14.77 ± 0.3	15.98 ± 0.22	16.10 ± 0.10	15.80 ± 0.10
A_{iso}	14.78 ± 0.02	15.97 ± 0.030	16.10 ± 0.10	15.80 ± 0.14

^a Polnaszek C.F. and J.H. Freed, *J. Phys. Chem.*, 79:2283-2306 (1975).

the central region in the spectrum were relatively high compared to the two outer hyperfine extrema. As a result, if the central region of the spectrum was fitted, the two outer hyperfine extrema from the simulation would be much higher than the corresponding experimental peaks, and vice versa. In addition, if the positive portion of the central region and the two outer hyperfine extrema were fitted, the negative portion of the central region from the simulation would deviate substantially from the experimental values. The fit shown in the figure was a compromise between the different contradicting features.

The resolution of the central region was low compared with the rigid limit spectra of PD-Tempone in solvents like phase V liquid crystals (Polnaszek and Freed, 1975; see also Table VI.1). The reduction in resolution of the central region could be attributed to interproton hyperfine interactions with water molecules and to a lesser extent with protons in the phospholipids. Moreover, nitroxide radicals form hydrogen bonds, and in the presence of water molecules, the relatively large changes in the appearance of this spectra and the magnetic parameters derived from it is not unexpected.

The rigid limit spectra of PD-Tempone in the phospholipid systems DMPC/DHPC+Yb³⁺ and DMPC/DHPC+Y³⁺ at 77 K are shown in Figure VI.4. The magnetic parameters which gave the best fit are given in Table VI.1. The fits were obtained with Lorentzian line widths of 3.3 G and 4.6 G, respectively, for the phospholipid systems DMPC/DHPC+Yb³⁺ and DMPC/DHPC+Y³⁺.

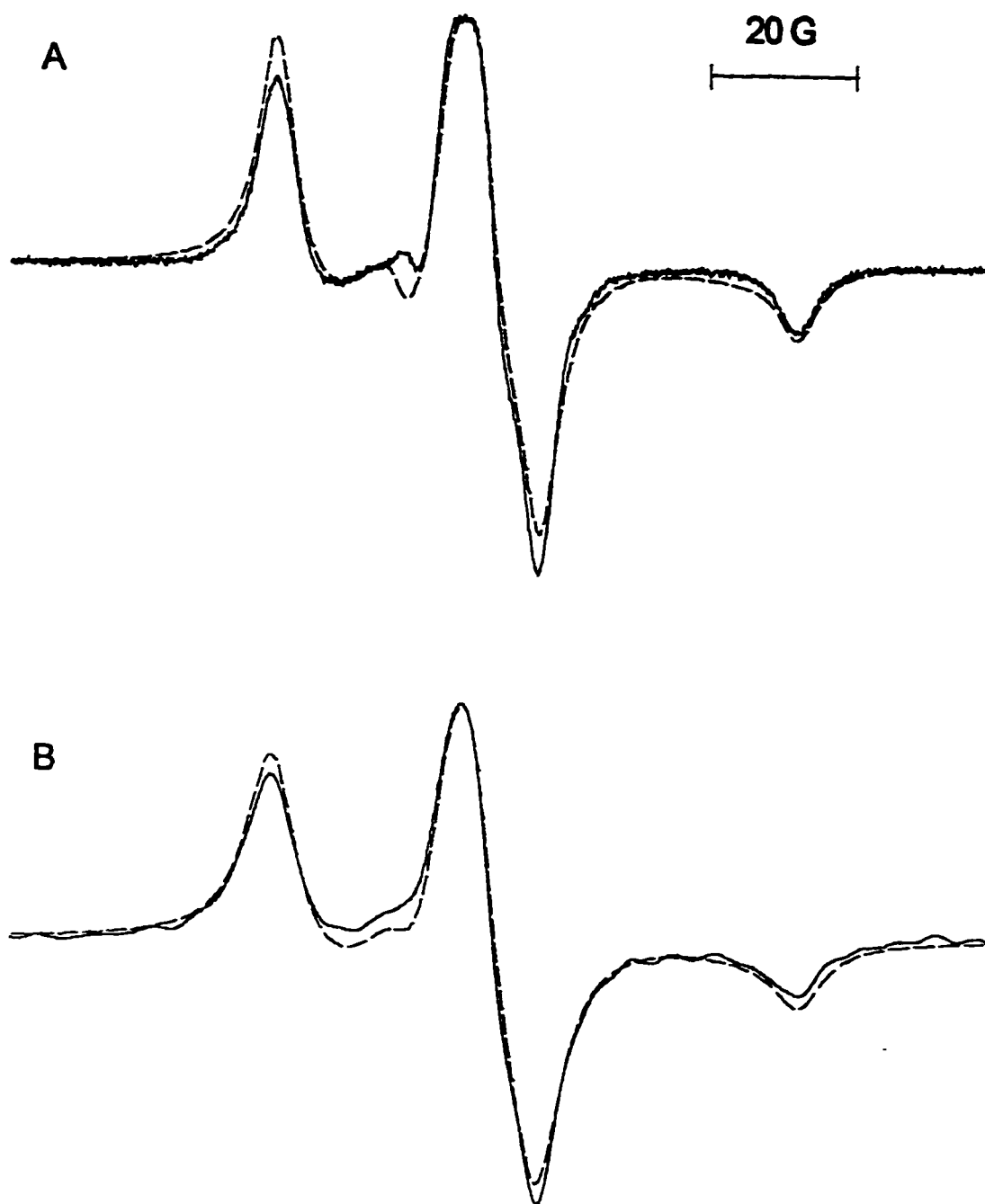


Figure VI.4. Rigid limit spectra for PD-Tempone in the phospholipid systems DMPC/DHPC+Yb³⁺ (A) and DMPC/DHPC+Y³⁺ (B), and simulations (dashed lines) based on magnetic parameters given in Table VI.1.

The two spectra were similar but the resolution of the central region in both spectra was lower than the resolution of the same region in the rigid limit spectra of PD-Tempone in DMPC/DHPC. Clearly this can be attributed to the presence of the paramagnetic Yb^{3+} and the diamagnetic Y^{3+} . The improved fit of these simulations could also be explained by the presence of Yb^{3+} and Y^{3+} . The water molecules would aggregate around the paramagnetic-phospholipid complexes (Hauser et al, 1977; Grasdalen et al, 1977) and therefore would become less available for interaction with the nitroxide radicals. Moreover, the rare earth metal ions interact preferentially with the head-groups of the phosphatidylcholine (Prosser et al, 1996) therefore reducing the extent of interaction between PD-Tempone and the phosphatidylcholine head-groups. This would contribute to the similarity of the two rigid limit spectra in the presence of the two rare earth metal ions as compared to the rigid limit spectrum measured in their absence.

Albeit the similarity of the two spectra in Fig VI.4, some slight differences can still be observed. The positive portion of the central region in the rigid limit spectrum of DMPC/DHPC+ Yb^{3+} is flatter at the top than the same portion in the spectrum of DMPC/DHPC+ Y^{3+} . Another difference is the hump close to the central peak. This hump was more resolved in the spectrum of DMPC/DHPC+ Yb^{3+} than in the spectrum of DMPC/DHPC+ Y^{3+} . Hence, it can be concluded from this that the interaction of Yb^{3+} with the system DMPC/DHPC +

PD-Tempone is slightly different from the interaction of Y^{3+} with the same system.

VI.4.2. Variable Temperature Experiments

The objectives of this section were to study the variations of the hyperfine spacings and the g -factor as a function of temperature for the three phospholipid systems. Based on the values of the hyperfine spacings and the g -factor, it was possible to calculate the order parameter $\langle D_{00}^2 \rangle_z$ and the potential expansion coefficient, or the solvent order parameter, λ . Finally, the principal ordering matrix tensors S_{11} , S_{22} , and S_{33} were calculated for the three phospholipid systems.

VI.4.2.1. *PD-Tempone in DMPC/DHPC-* The study of PD-Tempone in DMPC/DHPC at X-band with 100-KHz field modulation, was performed over a range of temperatures from 22.4 to , *ca.*, 76.8 °C and selected spectra are shown in Figure VI.5. These spectra were obtained after the system (PD-Tempone + DMPC/DHPC) was exposed to a static magnetic field of 10,000 Gauss (1 Tesla) for one hour. The general features of these spectra are similar to the EPR spectra of the spin nitroxide TEMPO obtained by Wu and McConnell (1975) for binary mixtures containing dielaidoylphosphatidylcholine together with dimyristoylphosphatidylcholine and several other phosphatidylcholines.

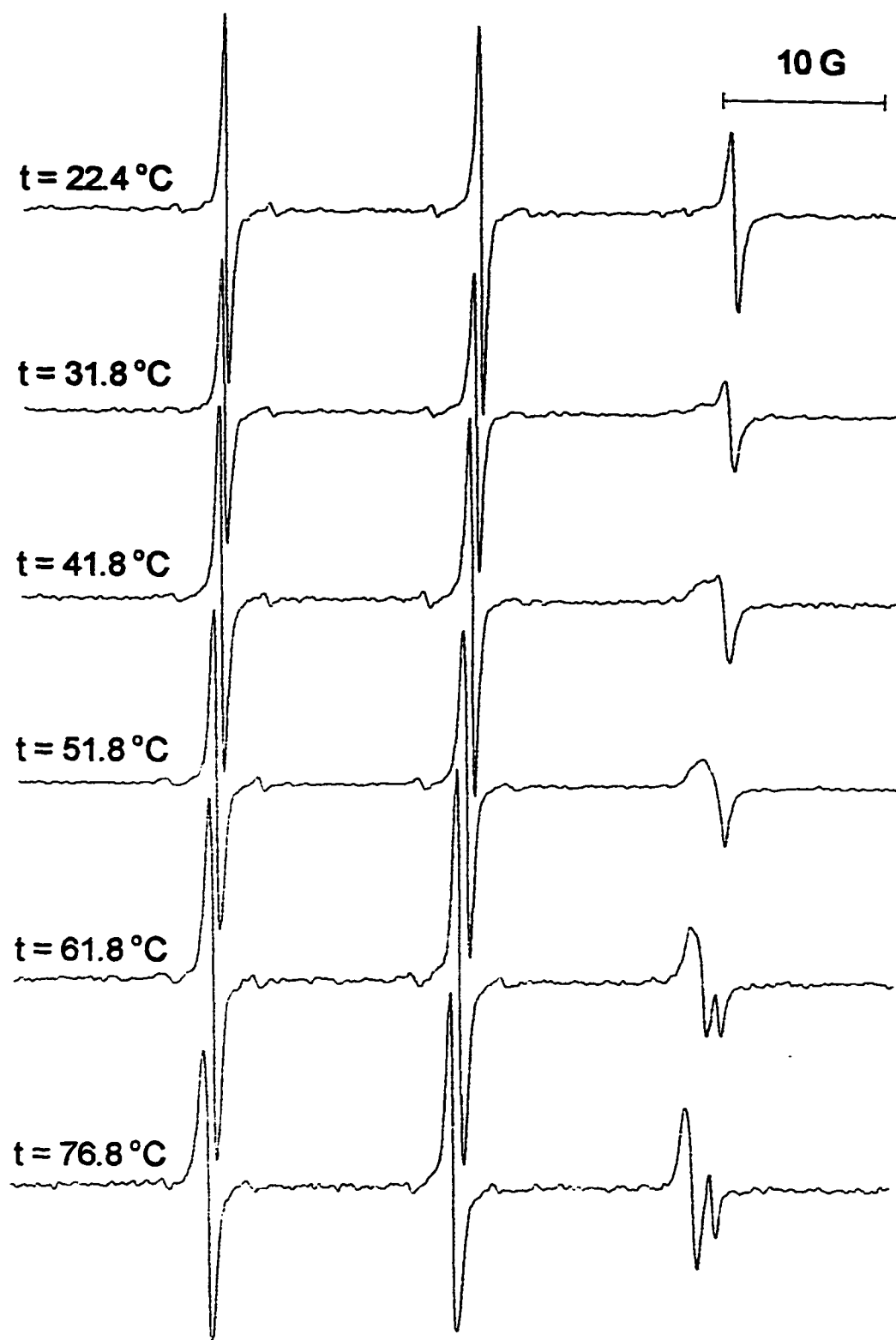


Figure VI.5. Selected experimental EPR spectra of PD-Tempone in DMPC/DHPC at different temperatures.

The splitting in the high field spectral line ($M_I = -1$) is due to the proportionation of PD-Tempone into the fluid lipid region which is indicated as H in Fig. VI.8 (page 203), and the aqueous region indicated as P in Fig. VI.8 (Wu & McConnell, 1975). Qualitatively, fractions of PD-Tempone in the fluid lipid region extend to values higher than one in this study, whereas fractions observed in previous studies (Wu & McConnell, 1975; Smimov et al, 1995) did not exceed one. This could be attributed to the relatively higher concentrations of phosphatidylcholines in this study (25% w/v) compared with previous studies (8-11% w/w) (cf. Wu & McConnell, 1975). Besides the approximate doubling of the phospholipid concentration, the presence of rare earth metal ions (in the two systems presented in the coming sections) possibly allowed further mixing of water molecules and therefore of PD-Tempone with the lipid bilayer.

Figure VI.6 shows the variation of the hyperfine splitting a and the g -factor with temperature for PD-Tempone in DMPC/DHPC. Also shown in the Figure are the variation of both the solute order parameter $\langle D_{00}^2 \rangle_z$ and the solvent order parameter λ with temperature for the same system. The g -factor, the solute order parameter $\langle D_{00}^2 \rangle_z$, and the solvent order parameter λ increased as the temperature increased, whereas the hyperfine splitting a decreased as the temperature increased. This behavior is opposite to the behavior of the thermotropic liquid crystals 5CB, 6CB, 7CB, and 8CB (Oweimreen & Hwang, 1989; Hwang et al, 1994; Oweimreen et al, 1995; Morsy et al, 1996) and in accordance with the behavior of previously studied phospholipid bilayers (Jost et

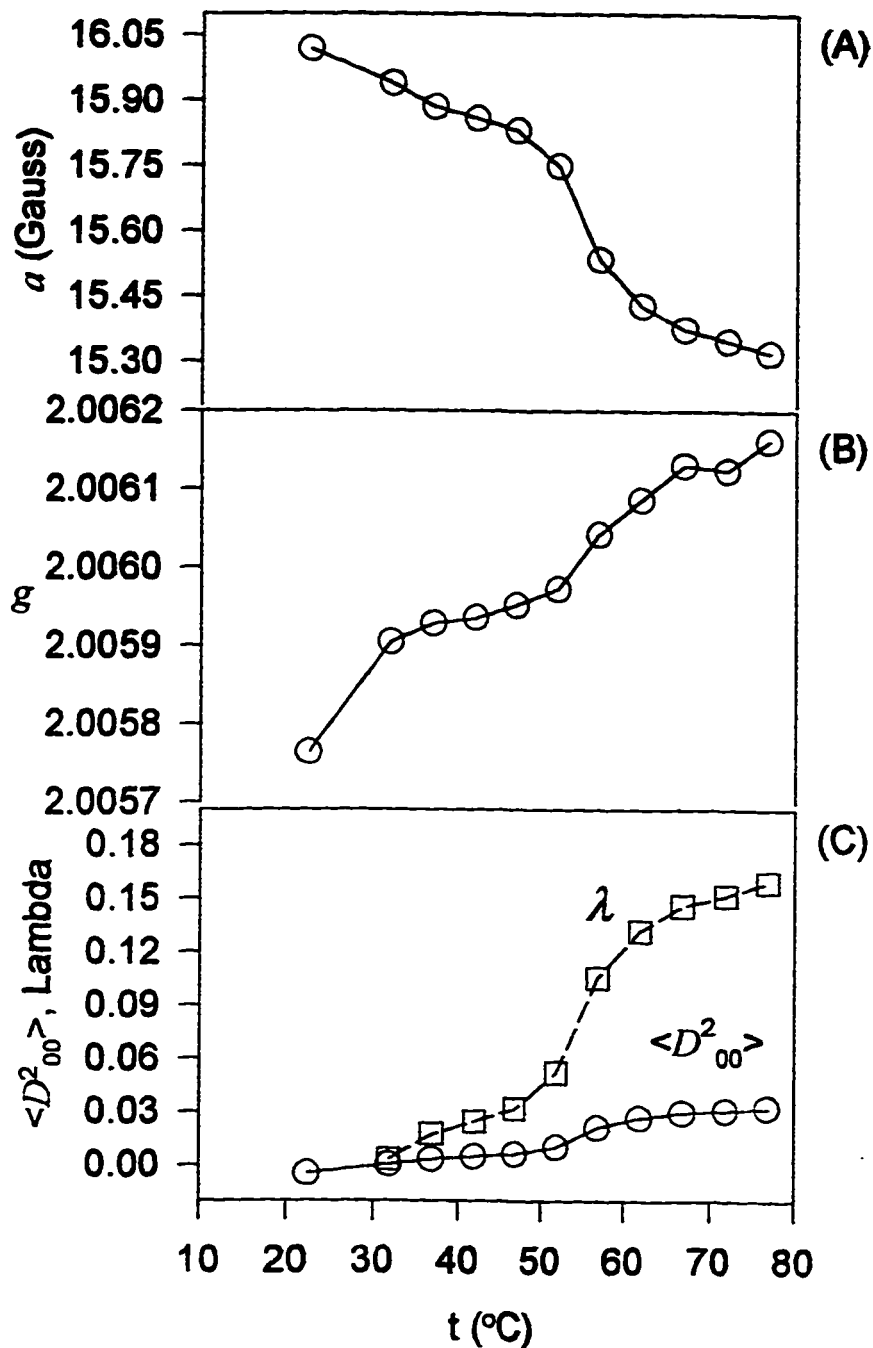


Figure VI.6. Parameters calculated are for the system PD-Tempone in DMPC/DHPC. (A) Hyperfine splitting a versus temperature. (B) g -Factor versus temperature. (C) Solute order parameter $\langle D^2_{00} \rangle$ and solvent order parameter λ versus temperature.

al, 1971, Libertini et al, 1974). (The liquid crystals are homologous members of the *p-n*-alkyl-*p'*-cyanobiphenyl with the alkyl groups in 5CB, 6CB, 7CB, and 8CB corresponding to, respectively, pentyl, hexyl, heptyl, and octyl.) A phase transition can be noticed in the temperature range 50-60 °C. Figure VI.7 shows the variation of the *f*-factor (Eq. [VI.33]), the order parameters S_{11} and S_{22} , and S_{33} and $\langle D_{00}^2 \rangle_z$ versus temperature. Fig.'s VI.7(B) and VI.7(C) indicates that $|S_{11}|$ and $|S_{22}|$ are almost equal and both are generally greater than $|S_{33}|$. The good agreement between S_{33} and $\langle D_{00}^2 \rangle_z$ is demonstrated in Fig. VI.7(C).

VL4.2.2. PD-Tempone in DMPC/DHPC+Yb³⁺- The EPR study of the weakly ordered nitroxide spin probe PD-Tempone in DMPC/DHPC+Yb³⁺ at X-band with 100-KHz field modulation, was performed over a range of temperatures from 22.8 to, *ca.*, 81.8 °C. Selected spectra are shown in Figure VI.8. These spectra were obtained after the system (PD-Tempone + DMPC/DHPC+Yb³⁺) was exposed to a static magnetic field of 10,000 Gauss (1 Tesla) for one hour, similar to the treatment applied to the system (PD-Tempone + DMPC/DHPC). The splitting in the high field spectral line ($M_l = -1$) is due to differences in the polarity of the spin-label environment (Shimshick & McConnell, 1973). The two signals are due to the proportionation of PD-Tempone into the fluid lipid region H, and the aqueous region P. This splitting would allow the calculation of the spectral parameter, *f*, which is equal to H/(H+P) defined by Shimshick and McConnell (1973). From the results of this preliminary study, the

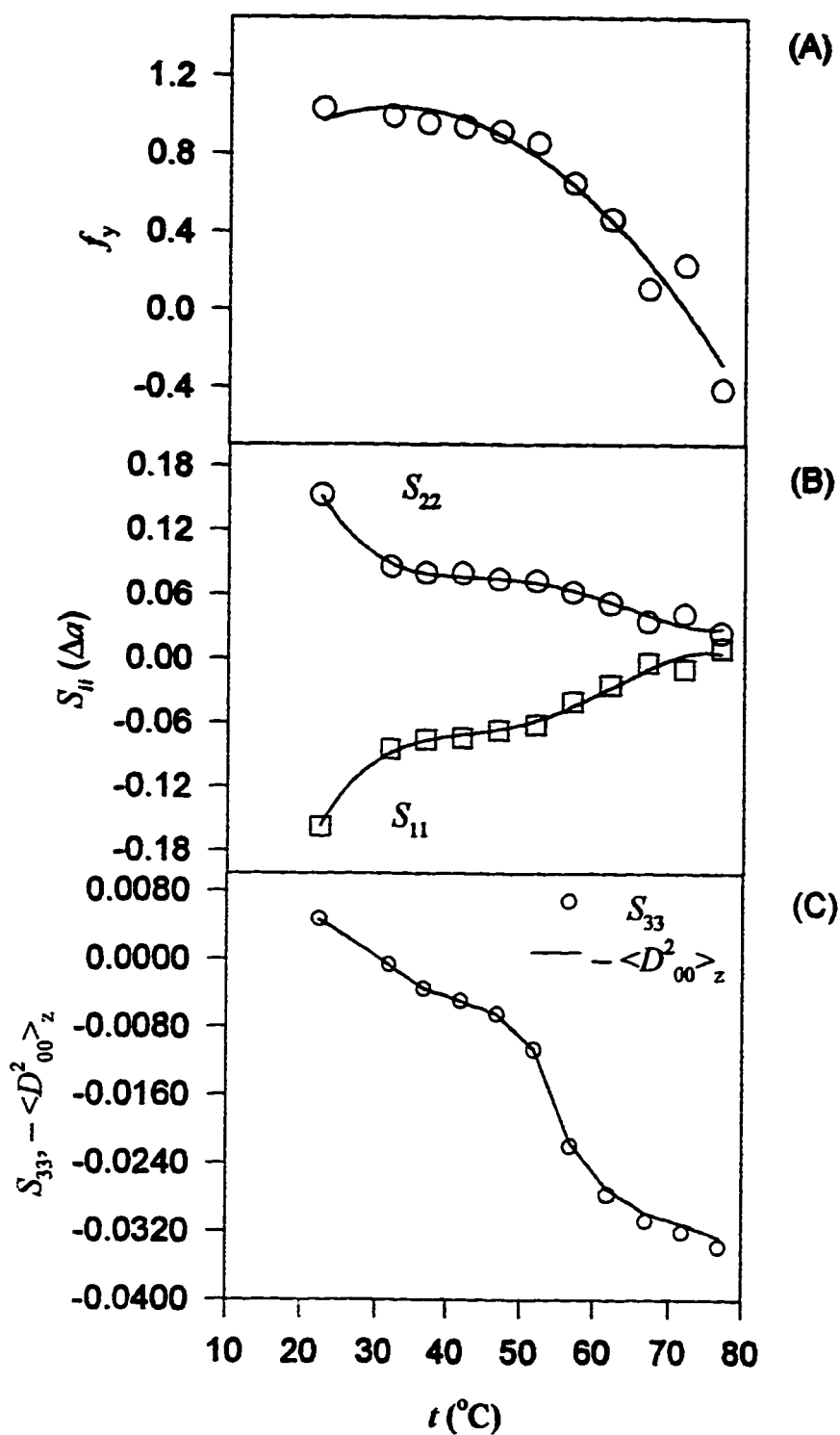


Figure VI.7. Parameters calculated are for the system PD-Tempone in DMPC/DHPC. (A) f -Factor versus temperature. (B) Order parameters S_{11} and S_{22} versus temperature. (C) S_{33} and $-\langle D_{00}^2 \rangle_z$ versus temperature.

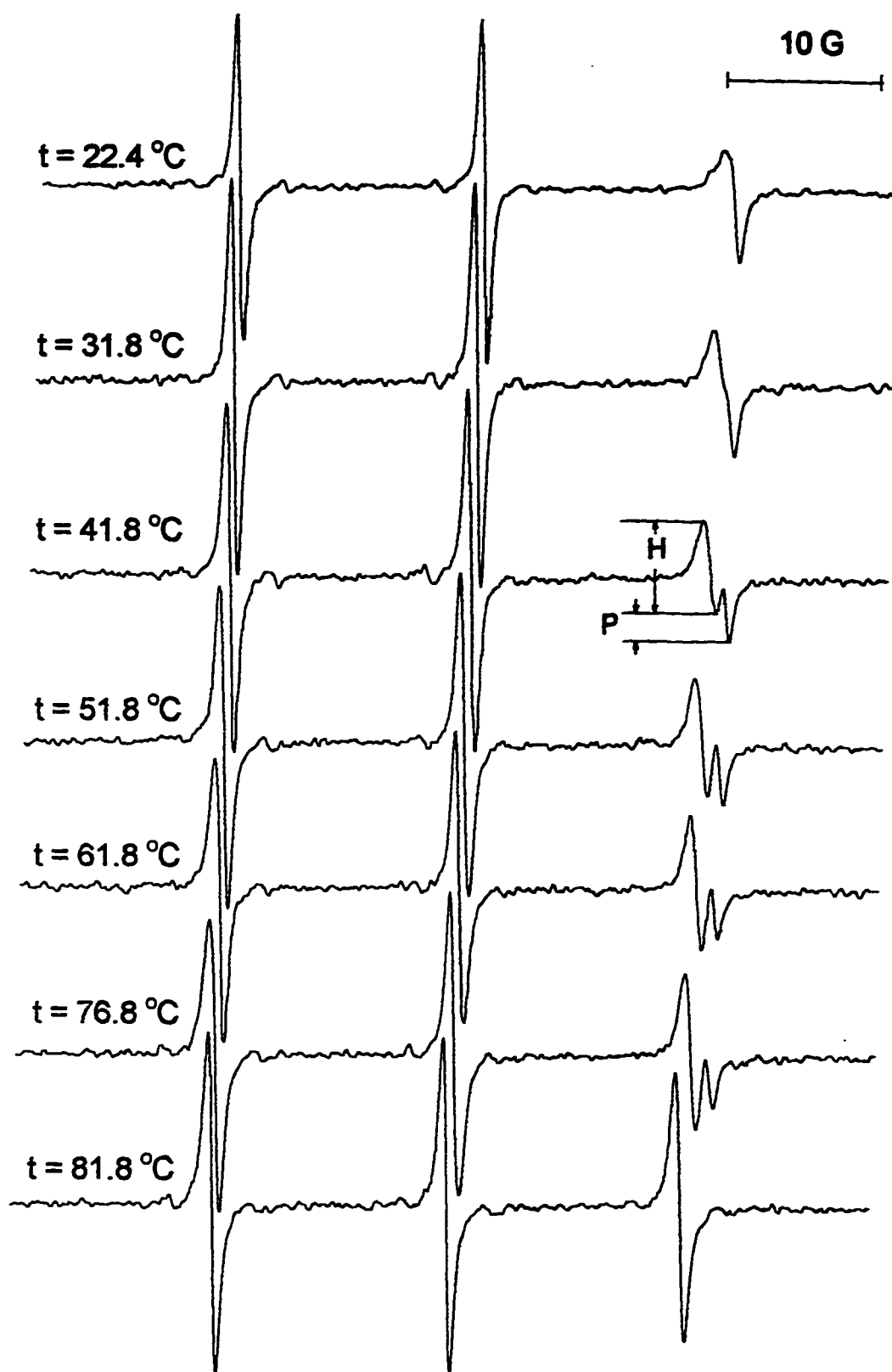


Figure VI.8. Selected experimental EPR spectra of PD-Tempone in DMPC/DHPC+Yb³⁺ at different temperatures.

temperature intervals at which phase transitions take place are wide. Further investigations are required. These include visual studies of phase alterations as a function of temperature varied in small intervals (0.5 to 1.0 °C close to the phase transition regions). Moreover, the same experiments should be performed by EPR and Differential Scanning Calorimetry (DSC).

The variation of the hyperfine splitting a and the g -factor with temperature is shown in Figure VI.9 for PD-Tempone in DMPC/DHPC+Yb³⁺. Also shown in the Figure are the variation of both the solute order parameter $\langle D_{00}^2 \rangle_z$ and the solvent order parameter λ with temperature for the same system. Two phase transition regions can be identified in the temperature ranges 30–40 °C and 70–80 °C. Variations of the hyperfine splitting a , the g -factor, the solute order parameter $\langle D_{00}^2 \rangle_z$, and the solvent order parameter λ as a function of temperature follow the same behavior observed for the DMPC+DHPC system.

Figure VI.10 shows the variation of the f -factor, the order parameters S_{11} and S_{22} , and S_{33} and $\langle D_{00}^2 \rangle_z$ versus temperature. The two relatively abrupt phase transitions are again displayed as a function of temperature by the factor f in Fig. VI.10(A). Fig.'s VI.10(B) and VI.10(C) indicates that $|S_{11}|$ is relatively greater than $|S_{22}|$, and $|S_{22}|$ and $|S_{33}|$ are almost equal. The variation of S_{22} as a function of temperature is almost opposite to the variation of S_{33} with temperature. Again, the good agreement between S_{33} and $\langle D_{00}^2 \rangle_z$ is demonstrated in Fig. VI.10(C).

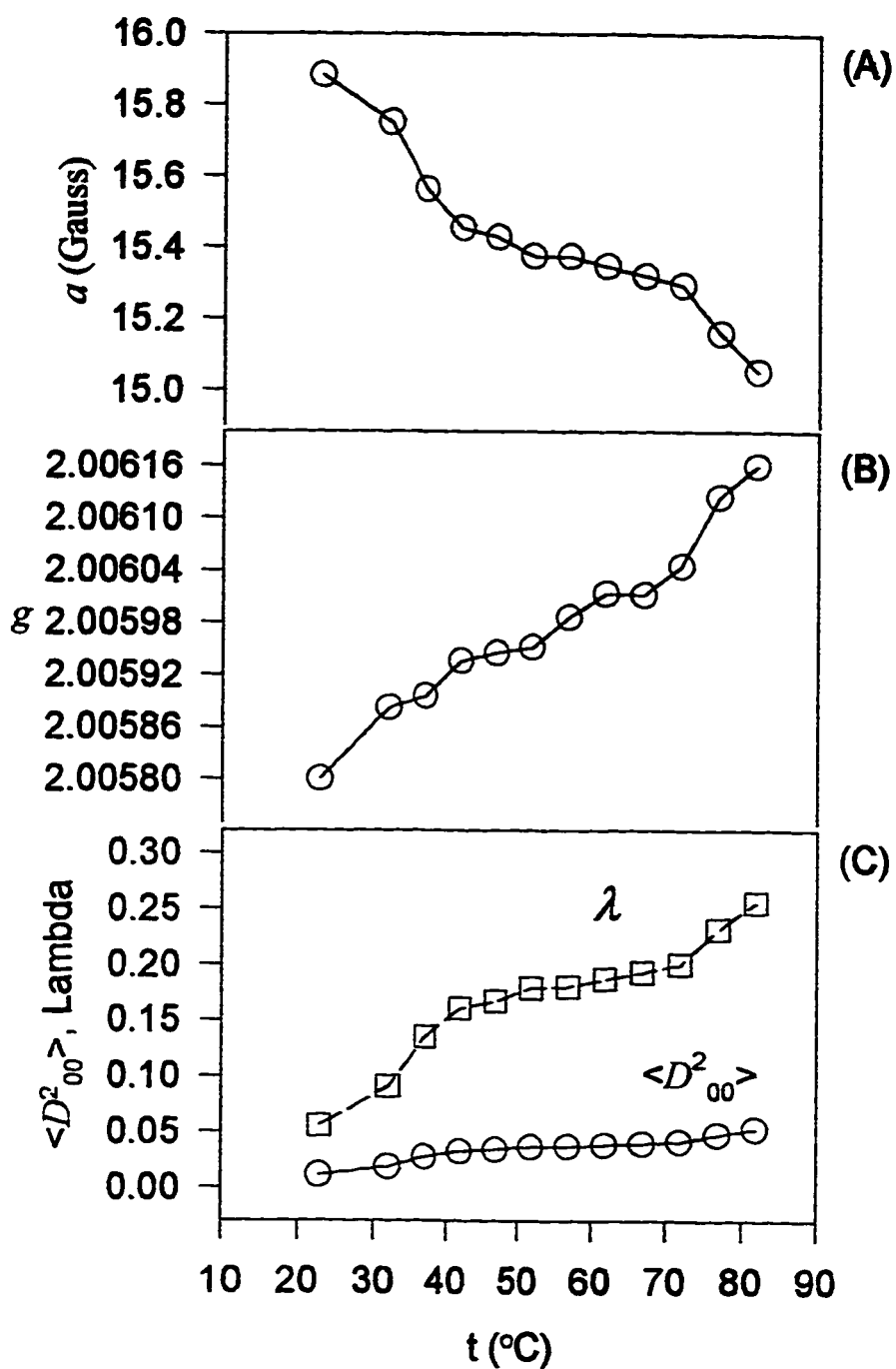


Figure VI.9. Parameters calculated are for the system PD-Tempone in DMPC/DHPC+Yb³⁺. (A) Hyperfine splitting a versus temperature. (B) g -Factor versus temperature. (C) Solute order parameter $\langle D^2_{00} \rangle$ and solvent order parameter λ versus temperature.

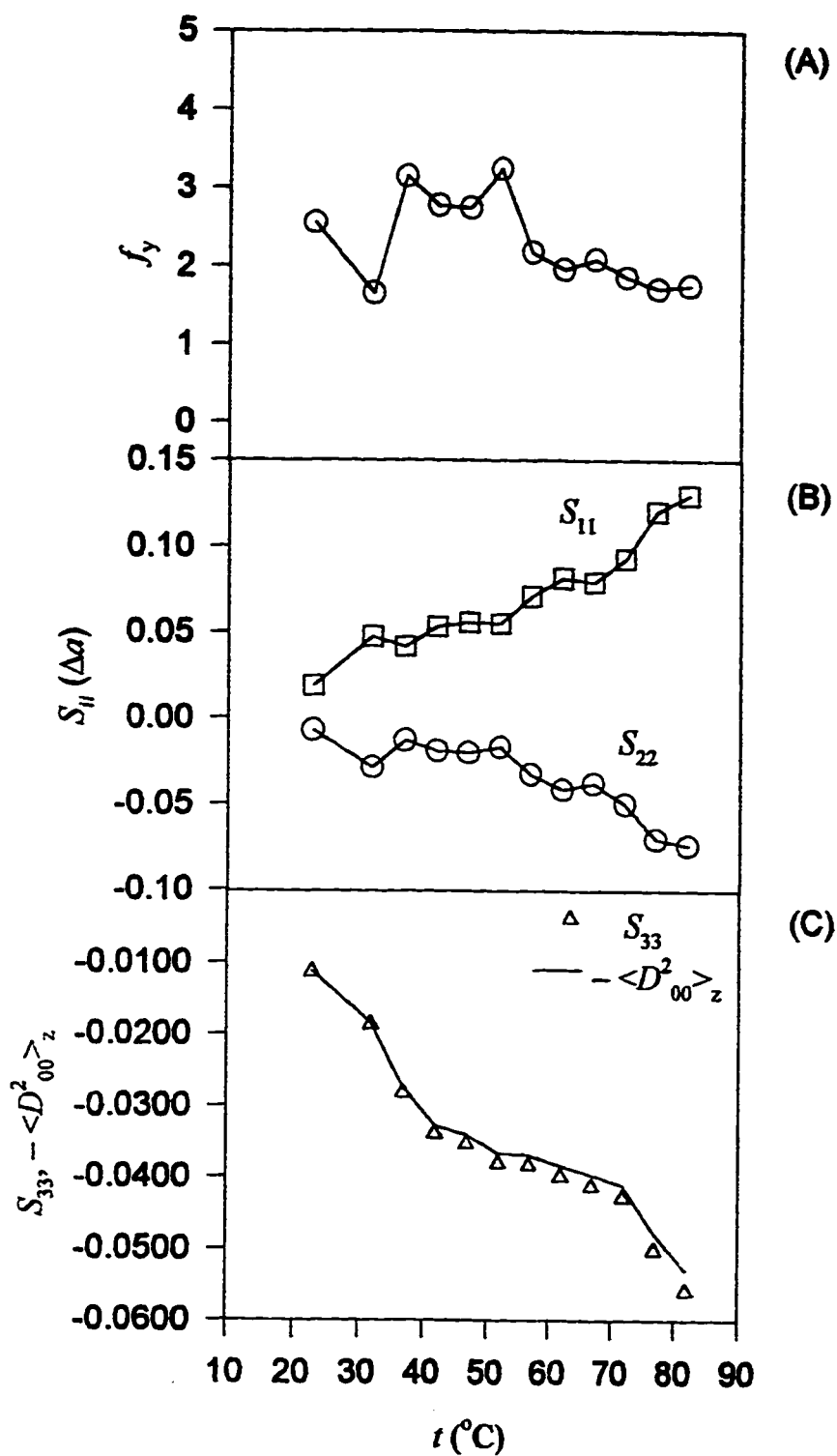


Figure VI.10. Parameters calculated are for the system PD-Tempone in DMPC/DHPC+Yb³⁺. (A) f -Factor versus temperature. (B) Order parameters S_{11} and S_{22} versus temperature. (C) S_{33} and $-\langle D^2_{00} \rangle_z$ versus temperature.

VI.4.2.3. PD-Tempone in DMPC/DHPC+Y³⁺. The study of PD-Tempone in DMPC/DHPC+Y³⁺ at X-band with 100-KHz field modulation, was performed over a range of temperatures from -13.2 to, *ca.*, 76.8 °C and selected spectra are shown in Figure VI.11. These spectra were obtained after the system (PD-Tempone + DMPC/DHPC+Y³⁺) was exposed to a static magnetic field of 10,000 Gauss (1 Tesla) for one hour. Apparently, the extent of interaction between the charge on yttrium(III) and PD-Tempone is relatively more than in the system with Yb³⁺. This seems to broaden the EPR signal of the system (PD-Tempone + DMPC/DHPC+Y³⁺) and consequently the splitting in the high-field line was obscured.

Figure VI.12 shows the variation of the hyperfine splitting α and the g -factor with temperature for PD-Tempone in DMPC/DHPC+Y³⁺. Variations of both the solute order parameter $\langle D_{00}^2 \rangle_z$ and the solvent order parameter λ with temperature for the same system are also shown in the same Figure. Although these variations are smoother than previous results (Fig.'s VI.6 & VI.9), the same general trend is maintained.

Figure VI.13 shows the variation of the f -factor, the order parameters S_{11} and S_{22} , and S_{33} and $\langle D_{00}^2 \rangle_z$ versus temperature. The variation of the f -factor as a function of temperature shown in Fig. VI.13(A) displays a sharp transition at ~45 °C. The possibility of multiple transitions cannot be excluded. Although S_{11} and S_{22} cross each other, Fig. VI.13(B), generally $|S_{11}|$ is greater than $|S_{22}|$, whereas $|S_{33}|$, Fig. VI.13(C), is intermediate between $|S_{11}|$ and $|S_{22}|$. The variation of S_{22} as

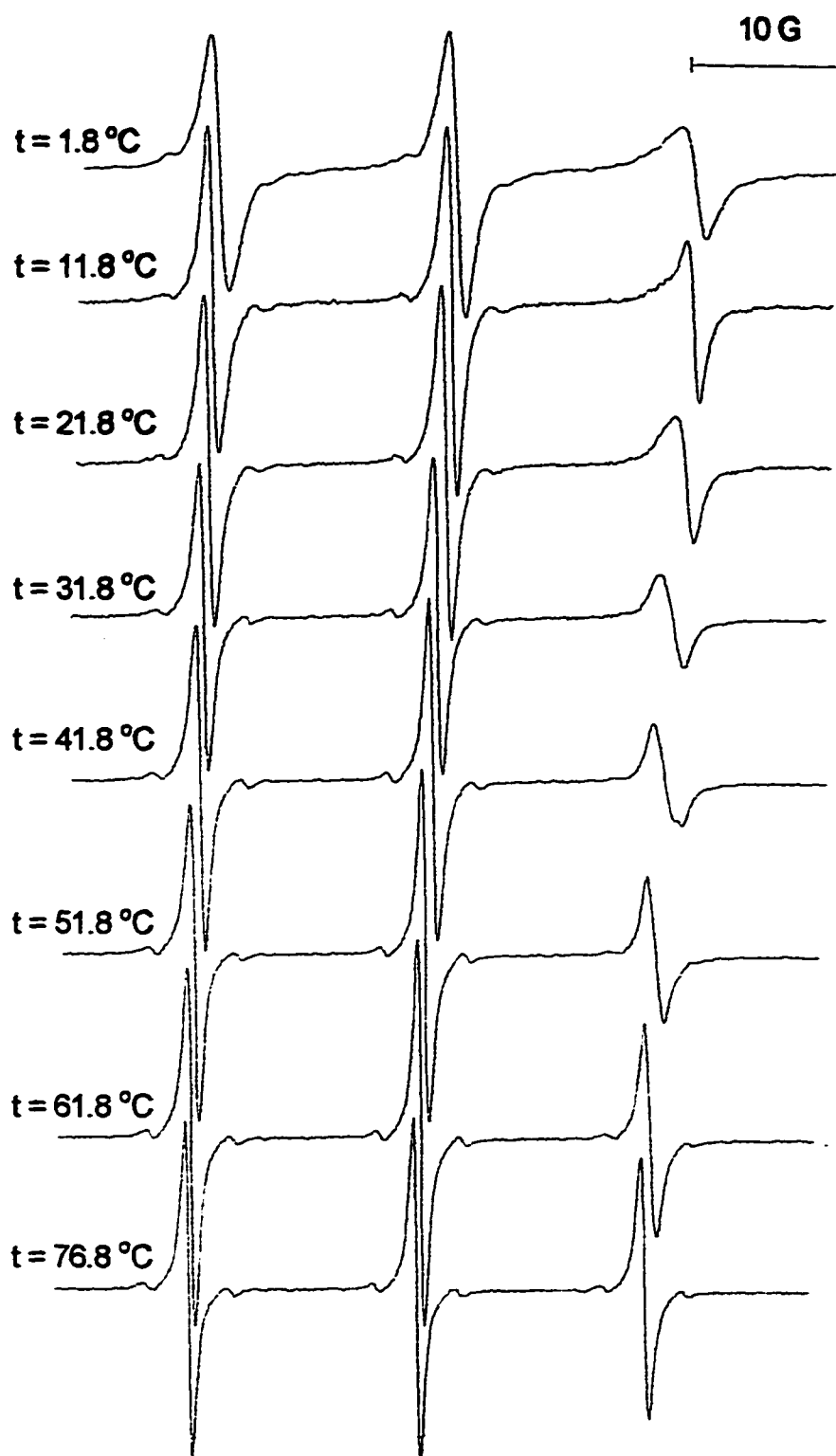


Figure VI.11. Selected experimental EPR spectra of PD-Tempone in DMPC/DHPC+Y³⁺ at different temperatures.

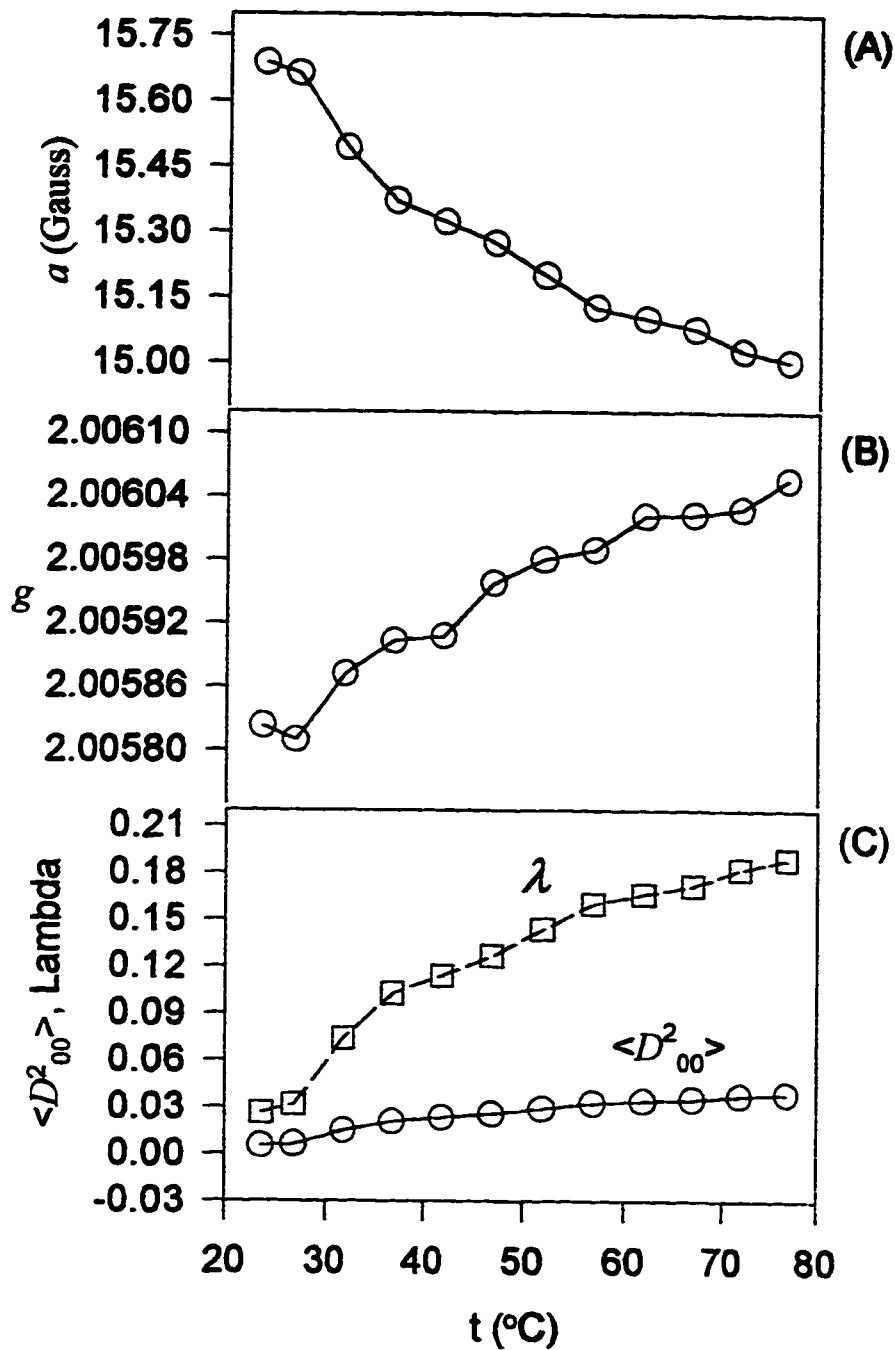


Figure VI.12. Parameters calculated are for the system PD-Tempone in DMPC/DHPC+Y³⁺. (A) Hyperfine splitting a versus temperature. (B) g -Factor versus temperature. (C) Solute order parameter $\langle D^2_{00} \rangle$ and solvent order parameter λ versus temperature.

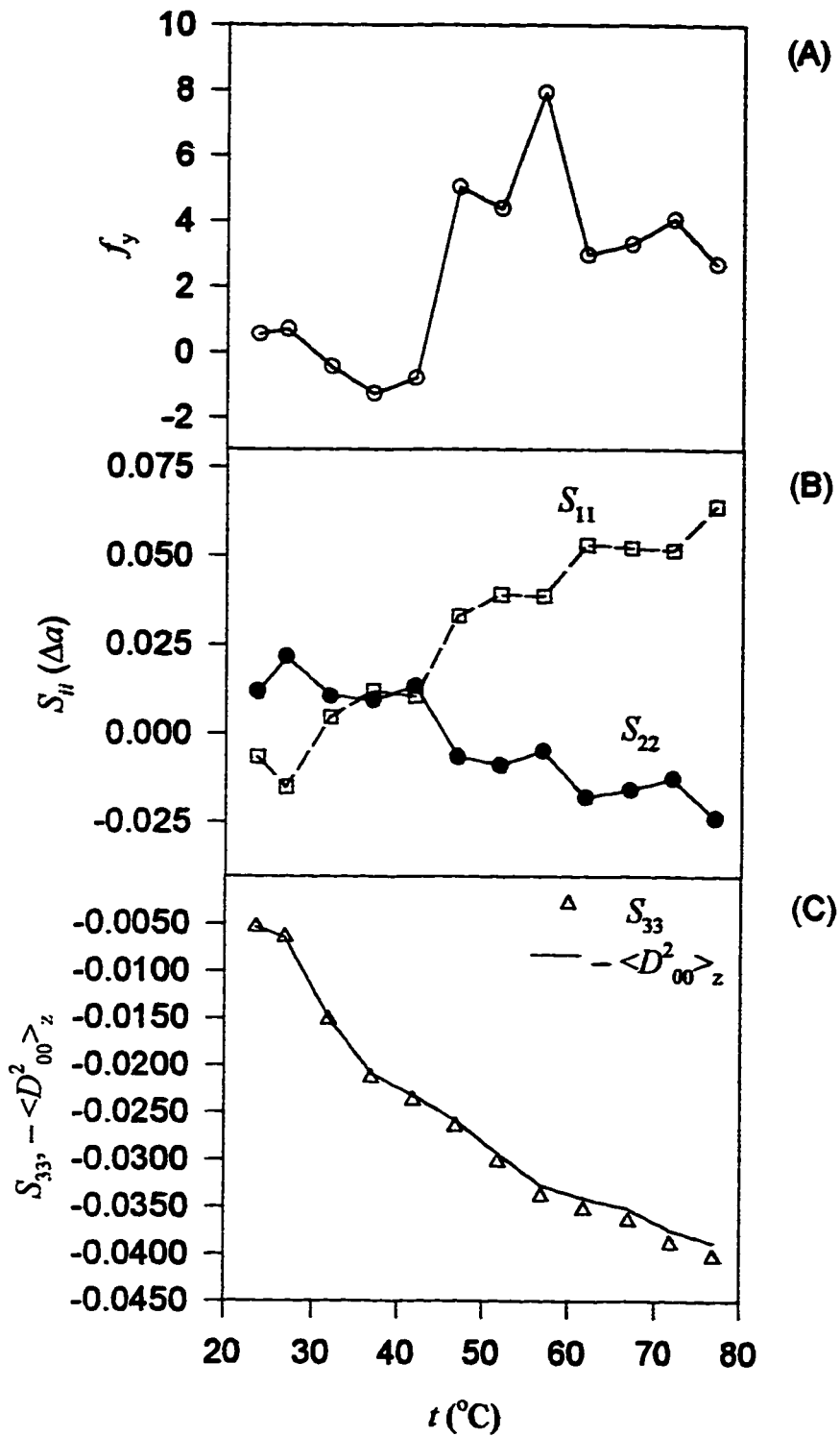


Figure VI.13. Parameters calculated are for the system PD-Tempone in DMPC/DHPC+Y³⁺. (A) f -Factor versus temperature. (B) Order parameters S_{11} and S_{22} versus temperature. (C) S_{33} and $\langle D_{00}^2 \rangle_z$ versus temperature.

a function of temperature is almost opposite to the variation of S_{11} with temperature. A satisfactory agreement between S_{33} and $\langle D_{00}^2 \rangle_z$ is shown in Fig. VI.13(C). Comparisons between the values of the order parameter S_{22} calculated using the g -factor, $S_{22}(\Delta g)$, and using the hyperfine splitting a , $S_{22}(\Delta a)$, are shown in Figure VI.14 for PD-Tempone in the three phospholipid systems. Linearity is fully satisfied between $S_{22}(\Delta g)$ and $S_{22}(\Delta a)$.

From these *preliminary* studies the following observations can be deduced. Firstly, addition of the lanthanide ion ytterbium(III) has a clear effect on the alignment of the highly ordered binary mixture of the phosphatidylcholines DMPC and DHPC. Addition of yttrium(III) effects the alignment of this mixture to a lesser extent. Ytterbium(III) interacts with the polar head group of the phospholipid bilayers through both its positive charge and the pseudocontact effect (Bleaney, 1972), whereas yttrium(III) interacts via its positive charge only. This trend can be clearly seen from Figure VI.15, which shows the variation of the order parameters $S_{22}(\Delta a)$, $S_{33}(\Delta a)$, and $S_{11}(\Delta a)$ as a function of temperature. The effect of adding yttrium(III) to the bicelles is always intermediate between when no lanthanide ion is added and when ytterbium(III) is added. In the absence of lanthanide ions and in the presence of Y^{3+} , only S_{11} and S_{22} seem to correlate, while in the presence of Yb^{3+} , all order parameters appear to correlate with each other. Secondly, the order parameters S_{11} and S_{22} flipped positions on going from bicelles with no lanthanon, passing through bicelles with yttrium(III), and ending at bicelles with ytterbium(III). This can be verified by examining

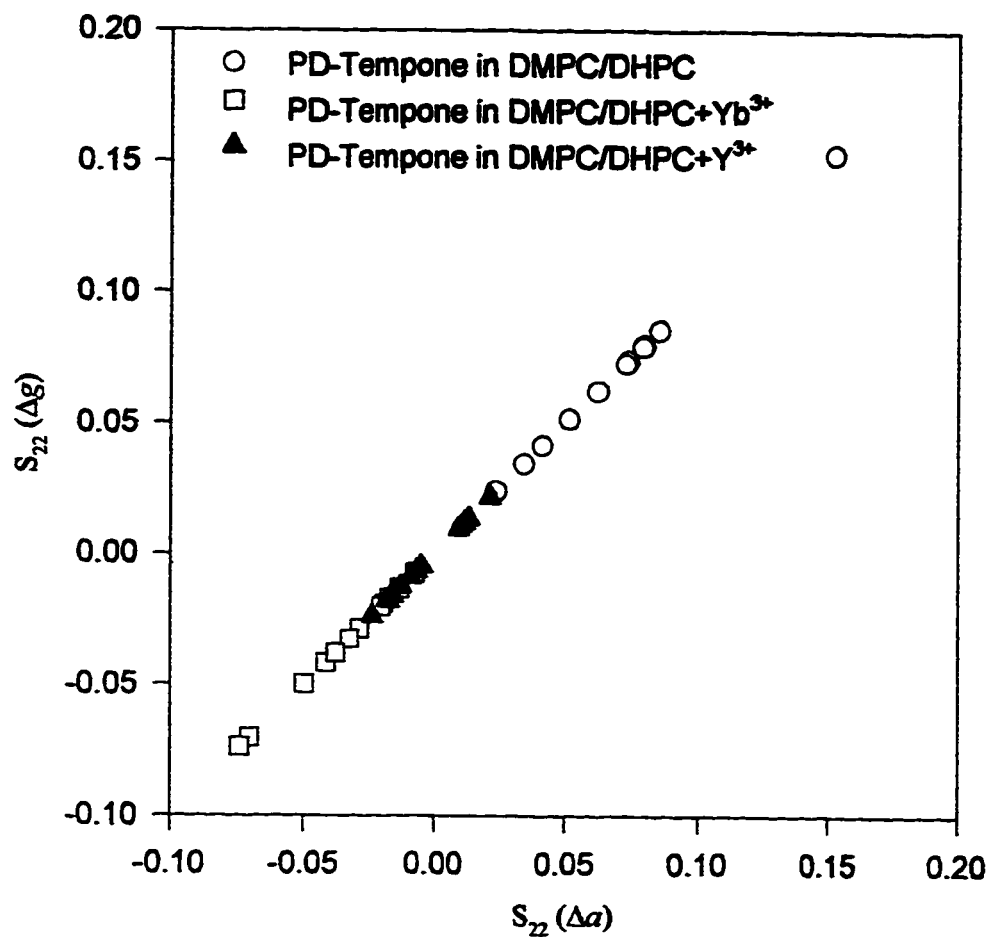


Figure VI.14. The order parameter S_{22} calculated using the g -factor and using the hyperfine splitting a for PD-Tempone in the three phospholipid systems: DMPC/DHPC, DMPC/DHPC+Yb³⁺, and DMPC/DHPC+Y³⁺.

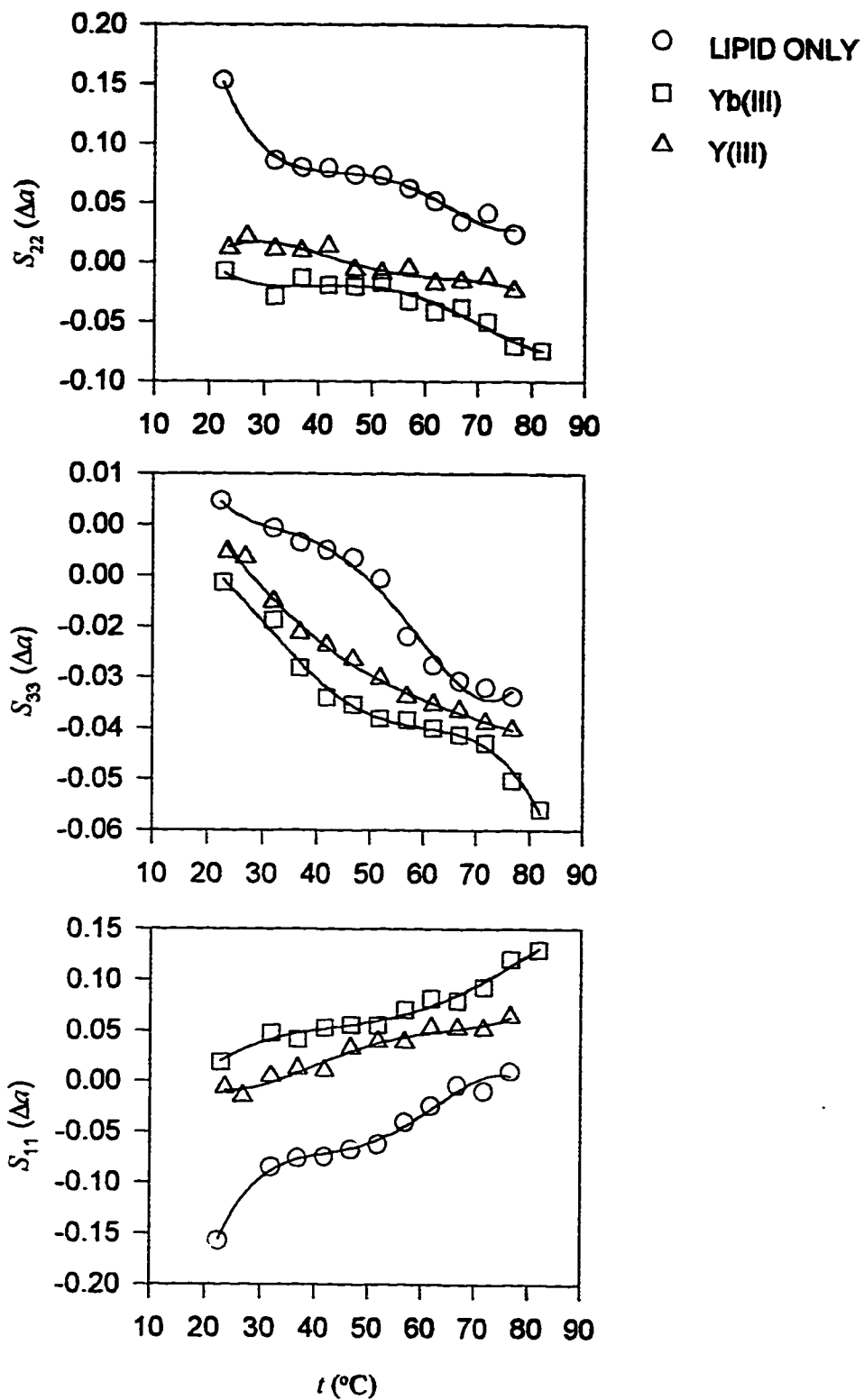


Figure VI.15. Order parameters S_{ii} calculated using the hyperfine splitting α for PD-Tempone as a function of temperature in the three phospholipid systems: DMPC/DHPC, DMPC/DHPC+Yb³⁺, and DMPC/DHPC+Y³⁺.

curves labeled (B) in Fig.'s VI.7, VI.13, and VI.10, respectively. The flipping of these order parameter, where S_{11} and S_{22} correspond to ordering in the molecular x-axis and y-axis directions, respectively, could be an indication of the flipping of this bicelles system (Prosser et al, 1996; Prosser et al, 1997). This flipping is also presented schematically in Figure VI.16. Thirdly, the agreement between S_{33} and $\langle D_{00}^2 \rangle_z$ is quite satisfactory and transformation (Polnaszek & Freed, 1975) to the Maier-Saupe potential expansion coefficient λ could be performed using either S_{33} or $\langle D_{00}^2 \rangle_z$.

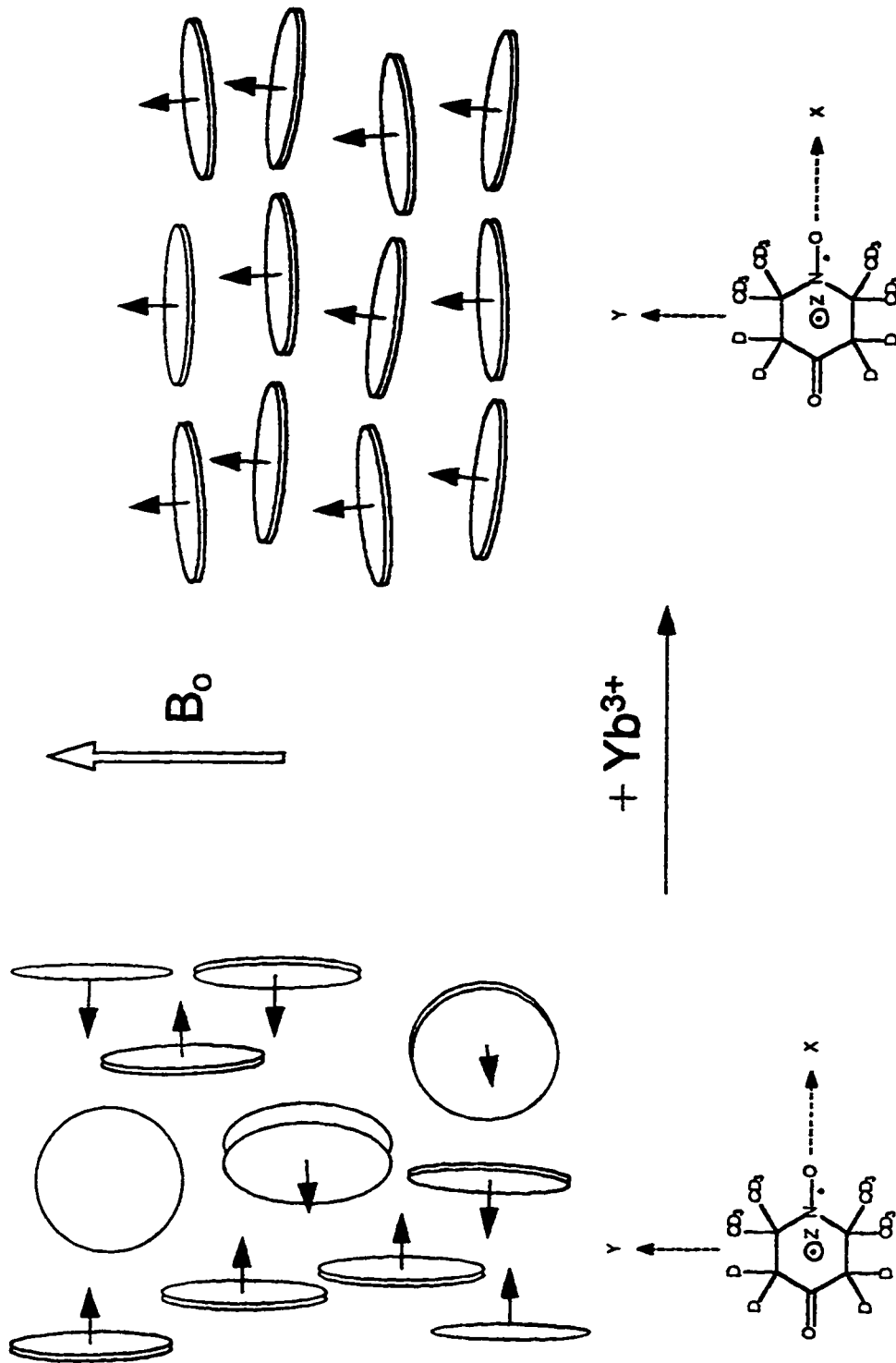


Figure VI.16. Long-range order for DMPC/DHPC discoidal bicelles for perpendicular alignment (left) and parallel alignment (right) relative to the applied magnetic field B_0 . The flipping is induced by the addition of ytterbium(III). The discs at the left form cylindrical distribution whereas the discs on the right organize into layers representing a smectic mesophase all with their unique axes pointing basically in the same direction. The suggested orientation of PD-Tempone is also depicted. (This sketch was adapted from Prosser et al, 1997.)

CHAPTER VII

NITRIC OXIDE AND NITROXIDE SPIN PROBE ADDUCTS OF BUCKMINSTERFULLERENE

VII.1. Introduction

In this work we studied the gas-solid interaction between nitric oxide (NO) and buckminsterfullerene and we synthesized a nitroxide spin probe derivatized from buckminsterfullerene. The chemistry and physics of buckminsterfullerene has been studied intensively (Hammond and Kuck, 1992; McLafferty, 1992; Kadish and Ruoff, 1994; Foote, 1994) since its discovery in 1985 (Kroto, *et al.*, 1985). Also, several reviews of the synthetic aspects of the nitroxide spin probes have appeared in the literature (Rozantsev, 1970; Keana, 1978; Gaffney, 1976). However, and to the best of our knowledge, this is the first time a nitroxide spin probe was derivatized from buckminsterfullerene. The importance of such adduct becomes evident when probing the behavior of buckminsterfullerene in different systems using EPR (e.g., studying the

translational diffusion of the adduct **8**, which resembles buckminsterfullerene, in different solvents).

The chemistry of buckminsterfullerene (C_{60}) has become a rapidly developing area of research. Chemical modifications of fullerenes by selective bond formation provide a vital tool in fullerene science and technology. Intensive efforts in the past few years have laid an organic foundation on the C_{60} sphere that includes ring systems of different sizes (Rubin, *et al.*, 1993; Khan, *et al.*, 1993; Prato, *et al.*, 1993; Rotello, *et al.*, 1993). The next step was to construct useful functionalities on such foundations.

VII.1.1. Buckminsterfullerene

The 1996 Nobel Prize in Chemistry went to R. F. Curl, H. W. Kroto, and R. E. Smalley for the discovery of buckminsterfullerene (C_{60}) in 1985 (Kroto, *et al.*, 1985). Numerous work has resulted since the discovery of a new method to produce and purify macroscopic quantities of fullerenes (Krätschmer, *et al.*, 1990; Ajie, *et al.*, 1990; Haufler, *et al.*, 1990; Cox, *et al.*, 1991). Buckminsterfullerene is stable due to geodesic and electronic properties inherent in the truncated icosahedral (symmetry group I_h) cage structure (Kroto, *et al.*, 1985). The stability of geodesic structures was realized by Muslim architects hundreds of years ago, where it constitute an integral part of mosques

and holy places. This stability was explored by R. Buckminster Fuller, who himself was an architect.

The molecule C_{60} consists of 20 six-membered rings and 12 five-membered rings. Curvature is provided by the five-membered rings while strain is minimized since no two five-membered rings are adjacent. Fullerenes manifest a compromise between strain and conjugation which should provide more insight into theoretical considerations of the nature of aromaticity. The diameter calculated for the C_{60} cage obtained via theoretical modeling is 7.1 Å (Krätschmer, *et al.*, 1990) and, since all of the carbons are equivalent, has a single pyramidalization angle of 11.6° (Rabideau and Sygula, 1996).

Several mechanisms were proposed for the formation of fullerenes (Goroff, 1996). However, none completely fit the experimental results. On the other hand, the possibility of producing fullerene-related hydrocarbons like corannulene, $C_{20}H_{10}$, when buckminsterfullerene is symmetrically chopped was envisaged (Rabideau and Sygula, 1996). All available spectroscopic and analytical techniques were employed to study buckminsterfullerene and related compounds; for example, fluorescence and phosphorescence spectroscopy (Wang, 1992), scanning tunneling microscopy (Zhang, *et al.*, 1992), Raman spectroscopy (Duclos, *et al.*, 1991), ^{13}C MAS NMR (Kanowski, *et al.*, 1995), neutron inelastic scattering spectroscopy (Coulombeau, *et al.*, 1992), and thermogravimetric analysis (Saxby, *et al.*, 1992), to name a few.

VII.1.2. The Study of Buckminsterfullerene by EPR

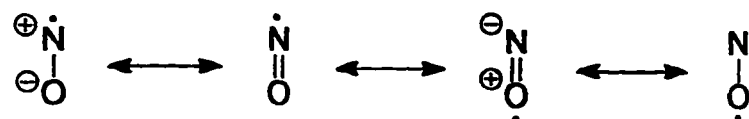
The single crystal of buckminsterfullerene is diamagnetic and has no EPR signal. The observed signal in the EPR spectrum of C_{60} is believed to be due to indigenous paramagnetic impurities associated with C_{60} during its formation. The valence values of charged C_{60}^{ν} molecules which are, for example, generated either photochemically or electrochemically, range from $\nu = -6$ to $\nu = +1$ (Allemand, *et al.*, 1991; Dubios, *et al.*, 1991; Stankowski, *et al.*, 1994; Khaled, *et al.*, 1994; Friedrich, *et al.*, 1994). Upon purification of crude C_{60} samples, an increase in the EPR signal intensity and a possible phase transition at 90 K were observed (Kempiński, *et al.*, 1995). The majority of C_{60} and its related fullerenes have a single EPR signal with varying features. (Krusic, *et al.*, 1991). However, the EPR spectrum of $La@C_{82}$ exhibited an octet of lines centered in the region characteristic of fullerenes anion radicals (Johnson, *et al.*, 1991).

EPR signals can be observed for odd ν and for $\nu = 2$ when a fullerene molecule (C_{60}^{ν}) is in the triplet state. EPR has been utilized in the study of the triplet state of C_{60} . The electronic structure of ${}^3C_{60}$ was investigated by measuring its EPR spectra at 5 K, while the triplet state lifetime for C_{60} was measured using time-resolved EPR of samples at 9 K (Wasielowski, *et al.*, 1991). The study suggests that the electrons in the triplet state reside, on the average, at opposite sides of the molecule. Continuous wave (CW), time-resolved (TR), and Fourier transform (FT) EPR were also used to study the rotational dynamics of the triplet state of C_{60} (Zhang, *et al.*, 1993; Steren, *et al.*,

1993). Triplet-triplet annihilation of $^3\text{C}_{60}$ and triplet quenching by the TEMPO radical were measured by TR-EPR (Goudsmit and Paul, 1993). Photoexcited triplet state of C_{60} , oriented in a nematic liquid crystal, was studied by time-domain EPR (Levanon, et al., 1992). Misra and Petkov reviewed the various EPR studies of C_{60} fullerenes that appeared in the literature up to middle 1994 (Misra and Petkov, 1995).

VII.1.3. Nitric Oxide (NO)

Nitric oxide has a wide range of functions in the body. It regulates blood pressure, dilates blood vessels, transmits messages between nerve cells, destroys certain microorganisms, participates in learning and memory, and might be used by the immune system to fight viral infections. On the other hand, NO is a major atmospheric pollutant that has been implicated in ozone depletion. The valence state of nitric oxide can be described as $\text{NO}[\text{KK}(\text{N}:2s)^2(\text{O}:2s)^2(2p\sigma)^2(2p\pi)^4(2p\pi^*)]$, where the filled orbitals $(2p\sigma)^2$ and $(2p\pi)^4$ correspond to a triple bond and $(2p\pi^*)$ is the orbital with the unpaired electron. The unusually low level of the ground state of the radical was explained by the quantum-mechanical resonance of four valence structures (Pauling, 1960):



Based on Pauling's idea of the three-electron bond, nitric oxide was described by a single formula: $\text{N} \equiv \text{O} \cdot$ (Dousmanis, 1955; Rozantsev, 1970).

A prevailing feature in almost all reactions of nitric oxide, the additional covalent bond is formed with the nitrogen atom (Herschbach, *et al.*, 1956; Rozantsev, 1970). An analysis of the parameters of the hyperfine structure of the EPR spectrum of nitric oxide also leads to the conclusion that the probability of the electron being on the nitrogen atom is about 60% (Dousmanis, 1955; Beringer and Castle, 1950). The hyperfine structure (HFS) of the NO EPR spectrum was attributed to the strong interaction between the moment of the unpaired electron and the rotation of the whole molecule (Beringer, *et al.*, 1954).

The ground electronic level of the NO molecule, ${}^2\Pi$, is split into a lower level, ${}^2\Pi_{1/2}$, and an upper level, ${}^2\Pi_{3/2}$. Paramagnetism of the gas is due to the upper or ${}^2\Pi_{3/2}$ doublet component which possesses an electronic magnetic moment (Beringer and Castle, 1950). This level, because of interaction with the rotational motion of the molecule, is split into four states, $M_J = \frac{3}{2}, \frac{1}{2}, -\frac{1}{2}, -\frac{3}{2}$. These four states will result in three absorption lines with the selection rule $m_S = \pm 1$. The experimentally observed EPR spectrum of NO consists of nine lines, where each of the three absorption lines is further split into three components because of interaction with the spin of the nitrogen nucleus ($a_N = 14.2$ G).

The study of the interaction of nitric oxide with buckminsterfullerene was stimulated by the work of Pace, *et al.*, in which the effect of O₂ on the EPR signal intensity of C₆₀ was investigated (Pace, *et al.*, 1992). The intensity of the single peak characteristic of the EPR spectrum of C₆₀ was found to be oxygen-dependent. The same group studied the interaction of NO₂ with C₆₀ (Pace, *et*

al., 1994). The EPR spectrum of the NO₂ trapped in C₆₀ was line broadened at room temperature. The sample had to be cooled to 77 K, before a clear EPR spectrum could be recorded. It was concluded from their study that NO₂ interacts with C₆₀ to form a trapped product which was hypothesized to be HNO₂⁻ based on a hyperfine coupling of 32 Gauss. The adsorption of NO and CO on C₆₀ was studied using IR spectroscopy (Fastow, *et al.*, 1992). The interaction of these gases with C₆₀ was found to be relatively strong.

VII.2. Results and Discussion

VII.2.1. Nitric Oxide and Buckminsterfullerene

Buckminsterfullerene was exposed to nitric oxide (NO) gas to investigate their mutual interaction using EPR spectroscopy. NO gas was prepared according to the following reaction (Bostrup, 1966)



The usual EPR signal of buckminsterfullerene was observed before it was exposed to NO gas. The g value was calculated to be 2.00247 ± 0.00006 as compared to a g value of 2.0021 obtained in the literature (Pace, *et al.*, 1992). The difference could be due to slightly different samples of C₆₀. The usual EPR signal of buckminsterfullerene disappeared shortly after it was exposed to NO

gas. Characteristic EPR signals emerged the next day (approximately, ca., 18 hours after exposure to NO gas) along with an overlapping central peak. These six doublet peaks along with the central peak are shown in Figure VII.1. The six peaks disappeared afterwards but the central peak persisted. Apparently an interaction of chemical nature takes place between NO gas and buckminsterfullerene. Moreover, the rate determining step in the interaction process is kinetically very slow. An analysis of the experimental observations will be presented in the following paragraphs.

A glass cell filled with nitric oxide gas did not give any EPR signal in the magnetic field ranges 3200 - 3700 G and 8000 - 9100 G. The EPR spectrum of the $^2\Pi_{3/2}$ state of NO gas appears at magnetic fields in the range 8400 to 8900 G at X-band with a g-value of 0.78 Gauss (Beringer and Castle, 1950). The theoretical g-value of the $^2\Pi_{3/2}$ state of NO is $\frac{4}{5}$ (Margenau and Henry, 1950; Wertz and Bolton, 1986). A gas cell of large volume was required to observe the EPR spectrum of NO gas. That the spectrum is due to the interaction of NO with C_{60} was verified experimentally by excluding other possibilities. The observed g-value of the EPR spectrum of NO+ C_{60} calculated at the center of the six peaks is 2.0018.

The observed g-values of the EPR spectrum of gaseous NO, gaseous NO_2 , and NO_2 in solution are, respectively, 0.78 Gauss (Beringer and Castle, 1950), 2.0029 Gauss (Castle and Beringer, 1950), and 2.008 Gauss (Bird, *et al.*, 1958). The value (2.0018) is in the neighborhood of the g-values of gaseous

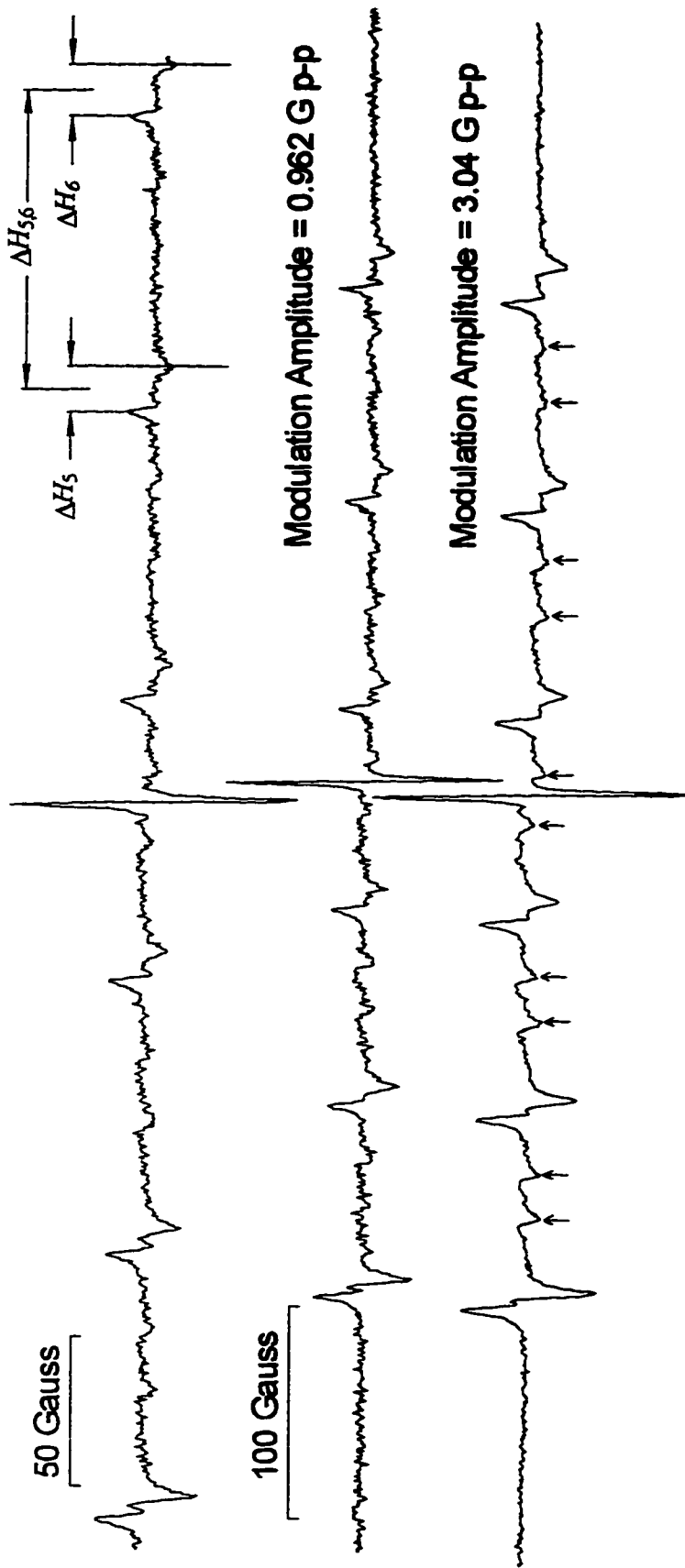


Figure VII.1. EPR spectra of interacting NO with buckminsterfullerene. The uppermost spectrum was used to calculate the field intervals ΔH_i 's, in Gauss, for the six doublet-peaks, and the center-to-center field intervals ΔH_{ij} 's, in Gauss, between the consecutive doublet-peaks. The middle and lowermost spectra have the same sweep width but different peak-to-peak modulation amplitudes. The arrows in the lowermost spectrum indicate the lower extrema of hyperfine doublet structures observed between the larger peaks.

NO₂ and buckminsterfullerene systems (Misra and Petkov, 1995). The observation of an EPR signal, which could not be detected in the gas phase, at the gas-solid interface reminds of Raman spectroscopy amplified by surface enhancement. Although it is too early to conclude such a resemblance with Raman spectroscopy, the current incident could be termed "surface enhanced EPR spectroscopy."

There are obvious features in the spectra shown in Fig. VII.1. First, the separation, ΔH_i (defined in Fig. VII.1), increases between the maximum and minimum points in each of the six peaks as the magnetic field increases. The symbol ΔH_i refers to the first peak at the lower end of the magnetic field, i.e., to the extreme left of the spectra shown in Fig. VII.1, ΔH_2 to the second peak, and so on. The separations, ΔH_i in Gauss, for the six peaks with the corresponding local central field values H_i^{CF} are given in Table VII.1. Second, the peaks center-to-center field separations, ΔH_{ij} (also defined in Fig. VII.1), display similar behavior, i.e., the separation increases as the magnetic field increases. The indices i and j refer, respectively, to the preceding and following peaks from left to right according to the spectra shown in Fig. VII.1. The separations, ΔH_{ij} in Gauss, between the six peaks are given in Table VII.1. The dependences of ΔH_i and ΔH_{ij} on the magnetic field is shown graphically in Figures VII.2(A) and (B), respectively. From Fig. VII.2(B), ΔH_{ij} display a linear dependence on the magnetic field, while in Fig. VII.2(A) ΔH_i deviated from linearity. Third, the unresolved hyperfine structures in the middle of the major six peaks and in the

TABLE VII.1. Values in Gauss of the Local Central Fields H_i^{CF} , Peak Widths ΔH_i , and Peak-to-Peak Separations ΔH_{ij} , for EPR Spectra of NO Interacting with Buckminsterfullerene.

$H_1^{CF} = 3233.57$	$\Delta H_1 = 8.31$	$\Delta H_{1,2} = 89.47$
$H_2^{CF} = 3323.26$	$\Delta H_2 = 8.80$	$\Delta H_{2,3} = 91.94$
$H_3^{CF} = 3415.39$	$\Delta H_3 = 10.26$	$\Delta H_{3,4} = 95.46$
$H_4^{CF} = 3510.45$	$\Delta H_4 = 12.71$	$\Delta H_{4,5} = 97.57$
$H_5^{CF} = 3608.94$	$\Delta H_5 = 15.15$	$\Delta H_{5,6} = 100.04$
$H_6^{CF} = 3708.15$	$\Delta H_6 = 17.11$	

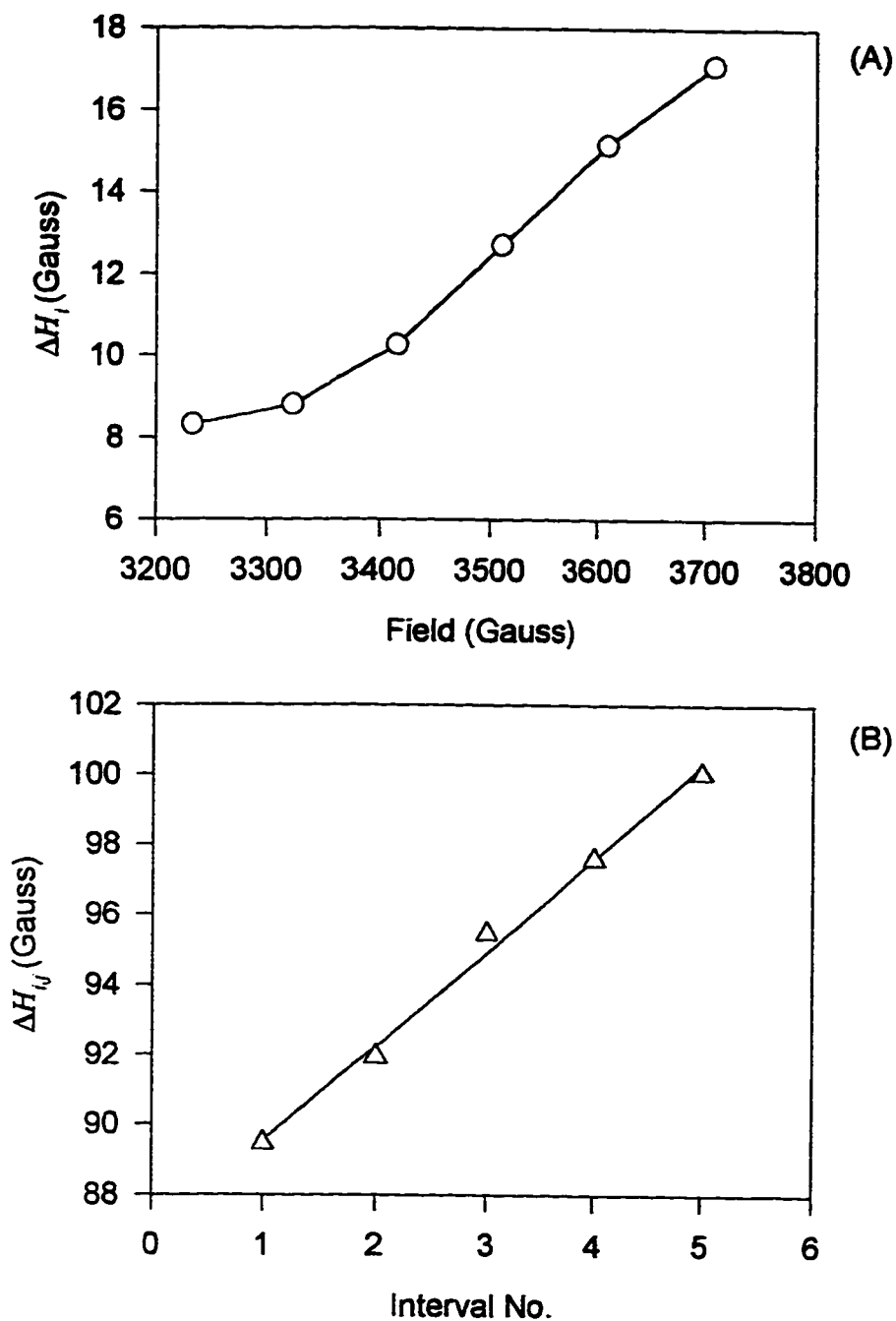


Figure VII.2. (A) The field intervals ΔH_i , in Gauss, versus field values, also in Gauss, for the six doublet-peaks observed in the EPR spectrum of interacting NO with buckminsterfullerene. (B) The field intervals $\Delta H_{i,j}$, in Gauss, versus intervals sequence number. Here i refers to the preceding peak and j refers to the following peak in the calculation. Both ΔH_i and $\Delta H_{i,j}$ were explained in Fig. VII.1.

minor ten peaks indicated by small arrows in the lowermost spectrum of Fig. VII.1. Moreover, the minor ten peaks show less or no dependence on the magnetic field value. Attempts will be made to explain the origin of these three features.

The doublet feature in the major peaks could be attributed to "*l* doubling," an important interaction in microwave spectroscopy (Steinfeld, 1989). The *l* doubling occurs in linear polyatomic molecules and results from the interaction of the molecular rotation with a doubly degenerate bending mode of the vibrational motion in the molecule. A plausible consequence for the requirement of linearity for *l* doubling, is an interaction between NO and C₆₀ via the nitrogen in NO (Maschke, *et al.*, 1963; Yamashita, *et al.*, 1995; Giamello, *et al.*, 1992) and a π cloud in an aromatic ring of C₆₀ (Fagan, *et al.*, 1992) forming a linear C₆₀-NO adduct. The unequally spaced ΔH_i and $\Delta H_{i,j}$ separations are characteristics of rotational spectroscopy, and anharmonicity could also be present in ΔH_i if the assumption of *l* doubling holds.

The peaks center-to-center field separations, $\Delta H_{i,j}$, include both coupling and rotational constants for the NO-C₆₀ adduct. The separations $\Delta H_{i,j}$ between the six successive components range from 89.5 to 100.0 Gauss. The average *J* coupling and hyperfine coupling constants for gaseous NO are, respectively, 104.0 and 27.4 Gauss (Beringer and Castle, 1950). The average separations between the successive triplet components in gaseous NO₂ and NO₂ in solution are, respectively, 47.5 and 107 Gauss. The EPR spectrum of NO at X-band

shows a triplet of a triplet (Beringer and Castle, 1950) and the EPR spectrum of NO₂ at X-band shows a broad triplet (Castle and Beringer, 1950). The g-value of the central peak (2.0019) is close to the g-value of NO₂-buckminsterfullerene system, which is 2.0021 (Pace, *et al.*, 1994). Hence, the central peak would be due to NO₂ interacting with buckminsterfullerene. The difference in g-values from this study and the literature suggests that buckminsterfullerene is modified by NO interaction.

The observed sextet spectrum could be explained in several ways (e.g., a triplet of doublet or vice versa). However, it cannot be due to adsorbed NO nor to adsorbed NO₂, since then either nine or three peaks would be observed. Moreover, the peak due to adsorbed NO₂ is already present and is different from these six peaks. One possible explanation for the observed sextet spectrum, combining previous findings, is that twelve NO molecules are associated with the twelve pentagons in the C₆₀ cage via η^5 -type of bonding. The adsorbed NO₂ would reduce the symmetry of C₆₀ resulting in six different groups of two equivalent pentagons. The unresolved hyperfine structures in the middle of the major six peaks could be due to the delocalization (Rozantsev, 1973) of the unpaired electrons over the π -orbital systems of the pentagons, while the minor ten peaks could be due to the delocalization of the unpaired electrons over the π -orbital systems of the remaining hexagons of the aromatic C₆₀ (the twenty hexagons can be divided into two symmetrical groups of ten different hexagons).

A scenario for the interaction of the gaseous NO with the solid buckminsterfullerene can be drawn from the above discussion.

Step 1- The NO gas inhibits the paramagnetic centers on buckminsterfullerene rendering them diamagnetic (Maschke, *et al.*, 1963; Phillips, 1961); the evidence is the disappearance of the EPR signal.

Step 2- The species formed in step1 dissociate to form adsorbed NO₂ (Bodenstein, 1922); the evidence is the observation of a single peak characteristic of adsorbed NO₂.

Step 3- NO molecules interact with buckminsterfullerene to give the sextet EPR spectrum; the evidence is the observed EPR signal.

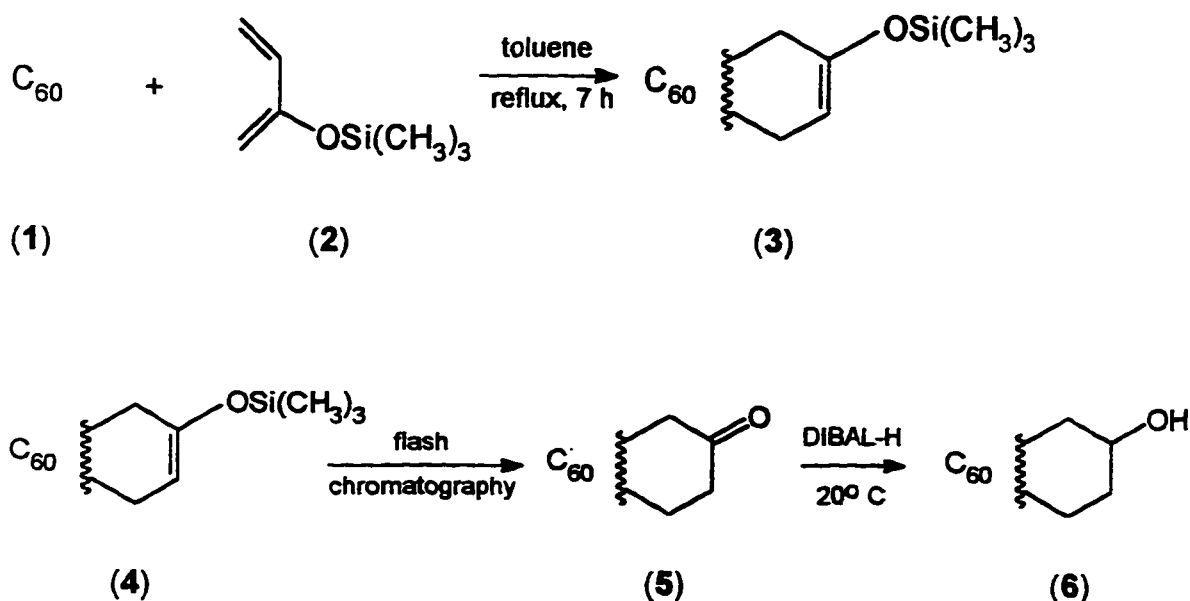
Step 4- The NO in the adduct formed in step3 dissociates to adsorbed N₂ and O₂ (Vijayakrishnan, *et al.*, 1992); evidences are the disappearance of the sextet EPR spectrum, no increase in the EPR signal characteristic of adsorbed NO₂, and the low pressure in the interior of the EPR sample tube noticed upon opening it.

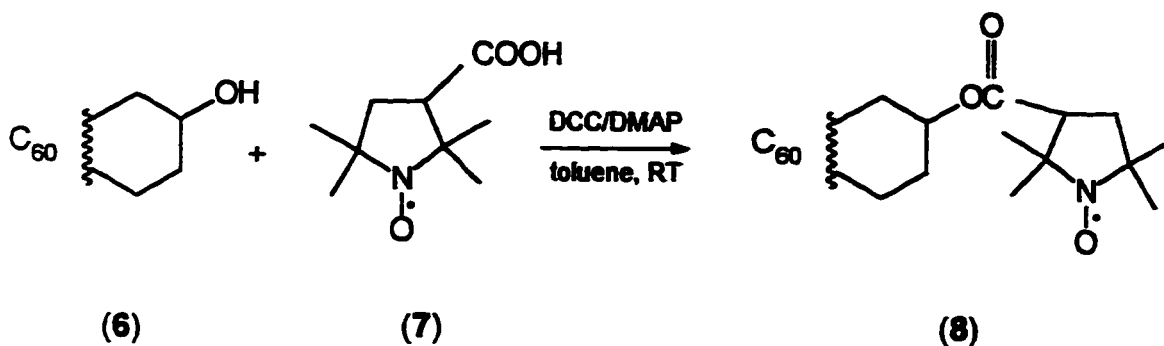
VII.2.2. Nitroxide Spin Probe Adduct of Buckminsterfullerene

At the beginning, we attempted to react Tempamine, 4-amino-2,2,6,6-tetramethylpiperidine *N*-oxide, with buckminsterfullerene in toluene. The reaction did not proceed in spite of modifying the conditions of concentration, temperature and time. Apparently, the Tempamine should have been the solvent as well as the reactant (Wudl, *et al.*, 1992). However, our objective was

to synthesize a monoadduct of C_{60} and tempamine. Use of tempamine in excessive amount would complicate the process as far as formation of monoadduct is concerned. An alternative reaction route was selected.

The nitroxide spin probe adduct of buckminsterfullerene **8**, 1,9-[4-(2,2,5,5-tetramethylpyrrolidine-1-oxyl-3-carboxylate)cyclohexano] buckminsterfullerene, was prepared by the esterification of alcohol **6**, namely 1,9-(4-hydroxycyclohexano)-buckminsterfullerene, with 2,2,5,5-tetramethyl pyrrolidine-1-oxyl-3-carboxylic acid (**7**). The synthetic route was based on the Diels-Alder reaction (An, *et al.*, 1993) of 2-[(trimethylsilyl)oxy]-1,3-butadiene (**2**) with C_{60} (**1**), followed by the esterification (Yamago, *et al.*, 1993) of **6** with **7**. Alcohol **6** was obtained by the reduction of ketone **5**. The reaction steps involved in the synthesis are outlined below.





Rigid limit spectra measured at 77 K in toluene and shown in Figure VII.3 of both the adduct **8** and the nitroxide spin probe **7** had similar features. However, the central peak in the rigid limit spectrum of the adduct **8** is relatively less broader than the central peak in the rigid limit spectrum of the nitroxide spin probe. The relatively sharper peak is an indication of less hydrogen bonding in the ester adduct than in the free carboxylic acid nitroxide spin probe. The behavior, studied by EPR, of both **8** and **7** in toluene at the different temperatures appeared to be slightly different in terms of observed linewidths and hyperfine splittings specially at lower temperatures. Figure VII.4 shows the EPR spectra of **8** and **7** in toluene at room temperature. However, when the liquid crystal 5CB (i.e., *p-n*-pentyl-*p*-cyanobiphenyl) was used as the solvent, clear distinction between the room temperature EPR spectra of the adduct **8** and the nitroxide spin probe **7** was observed. These spectra are shown in Figure VII.5. The adduct appeared to be tumbling at a slower rate in 5CB than the nitroxide spin probe. This was obvious from the observed linewidths of the EPR spectra of the adduct and the free spin probe. The observed linewidths for the

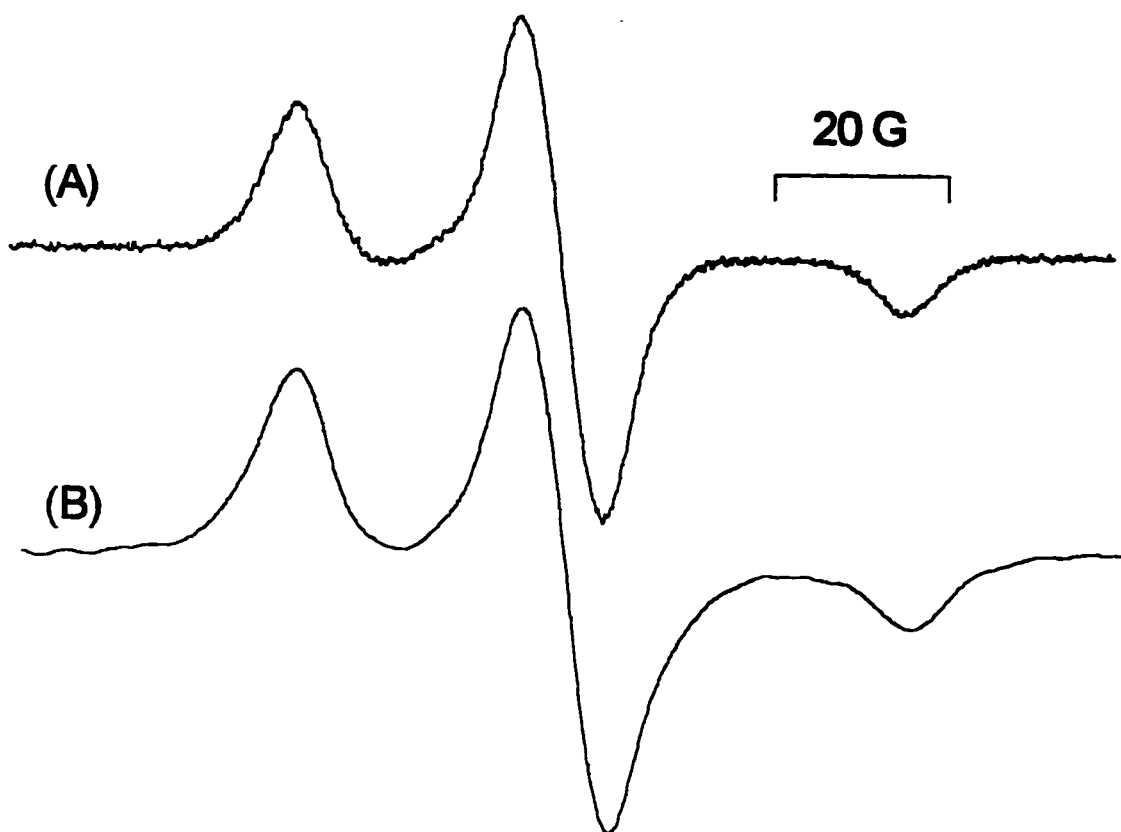


Figure VII.3. (A) The rigid limit spectrum of the adduct **8** in toluene obtained at 77 K. (B) The rigid limit spectrum of the nitroxide spin probe **7** in toluene obtained at 77 K.

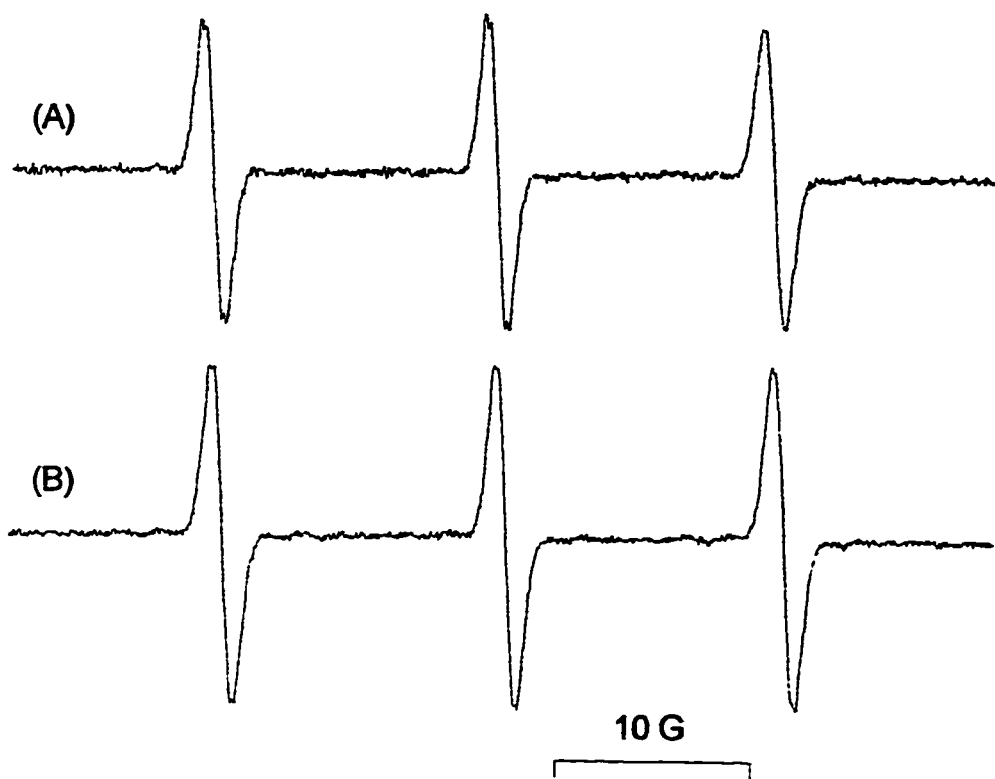


Figure VII.4. (A) The room temperature spectrum of the adduct **8** in toluene.

(B) The room temperature spectrum of the nitroxide spin probe **7** in toluene.

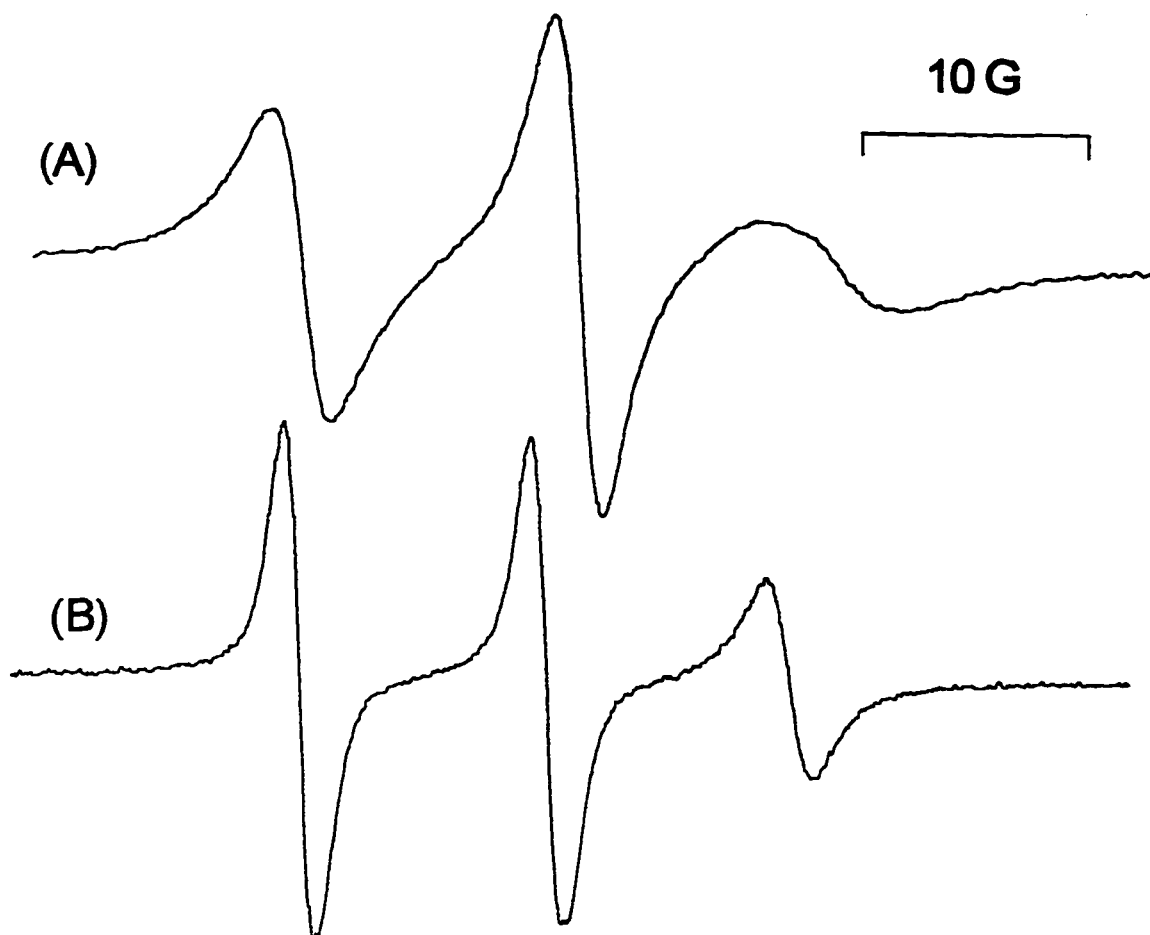
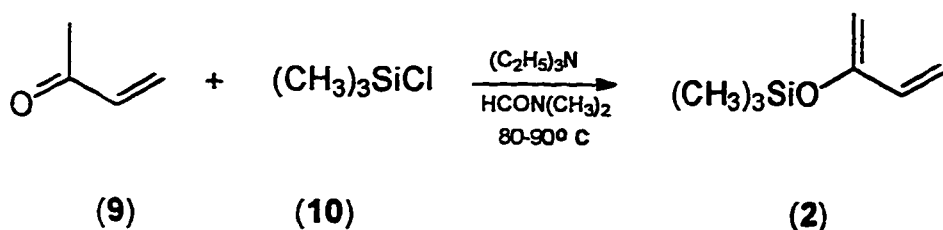


Figure VII.5. (A) The EPR room temperature spectrum of the adduct **8** in the liquid crystal 5CB. (B) The EPR room temperature spectrum of the nitroxide spin probe **7** in the liquid crystal 5CB.

three peaks in the EPR spectrum of the adduct **8** were larger than the corresponding linewidths of the nitroxide spin probe **7**.

An additional test for the formation of the adduct **8** was by preparing an EPR sample in which both the adduct **8** and the nitroxide spin probe **7** were added. The EPR spectrum, shown in Figure VII.6, can be visualized as the summation of the separate spectra of the adduct and the free nitroxide spin probe. The qualitative results of the thin layer chromatography were in accordance with these findings. Due to the tiny quantities that are dealt with here (in the range of few mg), the NMR and the FTIR spectra of the adduct **8** were noisy and not much information could be extracted from them.

2-[(trimethylsilyl)oxy]-1,3-butadiene (**2**), was prepared (Jung and McCombs, 1978) according to the reaction:



In the next section, the experimental procedure for the interaction of gaseous NO with buckminsterfullerene and the preparation of **2**, **6**, and **8** will be described in details.

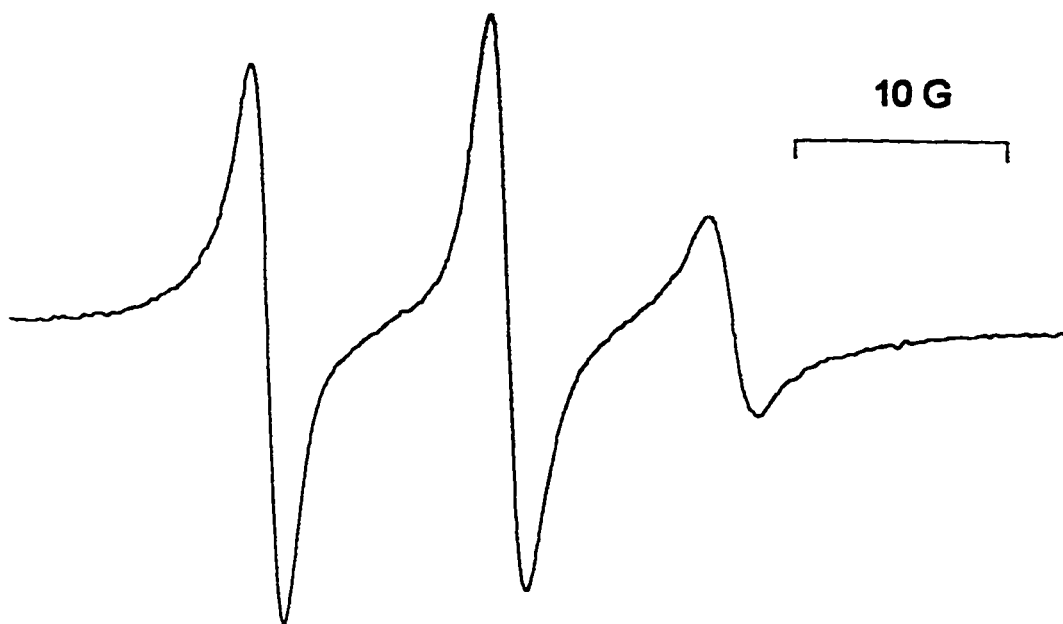


Figure VII.6. The room temperature EPR spectrum of a mixture of the adduct **8** and the nitroxide spin probe **7** in 5CB liquid crystal.

VII.3. Experimental

VII.3.1. Nitric Oxide and Buckminsterfullerene

Adopting the procedure outlined by Bostrup for NO gas production (Bostrup, 1966), a 500-ml, three-necked, round-bottomed flask was fitted with a 100-ml dropping funnel, a nitrogen gas inlet, and a glass stopper. Sodium nitrite (NaNO_2) in the powder form was placed (250 g) in the round-bottomed flask, and 2M H_2SO_4 was placed (100 ml) in the 100-ml dropping funnel. Liberated nitric oxide was purified and dried by passing through two 1-L glass containers half-filled with 10M NaOH and a third container completely filled with NaOH pellets which were covered on the top by glass wool. Both H_2SO_4 and NaNO_2 were obtained from Fluka and NaOH was obtained from Riedel-deHaën. The general procedure for producing NO gas was to purge the complete apparatus with nitrogen gas for ten minutes, add H_2SO_4 to NaNO_2 dropwise, discard the initial batch of NO gas, and then use the produced NO gas. The flow rate of NO gas produced was controlled by adjusting the rate of adding H_2SO_4 to NaNO_2 .

The procedure for reacting NO gas with buckminsterfullerene can be described by referring to the schematic depicted in Figure VII.7. A cell was constructed so that the reaction of NO gas with C_{60} could be achieved without any interference from oxygen or moisture. The reaction cell consisted of a four-port glass manifold to which a modified Pyrex tube with a gas-seal valve was connected using quick-fit metal connectors. The sample to be studied was placed in a quartz tube which was connected to the Pyrex tube via the cap of the

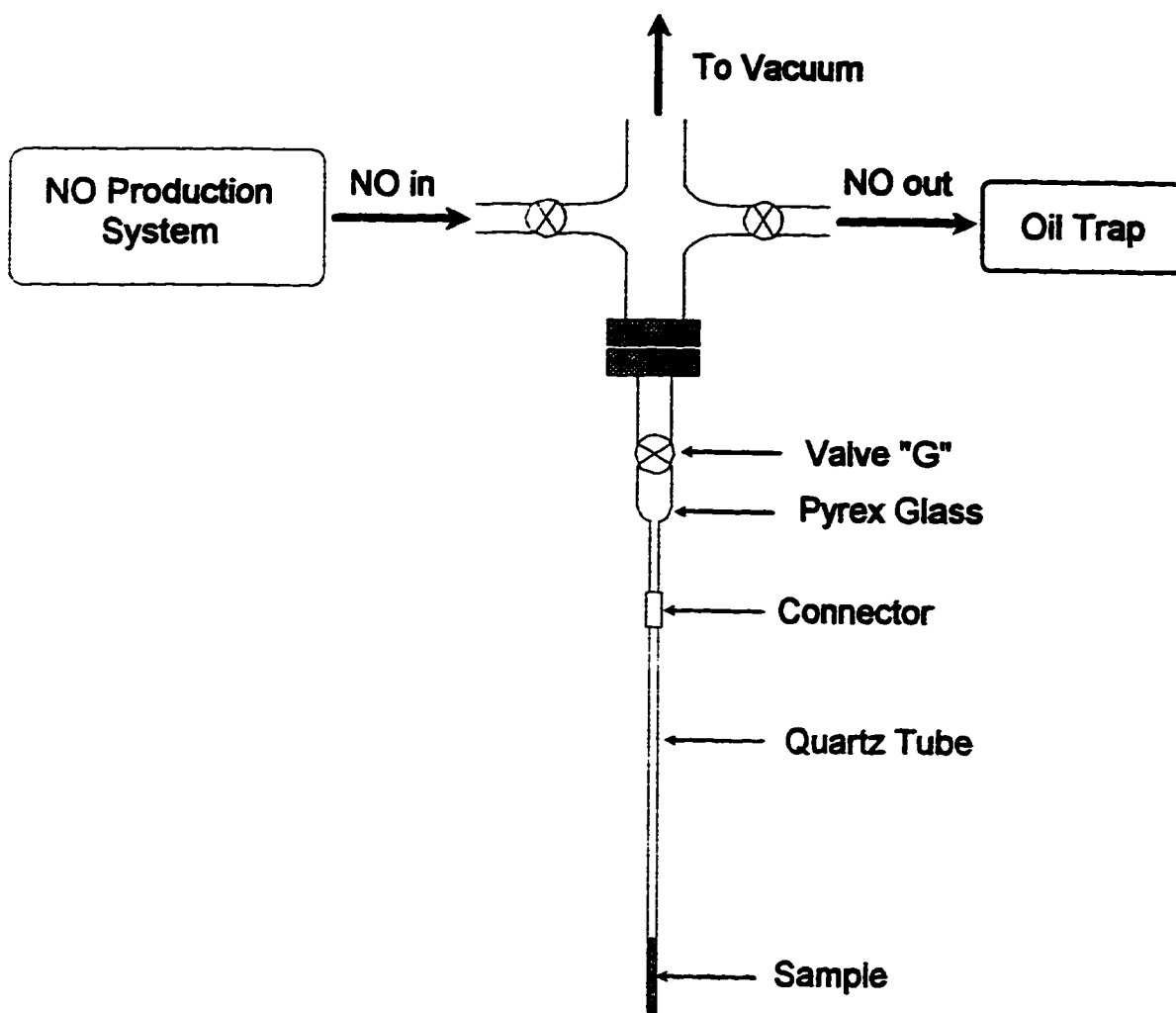


Figure VII.7. A schematic of the of the system used to react NO gas with buckminsterfullerene.

quartz tube. Teflon tape underneath the cap and black wax on the top were used to ensure maximum seal. The nitric oxide production system was connected to one side arm of the manifold and an oil trap was connected to the other. The cell was evacuated through the top port.

To study the interaction of NO with buckminsterfullerene, the latter (~8 mg) was placed in a TPX-1 capillary (purchased from Wilmad) sealed from the bottom with Critoseal[®]. TPX, a methylpentene gas permeable polymer, has been used in EPR studies (Popp and Hyde, 1980; Froncisz, et al., 1985). The TPX capillary was placed inside a quartz tube which was connected to the Pyrex tube with the cap. After that, the system depicted in Fig. VII.7 was purged for 15 minutes with nitrogen gas while valve "G" was closed, which prevented any residual NO₂ from coming in contact with C₆₀. The system was then purged for 5 minutes with NO gas at a flow rate of 15 ml/min, while valve "G" was kept open. The reaction cell was evacuated to a pressure of 0.015 mmHg, and the process of purging with NO gas and evacuation was repeated one more time. The NO gas was passed through the reaction cell for 90 minutes at a flow rate of 15 ml/min, while the quartz tube was immersed in liquid nitrogen. The liquid nitrogen was removed and returned repeatedly at the beginning to ensure that only NO gas was retained while other gases (like NO₂ and O₂) were purged out. The valve "G" was closed, the system was purged with N₂ gas, the Pyrex and quartz tubes were disconnected from the manifold, and while still immersed in liquid nitrogen the tubes were carried to the EPR spectrometer for

measurements. The usual EPR signal of buckminsterfullerene was observed before it was exposed to NO gas. The usual EPR signal of buckminsterfullerene disappeared shortly after it was exposed to NO gas. Characteristic EPR signals emerged the next day (approximately, ca., 18 hours after exposure to NO gas) along with an overlapping central peak. The six peaks disappeared afterwards but the central peak persisted. The same experiment was repeated in the absence of buckminsterfullerene to study the interaction of NO with the TPX capillary and no EPR signal was observed.

In another experiment, nitric oxide gas was bubbled through a solution of buckminsterfullerene in toluene. The color of the solution changed from purple to light amber color, which is characteristic of the addition to C₆₀ of toluene and benzene radicals generated by NO. These types of reactions, in which the radicals were generated photochemically, were studied extensively in the literature (Krusic, *et al.*, 1991(a); Krusic, *et al.*, 1991(b); Krusic, *et al.*, 1993). Consequently, neither complete identification of the compound formed was conducted nor similar reaction schemes were pursued.

VII.3.2. Nitroxide Spin Probe Adduct of Buckminsterfullerene

The EPR spectra were acquired using the Bruker EPR spectrometer described in the previous chapters of this Dissertation. A Varian XL-200 operating at a proton frequency of 200.0 MHz was used to record the ¹H NMR spectra. Thin layer chromatography (TLC) silica gel plates with fluorescent

indicator (Eastman, No. 6060) were used to monitor the reaction progress, and to determine the suitable solvent system for elution of the silica gel chromatographic separations which were performed with flash chromatography silica. All glassware were washed thoroughly with acid and distilled water and were dried in the oven, and when necessary the glassware were kept in the desiccator until the time of use.

VII.3.2.1. Preparation of 2-[(trimethylsilyl)oxy]-1,3-butadiene (2)- *N,N*-dimethyl formamide, obtained from Fluka, was distilled before use under a positive pressure of nitrogen atmosphere. Methyl vinyl ketone and chlorotrimethylsilane obtained from Fluka and triethylamine obtained from BDH were all distilled from calcium hydride under a positive pressure of nitrogen atmosphere. A 500-ml, three-necked, round-bottomed flask was fitted with two addition funnels, a glass stopper, and a magnetic stirrer, and placed in a 80-90 °C oil bath. Under nitrogen atmosphere, methyl vinyl ketone (10 g) in 10 ml of *N,N*-dimethyl formamide and chlorotrimethylsilane (17 g) in 12 ml of *N,N*-dimethyl formamide were added over 45 minutes to a magnetically stirred solution of triethylamine (16 g) in 80 ml of *N,N*-dimethyl formamide. The reaction was set up to run overnight, or ca. 15 hours.

The reaction was cooled to room temperature, filtered, and transferred to a 2-l separatory funnel containing 120 ml of pentane. To this solution was added 400 ml of cold 5% (25 g in 500 ml) sodium bicarbonate solution. The

mixture was shaken briskly for 10 seconds and separated as soon as foaming ceased. The bicarbonate extractions were performed quickly because the product slowly hydrolyzes in the presence of water. The pentane layer was separated and the aqueous layer was extracted twice with 120-ml portions of pentane. The pentane extracts were combined and washed with 80 ml of cold distilled water. The pentane layer was left overnight to dry over powdered anhydrous sodium sulfate. The pentane extracts were placed in a 500-ml round-bottomed flask, and fractional distillation, at an oil bath temperature of 70 °C, was carried out with a 30 cm vigreux column. The fractional distillation was conducted under vacuum (46 mmHg) and the inside temperature at which condensation took place was 46 °C. The distillate was collected in a four finger glass flask where samples were drawn from the second and third batches of distillate. The structure of the diene **2** was confirmed with NMR.

VII.3.2.2. *Preparation of 1,9-(4-hydroxycyclohexano)buckminsterfullerene*

(6)- Toluene, obtained from Fluka, was distilled before use under positive nitrogen atmosphere. Buckminsterfullerene was obtained from Sigma and was used as received. All glassware were washed thoroughly with acid and distilled water, dried in the oven, stored in the desiccator, and flushed with dry nitrogen gas before use. A 5-ml, round-bottomed flask was fitted with a condenser cooled to 0 °C by a circulating water bath, and a magnetic stirrer, and placed in a 120-125 °C oil bath. Under an inert atmosphere of dry nitrogen gas, the diene

(2) (47 mg) was added dropwise to a magnetically stirred solution of buckminsterfullerene (38 mg) in 10 ml of toluene at reflux. The reaction was set up to run for 7 hours. The uncharacterized intermediate silyl enol ether was checked with TLC (CS_2 , then toluene) and separated by column chromatography on silica gel (6.5 g of 100-200 mesh size silica obtained from Fisher Scientific, elution with CS_2 followed by toluene). This intermediate was hydrolyzed through flash chromatography on silica gel (5 g 100-300 mesh size silica, solution was left in the column for 2 hours, elution with CS_2 followed by toluene). A characteristic spot was observed with TLC (CS_2 , then toluene). The solvent in the collected eluant was removed by bubbling nitrogen gas through the solution to give **5** as a black solid (26.7 mg). This sample was further purified through silica gel column chromatography (silica gel 9.5 g, 1 cm \times 50 cm burette) by elution of different ratios of CS_2 :toluene starting with 1:0 and ending with 0:1. The ketone **5** was reduced with 23 μl solution of 1.2 M diisobutyl aluminum hydride (DIBAL-H) in toluene. The solution was stirred for 5 minutes and the reaction was quenched with ethanol (15 μl) after the progress of the reaction was checked with TLC. After an aqueous work-up with deionized water, the organic phase was separated and dried with Na_2SO_4 (5 g) and the product **6** was filtered (11.8 mg). Albeit the weak signals observed, the structure of the alcohol **6** was also verified with NMR.

VII.3.2.3. Synthesis of the Nitroxide Spin Probe-Buckminsterfullerene Adduct- *N,N*-dicyclohexylcarbodiimide (DCC) and 4-dimethylaminopyridine (DMAP), purchased from Fluka, and 2,2,5,5-tetramethylpyrrolidine-1-oxyl-3-carboxylic acid), purchased from Molecular Probes, Inc., were used without further purification. Esterification of the alcohol **6** with the nitroxide spin probe **7** was performed in a capped glass vial fitted with a magnetic stirrer. A mixture of the alcohol **6** (10 mg), the nitroxide spin probe **7** (5 mg), DCC (5 mg), and DMAP (0.5 mg) in 4 ml of toluene was stirred at room temperature under nitrogen for 12 hours. Many runs of TLC in toluene of the reaction mixture (while adding to the eluant drops of 5% ethylacetate in toluene), was used to observe the progress of the reaction. A TLC of the reactants only, the reactants and the products, and the products only confirmed that the products were different from the reactants.

The unreacted nitroxide carboxylic acid spin probe (**7**) was removed from the reaction mixture by three times extraction with 50 ml solution of 5% NaHCO₃ in deionized water. To assess the effectiveness of the 5% NaHCO₃ solution in extracting the nitroxide carboxylic acid spin probe (**7**), a solution of 1 mg of the free nitroxide spin probe in 100 ml toluene was examined with EPR before and after extraction. The 5% NaHCO₃ solution was 100% effective in extracting the nitroxide carboxylic acid spin probe. Further extraction with two 100-ml portions of 5% Na₂CO₃ in deionized water, drying on Na₂SO₄, and purification by silica gel column chromatography (silica gel 6 g, elution with toluene) was performed

to completely ascertain the removal of any unreacted nitroxide carboxylic acid spin probe.

The EPR samples in toluene were prepared in the usual manner described previously in details. The EPR samples of the adduct **8** in the liquid crystal 5CB were prepared by filling a quartz EPR sample tube to a height of 6 cm with the adduct solution in toluene. The toluene was evaporated under vacuum, 0.2 ml of the 5CB liquid crystal (Merk, Ltd.) was added, and the sample was mixed by heating the liquid crystal to the isotropic phase and shaking the EPR sample tube.

CHAPTER VIII

CONCLUSIONS

VIII.1. PD-Tempone

In this chapter, the anisotropic interaction parameter κ for PD-Tempone in toluene at the four microwave frequencies L-, S-, X-, and Q-Bands was studied. Related to this is the effect of modifying the Debye spectral densities by introducing the Cole-Davidson parameter β .

Molecules of PD-Tempone in toluene at the four bands were found to align under the applied magnetic field such that the molecular Y axis was parallel to the direction of the applied magnetic field. Values of the anisotropic rotational reorientation N were close to one, where N is the ratio of R_{\parallel}/R_{\perp} , R_{\parallel} is the rotational diffusion constant along the longer molecular axis R_x , and R_{\perp} is the rotational diffusion constant perpendicular to the longer molecular axis ($R_{\perp} = R_y = R_z$). At ~ 1 GHz and ~ 4 GHz, PD-Tempone underwent isotropic rotational diffusion, whereas at ~ 9.5 GHz and ~ 35 GHz its rotational diffusion became

slightly anisotropic. The slow tumbling region started at a lower temperature in the Q-Band than in the other three bands. This suggested that the strength of the applied magnetic field had a clear effect on the molecular motion of PD-Tempone, and consequently on the anisotropy of the rotational diffusion represented by the N values.

Values of the anisotropic interaction parameter κ determined in this study for PD-Tempone in toluene were similar at the four microwave bands. This similarity is predicted by theory for linear or spherical molecules undergoing isotropic molecular motion. Values of the anisotropy of molecular reorientation (N) which were close to one indicate isotropic molecular motions.

The Cole-Davidson parameter β was introduced to the spectral densities for the first time. A β value of 0.55 was used at L-Band to unify the results for the alignment of PD-Tempone in toluene, the anisotropic rotational reorientation N , and for the anisotropic interaction parameter κ determined at the four microwave bands. A β value of less than one suggested the existence of multiple intermolecular motions, or equivalently a broader distribution of relaxation times associated with different types of motions. At least there are two types of correlation times: the correlation time for angular momentum which is a characteristic time for "free rotations" of the molecules in the liquid, and the correlation time for molecular reorientation. Most probably, the distinction between these types of motions became clear in the L-Band range for PD-Tempone in toluene, which necessitated setting β equal to < 1 .

The value of the anisotropic interaction parameter κ determined for PD-Tempone in toluene at the Q-Band depended significantly on whether the scale of the axes used for plotting τ_R versus (η/T) was logarithmic or linear. Axes with a logarithmic scale gave a κ value which was similar to the values obtained at the other microwave bands. Applying a logarithmic scale to the axes of the τ_R versus η/T plots minimized the effect of anisotropy which became amplified at lower temperatures. A summary of the results obtained for PD-Tempone in toluene at the four microwave bands L, S, X, and Q is given in Table III.15.

VIII.2. BBTMPO

In this part, similar to the work conducted on PD-Tempone, the anisotropic interaction parameter κ for BBTMPO in toluene at the four microwave frequencies L-, S-, X-, and Q-Bands was studied. The effect of modifying the Debye spectral densities was also investigated by introducing the Cole-Davidson parameter β . To perform this study, however, an accurate value of the hydrodynamic radius for BBTMPO in toluene was determined experimentally. The hydrodynamic radius for BBTMPO in toluene was found to be 5.6 Å. This was calculated using a D value of 1.0×10^{-5} cm²/sec determined from the capillary translational diffusion experiment conducted at room temperature. The calculation was performed assuming a slip boundary condition in the Stokes-Einstein equation. The corresponding hydrodynamic volume for the slip boundary condition, also assuming a hard sphere geometry,

was 735.6 \AA^3 . The difference between the experimental results and the values obtained using models is most probably due to anisotropic BBTMPO, BBTMPO undergoing thermal rotations, and solvation of BBTMPO by toluene.

Lineshape analysis was performed for the first time on the EPR spectra of BBTMPO to determine intrinsic linewidths from experimentally observed linewidths. The peaks in the EPR spectra of BBTMPO, like in PD-Tempone, were inhomogeneously broadened. In the EPR spectra of PD-Tempone, the source of inhomogeneous broadening was the unresolved hyperfine structures resulting from the interaction of the spin magnetic moments of the unpaired electron and the twelve deuterons, whereas in BBTMPO the twelve deuterons were substituted by twelve protons. This was reflected in the type of lineshape function used to fit the experimental EPR lines. For PD-Tempone, a Lorentzian lineshape function was sufficient to fit all of the experimental EPR lines, however for BBTMPO, mixtures of Lorentzian and Gaussian lineshape functions were necessary for the fitting.

A Gaussian lineshape function was required possibly due to Doppler effect which arose from mass differences between deuterons and protons. The spectral distribution of the lighter protons assumed a mixture of Gaussian and Lorentzian lines, whereas the heavier deuterons assumed a Lorentzian distribution. Moreover, as the temperature was lowered for the BBTMPO system at the four microwave bands, the lineshape function became more Lorentzian (*cf.*, Table V.5).

Molecules of BBTMPO in toluene at the four microwave frequencies aligned under the applied magnetic field such that the molecular X axis was parallel to the direction of the applied magnetic field. Values of the anisotropic rotational reorientation N were equal to 7, which implied that at the four microwave bands, BBTMPO underwent anisotropic rotational diffusion.

Values of the anisotropic interaction parameter κ determined in this study for BBTMPO in toluene were similar at the three microwave bands L, S, and X, whereas at Q-Band the value of the anisotropic interaction parameter κ was much smaller. Apparently, variations among the three bands were not significant enough to be reflected in the value of the anisotropic interaction parameter κ . However, at Q-Band the difference became clear. A logarithmic scale was used for the axes of the τ_R versus η/T plots at the four bands, and the value obtained for κ at Q-band was only slightly improved.

To unify the results for BBTMPO in toluene, a value for the Cole-Davidson parameter β of 0.7 was used at both L- and S-Bands. Unlike PD-Tempone, the existence of multiple intermolecular motions, or equivalently a broader distribution of relaxation times associated with different types of motions, extended from L-Band only for PD-Tempone to both L- and S-Bands for BBTMPO. This was attributed to the larger size of the BBTMPO molecules. The distinction between the two types of motions, i.e. free rotations and molecular reorientation, became evident in the L- and S-Bands for BBTMPO, which necessitated setting β equal to < 1 .

The smaller value of the anisotropic interaction parameter κ determined for BBTMPO in toluene at the Q-Band showed that the coupling between the spin probe and the solvent was minimal. Due to high magnetic fields applied at Q-Band, the spin probe precessed at higher rates and since its motion was highly anisotropic, a weak coupling resulted between the rotational motion of the spin probe and the translational modes of the solvent. From this study, it is highly recommended that comparing the values of κ for different systems (e.g., PD-Tempone in toluene and BBTMPO in toluene) has to be performed with great caution. A summary of the results obtained for BBTMPO in toluene at the four microwave bands L, S, X, and Q is given in Table V.14.

VIII.3. Lipid

To the best of our knowledge, this is the first time a bilayer system with lanthanide ions was studied by observing the EPR spectra of weakly ordered nitroxide spin probe as a function of temperature. The systems studied were DMPC/DHPC, DMPC/DHPC+Yb³⁺, and DMPC/DHPC+Y³⁺. Studying coarse phospholipid dispersions and adding ions of different magnetic properties did not form serious limitations to EPR, which is contrary to the NMR techniques

Values of the g and A tensors were obtained by simulation of the rigid limit spectra. The magnetic parameters, which gave the best fit for the rigid limit (77 K) EPR spectrum of PD-Tempone in the phospholipid system DMPC/DHPC, are given in Table VI.1. The fit was obtained with a Lorentzian linewidth of 3.3

G. The magnetic parameters which gave the best fit for the rigid limit spectra of PD-Tempone in the phospholipid systems DMPC/DHPC+Yb³⁺ and DMPC/DHPC+Y³⁺ at 77 K are also given in Table VI.1. The fits were obtained with Lorentzian linewidths of 3.3 G and 4.6 G, respectively, for the phospholipid systems DMPC/DHPC+Yb³⁺ and DMPC/DHPC+Y³⁺. The two spectra were similar but the resolution of the central region in both spectra was lower than the resolution of the same region in the rigid limit spectrum of PD-Tempone in DMPC/DHPC. This was attributed to the presence of the paramagnetic Yb³⁺ and the diamagnetic Y³⁺, which allowed more interaction between the water molecules and the carbonyl group in PD-Tempone through hydrogen bonding.

EPR spectroscopy of PD-Tempone in DMPC/DHPC at X-band was studied as a function of temperature. The splitting in the high field spectral line ($M_l = -1$) was due to the proportionation of PD-Tempone into the fluid lipid region and the aqueous region. Qualitatively, fractions of PD-Tempone in the fluid lipid region extended to values higher than one in this study, which was attributed to the relatively higher concentrations of phosphatidylcholines (25% w/v) compared with previous studies (8-11% w/w) (cf. Wu & McConnell, 1975). Besides the approximate doubling of the phospholipid concentration, the presence of rare earth metal ions possibly allowed further mixing of water molecules and therefore of PD-Tempone with the lipid bilayer. The g -factor, the solute order parameter $\langle D_{00}^2 \rangle_z$, and the solvent order parameter λ increased as the temperature increased, whereas the hyperfine splitting α decreased as the

temperature increased. A phase transition occurred in the temperature range 50–60 °C. Finally, the values of $|S_{11}|$ and $|S_{22}|$ were almost equal and both were generally greater than $|S_{33}|$, and a good agreement between S_{33} and $\langle D_{00}^2 \rangle_z$ was demonstrated.

EPR spectroscopy of PD-Tempone in DMPC/DHPC+Yb³⁺ at X-band was performed as a function of temperature. From the results of this study, the temperature intervals at which phase transitions took place were wide. Further investigations are required which could include visual studies of phase alterations as a function of temperature varied in small intervals (1.0 °C, and 0.5 °C close to phase transition regions). Then, these same experiments should be performed by EPR and Differential Scanning Calorimetry (DSC). Two phase transition regions were identified for this system, DMPC/DHPC+Yb³⁺, in the temperature ranges 30–40 °C and 70–80 °C. The values of $|S_{11}|$ were relatively higher than $|S_{22}|$, and the values of $|S_{22}|$ and $|S_{33}|$ were almost equal. Variations of S_{22} and S_{33} as a function of temperature were almost opposite to each other.

PD-Tempone in DMPC/DHPC+Y³⁺ was studied at X-band over a range of temperatures. Apparently, the extent of interaction between the charge on yttrium(III) and PD-Tempone is relatively higher than the interaction between Yb³⁺ and PD-Tempone. This was concluded from the broader EPR signal of the system PD-Tempone + DMPC/DHPC + Y³⁺. Consequently, the splitting in the high-field line was obscured. Although, variations of the hyperfine splitting a , the

g -factor, the solute order parameter $\langle D_{00}^2 \rangle$, and the solvent order parameter λ with temperature in this system were smoother than in the other two systems, the variation of the f -factor displayed a sharp transition at $\sim 45^\circ\text{C}$. The possibility of multiple transitions could not be excluded. Generally $|S_{11}|$ was greater than $|S_{22}|$, whereas $|S_{33}|$ was intermediate between $|S_{11}|$ and $|S_{22}|$. Variations of S_{11} and S_{22} as a function of temperature were almost opposite to each other. Linearity was fully satisfied between $S_{22}(\Delta g)$ and $S_{22}(\Delta\alpha)$ calculated for the three phospholipid systems.

From these *preliminary* studies the following observations were deduced. Firstly, addition of the lanthanide ion ytterbium(III) had a clear effect on the alignment of the highly ordered binary mixture of the phosphatidylcholines DMPC and DHPC. Addition of yttrium(III) effected the alignment of this mixture to a lesser extent. Ytterbium(III) interacts with the polar head groups of the phospholipid bilayers through both its positive charge and the pseudocontact effect (Bleaney, 1972), whereas yttrium(III) interacts via its positive charge only. The effect of adding yttrium(III) to the bicelles was always intermediate between when no lanthanide ion was added and when ytterbium(III) was added. In the absence of lanthanide ions and in the presence of Y^{3+} , only S_{11} and S_{22} seem to correlate, while in the presence of Yb^{3+} , all order parameters appear to correlate with each other. Secondly, the order parameters S_{11} and S_{22} flipped positions on going from bicelles with no lanthanon, passing through bicelles with yttrium(III), and ending at bicelles with ytterbium(III). The flipping of these order parameter,

where S_{11} and S_{22} correspond to ordering in the molecular x-axis and y-axis directions, respectively, could be an indication of the flipping of this bicelles system (Prosser et al, 1996; Prosser et al, 1997). Thirdly, the agreement between S_{33} and $\langle D_{00}^2 \rangle_z$ was quite satisfactory and transformation (Polnaszek & Freed, 1975) to the Maier-Saupe potential expansion coefficient λ could be performed using either S_{33} or $\langle D_{00}^2 \rangle_z$.

VIII.4. Buckminsterfullerene Adducts

This part included two studies. *In the first study*, buckminsterfullerene was exposed to nitric oxide (NO) gas to investigate their mutual interaction using EPR spectroscopy. The usual EPR signal of buckminsterfullerene was observed before it was exposed to NO gas. The g value was calculated to be 2.00247 ± 0.00006 . This EPR signal disappeared shortly after exposure to NO gas. Six characteristic EPR signals emerged the next day (approximately, ca., 18 hours after exposure to NO gas) along with an overlapping central peak. The six peaks disappeared afterwards but the central peak persisted. Apparently an interaction of chemical nature took place between NO gas and buckminsterfullerene. Moreover, the rate determining step in the interaction process was kinetically very slow. That the spectrum was due to the interaction of NO with C_{60} was verified experimentally by excluding other possibilities. The observed g-value of the EPR spectrum of NO+ C_{60} calculated at the center of the six peaks was 2.0018.

The observation of an EPR signal, which could not be detected in the gas phase, at the gas-solid interface reminds of Raman spectroscopy amplified by surface enhancement. Although it is too early to conclude such a resemblance with Raman spectroscopy, the current incident could be termed "surface enhanced EPR spectroscopy."

The doublet feature in the major peaks was attributed to "*l* doubling," an important interaction in microwave spectroscopy (Steinfeld, 1989). The *l* doubling occurs in linear polyatomic molecules and results from the interaction of the molecular rotation with a doubly degenerate bending mode of the vibrational motion in the molecule. A plausible consequence for the requirement of linearity for *l* doubling, is an interaction between NO and C₆₀ via the nitrogen in NO and a π cloud in an aromatic ring of C₆₀ (Fagan, *et al.*, 1992) forming a linear C₆₀-NO adduct. The unequally spaced ΔH_i and $\Delta H_{i,j}$ separations (defined in section VII.2.1) are characteristics of rotational spectroscopy, and anharmonicity could also be present in ΔH_i if the assumption of *l* doubling holds.

The central peak was due to NO₂ interacting with buckminsterfullerene. The difference in g-values from this study and the literature suggests that buckminsterfullerene was slightly modified by NO interaction. The observed sextet could not be due to absorbed NO nor to absorbed NO₂, since then either nine or three peaks would be observed. Moreover, the peak due to adsorbed NO₂ was already present and was different from these six peaks. A possible explanation for the observed sextet spectrum was that twelve NO molecules

were associated with the twelve pentagons in the C_{60} cage via η^5 -type of bonding. The adsorbed NO_2 would reduce the symmetry of C_{60} resulting in six equivalent pentagons. The unresolved hyperfine structures in the middle of the major six peaks could be due to the delocalization (Rozantsev, 1973) of the unpaired electrons over the π -orbital systems of the pentagons, while the minor ten peaks could be due to the delocalization of the unpaired electrons over the π -orbital systems of the remaining hexagons of the aromatic C_{60} (the twenty hexagons can be divided into two symmetrical groups of ten hexagons).

A scenario for the interaction of the gaseous NO with the solid buckminsterfullerene was deduced from the above observations. Step 1- The NO gas inhibited the paramagnetic centers on buckminsterfullerene rendering them diamagnetic; the evidence was the disappearance of the EPR signal. Step 2- The species formed in step1 dissociated to form adsorbed NO_2 ; the evidence was the observation of a single peak characteristic of adsorbed NO_2 . Step 3- NO molecules interacted with buckminsterfullerene to give the sextet EPR spectrum; the evidence was the observed EPR signal. Step 4- The NO in the adduct formed in step3 dissociated to adsorbed N_2 and O_2 ; evidences were the disappearance of the sextet EPR spectrum, no increase in the EPR signal of adsorbed NO_2 , and the low pressure in the interior of the EPR sample tube noticed upon opening it.

The nitroxide spin probe adduct of buckminsterfullerene **8**, 1,9-[4-(2,2,5,5-tetramethyl pyrrolidine-1-oxyl-3-carboxylate)cyclohexano] buckminsterfullerene,

was prepared by the esterification of alcohol **6**, namely 1,9-(4-hydroxycyclohexano)-buckminsterfullerene, with 2,2,5,5-tetramethyl pyrrolidine-1-oxy-3-carboxylic acid (**7**). *In this second study*, the synthetic route was based on the Diels-Alder reaction (An, *et al.*, 1993) of 2-[(trimethylsilyl)oxy]-1,3-butadiene (**2**) with C₆₀ (**1**), followed by the esterification (Yamago, *et al.*, 1993) of **6** with **7**. Alcohol **6** was obtained by the reduction of ketone **5**. The reaction steps involved in the synthesis are presented in section VII.2.2.

Rigid limit spectra measured at 77 K in toluene for both the adduct **8** and the nitroxide spin probe **7** had similar features. However, the central peak in the rigid limit spectrum of the adduct **8** was relatively less broader than the central peak in the rigid limit spectrum of the nitroxide spin probe. The relatively sharper peak was an indication of less hydrogen bonding in the ester adduct than in the free carboxylic acid nitroxide spin probe. The behavior, studied by EPR, of both **8** and **7** in toluene at the different temperatures appeared to be slightly different in terms of observed linewidths and hyperfine splittings specially at lower temperatures. However, when the liquid crystal 5CB (i.e., *p-n*-pentyl-*p'*-cyanobiphenyl) was used as the solvent, clear distinction between the room temperature EPR spectra of the adduct **8** and the nitroxide spin probe **7** was observed. The adduct appeared to be tumbling at a slower rate in 5CB than the nitroxide spin probe. This was obvious from the observed linewidths of the EPR spectra of the adduct and the free spin probe. The observed linewidths for

the three peaks in the EPR spectrum of the adduct **8** were larger than the corresponding linewidths of the nitroxide spin probe **7**.

An additional test for the formation of the adduct **8** was by preparing an EPR sample in which both the adduct **8** and the nitroxide spin probe **7** were added. The EPR spectrum was a summation of the separate spectra of the adduct and the free nitroxide spin probe. The qualitative results of the thin layer chromatography were in accordance with these findings. Due to the tiny quantities that were dealt with here (in the range of few mg), the NMR and the FTIR spectra of the adduct **8** were noisy and not much information could be extracted from them.

BIBLIOGRAPHY

- Abragam A. **1994**. "Principles of Nuclear Magnetism," reprint. Oxford University Press: Hong Kong.
- Abramowitz M. and I. Stegun, **1964**. "Handbook of Mathematical Functions." National Bureau of Standards. Applied Mathematical Series; U. S. Government Printing Office: Washington, D. C., Vol. 55.
- Ahn M.-K., **1976**. Diffusion coefficients of paramagnetic species in solution. *J. Magn. Res.* 22:289-293.
- Ahn M.-K. and C.S. Johnson, **1969**. Electron spin relaxation in the *N,N*-dimethylpyrazine cation radical. *J. Chem. Phys.* 50:632-640.
- Ahn M.-K. and D.E. Ormond, **1978**. Electron spin resonance studies of translational and reorientational motions of vanadyl acetylacetonate in tetrahydrofuran. *J. Phys. Chem.* 82:1635-1637.
- Ahn M.-K. and Z.J. Deriacki, **1978**. Translational diffusion coefficients of vanadyl acetylacetonate in organic solvents. *J. Phys. Chem.* 82:1930-1933.
- Ahn M.-K., S.J.K. Jensen, and D. Kivelson, **1972**. Molecular theory of diffusion constants in liquids. *J. Chem. Phys.* 57:2940-2951.
- Ajie H., M.M. Alvarez, S.J. Anz, R.D. Beck, F. Diederich, K. Fostiropoulos, D.R. Huffman, W. Krätschmer, Y. Rubin, K.E. Schriver, D. Sensharma. and

- R.L. Whetten, **1990**. Characterization of the soluble all-carbon molecules C_{60} and C_{70} . *J. Phys. Chem.* 94: 8630-8633.
- Akutsu H. and J. Seelig, **1981**. Interaction of metal ions with phosphatidylcholine bilayer membranes. *Biochemistry* 20:7366-7373.
- Allemand P.-M., G. Srdanov, A. Koch, K. Khemani, F. Wudl, Y. Rubin, F. Diederich, M.M. Alvarez, S.J. Anz, and R.L. Whetten, **1991**. The unusual electron spin resonance of fullerene $C_{60}^{\cdot-}$. *J. Am. Chem. Soc.* 113:2780-2781.
- An Y.-Z., J.L. Anderson, and Y. Rubin, **1993**. Synthesis of α -amino acid derivatives of C_{60} from 1,9-(4-hydroxycyclohexano)-buckminsterfullerene. *J. Org. Chem.* 58: 4799-4801, and supplementary materials.
- Atherton N.M. **1973**. "Electron Spin Resonance." Ellis Horwood Ltd.: Chichester, England.
- Bales B.L., **1989**. Inhomogeneously broadened spin-label spectra, in "Spin Labelling: Theory and Applications," L. J. Berliner and J. Reuben, Eds., Chap. 2. Plenum Press: New York.
- Balkhoyor H.B., **1993**. "A Study of Translational Diffusion Constants of Paramagnetic Species in Solution," M. S. Thesis, King Fahd University of Petroleum and Minerals, Dhahran 31261, Saudi Arabia.
- Barlow A.J., J. Lamb, and A.J. Matheson, **1966**. Viscous behaviour of supercooled liquids. *Proc. R. Soc.* 292A:322-342.

- Beardwood P. and J.F. Gibson, **1983**. Electron spin resonance spectra of reduced $[\text{Fe}_2\text{S}_2(\text{SC}_6\text{H}_4\text{Y}-p)_4]^{2-}$ (Y=Cl, H, or Me) complexes and their selenium-ligated homologues. *J. Chem. Soc. Dalton Trans.* 737-748.
- Beckmann P.A., **1988**. Spectral densities and nuclear spin relaxation in solids. *Physics Reports* 171:85-128.
- Beringer R., and J.G. Castle, **1950**. Magnetic resonance absorption in nitric oxide. *Phys. Rev.* 78:581-586.
- Beringer R., E.B. Rawson, and A.F. Henry, **1954**. Microwave resonance in nitric oxide: Lambda doubling and hyperfine structure. *Phys. Rev.* 94:343-349.
- Bird G., J. Baird, and R. Williams, **1958**. Fine structure in the electron spin resonance spectra of NO_2 solutions. *J. Chem. Phys.* 28:738-739.
- Bleaney, B., **1972**. Nuclear magnetic resonance shifts in solution due to lanthanide ions. *J. Magn. Res.* 8:91-100.
- Bodenstein M., **1922**. Bildung und zersetzung der höheren stickoxyde. *Z. Phys. Chem.* 100:68-123.
- Bostrup O.L.E., **1966**. 49. Nitrosylpentaaminocobalt(II) chloride, in "Inorganic Syntheses," H.F. Holtzclaw, Ed. McGraw-Hill Book Company: New York, VIII:191-195.
- Brown M.F., **1996**. Membrane structure and dynamics studied with NMR spectroscopy, in "Biological Membranes," K. Merz and B. Roux, Eds., Chap. 8. Birkhäuser: Boston.

- Carrington A. and A.D. McLachlan, **1980**. "Introduction to Magnetic Resonance."
Chapman and Hall: New York.
- Castle J.G. and R. Beringer, **1950**. Microwave magnetic resonance absorption in
nitrogen dioxide. *Phys. Rev.* 80:114-115.
- Chapman D., W.E. Peel, B. Kingston, and T.H. Lilley, **1977**. The interaction of
ions with phosphatidylcholine bilayers. *Biochim. Biophys. Acta* 464:260-
275.
- Coulombeau C., H. Jobic, P. Bernier, C. Fabre, D. Schütz, and A. Rassat, **1992**.
Neutron inelastic scattering spectrum of footballen C_{60} . *J. Phys. Chem.*
96:22-24.
- Cox D. M., S. Behal, M. Disko, S.M. Gorum, M. Greaney, C.S. Hsu, E.B. Kollin,
J. Millar, J. Robbins, W. Robbins, R.D. Sherwood, and P. Tindall, **1991**.
Characterization of C_{60} and C_{70} clusters. *J. Am. Chem. Soc.* 113: 2940-
2944.
- Davidson D.W., **1961**. Dielectric relaxation in liquids. I. The representation of
relaxation behavior. *Can J. Chem.* 39:571-594.
- Davidson D.W., and R.H. Cole, **1951**. Dielectric relaxation in glycerol, propylene
glycol, and n-propanol. *J. Chem. Phys.* 19:1484-1490.
- Debye P., 1945. "Polar Molecules." Dover: New York, pp. 77-89.
- Dousmanis G.C., **1955**. Magnetic hyperfine effects and electronic structure of
 NO^* . *Phys. Rev.* 97:967-970.

- Dubois D., K.M. Kadish, S. Flanagan, R.E. Haufler, L.P.F. Chibante, and L.J. Wilson, **1991**. Spectroelectrochemical study of the C₆₀ and C₇₀ fullerenes and their mono-, di-, tri-, and tetraanions. *J. Am. Chem. Soc.* 113: 4364-4366.
- Duclos S.J., R.C. Haddon, S. Glarum, A.F. Hebard, and K.B. Lyons, **1991**. Raman studies of alkali-metal doped A_xC₆₀ films (A = Na, K, Rb, and Cs; x = 0, 3, and 6). *Science* 254:1625-1627.
- Eaton S.S., H.V. Willigen, M.J. Heinig, and G.R. Eaton, **1980**, EPR measurement of long-range hyperfine coupling in a nitroxyl radical. *J. Magn. Res.* 38:325-330.
- Evans A.G., J.C. Evans, and E.H. Moon, **1974**. Electron spin resonance studies of Ziegler-type catalysts. Part I. Characterisation of a vanadium-aluminium complex obtained on mixing dichlorobis(η -cyclopentadienyl) vanadium with ethylaluminium di-chloride. *J.C.S. Dalton* 2390-2395.
- Fagan P.J., J.C. Calabrese, and B. Malone, **1992**. Metal complexes of buckminsterfullerene (C₆₀). *Acc. Chem. Res.* 25:134-142.
- Fastow M., Y. Kozirovski, M. Folman, and J. Heidberg, **1992**. IR spectra of CO and NO adsorbed on C₆₀. *J. Phys. Chem.* 96:6126-6128.
- Ferruti P., D. Gill, M.A. Harpold, and M.P. Klein, **1969**. ESR of spin-labeled nematogenlike probes dissolved in nematic liquid crystals. *J. Chem. Phys.* 50: 4545-4550.

- Footo C.S., **1994**. Photophysical and photochemical properties of fullerenes, in "Topics in Current Chemistry 169: Electron Transfer I," M.J.S. Dewar, *et al.*, Eds. Springer-Verlag: Berlin, pp. 347-363.
- Freed J.H. and G.K. Fraenkel, **1963**. Theory of linewidths in electron spin resonance spectra. *J. Chem. Phys.* 39:326-348.
- Freed J.H., **1964**. Anisotropic rotational diffusion and electron spin resonance linewidths. *J. Chem. Phys.* 41:2077-2083.
- Freed J.H., **1977**. ESR studies of spin probes in anisotropic media, in "Spin Labelling: Theory and Applications," L. J. Berliner and J. Reuben, Eds., Chap. 1. Plenum Press: New York.
- Friedrich J., P. Schweitzer, K.-P. Dinse, P. Rapta, and A. Stasko, **1994**. EPR study of radical anions of C_{60} and C_{70} . *Appl. Magn. Reson.* 7:415-425.
- Francisz W., C.-S. Lai, and J.S. Hyde, **1985**. Spin-label oximetry: kinetic study of cell respiration using a rapid-passage T_1 -sensitive electron spin resonance display. *Proc. Natl. Acad. Sci.* 82:411-415.
- Gaffney B.J., **1976**. The chemistry of spin labels, in "Spin Labelling: Theory and Applications," L. J. Berliner, Ed., Chap. 5. Academic Press, Inc.: New York.
- Giamello E., D. Murphy, G. Maganacca, C. Morterra, Y. Shioya, T. Nomura, and M. Anpo, **1992**. The interaction of NO with copper ions in ZSM5: an EPR and IR investigation. *J. Catal.* 136:510-520.

- Goldman S.A., G.V. Bruno, and J.H. Freed, **1972**. An ESR study of anisotropic rotational reorientation and slow tumbling in liquid and frozen media. *J. Chem. Phys.* 56:716-735.
- Goldman S.A., G.V. Bruno, and J.H. Freed, **1973**. ESR studies of anisotropic rotational reorientation and slow tumbling in liquid and frozen media. II. Saturation and nonsecular effects. *J. Chem. Phys.* 59:3071-3091.
- Goldstein H., **1980**. "Classical Mechanics," 2nd Ed. Addison-Wesley Publishing Company, Inc.:Massachusetts, p. 143.
- Goroff N.S., **1996**. Mechanism of fullerene formation. *Acc. Chem. Res.* 29:77-83.
- Goudsmit G.-H., and H. Paul, **1993**. Time-resolved EPR investigation of triplet state C_{60} . Triplet-triplet annihilation, CIDEP, and quenching by nitroxide radicals. *Chem. Phys. Lett.* 208:73-78.
- Grasdalen H., L.E.G. Eriksson, J. Westman, and A. Ehrenberg, **1977**. Surface potential effects on metal ion binding to phosphatidylcholine membranes. ^{31}P NMR study of lanthanide and calcium ion binding to egg-yolk lecthin vesicles. *Biochim. Biophys. Acta* 469:151-162.
- Griffith O.H. and P.C. Jost, **1976**. Lipid spin labels in biological membranes, in "Spin Labelling: Theory and Applications," L.J. Berliner, Ed., Chap. 12. Academic Press, Inc.: New York.

- Hammond G.S. and V.J. Kuck, Eds., **1992**. "Fullerenes: Synthesis, Properties, and Chemistry of Large Carbon Clusters." ACS Symposium Series 481, American Chemical Society: Washington, DC.
- Hauffler R.E., J. Conceicao, L.P.F. Chibante, Y. Chai, N.E. Byrne, S. Flanagan, M.M. Haley, S.C. O'Brien, C. Pan, Z. Xiao, W.E. Billups, M.A. Ciufolini, R.H. Hauge, J.L. Margrave, L.J. Wilson, R.F. Curl, and R.E. Smalley, **1990**. Efficient production of C_{60} (buckminsterfullerene), $C_{60}H_{36}$, and the solvated buckide ion. *J. Phys. Chem.* 94: 8634-8636.
- Hauser H., C.C. Hinckley, J. Krebs, B.A. Levine, M.C. Phillips, and R.J.P. Williams. **1977**. The interaction of ions with phosphatidylcholine bilayers. *Biochim. Biophys. Acta* 468:364-377.
- Herschbach D.R., H.S. Johnston, K.S. Pitzer, and R.E. Powell, **1956**. Theoretical pre-exponential factors for twelve bimolecular reactions. *J. Chem. Phys.* 25:736-741.
- Hudson A. and G.R. Luckhurst, **1969**. The electron resonance line shapes of radicals in solution. *Chem. Rev.* 69:191-225.
- Hwang J.S., and H.B. Balkhoyor, **1995**. ESR studies of the coupling of translational and reorientational motions of dichlorobis(η -cyclopentadienyl)vanadium in solution. *J. Phys. Chem.* 99:8447-8452.
- Hwang J.S., M.A. Morsy, and G.A. Oweimreen, **1994**. Nonmesomorphic solute-mesomorphic solvent interaction studies. 1. Visual and ESR studies on nitroxide radicals in the nematic and isotropic phases of 4-cyano-4'-n-

pentylbiphenyl (5CB) liquid crystalline solvent. *J. Phys. Chem.* 98: 9056-9062.

Hwang J.S., and M.H. Rahman, **1992**. Determination of the anisotropy of rotational reorientation from ESR line width data. *Chem. Phys. Lett.* 199:286-292.

Hwang J.S., P. Pollet, and M.M. Saleem, **1986**. ESR line shape studies of *N*-(4-*n*-butyl benzilidene) 4-amino 2,2,6,6-tetramethyl piperidine 1-oxide (BBTMPO) in toluene. *J. Chem. Phys.* 84:577-583.

Hwang J.S., R.P. Mason, L.-P. Hwang, and J.H. Freed, **1975**. Electron spin resonance studies of anisotropic rotational reorientation and slow tumbling in liquid and frozen media. III. Perdeuterated 2,2,6,6-tetramethyl-4-piperidone *N*-oxide and an analysis of fluctuating torques. *J. Phys. Chem.* 79:489-511.

Johnson R.D., C.S. Yannoni, M.S. de Vries, H.C. Dorn, J.R. Salem, and D.S. Bethune, **1992**. C₆₀ solid state rotational dynamics and production and EPR spectroscopy of fullerenes containing metal atoms. *Nanotechnology* 3:164-166.

Jost P., L.J. Libertini, V.C. Hebert, and O.H. Griffith, **1971**. Lipid spin labels in lecithin multilayers. A study of motion along fatty acid chains. *J. Mol. Biol.* 59:77-98.

- Jung M.E. and C.A. McCombs, **1978**. 2-trimethylsilyloxy-1,3-butadiene as a reactive diene: Diethyl *trans*-4-trimethylsilyloxy-4-cyclohexene-1,2-dicarboxylate. *Org. Synth.* 58:163-168.
- Kadish K.M. and R.S. Ruoff, Eds., **1994**. "Recent Advances in the Chemistry and Physics of Fullerenes and Related Materials." The Electrochemical Society, Inc.: New Jersey.
- Kanowski M., H. Werner, R. Schlögl, H.-M. Vieth, and K. Lüders, **1995**. ^{13}C MAS NMR investigations of alkali doped C_{60} . *Appl. Magn. Res.* 8:173-180.
- Keana J.F.W., **1978**. Newer aspects of the synthesis and chemistry of nitroxide spin lables. *Chemical Reviews* 78: 37-64.
- Kempiński W., J. Stankowski, Z. Trybula, and Sz. Loš, **1995**. EPR evidence of the low temperature phase transition in C_{60} . *Appl. Magn. Reson.* 8:127-132.
- Khaled M.M., R.T. Carlin, P.C. Trulove, G.R. Eaton, and S.S. Eaton, **1994**. Electrochemical generation and electron paramagnetic resonance studies of C_{60}^- , C_{60}^{2-} , and C_{60}^{3-} . *J. Am. Chem. Soc.* 116:3465-3474.
- Khan S.I., A.M. Oliver, M.N. Paddon-Row, and Y. Rubin, **1993**. Synthesis of a rigid "ball-and-chain" donor-acceptor system through Diels-Alder functionalization of buckminsterfullerene (C_{60}). *J. Am. Chem. Soc.* 115: 4919-4920.

- Kivelson D., **1972**. Electron spin relaxation in liquids, *In* "Electron Spin Relaxation in Liquids," L.T. Muss and P.W. Atkins, Eds. Plenum: New York, pp. 213-277.
- Kivelson D., M.G. Kivelson and I. Oppenheim, **1970**. Rotational Relaxation in Fluids. *J. Chem. Phys.* 52:1810-1821.
- Krätschmer W., L.D. Lamb, K. Fostiropoulos, and D.R. Huffman, **1990**. Solid C₆₀: a new form of carbon. *Nature* 347: 354-358.
- Kroto H.W., J.R. Heath, S.C. O'Brien, R.F. Curl, and R.E. Smalley, **1985**. C₆₀: Buckminsterfullerene. *Nature* 318: 162-163.
- Krusic P.J., D.C. Roe, E. Johnson, J.R. Morton, and K.F. Preston, **1993**. EPR study of hindered internal rotation in alkyl-C₆₀ radicals. *J. Phys. Chem.* 97:1736-1738.
- Krusic P.J., E. Wasserman, B.A. Parkinson, B. Malone, E.R. Holler, P.N. Keizer, J.R. Morton, and K.F. Preston, **1991(a)**. Electron spin resonance study of the radical reactivity of C₆₀. *J. Am. Chem. Soc.* 113:6274-6275.
- Krusic P.J., E. Wasserman, P.N. Keizer, J.R. Morton, and K.F. Preston, **1991(b)**. Radical reactions of C₆₀. *Science* 254:1183-1185.
- Lang J.C. and J.H. Freed, **1972**. ESR study of Heisenberg spin exchange in a binary liquid solution near the critical point. *J. Chem. Phys.* 56:4103-4114.
- Lefebvre R. and J. Maruani, **1965(a)**. Use of computer programs in the interpretation of electron paramagnetic resonance spectra of dilute radicals in amorphous solid samples. I. High-field treatment. X-band

spectra of π -electron unconjugated hydrocarbon radicals. *J. Chem. Phys.* 42:1480-1496.

Lefebvre R. and J. Maruani, **1965(b)**. Use of computer programs in the interpretation of electron paramagnetic resonance spectra of dilute radicals in amorphous solid samples. II. Zero-field treatment for several nuclei of spin 1/2. *J. Chem. Phys.* 42:1496-1502.

Lenk R. **1977**. "Brownian Motion and Spin Relaxation." Elsevier: Amsterdam.

Levanon H., V. Meiklyar, A. Michaeli, S. Michaeli, and A. Regev, **1992**. Paramagnetic states and dynamics of photoexcited C_{60} . *J. Phys. Chem.* 96:6128-6131.

Li A.S.W., and J.S. Hwang, **1984**. Determination of intrinsic linewidth and deuterium isotropic hyperfine coupling constant of pd-tempone in jojoba oil and microemulsion: an esr study. *Arabian J. Sci. Eng.* 9:233-238

Li A.S.W., and J.S. Hwang, **1985**. Anisotropic rotational reorientation of perdeuterated 2,2,6,6-tetramethyl-4-piperidone *N*-oxide in jojoba oil: an esr line shape study. *J. Phys. Chem.* 89:2556-2560.

Libertini L.J., C.A. Burke, P.C. Jost, and O.H. Griffith, **1974**. An orientation distribution model for interpreting ESR line shapes of ordered spin labels. *J. Magn. Reson.* 15:460-476.

Likhtenshtein G.I. **1976**. "Spin Labelling Methods in Molecular Biology." Jhon Wiley & Sons, Inc.: New York.

Margenau H. and A. Henry, **1950**. Theory of magnetic resonance in nitric oxide.

Phys. Rev. 78:587-592.

Maschke A., B.S. Shapiro, and F.W. Lampe, **1963**. Mechanism of the low-temperature scavenging of methyl- d_3 radicals by nitric oxide. *J. Am. Chem. Soc.* 85:1876-1878.

McClung R.E.D. and D. Kivelson, **1968**. ESR linewidths in solution. V. Studies of spin-rotational effects not described by rotational diffusion theory. *J. Chem. Phys.* 49:3380-3391.

McConnell H.M. **1976**. Molecular motion in biological membranes, in "Spin Labeling Theory and Applications," L.J. Berliner, Ed. Academic Press: New York, pp. 525-560.

McLafferty F.W., Ed., **1992**. *Acc. Chem. Res.* 25: 97-175. Special Issue on Buckminsterfullerenes.

Misra S.K. and V. Petkov, **1995**. Electron paramagnetic and muon spin resonance studies in fullerenes. *Appl. Magn. Res.* 8:277-310.

Morsy M.A., G.A. Oweimreen, and J.S. Hwang, **1997**. Nonmesomorphic solute-mesomorphic solvent interactions studies: 2. ESR studies on the different phases of 5CB, 6CB, 7CB, and 8CB liquid crystals using PD-Tempone and Tempo-palmitate as probes. Structural and conformational effects. *J. Phys. Chem.* 100:8331-8337.

Morsy M.A., J.S. Hwang, and G.A. Oweimreen, **1997**. Nonmesomorphic solute-mesomorphic solvent interactions studies. 3. A unified approach to probe

- liquid crystalline order by electron spin resonance spectroscopy. *J. Phys. Chem.* 101:2120-2125.
- Nordio P.L. **1976**. General magnetic resonance theory, in "Spin Labelling: Theory and Applications," L.J. Berliner, Ed., Chap. 2. Academic Press, Inc.: New York.
- Oweimreen G.A. and J.S. Hwang, **1989**. The nematic-isotropic two phase region in mixtures of quasi-spherical solutes in alkylcyanobiphenyls: an E.S.R. study using tempone as a probe. *Liq. Cryst.* 5:585-593.
- Oweimreen G.A., M.A. Morsy, and J.S. Hwang, **1995**. Phase Diagrams from spin probe studies for binary mixtures of Non-mesomorphic solutes in 5CB. *Appl. Magn. Reson.* 9:61-71.
- Pace M.D., T.C. Christidis, J.J. Yin, and J. Milliken, **1992**. EPR of a free radical in C₆₀: Effect of O₂. *J. Phys. Chem.* 96:6855-6858.
- Pace M.D., J. Milliken, J.J. Yin, and T.C. Christidis, **1994**. EPR detected interactions of oxygen, nitrogen, and nitrogen dioxide with C₆₀, in "Recent Advances in the Chemistry and Physics of Fullerenes and Related Materials," K.M. Kadish and R.S. Ruoff, Eds. The Electrochemical Society, Inc.: New Jersey, pp.1057-1067.
- Pake G.E. and T.L. Estle, **1973**. "The Physical Principles of Electron Paramagnetic Resonance." W. A. Benjamin, Inc.: Massachusetts, p. 171.
- Pauling L., **1960**. "The Nature of the Chemical Bond," 3rd ed. Cornell University Press: New York.

- Phillips L., **1961**. The addition of methyl radicals to nitrosomethane in the vapour phase: trimethylhydroxylamine. *Proc. Chem. Soc.* 204-205.
- Polnaszek C.F., **1975**. An ESR Study of Rotational Reorientation and Spin Relaxation in Liquid Crystal Media, Ph.D. Thesis, Cornell University, Ithaca, New York.
- Polnaszek C.F. and J.H. Freed, **1975**. Electron spin resonance studies of anisotropic ordering, spin relaxation and slow tumbling in liquid crystalline solvents. *J. Phys. Chem.* 79: 2283-2306.
- Poole C.P., **1983**. "Electron Spin Resonance," 2nd Ed. John Wiley & Sons, Inc.: New York.
- Popp C.A. and J.S. Hyde, **1981**. Effects of oxygen on EPR spectra of nitroxide spin-label probes of model membranes. *J. Magn. Reson.* 43:249-258.
- Prosser R.S., J.S. Hwang, and R.R. Vold, **1996**. Characterization of a magnetically oriented phospholipid/lanthanide bilayer with a positive order parameter - a deuterium solid state NMR study. *Submitted for publication*.
- Prosser R.S., S.A. Hunt, J.A. DiNatale, and R.R. Vold, **1996**. Magnetically aligned membrane model systems with positive order parameter: switching the sign of S_{zz} with paramagnetic ions. *J. Am. Chem. Soc.* 118:269-270.
- Prato M., T. Suzuki, H. Foroudian, Q. Li, K. Khemani, and F. Wudl, **1993**. [3+2] and [4+2] cycloadditions of C_{60} . *J. Am. Chem. Soc.* 115: 1594-1595.

Press W.H., B.P. Flannery, S.A. Teukolsky, and W.T. Vetterling, **1987**.

"Numerical Recipes." Cambridge:New York, pp. 86-89.

Rabideau P.W. and A. Sygula, **1996**. Buckybowls: polynuclear aromatic hydrocarbons related to the buckminsterfullerene surface. *Acc. Chem. Res.* 29: 235-242, and references therein.

Rahman M.H., **1988**. "EPR Studies of Anisotropic Rotational Reorientation and Slow Tumbling in Liquids and Frozen Media," M.Sc. Thesis, King Fahd University of Petroleum & Minerals, Dhahran 31261, Saudi Arabia.

Rao K.V.S., J.S. Hwang, and J.H. Freed, **1976**. Symmetry of orientational order fluctuations about the nematic-isotropic phase transition: an ESR study. *Phys. Rev. Lett.* 37:515-518.

Rotello V.M., J.B. Howard, T. Yadav, M.M. Conn, E. Viani, L.M. Giovane, and A.L. Lafleur, **1993**. Isolation of fullerene products from flames: structure and synthesis of the C₆₀-cyclopentadiene adduct. *Tetrahedron. Lett.* 34: 1561-1562.

Rozantsev E.G., **1970**. "Free Nitroxyl Radicals." Plenum Press, New York.

Rubin Y., S. Khan, D.I. Freedberg, and C. Yeretian, **1993**. Synthesis and X-ray structure of a Diels-Alder adduct of C₆₀. *J. Am. Chem. Soc.* 115: 344-345.

Samirnov A.I., T.I. Smirnova, and P.D. Morse II, **1995**. Very high frequency electron paramagnetic resonance of 2,2,6,6-tetramethyl-1-piperidinyloxy in 1,2-dipalmitoyl-*sn*-glycero-3-phosphatidylcholine liposomes: partitioning and molecular dynamics. *Biophys. J.* 68:2350-2360.

- Sanders C.R. and G.C. Landis, **1995**. Reconstitution of membrane proteins into lipid-rich bilayered mixed micelles for NMR studies. *Biochemistry* 34:4030-4040.
- Sanders C.R. and J.P. Schwonek, **1992**. Characterization of magnetically orientable bilayers in mixtures of dihexanoylphosphatidylcholine and dimyristoylphosphatidylcholine by solid-state NMR. *Biochemistry* 31: 8898-8905.
- Saupe, A., **1968**. Recent results in the field of liquid crystals. *Angew. Chem. internat. Edit.* 7:97-112.
- Saxby J.D., S.P. Chatfield, A.J. Palmisano, A.M. Vassallo, M.A. Wilson, and L.S.K. Pang, **1992**. Thermogravimetric analysis of buckminsterfullerene and related materials in air. *J. Phys. Chem.* 96:17-18.
- Seelig J., **1976**. Anisotropic motion in liquid crystalline structures, in "Spin Labelling: Theory and Applications," L.J. Berliner, Ed., Chap. 10. Academic Press, Inc.: New York.
- Schorn K. and D. Marsh, **1996**. Lipid chain dynamics and molecular location of diacylglycerol in hydrated binary mixtures with phosphatidylcholine: spin label ESR studies. *Biochemistry* 35:3831-3836.
- Shimshick E.J. and H.M. McConnell, **1973**. Lateral phase separation in phospholipid membranes. *Biochemistry* 12:2351-2360.
- Slichter C.P., **1992**. "Principles of Magnetic Resonance," 3rd Ed. Springer-Verlag: New York.

- Stankowski J., W. Kempniński, A. Koper, and J. Martinek, **1994**. Valence state of paramagnetic centers in fullerenes. *Appl. Magn. Reson.* 6:145-154, and references therein.
- Steinfeld J.I., **1989**. "Molecules and Radiation: An Introduction to Modern Molecular Spectroscopy," 2nd Ed. The MIT Press: Massachusetts, p. 224.
- Stern C.A., P.R. Levstein, H. van Willigen, H. Linschitz, and L. Biczok, **1993**. FT-EPR study of the triplet state C_{60} . Spin dynamics and electron transfer quenching. *Chem. Phys. Lett.* 204:23-28.
- Trousseau P. and Y. Lion **1985**. Fourier transform numerical analysis of the long-range proton hyperfine coupling in nitroxide radicals. *J. Phys. Chem.* 89:1954-1958.
- Vijayakrishnan V., A.K. Santra, T. Pradeep, R. Seshadri, R. Nagarajan, and C.N.R. Rao, **1992**. Interaction of nitrogen and oxygen with C_{60} . *J. Chem. Soc., Chem. Commun.* 198-199.
- Wang J.H., **1951**. Self-diffusion and structure of liquid water. I. Measurement of self-diffusion of liquid water with deuterium as tracer. *J. Am. Chem. Soc.* 73: 510-513.
- Wang Y., **1992**. Photophysical properties of fullerenes and fullerene/*N,N*-diethylaniline charge-transfer complexes. *J. Phys. Chem.* 96: 764-767.
- Wasielowski M.R., M.P. O'Neil, K.R. Lykke, M.J. Pellin, and D.M. Gruen, **1991**. Triplet states of fullerenes C_{60} and C_{70} : Electron paramagnetic resonance

spectra, photophysics, and electronic structures. *J. Am. Chem. Soc.* 113:2774-2776.

Witherspoon P.A. and D.N. Saraf, **1965**. Diffusion of methane, ethane, propane, and *n*-butane in water from 25 to 43°. *J. Phys. Chem.* 69:3752-3755.

Wu S.H.-w. and H.M. McConnell, **1975**. Phase separations in phospholipid membranes. *Biochemistry* 14:847-854

Wudl F., A. Hirsch, K.C. Khemani, T. Suzki, P.-M. Allemand, A. Koch, H. Eckert, G. Srdanov, and H.M. Webb, **1992**. Survey of chemical reactivity of C₆₀, electrophile and dieno-polarophile par excellence, in "Fullerenes: Synthesis, Properties, and Chemistry of Large Carbon Clusters," G.S. Hammond and V.J. Kuck, Eds., ACS Symposium Series 481, American Chemical Society, Washington, DC, pp. 161-175.

Yamago S., H. Tokuyama, E. Nakamura, M. Prato, and F. Wudl. **1993**. Chemical derivatization of organofullerenes through oxidation, reduction, and C-O and C-C bond-formation reactions. *J. Org. Chem.* 58: 4796-4798, and supplementary materials.

Yamashita H., M. Matsuoka, K. Tsuji, Y. Shioya, E. Giamello, M. Che, and M. Anpo, **1995**. In situ investigation on the interaction of NO and CO with Cu⁺/ZSM-5 catalyst, in "Science and Technology in Catalysis 1994," Y. Izumi, H. Arai, and M. Iwamoto, Eds., Kodansha Ltd., Tokyo, pp. 227-232.

Zavoisky, E. **1945**. *J. Phys. USSR* 9:211.

Zhang Y., X. Gao, and M.J. Weaver, **1992**. Scanning tunneling microscopy of C_{60} and C_{70} on ordered Au(111) and Au(110): Molecular structure and electron transmission. *J. Phys. Chem.* 96:510-513.

Zhang D., J.R. Norris, P.J. Krusic, E. Wasserman, C.-C. Chen, and C.M. Lieber, **1993**. Time-resolved EPR and Fourier transform EPR study of triplet C_{60} . Determinations of T_1 and ^{13}C hyperfine coupling constant. *J. Phys. Chem.* 97:5886-5889.

APPENDIX

Appendix A

LWA.FOR

```

PROGRAM LWA
DOUBLE PRECISION BFLD(2500),INT(2500),BMAX(3),
1IMAX(3),IMIN(3),OLW(3),PTPI(3), CFLD(3),
2AMAXI, AINT, TEMP, BMIN(3)
INTEGER*2 N, NSET, DPN(2500), NI, NF,
1 NMAX(3), NMIN(3), THIRD, L
CHARACTER FDATIM*65, MODF*60, FNAME*2, EXTI*4, EKTO*4,
1FNAME*9, FONAME*7, DATIM*60, DASH, SOLUTE*60, SOLVNT*60,
2 FREQ*6, RBQ*5, F*1, CNAME*3
REQ = '-Band'
EXTI = '.TXT'
EXTO = '.DAT'
WRITE (*,114)
114 FORMAT (//,2X,'Name of the solute --> '\)
READ (*,110) SOLUTE
WRITE (*,115)
115 FORMAT (//,2X,'Name of the Solvent --> '\)
READ (*,110) SOLVNT
WRITE (*,116)
117 WRITE (*,116)
READ (*,165, err=117) F
116 FORMAT (//,2X,'Microwave Frequency (L, S, X, OR Q) --
> '\)
165 FORMAT(A1)
WRITE (*,210)
210 FORMAT (//,2X,'Number of files for analysis --> '\)
READ(*,*) NSET
FREQ(1:1) = F
FREQ(2:1+5) = REQ
FONAME(1:1) = F
FONAME(2:1+2) = SOLUTE
FONAME(3:2+1) = SOLVNT
FONAME(4:3+4) = EXTO
OPEN(UNIT=4,FILE=FONAME, STATUS='NEW', FORM='FORMATTED',
* ACCESS = 'SEQUENTIAL')
WRITE (4,118) SOLUTE, SOLVNT, FREQ
118 FORMAT (2X,'THE SOLUTE IS --> ',A,/,2X,'THE SOLVENT
IS --> '
1,A,/,2X,'THE MICROWAVE FREQUENCY RANGE: ',A6,/)
WRITE(4,200)
200 FORMAT(96('='),/,18X,'m = -1',24X,'m = 0',24X,
1'm=+1',/,96('-'
),/,1X,'TEMP.',3(3X,'OLW',6X,'PTPI',8X,'CFLD',2X
2),/,2X,'(K)',2X,3('GAUSS)',14X,'(GAUSS)',2X)/,96('='),/)
301 WRITE (*,300)
300 FORMAT (//, 8X, '*** THE NAME OF THE FILE MUST BE OF
THE FORM
1 ?????.TXT ***,/,
2 2X, 'INPUT THE FIRST THREE CHARACTERS IN COMMON -->
',S)
READ (*,110, ERR=301) CNAME
FINAME(1:3) = CNAME
FINAME(6:5+4) = EXTI
DO 60 L = 1, NSET
NI = 1
DO 10 I = 1,3
IMAX(I) = 0.0D0
IMIN(I) = 0.0D0
10 CONTINUE
101 WRITE (*,100)
100 FORMAT (//,2X, 'INPUT DATA FILE NAME IDENTIFIERS (TWO
CHARACTERS
IONLY) --> ',S)
READ (*,110, ERR=101) FNAME
110 FORMAT(A)
FINAME(4:3+2) = FNAME
OPEN(UNIT=3,FILE=FINAME, STATUS='OLD', FORM='FORMATTED',
* ACCESS = 'SEQUENTIAL')
READ (3,110) FDATIM
DATIM = FDATIM(10:65)
READ (3,120) MODF
120 FORMAT(A)
WRITE (*,145)
145 FORMAT (//,2X,'ENTER THE TEMPERATURE IN KELVIN -->
',\)
READ (*,*) TEMP
WRITE (*,140)
140 FORMAT (//,2X,'ENTER NUMBER OF DATA POINTS --> ',\)

```

```

READ (*,*) N
READ (3,150) DASH
150 FORMAT(//A)
READ (3,155) (DPN(I),BFLD(I), INT(I), I=1,N)
155 FORMAT(4X,I4,3X,F10.4,4X,E12.4E3)
CLOSE (3, STATUS = 'KEEP')
THIRD = N/3
NF = THIRD
DO 20 K = 1,3
DO 30 I=NI,NF
IF (INT(I) .GE. IMAX(K)) THEN
IMAX(K) = INT(I)
BMAX(K) = BFLD(I)
NMAX(K) = DPN(I)
ENDIF
IF (INT(I) .LE. IMIN(K)) THEN
IMIN(K) = INT(I)
BMIN(K) = BFLD(I)
NMIN(K) = DPN(I)
ENDIF
OLW(K) = BMIN(K) - BMAX(K)
PTPI(K) = IMAX(K) - IMIN(K)
CFLD(K) = BMAX(K) + OLW(K)/2.
30 CONTINUE
NI = NI + THIRD
NF = NF + THIRD
CONTINUE
WRITE (4,119) TEMP, (OLW(J), PTP(I), CFLD(J), J=1,3)
119 FORMAT(1X,F5.1,3(1X,F6.4,E12.4E3,1X,F10.4))
60 CONTINUE
CLOSE (4, STATUS = 'KEEP')
WRITE (*,70) FONAME
70 FORMAT (//,2X,'THE RESULTS ARE STORED IN --> ',A)
STOP
END

```

EXDEL.FOR

```

PROGRAM EXDEL
COMMON/YURCOM/ DPN, BFLD, INT, N
DIMENSION X(11), Y(11)
DOUBLE PRECISION BFLD(2500),INT(2500),BMAX,BMIN,IMAX,IMIN,
PP
1WIDTH,DEL,CFLD,CINT,LFLD,RFLD,ILFLD,IRFLD,IFLD,AINT,
NDEL,AIMAX
INTEGER*2 DPN(2500), N, NMAX, NMIN, NSET,L
CHARACTER FDATIM*65, MODF*60,CFNAME*3, EXTI*4, EKTO*4,
1 FNAME*9, FONAME*9, DATIM*60, DASH, SOLUTE*60,
SOLVNT*60
CHARACTER FREQ*6, REQ*5, F*1, ANS*1,VNAME*2
WRITE (*,1140)
1140 FORMAT (//,2X,'Enter the Name of the Solute --> '\)
READ (*,1010) SOLUTE
WRITE (*,1150)
1150 FORMAT (//,2X,'Enter the Name of the Solvent --> '\)
READ(*,1010) SOLVNT
1170 WRITE (*,1160)
READ (*,1165, err=1170) F
1160 FORMAT (//,2X,'Enter the Microwave Frequency (L, S,
...)--> '\)
1165 FORMAT(A1)
FREQ(1:1) = F
FREQ(2:1+5) = REQ
REQ = '-Band'
EXTI = '.TXT'
EXTO = '.OUT'
WRITE (*,90)
90 FORMAT (//, 12X, '*** THE NAME OF THE FILE MUST BE OF
THE FORM
1 ????.TXT ***,/,,,
2 2X, 'INPUT THE FIRST THREE COMMON CHARACTERS --> ',S)
READ (*,1010) CFNAME
1010 FORMAT(A)
FINAME(1:3) = CFNAME
FINAME(6:5+4) = EXTI
FONAME(1:3) = CFNAME
FONAME(6:5+4) = EXTO
WRITE (*,2140)
2140 FORMAT (//,2X,'HOW MANY FILES TO PROCESS? --> '\)
READ (*,*) NSET
C
DO 4 L = 1, NSET
IMAX = 0.0D0

```

```

IMIN = 0.000
AIMAX = 0.000
WRITE (*,100)
100  FORMAT (//,2X, 'INPUT THE TWO NUMBERS IDENTIFIER -->
',5)
    READ (*,1010) VFNAM
    FINAME(4:3+2) = VFNAM
    FONAME(4:3+2) = VFNAM
    OPEN(UNIT=3,FILE=FINAME, STATUS='OLD', FORM='FORMATTED',
    * ACCESS = 'SEQUENTIAL')
    OPEN(UNIT=4,FILE=FONAME, STATUS='NEW', FORM='FORMATTED',
    * ACCESS = 'SEQUENTIAL')
    READ (3,1010) FDATE
    DATIM = FDATE(10:65)
    READ (3,1020) MODF
1020  FORMAT(/A)
    WRITE (*,1040)
1040  FORMAT (//,2X, 'ENTER NUMBER OF DATA POINTS --> ',\
)
    READ (*,*) N
    C   WRITE (*,*) 'N= ', N
    WRITE (*,45)
    45  FORMAT (//,2X, 'Enter the "m" Value (-1, 0, 1) -->
'\)
    READ (*,1145) MVALUE
1145  FORMAT(I2)
    READ (3,1050) DASH
1050  FORMAT(/A)
    READ (3,1055) (DPN(I),BFLD(I), INT(I), I=1,N)
1055  FORMAT(4X,I4,3X,F10.4,4X,E12.4E3)
    CLOSE (3, STATUS = 'KEEP')
    WRITE (4,1010) DATIM
    WRITE (4,1070) MODF
1070  FORMAT(/A)
    WRITE (4,1180) SOLUTE, SOLVMT, FREQ, MVALUE
1180  FORMAT (2X, 'THE SOLUTE IS --> ',A,/,2X, 'THE SOLVENT
IS --> ',
1,A,/,2X, 'THE MICROWAVE FREQUENCY RANGE: ',A6,/,2X,
2'THE "m" VALUE IS --> ',I2)
    DO 1 I=1,N
    AINT=ABS(INT(I))
    IF (AINT .GE. AIMAX) AIMAX = AINT
    IF (INT(I) .GE. 0 .AND. INT(I+1) .LT. 0.) THEN
    PP = (0. - INT(I+1))/(INT(I)-INT(I+1))
    CFLD = BFLD(I) + PP * (BFLD(I+1)-BFLD(I))
    ENDIF
    IF (INT(I) .GE. IMAX) THEN
    IMAX = INT(I)
    BMAX = BFLD(I)
    NMAX = DPN(I)
    ENDIF
    IF (INT(I) .LE. IMIN) THEN
    IMIN = INT(I)
    BMIN = BFLD(I)
    NMIN = DPN(I)
    ENDIF
1    CONTINUE
    DO 2 J=1,N
    INT (J) = INT(J)/AIMAX
2    CONTINUE
    WIDTH = BMIN - BMAX
    WRITE (*,110) WIDTH
110  FORMAT (/,2X, 'OBSERVED LINEWIDTH = ',F10.4/)
    DEL = WIDTH/4.
    WRITE (*,1190) CFLD
1190  FORMAT(2X, 'THE CALCULATED CENTRAL FIELD = ',F10.4,2X,
1 'GAUSS')
    WRITE (*,1200)
1200  FORMAT(2X, 'WOULD YOU LIKE TO INPUT ANOTHER VALUE?
(Y/N) '\)
    READ (*,1210) ANS
1210  FORMAT(A)
    IF (ANS .EQ. 'Y' .OR. ANS .EQ. 'y') THEN
    WRITE (*,1220)
1220  FORMAT(2X, 'INPUT THE NEW CF VALUE --> '\)
    READ (*,*) CFLD
    END IF
    NDEL = 0.000
    DO 3 K = 1, 11
    LFLD = CFLD - NDEL * DEL
    RFLD = CFLD + NDEL * DEL
    CALL INTSTY (LFLD, ILFLD)
    CALL INTSTY (RFLD, IRFLD)
    IFLD = (ILFLD + ABS(IRFLD))/2.
    X(K) = NDEL
    Y(K) = IFLD
    NDEL = NDEL + 1.
3    CONTINUE
    WRITE (4,1080) AIMAX
1080  FORMAT (/,2X, 'ABSOLUTE MAXIMUM INTENSITY =
',E14.6E3)
    WRITE (4,1090) NMAX, BMAX, IMAX
1090  FORMAT (2X, 'MAXIMUM: ',I4,2X,F10.4,2X,E14.6E3)
    WRITE (4,1100) NMIN, BMIN, IMIN

```

```

1100  FORMAT (2X, 'MINIMUM: ',I4,2X,F10.4,2X,E14.6E3)
    WRITE (4, 1110) WIDTH, CFLD, DEL
1110  FORMAT (/,2X, 'OBSERVED LINEWIDTH = ',F10.4,2X, 'GAUSS' /,
1 2X, 'CENTRAL FIELD = ',F10.4,2X, 'GAUSS' /,2X, '1/4 DEL
= .
2 ,F10.4,2X, 'GAUSS')
    WRITE (4,80) BFLD(N)-BFLD(1)
80  FORMAT (2X, 'THE SWEEP WIDTH = ',F10.4,2X, 'GAUSS')
    WRITE (4,1120)
1120  FORMAT (///,2X, 'MULTIPLES OF 1/4 DEL',6X,
1 'AVERAGE AMPLITUDE')
    WRITE (4,1125)
1125  FORMAT(2X, '-----',6X, '-----
',/)
    WRITE (4,1130) (X(I), Y(I), I = 1, 11)
1130  FORMAT (4X, F10.4, 14X, E14.6E3)
    C
    CLOSE (4, STATUS = 'KEEP')
    WRITE (*,70) FONAME
70  FORMAT (//,2X, 'THE RESULTS ARE STORED IN --> ',A)
4    CONTINUE
    END
    C
    SUBROUTINE INTSTY (FLD,CI)
    COMMON/YURCOM/ DPN, BFLD, INT, N
    DOUBLE PRECISION BFLD(2500), INT(2500), FLD, CI, P
    INTEGER*2 T1,T2, DPN(2500), N
    C
    DO 100 I = 1, N
    IF (BFLD(I) .LT. FLD) GOTO 100
    IF (BFLD(I) .EQ. FLD) CI = INT(I)
    IF (BFLD(I) .GT. FLD) THEN
    T1 = I - 1
    T2 = I
    P = (FLD - BFLD(T1))/(BFLD(T2) - BFLD(T1))
    CI = INT(T1) + (P * (INT(T2) - INT(T1)))
    GOTO 200
    ENDIF
100  CONTINUE
200  RETURN
    END

```

GSUM.H.FOR

```

DIMENSION DEG(25),BRES(25),BFLD(1001),DERAB(1001),EMP(9),
1XT2IN(25),A(25),QNO(25),MOD(25),X(11),Y(11)
CHARACTER FNAME*3, EXTI*4, EXTO*4, FINAME*7, FONAME*7
REAL*8 MDERAB
C
EXTI = '.DAT'
EXTO = '.TXT'
WRITE(*,900)
900  FORMAT (//,12X, '*** THE NAME OF THE FILE MUST BE OF THE
FORM ????.da
1t ***',///,
2 2X, 'INPUT DATA FILE NAME WITHOUT THE EXTENSION .dat-
-> ',5)
    READ (*,910) FNAME
910  FORMAT(A)
    FINAME(1:3) = FNAME
    FINAME(4:3+4) = EXTI
    FONAME(1:3) = FNAME
    FONAME(4:3+4) = EXTO
    OPEN(UNIT = 3,FILE=FINAME, STATUS = 'OLD', FORM =
'FORMATTED',
    * ACCESS = 'SEQUENTIAL')
    OPEN(UNIT = 4,FILE=FONAME,STATUS='NEW', FORM =
'FORMATTED',
    * ACCESS = 'SEQUENTIAL')
    READ(3,1) N
1    FORMAT(I2)
    READ(3,4) (DEG(I),QNO(I),I=1,N)
4    FORMAT(8F10.7)
    SDBG=0.00
    DO 223 I=1,N
223  SDBG=SDBG+DEG(I)
    READ(3,257) NB,BI,BF
257  FORMAT(I4,6X,2D10.7)
    READ(3,1) NSETS
    DO 2 J=1,NSETS
    READ(3,4) A(J)
    WRITE (4,1050) A(J)
1050  FORMAT(35H NEW DEUTERON HYPERFINE COUPLING =
,F10.7,2X, 'GAUSS',/)
    DO 6 I=1,N
6    BRES(I)=QNO(I)*A(J)
    C   WRITE(4,1040)
    READ(3,1020) NLW
1020  FORMAT(I4)
    READ(3,1030) (XT2IN(I), I=1,NLW)
1030  FORMAT(8F10.7)

```

```

DO 2 K=1,NLW
T2IN=XT2IN(K)
WRITE(4,255) T2IN,BI,BF,NB
255 FORMAT(48H FIRST DERIVATIVE LINWIDTH(NO-EXCHANGE) P-P
=
1E12.7,6H GAUSS , /
249H INITIAL FIELD SWEEP VALUE RELATIVE TO CENTER =
3E12.5,6H GAUSS , /
447H FINAL FIELD SWEEP VALUE RELATIVE TO CENTER =
5E12.5,6H GAUSS , /
642H NUMBER OF POINTS FOR "HALF-SPECTRUM" = I4)
T2IN=T2IN*(SQRT(3.)/2.)
DEL=(BF-BI)/FLOAT(NB-1)
RES=BI
DO 261 IB=1,NB
GSUM=0.DO
DO 262 I=1,N
262GSUM=GSUM-2.*(DEG(I)/SDEG)*(BRES(I)-RES)*T2IN/(((BRES(I)-
RES)*
1(BRES(I)-RES)+T2IN*T2IN)*((BRES(I)-RES)*(BRES(I)-RES)+
2T2IN*T2IN))
DERAB(IB) = GSUM
BFLD(IB) = RES
261 RES=RES+DEL
C
C.....TO WRITE OUT THE FIELD AND NORMALIZED INTENSITY
-----
C GO TO 333
MDERAB=0.DO
DO 10 IBB=1,NB
IF(DERAB(IBB).LT.MDERAB) MDERAB=DERAB(IBB)
10 CONTINUE
WRITE(4,100) MDERAB
100 FORMAT(2X,'MINIMUM INTENSITY = ',D14.8)
DO 20 JB=1,NB
DERAB(JB)=DERAB(JB)/MDERAB
20 CONTINUE
WRITE(4,3010)
3010 FORMAT(/3X,'FIELD(GAUSS)',5X,'NORM. INTENSITY',/)
WRITE(4,3020)(BFLD(IB),DERAB(IB), IB=1,NB)
3020 FORMAT(1X,F12.5,7X,E14.8)
C
333 IMIN=1
YMIN=DERAB(1)
DO 4000 IB=2,NB
IF(DERAB(IB).LT.YMIN) IMIN=IB
IF(DERAB(IB).LT.YMIN) YMIN=DERAB(IB)
4000 CONTINUE
FPOS=BFLD(IMIN)
WRITE(4,400) FPOS,IMIN
400 FORMAT(7H FPOS= ,E13.6,10X,7H IMIN= ,I4)
WIDTH=2.*(ABS(FPOS))
WRITE(4,300) WIDTH
300 FORMAT(/29H THE OBSERVED LINWIDTH IS = ,E13.6,6H
GAUSS
,/)
DEL=0.5*FPOS
RES=BF
WRITE(4,499)
499 FORMAT(55H MULTIPLES OF 1/4 DEL PP FROM CENTER
REL AMPLITUDE)
DO 361 M=1,11
GSUM=0.DO
DO 362 I=1,N
362GSUM=GSUM-2.*(DEG(I)/SDEG)*(BRES(I)-RES)*T2IN/(((BRES(I)-
RES)*
1(BRES(I)-RES)+T2IN*T2IN)*((BRES(I)-RES)*(BRES(I)-RES)+
2T2IN*T2IN))
Y(M)=GSUM/YMIN
X(M)=RES/(0.5*FPOS)
WRITE(4,500) ABS(X(M)),ABS(Y(M))
500 FORMAT(13X,F12.8,16X,F12.8)
361 RES=RES-DEL
WRITE(4,1060)
1060 FORMAT(///)
2 CONTINUE
CLOSE (3,STATUS='KEEP')
CLOSE (4,STATUS='KEEP')
WRITE (*,70) FOWAME
70 FORMAT (//,2X,'THE RESULTS ARE STORED IN ---> ',A)
STOP
END

```

GSUMDP.FOR

```

DIMENSION DEG(25),BRES(25),BFLD(1001),DERAB(1001),EMP(9),
1XT2IN(25),A(25),QNO(25),MOD(25),X(11),Y(11), ETA(25)
CHARACTER FNAME*3, EXTI*4, EXTO*4, FNAME*7, FOWAME*7
C
PI = 3.141592654
EXTI = '.DAT'
EXTO = '.TXT'

```

```

WRITE(*,900)
900 FORMAT(//,12X,'*** THE NAME OF THE FILE MUST BE OF THE
FORM ????.dat
1 ****,////,
2 2X, 'INPUT DATA FILE NAME WITHOUT THE EXTENSION .dat-
-> ',S)
READ(*,910) FNAME
910 FORMAT(A)
FNAME(1:3) = FNAME
FNAME(4:3+4) = EXTI
FOWAME(1:3) = FNAME
FOWAME(4:3+4) = EXTO
OPEN(UNIT = 3,FILE=FNAME, STATUS = 'OLD', FORM =
'FORMATTED',
* ACCESS = 'SEQUENTIAL')
OPEN(UNIT = 4,FILE=FOWAME,STATUS='NEW', FORM =
'FORMATTED',
* ACCESS = 'SEQUENTIAL')
C
READ(3,1) N
FORMAT(12)
C
READ(3,4) (DEG(I),QNO(I),I=1,N)
4 FORMAT(8F10.7)
C
ETA = 1.0
SDEG=0.DO
DO 223 I=1,N
223 SDEG=SDEG+DEG(I)
READ(3,257) NB,BI,BF
257 FORMAT(14,6X,2D10.7)
READ(3,1) NSETS
DO 2 J=1,NSETS
READ(3,4) A(J), ETA(J)
WRITE (4,1050) A(J), ETA(J)
1050FORMAT(35H NEW HYDROGEN HYPERFINE COUPLING
=,F10.7,2X,'GAUSS',/,
11X,'ETA = ',F10.7)
DO 6 I=1,N
6 BRES(I)=QNO(I)*A(J)
READ(3,1020) NLW
1020 FORMAT(I4)
READ(3,1030) (XT2IN(I), I=1,NLW)
1030 FORMAT(8F10.7)
DO 2 K=1,NLW
T2IN=XT2IN(K)
WRITE(4,255) T2IN,BI,BF,NB
255 FORMAT(48H FIRST DERIVATIVE LINWIDTH(NO-EXCHANGE)P-P=
1E12.7,6H GAUSS , /
249H INITIAL FIELD SWEEP VALUE RELATIVE TO CENTER =
3E12.5,6H GAUSS , /
447H FINAL FIELD SWEEP VALUE RELATIVE TO CENTER =
5E12.5,6H GAUSS , /
642H NUMBER OF POINTS FOR "HALF-SPECTRUM" = I4)
T2IN=T2IN*(SQRT(3.)/2.)
DEL=(BF-BI)/FLOAT(NB-1)
RES=BI
DO 261 IB=1,NB
GSUM=0.DO
GSUM1=0.DO
GSUM2=0.DO
DO 262 I=1,N
GSUM1=ETA(J)*2./PI*(BRES(I)-RES)*T2IN/(((BRES(I)-RES)*
1(BRES(I)-RES)+T2IN*T2IN)*((BRES(I)-RES)*(BRES(I)-RES)+
2T2IN*T2IN))
GSUM2=(1.-ETA(J))/SQRT(2.*PI)*(BRES(I)-RES)/(T2IN*T2IN*T2IN)*
1EXP(-(BRES(I)-RES)*(BRES(I)-RES)/(2.*T2IN*T2IN))
262 GSUM=GSUM-DEG(I)/SDEG*(GSUM1+GSUM2)
DERAB(IB) = GSUM
BFLD(IB) = RES
261 RES=RES+DEL
C
WRITE(4,3010)
3010 FORMAT(/3X,'FIELD(GAUSS)',4X,'INTENSITY',/)
WRITE(4,3020)(BFLD(IB),DERAB(IB), IB=1,NB)
3020 FORMAT(1X,F12.8,2X,F12.8)
C
IMIN=1
YMIN=DERAB(1)
DO 4000 IB=2,NB
IF(DERAB(IB).LT.YMIN) IMIN=IB
IF(DERAB(IB).LT.YMIN) YMIN=DERAB(IB)
4000 CONTINUE
FPOS=BFLD(IMIN)
WRITE(4,400) FPOS,IMIN
400 FORMAT(7H FPOS= ,E13.6,10X,7H IMIN= ,I4)
WIDTH=2.*(ABS(FPOS))
WRITE(4,300) WIDTH
300 FORMAT(29H THE OBSERVED LINWIDTH IS = ,E13.6,6H
GAUSS)
DEL=0.5*FPOS
RES=BF
WRITE(4,499)

```

```

499  FORMAT(55H MULTIPLES OF 1/4 DEL PP FROM CENTERREL
AMPLITUDE)
DO 361 M=1,11
GSUM=0.00
DO 362 I=1,N
GSUM1=ETA(J)*2./PI*(BRES(I)-RES)*T2IN/(((BRES(I)-RES)*
1(BRES(I)-RES)+T2IN*T2IN)*((BRES(I)-RES)*(BRES(I)-RES)+
2T2IN*T2IN))
GSUM2=(1.-ETA(J))/SQRT(2.*PI)*(BRES(I)-RES)/(T2IN*T2IN*T2IN)*
1EXP(-(BRES(I)-RES)*(BRES(I)-RES)/(2.*T2IN*T2IN))
362  GSUM=GSUM-DBG(I)/SDBG*(GSUM1+GSUM2)
Y(M)=GSUM/YMIN
X(M)=RES/(0.5*FPOS)
WRITE(4,500) ABS(X(M)),ABS(Y(M))
500  FORMAT(13X,F12.8,16X,F12.8)
361  RES=RES-DEL
2    CONTINUE
CLOSE(3,STATUS='KEEP')
CLOSE(4,STATUS='KEEP')
STOP
END

```

T22.FOR

```

DIMENSION TITLE(18)
COMMON
ALWOB(450),ALWIN(450),HEIGHT(450),H2N,H3N,OW2,EIW2,A2,
1OW3,EIW3,A3,NPTS
OPEN(UNIT = 5,FILE='T22.DAT',STATUS='OLD',FORM='FORMATTED',
* ACCESS = 'SEQUENTIAL')
OPEN(UNIT = 6,FILE='T22.OUT',STATUS='NEW',FORM='FORMATTED',
* ACCESS = 'SEQUENTIAL')
OPEN(UNIT = 7,FILE='T22.TXT',STATUS='NEW',FORM='FORMATTED',
* ACCESS = 'SEQUENTIAL')
WRITE(7,2200)
2200  FORMAT(1X,'TEMP.(K)',1X,'INDEX',1X,' *** B *** ',1X,'
+ OR - ',
12X,' *** C *** ',1X,' + OR - ',1X,' C/B ')
C250  FORMAT(12,2X,2F7.2,3F11.2)
250   FORMAT(F5.1,I4,2F9.5,3F14.4)
350   FORMAT(3F9.5)
450   FORMAT(/' EXPERIMENTAL LINEWIDTH          INTRINSIC
LINEWIDTH
1     PP HEIGHT',8X,' (GAUSS)',21X,' (GAUSS)')
550   FORMAT(3(8X,F7.4,22X,F7.4,13X,E15.8/))
1000  FORMAT(18A4)
2000  FORMAT(//////////1X,18A4)
890   FORMAT(3X,'DEUTERIUM HYPERFINE SPLITTING IS',D12.5/)
READ(5,125) NPTS
125   FORMAT(18X,I4)
126   FORMAT(3X,'NO OF POINTS IS',I4/)
READ(5,89) AD
89    FORMAT(/35X,D12.5)
READ(5,145)
145   FORMAT(////)
READ(5,151) (ALWOB(I),ALWIN(I),HEIGHT(I),I=1,NPTS)
WRITE(6,151) (ALWOB(I),ALWIN(I),HEIGHT(I),I=1,NPTS)
151   FORMAT(4X,D16.8,12X,D16.8,8X,D16.8)
1     READ(5,1000,END=560) TITLE
WRITE(6,1000) TITLE
READ(5,*) TEMP,INDEX,WIDTH,FELW,H1,H2,H3
WRITE(6,250) TEMP,INDEX,WIDTH,FELW,H1,H2,H3
READ(5,350) FEA1,FEA2,FEA3
WRITE(6,350) FEA1,FEA2,FEA3
DO 100 K=1,NPTS
IF(ALWOB(K).EQ.WIDTH) GO TO 200
IF(ALWOB(K).GT.WIDTH) GO TO 300
100   CONTINUE
200   ELWIN=ALWIN(K)
AMP=HEIGHT(K)
GO TO 400
300   I2=K
I1=I2-1
P=(WIDTH-ALWOB(I1))/(ALWOB(I2)-ALWOB(I1))
ELWIN=ALWIN(I1)+P*(ALWIN(I2)-ALWIN(I1))
AMP=HEIGHT(I1)+P*(HEIGHT(I2)-HEIGHT(I1))
400   WRITE(6,450)
IF(INDEX) 10,20,30
10    FAC=AMP/SQRT(H1)
H2N=SQRT(H2)*FAC
H3N=SQRT(H3)*FAC
CALL SOB
OBLW1=WIDTH
EIN1=ELWIN
EIN2=CF/EIN1
AIN1=(3.*1.73205/(4.*3.1416))*T21**2
AMP1=AMP
OBLW2=OW2
EIN2=EIW2
EIN2=EIW2
C     T22=CF/EIN2
C     AIN2=(3.*1.73205/(4.*3.1416))*T22**2

```

```

AMP2=A2
OBLW3=OW3
EIN3=EIW3
C     T23=CF/EIN3
C     AIN3=(3.*1.73205/(4.*3.1416))*T23**2
AMP3=A3
FA=SQRT(FELW**2+0.25*FEA1**2+0.25*FEA2**2)
FB=SQRT((FEA3**2+FEA1**2)/(4.*(H3/H1)*(SQRT(H1/H3)-
1.)**2)+FELW**2
*)
FC=SQRT((0.25*(H1/H3)*(FEA3**2+FEA1**2)+(H1/H2)*(FEA1**2+FEA
2**2)+H1/SQRT(H3*H2)*FEA1**2)/(1.+SQRT(H1/H3)-
2.*SQRT(H1/H2))**2+
2FELW**2)
GO TO 500
20    FAC=AMP/SQRT(H2)
H2N=SQRT(H1)*FAC
H3N=SQRT(H3)*FAC
CALL SOB
OBLW1=OW2
EIN1=EIW2
AMP1=A2
OBLW2=WIDTH
EIN2=ELWIN
AMP2=AMP
OBLW3=OW3
EIN3=EIW3
AMP3=A3
FA=FELW
FB=SQRT(((H2/H3)*(FEA2**2+FEA3**2)+(H2/H1)*(FEA2**2+FEA1**2)
+
12.*H2/SQRT(H3*H1)*FEA2**2)/(4.*(SQRT(H2/H3)-
SQRT(H2/H1))**2)+FELW*
2**2)
FC=SQRT((0.25*(H2/H3)*(FEA2**2+FEA3**2)+0.25*(H2/H3)*(FEA2
1**2+FEA1**2)+0.5*H2/SQRT(H3*H1)*FEA2**2)/(SQRT(H2/H3)+
2SQRT(H2/H1)-2.)**2+FELW**2)
GO TO 500
30    FAC=AMP/SQRT(H3)
H2N=SQRT(H1)*FAC
H3N=SQRT(H2)*FAC
CALL SOB
OBLW1=OW2
EIN1=EIW2
EIN2=OW3
EIN2=EIW3
AMP2=A3
OBLW3=WIDTH
EIN3=ELWIN
AMP3=AMP
FA=SQRT(FELW**2+0.25*FEA3**2+0.25*FEA2**2)
FB=SQRT((FEA3**2+FEA1**2)/(4.*(H1/H3)*(1.-SQRT(H3/H1))**2)
1+FELW**2)
FC=SQRT((0.25*(H3/H1)*(FEA1**2+FEA3**2)+(H3/H2)*(FEA3**2+
1FEA2**2)+H3/SQRT(H1*H2)*FEA3**2)/(1.+SQRT(H3/H1)-
2.*SQRT
2(H3/H2))**2+FELW**2)
500WRITE(6,550)
OBLW1,EIN1,AMP1,OBLW2,EIN2,AMP2,OBLW3,EIN3,AMP3
CALL ABCT2(TEMP,INDEX,EIN1,EIN2,EIN3,FELW,FA,FB,FC)
GO TO 1
560   STOP
END
C-----
SUBROUTINE SOB
COMMON X(450),Y(450),Z(450),H2N,H3N,OBLW2,ELWIN2,AMP2,OBLW3,
1ELWIN3,AMP3,N
C     WRITE(6,100) N
C100  FORMAT(/,3X,'VALUE OF NPTS IS',I5)
DO 10 K=1,N
IF(Z(K).EQ.H2N) GO TO 20
IF(Z(K).LT.H2N) GO TO 30
10    CONTINUE
20    AMP2=Z(K)
ELWIN2=Y(K)
OBLW2=X(K)
30    I2=K
I1=I2-1
Q=(Z(I1)-H2N)/(Z(I1)-Z(I2))
OBLW2=X(I1)+Q*(X(I2)-X(I1))
ELWIN2=Y(I1)+Q*(Y(I2)-Y(I1))
AMP2=Z(I1)+Q*(Z(I2)-Z(I1))
C     WRITE(6,200) H3N
C200  FORMAT(/3X,'H3N IS',F15.6)
DO 40 M=1,N
IF(Z(M).EQ.H3N) GO TO 50
IF(Z(M).LT.H3N) GO TO 60

```

```

40 CONTINUE
50 OBLW3=X(M)
   ELWIN3=Y(M)
   AMP3=Z(M)
60 J2=M
   J1=J2-1
   P=(Z(J1)-H3N)/(Z(J1)-Z(J2))
   OBLW3=X(J1)+P*(X(J2)-X(J1))
   ELWIN3=Y(J1)+P*(Y(J2)-Y(J1))
   AMP3=Z(J1)+P*(Z(J2)-Z(J1))
   RETURN
   END
-----
SUBROUTINE ABCT2(TE,IN,DEL1,DEL2,DEL3,E,FA,FB,FC)
A=DEL2
EA=FA*A
B=0.5*(DEL3-DEL1)
EB=FB*B
C=0.5*(DEL3+DEL1-2.*DEL2)
EC=FC*C
FAC=2.*5.66818E-8/1.73205
T21=FAC/DEL1
T2INV1=1./T21
T22=FAC/DEL2
T2INV2=1./T22
T23=FAC/DEL3
T2INV3=1./T23
BOC=B/C
COB=C/B
AOB=A/B
BOA=B/A
AOC=A/C
COA=C/A
ET21=E*T21
ET22=E*T22
ET23=E*T23
ET2IN1=E*T2INV1
ET2IN2=E*T2INV2
ET2IN3=E*T2INV3
WRITE(6,150)A,EA,B,EB,C,EC,BOC,COB,AOB,BOA,AOC,COA,T21,ET21,
T22,
1ET22,T23,ET23,T2INV1,ET2IN1,T2INV2,ET2IN2,T2INV3,ET2IN3
150 FORMAT(/' A=',F12.8,2X,' +OR-',4X,F10.8,2X,' GAUSS'
1/' B=',F12.8,2X,' +OR-',4X,F10.8,2X,' GAUSS'
2/' C=',F12.8,2X,' +OR-',4X,F10.8,2X,' GAUSS'
3/' B/C=',E12.5,5X,' C/B=',F9.5// ' A/B=',F9.5,5X
4,' B/A=',F9.5,5X,' A/C=',E12.5,5X,' C/A=',F9.5//
T2(M=-1) =',E12.
55,' +OR-',E12.5,' SEC/RADIAN'// ' T2(M= 0) =',E12.5,'
+OR-',E12.
65,' SEC/RADIAN'// ' T2(M=+1) =',E12.5,' +OR-',E12.5,'
SEC/RADIAN'
7// ' T2 INVERSE(M=-1) =',E12.5,' +OR-',E12.5,'
RADIAN/SEC'//
8' T2 INVERSE(M= 0) =',E12.5,' +OR-',E12.5,'
RADIAN/SEC'//
9' T2 INVERSE(M=+1) =',E12.5,' +OR-',E12.5,'
RADIAN/SEC'//
WRITE(7,250) TE,IN,B,EB,C,EC,COB
250 FORMAT(2X,F5.1,2X,I4,2(1X,F12.8,1X,F10.8,1X),F9.5)
RETURN
END

```

BCT1.FOR

```

DIMENSION GFUN(5),AFUN(5),OUTPT(40,40)
REAL*4 HZ(4),GAME,W0,GAMEP,DO,D2,TAU0,TAU2,TAUR,I,DEL2,
1WA,C1,C2,C,B1,B2,B,A1,A2,A3,A4,A,NI,NF,NM,DEL1,
2N,GFUN,AFUN,GE,GX,GY,GZ,GN,AX,AY,AZ,AM,G0,G2,
3A0B,PI,TAURF,TAURM,TAURC,DELC,EXC,TEMP,COB,EXB,
4EM,EF,EI,EIM,EPM,EPP,EPI,EPIM,ALPHA,XC11,XC12,YC11,YC12,
5XC21,XC22,YC21,YC22,ALPHA1
COMPLEX ZC11,ZC12,ZFC11,ZFC12,ZC21,ZC22,ZFC21,ZFC22
INTEGER R,RR,IN,COUNT,NSBT,DELT,M,J1,J2,J3,J4,M1,IL,IK,J5,
*NV,IT,J6,IALPHA
CHARACTER ANS1,ANS2,ANS3,ANS4,ANS5,AXES,ANS6,ANS7,ANS8
CHARACTER FDATEIM*65,MODE*60,FNAME*2,EXTI*4,EXTO*4,
1
FINAME*10,FONAME*12,DATIM*60,DASH,SOLUTE*60,SOLVNT*60,
2 FREQ*6,REQ*5,F*1,CHAME*4
C
FONAME = 'PDTBCF03.TXT'
SOLUTE = 'PD-TEMPONE'
C
SOLUTE = 'BTHPO'
SOLVNT = 'TOLUENE'
OPEN ( UNIT= 3, FILE = FONAME, STATUS = 'NEW', FORM =
'FORMATTED',
* ACCESS = 'SEQUENTIAL')
C

```

```

WRITE(3,107) SOLUTE, SOLVNT
107 FORMAT(2X,'THE SOLUTE IS ---> ',A,',',2X,'THE SOLVENT
IS ---> ',
1,A)
C
PI = 3.141592654
EM = 1.
EF = 7.
EIM = .2
EPM = 1.
EPP = 6.
EPI = .1
EPIM = .1
NM = 1.
NI = 1.
NF = 6.
NP = 6.
NV = 6
DELCM = .25
IF(SOLUTE(1:1).EQ.'P') GOTO 10
C ----- BTHPO IN TOLUENE
GFUN(1) = 2.0023
GFUN(4) = GFUN(1)
GFUN(2) = 2.0097
GFUN(5) = GFUN(2)
GFUN(3) = 2.0060
AFUN(1) = 34.20
AFUN(4) = AFUN(1)
AFUN(2) = 7.0
AFUN(5) = AFUN(2)
AFUN(3) = 5.3
IF(SOLUTE(1:1).EQ.'B') GOTO 20
10 CONTINUE
C ----- PD-TEMPONE IN TOLUENE
GFUN(1) = 2.0022
GFUN(4) = GFUN(1)
GFUN(2) = 2.0096
GFUN(5) = GFUN(2)
GFUN(3) = 2.0063
AFUN(1) = 33.45
AFUN(4) = AFUN(1)
AFUN(2) = 4.1
AFUN(5) = AFUN(2)
AFUN(3) = 6.1
20 CONTINUE
HZ(1) = 1.12E9
HZ(2) = 3.99E9
HZ(3) = 9.54E9
HZ(4) = 34.2E9
GAME = 1.76409681E7
GE = 2.00232
I = 1.
TAURM = 1.E-12
TAURF = 2.5E-9
TAURC = 10.
IT=28
DO 101 JJ=1,4
C
ALPHA=.5
IF(JJ.GE.2) ALPHA = 1.
WRITE(3,500) HZ(JJ)
500 FORMAT(//1X,'MW F.(Hz) = ',E10.3)
C
R = 1
RR = R
IF (RR .EQ. 1) THEN
AXES = 'Y'
ELSE IF (RR .EQ. 2) THEN
AXES = 'Z'
ELSE IF (RR .EQ. 3) THEN
AXES = 'X'
END IF
WRITE(3,100) AXES
100 FORMAT(2X,'Z' = ',A1)
C
DO 11 IALPHA = 1,6
70
C
WRITE(3,110) ALPHA
110 FORMAT(1X,'ALPHA= ',F4.2)
TAUR = TAURM
N = NM
EP = EPM
E = EM
EI = EIM
GX = GFUN(R)
GY = GFUN(R+1)
GZ = GFUN(R+2)
AX = AFUN(R)
AY = AFUN(R+1)
AZ = AFUN(R+2)
W0 = 2*PI*HZ(JJ)
GN = (GX + GY + GZ)/3.
AN = (AX + AY + AZ)/3.
G0 = 1.5*.5 * (GZ - GN)
GZ = (GX - GY)/2.

```

```

GAMEP = GAME * GN/GE
DO = GAMEP / 2. / PI * .375**5 * (AN - AZ)
D2 = GAMEP/2. / PI * (AY - AX)/4.

C
J1 = 2
J5 = 1
DO 22 J = 1,NV
OUTPT(1,(J1)) = N
J2 = J5
J3 = J5 + 1
J4 = J5 + 2
C
J6 = J5 + 3
DO 33 M = 1,IT
M1 = M + 1
TAU0 = TAU0 * N**5
TAU2 = 3. * TAU0 / (1+ 2. * N)
WA = AN * GAMEP / 2.
XC11=1./ (1.+(WA*TAU0)*(WA*TAU0)*EP)
YC11=WA*TAU0*SQRT(EP)*XC11
ZC11=CMPLX(XC11,-YC11)
ZFC11=ZC11**ALPHA
XC12=1./ (1.+(W0*TAU0)*(W0*TAU0)*E)
YC12=W0*TAU0*SQRT(E)*XC12
ZC12=CMPLX(XC12,-YC12)
ZFC12=ZC12**ALPHA
C1 = 8./3.-REAL(ZFC11)-1./3.*REAL(ZFC12)
CC1=8./3.-1./ (1.+(WA*TAU0)*(WA*TAU0)*EP)-1./3./ (1.+(W0*TAU0)
1*(W0*TAU0)*E)
C
XC21=1./ (1.+(WA*TAU2)*(WA*TAU2)*EP)
YC21=WA*TAU2*SQRT(EP)*XC21
ZC21=CMPLX(XC21,-YC21)
ZFC21=ZC21**ALPHA
XC22=1./ (1.+(W0*TAU2)*(W0*TAU2)*E)
YC22=W0*TAU2*SQRT(E)*XC22
ZC22=CMPLX(XC22,-YC22)
ZFC22=ZC22**ALPHA
C2 = 8./3.-REAL(ZFC21)-1./3.*REAL(ZFC22)
C
C2 = 8./3.-1./ (1+(WA*TAU2)*(WA*TAU2)*EP)-1/3/ (1+(W0*TAU2)
1*(W0*TAU2)*E)
C
C = 2./3.**5/GAME*.8*PI*PI*(D0*D0*TAU0*C1+2*D2*D2*TAU2*C2)
B1 = 16./3. + 4.*REAL(ZFC12)
C
B1 = 16./3. + 4./ (1+(W0*TAU0)*(W0*TAU0)*E)
B2 = 16./3. + 4.*REAL(ZFC22)
C
B2 = 16./3. + 4./ (1+(W0*TAU2)*(W0*TAU2)*E)
B = 2./3.**5/GAME*.1*PI*W0*(G0*D0*TAU0*B1+2*G2*D2*TAU2*B2)
OUTPT((M1),1) = TAU0
OUTPT((M1),J3) = B
OUTPT((M1),J4) = C
IF(TAU0 .LT. 1E-10) THEN
TAU0 = TAU0 * TAURC
ELSE
TAU0 = TAU0 + 1.E-10
ELSE IF (TAU0 .GE. 1E-9 .AND. TAU0 .LT. 1E-8) THEN
TAU0 = TAU0 + 1.5E-9
ELSE IF (TAU0 .GE. 1E-8 .AND. TAU0 .LT. 1E-7) THEN
TAU0 = TAU0 + 1.5E-8
ENDIF
WRITE(3,200) TAU0, B, C
C200
FORMAT(1X,E12.6,2(2X,E12.6))
TAU0 = TAU0 * TAURC
C
33
CONTINUE
C
N = N + NI
TAUR = TAURM
J1 = J1 + 2
J5 = J5 + 2
22
CONTINUE
DO 44 IL = 1,IT
DO 55 IK = 1,21
WRITE(3,600) (OUTPT(IL,(IK)), IK = 1,2*NV+1)
FORMAT(30(E12.6))
CONTINUE
44
CONTINUE
DO 66 IL = 1,40
DO 77 IK = 1,40
OUTPT(IL,(IK)) = 0.0
CONTINUE
77
CONTINUE
66
CONTINUE
IF(JJ .EQ. 1) THEN
ALPHA = .05
ELSE IF(JJ.EQ.2.AND.IALPHA.EQ.1) THEN
ALPHA = 1.
ALPHA = 1.
ELSE IF(JJ.GT.2) THEN
ALPHA = 1.
ENDIF
ALPHA=ALPHA+ALPHA1
11
CONTINUE
101
CONTINUE
C
WRITE (*,120) FONAME
120
FORMAT (//,2X,'THE RESULTS ARE STORED IN ----> ',A)
STOP

```

END

ABCIFOR

```

DIMENSION
FUN(5),AFUN(5),HZ(100),TEMP(100),AOB(100),IN(100),
1EXB(100),KXC(100)
REAL*4 HZ, GAME, W0, GAMEP, DO, D2, TAU0, TAU2,
TAUR,I,DEL2,
1WA, C1, C2, C, B1, B2, B, A1, A2, A3, A4, A, NI, NF,
NM, DEL1,
2N, GFUN, AFUN, GE, GX, GY, GZ, GN, AX, AY, AZ, AN, G0,
GZ,MM,
3AOB, PI, TAURF, TAURM, TAURI, DELC, KXC, TEMP, COB,
EXB, DELB,
4TAURIM,
DELCM,EM,EF,EI,EPM,EPF,EPI,ALPHA,XC11,XC12,YC11,YC12,
5XC21,XC22,YC21,YC22
COMPLEX ZC11,ZC12,ZFC11,ZFC12,ZC21,ZC22,ZFC21,ZFC22
INTEGER R,RR, IN, COUNT, NSET, DELT,NPT
CHARACTER ANS1, ANS2, ANS3, ANS4, ANS5, AXES, ANS6,
ANS7,ANS8
CHARACTER PDATIM*65, NODF*60, FNAME*2, EXTI*4, EXTO*4,
1 FNAME*11, FONAME*12, DATIM*60, DASH, SOLUTE*60,
SOLVNT*60,
2 FREQ*6, REQ*5, F*1, CNAME*4
C
FONAME = 'PDTABCF2.TXT'
FINAME = 'TUPLPDT.DAT'
SOLUTE = 'PD-TEMPONE'
C
SOLUTE = 'BBTMO'
SOLVNT = 'TOLUENE'
OPEN (UNIT=5,FILE=FINAME,STATUS='OLD',FORM='FORMATTED',
* ACCESS = 'SEQUENTIAL')
OPEN (UNIT=3,FILE=FONAME,STATUS='NEW',FORM = 'FORMATTED',
* ACCESS = 'SEQUENTIAL')
C
WRITE (3,107) SOLUTE, SOLVNT
107
FORMAT (2X,'THE SOLUTE IS ----> ',A,/,2X,'THE SOLVENT
IS ----> ',
1,A//)
C
WRITE(3,2200)
2200
FORMAT(3X,'MW FREQ(Hz)',2X,'TEMP.(K)',1X,'IN.',1X,'***
A ***',
13X,'*** B ***',3X,'*** C ***',2X,'
',1X,'Taur(sec.)',
22X,' N ',2X,'Z ',1X,' E ')
C
PI = 3.141592654
EPM = 1.
EPF = 6.
EPI = .5
DELCM = .5
IF(SOLUTE(1:1).EQ.'P') GOTO 10
C
----- BBTMO IN TOLUENE
GFUN(1) = 2.0023
GFUN(4) = GFUN(1)
GFUN(2) = 2.0097
GFUN(5) = GFUN(2)
GFUN(3) = 2.0060
AFUN(1) = 34.20
AFUN(4) = AFUN(1)
AFUN(2) = 7.0
AFUN(5) = AFUN(2)
AFUN(3) = 5.3
IF(SOLUTE(1:1).EQ.'B') GOTO 20
10
CONTINUE
C
----- PD-TEMPONE IN TOLUENE
GFUN(1) = 2.0022
GFUN(4) = GFUN(1)
GFUN(2) = 2.0096
GFUN(5) = GFUN(2)
GFUN(3) = 2.0063
AFUN(1) = 33.45
AFUN(4) = AFUN(1)
AFUN(2) = 4.1
AFUN(5) = AFUN(2)
AFUN(3) = 6.1
20
CONTINUE
GAME = 1.76409681E7
GE = 2.00232
I = 1.
READ(5,400) NSET
400
FORMAT(I3)
DO 444 JJ=1,NSET
TAURIM = 1.E-15
READ(5,410) R,NM,ALPHA,EM,EF,EI,TAURM,TAURF
410
FORMAT(I3,5(1X,F5.2),2(1X,1PE8.2E3))
READ(5,4000) NPT
4000
FORMAT(I3)

```

```

READ(5,4100)
(HZ(J),TEMP(J),AOB(J),IN(J),EXB(J),EXC(J),J=1,NPT)
4100
FORMAT(E12.7E1,2X,F5.1,1X,F6.4,3X,I2,3X,F10.8,2X,F10.8)
RR = R
C
DO 22 J = 1, NPT
TAUR = TAURM
TAURI = TAURIM
N = NM
EP = EPM
E = EM
IF (EXC(J) .LT. 0.) GOTO 22
DEL1 = EXC(J)*1.E-3
DEL2 = EXB(J)*1.E-1
GX = GFUN(R)
GY = GFUN(R+1)
GZ = GFUN(R+2)
AX = AFUN(R)
AY = AFUN(R+1)
AZ = AFUN(R+2)
W0 = 2*PI*HZ(J)
GW = (GX + GY + GZ)/3.
AN = (AX + AY + AZ)/3.
G0 = 1.5*.5 * (GZ - GW)
G2 = (GX - GY)/2.
GAMEP = GAME * GW/GE
DO = GAMEP/2. / PI * .375*.5 * (AN - AZ)
D2 = GAMEP/2. / PI * (AY - AX)/4.
77 TAU0 = TAUR * N*.5
TAU2 = 3. * TAU0 / (1+ 2. * N)
WA = AN * GAMEP / 2.
44 XC11=1./(1.+(WA*TAU0)*(WA*TAU0)*EP)
YC11=WA*TAU0*SQRT(EP)*XC11
ZC11=CMPLX(XC11,-YC11)
ZFC11=ZC11**ALPHA
XC12=1./(1.+(W0*TAU0)*(W0*TAU0)*E)
YC12=W0*TAU0*SQRT(E)*XC12
ZC12=CMPLX(XC12,-YC12)
ZFC12=ZC12**ALPHA
C1 = 8./3.-REAL(ZFC11)-1./3.*REAL(ZFC12)
CC1=8./3.-1./(1.+(WA*TAU0)*(WA*TAU0)*EP)-1./3./(1.+(W0*TAU0)
C 1*(W0*TAU0)*E)
XC21=1./(1.+(WA*TAU2)*(WA*TAU2)*EP)
YC21=WA*TAU2*SQRT(EP)*XC21
ZC21=CMPLX(XC21,-YC21)
ZFC21=ZC21**ALPHA
XC22=1./(1.+(W0*TAU2)*(W0*TAU2)*E)
YC22=W0*TAU2*SQRT(E)*XC22
ZC22=CMPLX(XC22,-YC22)
ZFC22=ZC22**ALPHA
C2 = 8./3.-REAL(ZFC21)-1./3.*REAL(ZFC22)
C2 = 8./3.-1./(1.+(WA*TAU2)*(WA*TAU2)*EP)-1/3/(1+(W0*TAU2)
C 1*(W0*TAU2)*E)
C=2./3**5/GAME*.8*PI*PI*(D0*D0*TAU0*C1+2*D2*D2*TAU2*C2)
B1 = 16./3. + 4.*REAL(ZFC12)
C B1 = 16./3. + 4./(1+(W0*TAU0)*(W0*TAU0)*E)
B2 = 16./3. + 4.*REAL(ZFC22)
C B2 = 16./3. + 4./(1+(W0*TAU2)*(W0*TAU2)*E)
B=2./3**5/GAME*.1*PI*W0*(G0*D0*TAU0*B1+2*G2*D2*TAU2*B2
)
C
DELC = ABS (EXC(J) - C)
DELB = ABS (EXB(J) - B)
IF ( TAUR .LT. TAURF) THEN
C IF (DELC .GE. DELCM) GOTO 22
IF (DELC .GT. DEL1) THEN
DELT = INT(TAUR / TAURIM)
IF (DELT .EQ. 1000) THEN
C TAURI = TAURIM * 10
IF (DELT .EQ. 10000) THEN
C TAURI = TAURIM * 10
ELSE IF (DELT .EQ. 100000) THEN
C TAURI = TAURIM * 100
ELSE IF (DELT .EQ. 1000000) THEN
C TAURI = TAURIM * 1000
ELSE IF (DELT .EQ. 10000000) THEN
C TAURI = TAURIM * 10000
ELSE IF (DELT .EQ. 100000000) THEN
C TAURI = TAURIM * 100000
END IF
TAUR = TAUR + TAURI
WRITE (*,3100) J,TAUR,DELC,DELB,HZ(J)
3100
FORMAT(1X,'NO.',I2,1X,'Tau(R)=' ,E11.6,'DELC=',E11.6,
1'DELB=',E11.6,'FRQ=',E13.8)
GO TO 77
ELSE IF (DELB .LE. DEL2) THEN
ELSE
A1=REAL(ZFC11)+7./3.*REAL(ZFC12)
C A1=1./(1+(WA*TAU0)*(WA*TAU0)*EP)
C * +7./3./(1+(W0*TAU0)*(W0*TAU0)*E)
A2=REAL(ZFC21)+7./3.*REAL(ZFC22)

```

```

C A2=1./(1+(WA*TAU2)*(WA*TAU2)*EP)
C * +7./3./(1+(W0*TAU2)*(W0*TAU2)*E)
A3=8./3.+2.*REAL(ZFC12)
C A3=8./3.+2./(1+(W0*TAU0)*(W0*TAU0)*E)
A4=8./3.+2.*REAL(ZFC22)
C A4=8./3.+2./(1+(W0*TAU2)*(W0*TAU2)*E)
A=AOB(J)-
(I*(I+1)*.8*PI*PI*(D0*D0*TAU0*A1+2.*D2*D2*TAU2*A2
1)+W0*W0/80.*(G0*G0*TAU0*A3+2.*G2*G2*TAU2*A4))*2./3.**.5/GAM
EP
GO TO 88
C ELSE IF (E .LT. EP) THEN
C E = E + EI
C WRITE(*,*) 'E = ',E,' DELB = ',DELB
C GO TO 44
C ELSE IF (N .LT. NF) THEN
C N = N + NI
C TAUR = TAURM
C TAURI = TAURIM
C E = EM
C GO TO 77
END IF
ENDIF
C
88 IF (RR .EQ. 1) THEN
AXES = 'Y'
ELSE IF (RR .EQ. 2) THEN
AXES = 'Z'
ELSE IF (RR .EQ. 3) THEN
AXES = 'X'
END IF
C
COB = C/B
WRITE(3,3000)
HZ(J),TEMP(J),IN(J),A,B,C,COB,TAUR,N,AXES,E
3000
FORMAT(E14.8,3X,F5.1,3X,I2,F11.8,1X,F11.8,1X,F11.8,2X,F7.5,2
X,
1E11.6,2X,F4.1,1X,A1,3X,F4.1)
IF (TAUR .GE. 1.E-9) THEN
TAURM = TAUR
TAURIM = TAURI
ENDIF
22 CONTINUE
444 CONTINUE
CLOSE(5, STATUS = 'KEEP')
CLOSE(3, STATUS = 'KEEP')
WRITE (*,70) FONAME
70 FORMAT (//,2X,'THE RESULTS ARE STORED IN ---> ',A)
STOP
END

```

Appendix B

DIFFA.FOR

```

PROGRAM DIFFA
C
DIMENSION FILEN(500)
REAL*4
BFLD(2100),INT(2100),BMAX(3),INTSTY(500),INTC(500),
1IMAX(3),IMIN(3),OLW(3),PTPI(3),PTPIC(3),
CFLD(3),FOLW(3),AMAXIN,
2AMAXI,AMAXIC,AINT,TEMP,BMIN(3),PTPIC(3),PTPIN(3),INTN(500)
C
INTEGER*2 N, NSET, NI, NF,DAY(500),
HR(500),MIN(500),DPN(2100),
1 NMAX(3),NMIN(3),THIRD,L,SEC(500)
INTEGER*4 TIMEI(500),TIME0
C
CHARACTER FDATEIM*65,MODF*60,FNAME*2,EXTI*4,EXTO*4,
1 FINAME*11, FONAME*11,DATIM*60,DASH,SOLUTE*60,
SOLVNT*60,
2 FREQ*6,REQ*5,F*1,CNAME*3,FILEN*9
C
SOLUTE = 'BETMPO'
SOLVNT = 'TOLUENE'
FINAME = 'DIFFBET.DAT'
FONAME = 'DIFFBET5.TXT'
C
N = 1024
C
OPEN(UNIT=4,FILE=FONAME,STATUS='NEW',FORM='FORMATTED',
* ACCESS = 'SEQUENTIAL')
C
OPEN(UNIT=5,FILE=FINAME,STATUS='OLD',FORM='FORMATTED',
* ACCESS = 'SEQUENTIAL')

```



```

READ(5,1000) NSET
1000 FORMAT(I4)
READ(5,2000)
(DAY(J),HR(J),MIN(J),SEC(J),FILEN(J),J=1,NSET)
2000 FORMAT(4(4(1X,I2),1X,A9))
CLOSE(5, STATUS = 'KEEP')
C
WRITE(4,210) NSET
210 FORMAT(2X,'NO. OF POINTS IS ',I4)
WRITE(4,118) SOLUTE, SOLVNT
118 FORMAT(2X,'THE SOLUTE IS --> ',A,/,2X,'THE SOLVENT
IS --> ',
1,A,/)
C
CWRITE(4,2000)
(DAY(J),HR(J),MIN(J),SEC(J),FILEN(J),J=1,NSET)
C
TIME0 = DAY(1)*86400+HR(1)*3600+MIN(1)*60+SEC(1)
DO 1001 J = 1, NSET
TIMEI(J) = DAY(J)*86400+HR(J)*3600+MIN(J)*60+SEC(J)-
TIME0
1001 CONTINUE
C
AMAXI=0.000
AMAXIC=0.000
AMAXIN=0.000
DO 122 II=1,3
FOLW(II)=0.
122 CONTINUE
DO 60 L = 1, NSET
NI = 1
DO 10 I = 1,3
IMAX(I) = 0.000
IMIN(I) = 0.000
10 CONTINUE
OPEN(UNIT=3,FILE=FILEN(L),STATUS='OLD',FORM='FORMATTED',
* ACCESS = 'SEQUENTIAL')
C
READ(3,110) FDATEI
110 FORMAT(A)
READ(3,120) NODE
120 FORMAT(/A)
READ(3,150) DASH
150 FORMAT(/A)
READ(3,155) (DPN(I),BFLD(I), INT(I), I=1,N)
155 FORMAT(4X,I4,3X,F10.4,4X,E12.4E3)
CLOSE(3, STATUS = 'KEEP')
C
THIRD = N/3
NF = THIRD
C
DO 20 K = 1,3
DO 30 I=NI,NF
IF (INT(I) .GE. IMAX(K)) THEN
IMAX(K) = INT(I)
BMAX(K) = BFLD(I)
NMAX(K) = DPN(I)
ENDIF
IF (INT(I) .LE. IMIN(K)) THEN
IMIN(K) = INT(I)
BMIN(K) = BFLD(I)
NMIN(K) = DPN(I)
ENDIF
OLW(K) = BMIN(K) - BMAX(K)
PTPI(K) = IMAX(K) - IMIN(K)
CFLD(K) = BMAX(K) + OLW(K)/2.
30 CONTINUE
NI = NI + THIRD
NF = NF + THIRD
20 CONTINUE
IF (L.EQ.1) THEN
FOLW(1)=OLW(1)
FOLW(2)=OLW(2)
FOLW(3)=OLW(3)
ENDIF
C
DO 40 JJ=1,3
PTPIC(JJ)=PTPI(JJ)*(OLW(JJ)/FOLW(JJ))**2
PTPICC(JJ)=PTPI(JJ)*(OLW(JJ)/OLW(1))**2
PTPIN(JJ)=PTPICC(JJ)*(OLW(1)/FOLW(1))**2
40 CONTINUE
C
WRITE(4,11) PTPI(1),OLW(1),TIMEI(L), (PTPI(I),I=1,3)
C
* PTPI(2),PTPI(3))
C11 FORMAT(F10.1,1X,E6.4,1X,I10,1X,3(F10.1,1X))
INTSTY(L)=PTPI(1)+PTPI(2)+PTPI(3)
C
INTC(L)=INTSTY(L)*(OLW(1)/FOLW)**2
INTC(L) = PTPIC(1) + PTPIC(2) + PTPIC(3)
INTN(L) = PTPIN(1) + PTPIN(2) + PTPIN(3)
IF (INTSTY(L).GT.AMAXI) AMAXI=INTSTY(L)
IF (INTC(L).GT.AMAXIC) AMAXIC=INTC(L)
IF (INTN(L).GT.AMAXIN) AMAXIN=INTN(L)
60 CONTINUE
C

```

```

WRITE(4,2100) NSET,AMAXI,AMAXIC,AMAXIN
2100 FORMAT(2X,'# OF DATA= ',I10,/,2X,'MAX. PTP INT.
=',F10.1,/,
12X,'MAX. CORR. PTP INT. =',F10.1,/,2X,'MAX. NORM. PTP
INT. =',
2F10.1/)
WRITE(4,200)
200FORMAT(2X,'TIME(sec.)',3X,'OVERALL
INTENSITY',3X,'CORRECTED INTEN
*SITY',3X,'TOTAL NORM. INT. '/')
WRITE(4,220)
(TIMEI(KK),INTSTY(KK),INTC(KK),INTN(KK),KK=1,NSET)
220 FORMAT(2X,I10,7X,E14.8,10X,E14.8,10X,E14.8)
CLOSE(4, STATUS = 'KEEP')
WRITE(*,28) FOWAME
28 FORMAT(/' NAME OF OUTPUT FILE --> ',A)
STOP
END

```

FITDIF.FOR

```

COMMON LT,PI,R,D,ACCUR,XT,RINT
REAL R,RM,RF,RI,D,DM,DF,DI,ORV,ODV,MSTD,PI,ACCUR,LS,LT,MAXI,
1 X,Y,CY,DUMMY,XT,RINT,SMDIF,DIFSQ,VAR,STNDEV
INTEGER NP,IX,K,I,L,II
CHARACTER SOLUT*30,SOLNT*30,FINAME*11,FONAME*10,DASH,
* FTNAME*10
DIMENSION X(500),IX(500),Y(500),DUMMY(500),CY(500)
FINAME='DIFBBS.TXT'
FTNAME='BBS004.TXT'
OPEN (UNIT=5,FILE=FINAME,STATUS='OLD',FORM='FORMATTED',
1 ACCESS='SEQUENTIAL')
OPEN (UNIT=7,FILE=FTNAME,STATUS='NEW')
C
RM=1
RF=1.
RI=1.E-1
DM=1.E-10
DF=1.E-4
MSTD=10.
ORV=1.
ODV=1.
PI=3.1415926
ACCUR=1.E-5
LS=2.E0
LT=3.5E0
MAXI=0.50
C
READ(5,200) NP
200 FORMAT(19X,I4)
READ(5,16) SOLUT
READ(5,16) SOLNT
WRITE(7,16) SOLUT
WRITE(7,19) SOLNT
16 FORMAT(A)
19 FORMAT(A)
READ(5,17) DASH
17 FORMAT(/A)
C
READ(5,210) (IX(I),Y(I),I=1,NP)
C 210 FORMAT(2X,I10,31X,E14.8)
210 FORMAT(2X,I10,7X,E14.8)
CLOSE(5, STATUS = 'KEEP')
C
DO 221 L=1,NP
X(L)=FLOAT(IX(L))
221 CONTINUE
DO 222 L=1,NP
IF(Y(L).GT.MAXI) MAXI=Y(L)
222 CONTINUE
DO 333 L=1,NP
Y(L)=Y(L)/MAXI
333 CONTINUE
C
NM=1
NF=NP
C-----OPTIMIZATION LOOP-----
D=DM
R=RM
DI=DM
44 DO 18 I=1,NP
DUMMY(I)=0.E0
CY(I)=0.E0
18 CONTINUE
DO 13 I=NM,NF
XT=X(I)
CALL DIFSIM(R,LT,PI,ACCUR,D,XT,RINT)
DUMMY(I)=RINT
13 CONTINUE
C

```

```

SMDIF=0.
DO 60 K=NM,NF
DIPSQ=(Y(K)-DUMMY(K))**2
SMDIF=SMDIF+DIPSQ
60 CONTINUE
VAR=(SMDIF/(NF-NM-1))
STNDEV=SQRT(VAR)
WRITE(*,90) STNDEV,R,D
90 FORMAT(1X,'THE STDV = ',1PE12.5,2X,' R = ',1PE12.5,
2X,' DIFF. = ',1PE12.5)
IF(STNDEV.LT.MSTD) THEN
MSTD=STNDEV
ORV=R
ODV=D
ENDIF
IF(D.LT.DF) THEN
IF(D.GE.DM*1.E1.AND.D.LT.DM*1.E2) THEN
DI=DM*1.E1
IF(D.GE.DM*1.E1.AND.D.LT.DM*1.E3) THEN
DI=DM*1.E1
ELSE IF(D.GE.DM*1.E3.AND.D.LT.DM*1.E4) THEN
DI=DM*1.E2
ELSE IF(D.GE.DM*1.E4.AND.D.LT.DM*1.E5) THEN
DI=DM*1.E3
ELSE IF(D.GE.DM*1.E5.AND.D.LT.DM*1.E6) THEN
DI=DM*1.E4
ENDIF
D=D+DI
GOTO 44
C
ELSE IF (R.LT.RF) THEN
IF (R.LT.RF) THEN
R=R+RI
D=DM
DI=DM
GOTO 44
ENDIF
WRITE(*,217) ODV,ORV,MSTD
WRITE(7,217) ODV,ORV,MSTD
217 FORMAT(/2X,'DIFF.COEFFICIENT = ',1PE15.6,1X,'cm^2/sec',/
2X,'R-VALUE = ',1PE15.6,/2X,'MIN. STDV. =
',1PE15.6//)
DO 15 II=NM,NF
XT=X(II)
CALL DIFSIM(ORV,LT,PI,ACCUR,ODV,XT,RINT)
CY(II)=RINT
15 CONTINUE
WRITE(7,216)
216 FORMAT(4X,'TIME*1E5 (SEC)',4X,'** EXPT.INT. **',
4X,'** CALC.INT. **')
WRITE(7,215) (I,X(I)*1E-5,Y(I),CY(I),I=1,NP)
215 FORMAT(13,1X,1PE15.6,4X,1PE15.6,4X,1PE15.6)
CLOSE(7,STATUS='KEEP')
WRITE(*,28) FNAME
28 FORMAT(/' NAME OF OUTPUT FILE ----> ',A)
STOP
END
C
SUBROUTINE DIFSIM(R,LT,PI,ACCUR,D,XT,RINT)
REAL A,SUM,EEE,BBB,FFF,CCC,DDD,R,LT,PI,ACCUR,D,XT,RINT
C
A=8./(PI*PI*R)
N=0
SUM=0.
DO 22 J=1,1000
EEE=(((2*N)+1)**2)*(PI**2)*D*D*XT/((4.*LT**2)
BBB=(EXP(-EEE))/((2*N)+1)**2)
IF (BBB.LE.ACCUR) GO TO 33
FFF=((2*N)+1)*PI*R/2.
CCC=SIN(FFF)
DDD=(-1)**N*BBB*CCC
SUM=SUM+DDD
N=N+1
22 CONTINUE
33 CONTINUE
RINT=A*SUM
11 CONTINUE
RETURN
END

```

Appendix C

HGSUMJH.FOR

```

DIMENSION DEG(25),BRES(50),BFLD(1001),DERAB(1001),EMP(9),
1XT2IN(50),A(25),QNO(25),MOD(25),X(11),Y(11),STA(25)
CHARACTER FNAME*3,EXTI*4,EXTO*4,FNAME*7,FONAME*7,ANS*1
DOUBLE PRECISION MDERAB

```

```

PI = 3.141592654
EXTI = '.DAT'
EXTO = '.TXT'
WRITE(*,800)
800 FORMAT(/,12X,'WOULD YOU LIKE TO PLOT THE RESULTS
(Y/N)? [N] -->
*,9)
READ(*,910) ANS
WRITE(*,900)
900 FORMAT(/,12X,'*** THE NAME OF THE FILE MUST BE OF THE
FORM ????.da
1t ****',/,
2 2X, 'INPUT DATA FILE NAME WITHOUT THE EXTENSION .dat-
-> ',9)
READ(*,910) FNAME
910 FORMAT(A)
FNAME(1:3) = FNAME
FNAME(4:3+4) = EXTI
FONAME(1:3) = FNAME
FONAME(4:3+4) = EXTO
OPEN(UNIT = 3,FILE=FNAME, STATUS = 'OLD', FORM =
'FORMATTED',
* ACCESS = 'SEQUENTIAL')
OPEN(UNIT = 4,FILE=FONAME,STATUS='NEW', FORM =
'FORMATTED',
* ACCESS = 'SEQUENTIAL')
C
READ(3,1) N
1 FORMAT(I2)
C
READ(3,4) (DEG(I),QNO(I),I=1,N)
4 FORMAT(8F10.7)
C
ETA = 1.0
SDEG=0.DO
DO 223 I=1,N
223 SDEG=SDEG+DEG(I)
READ(3,257) NB,BI,BF
257 FORMAT(I4,6X,2D10.7)
READ(3,1) NSETS
DO 2 J=1,NSETS
READ(3,4) A(J), ETA(J)
WRITE (4,1050) A(J), ETA(J)
1050 FORMAT(35H NEW HYDROGEN HYPERFINE COUPLING =
,F10.7,2X,'GAUSS',/,
11X,'ETA = ',F10.7)
C23456789012345678901234567890123456789012345678901234567890
1234567890
DO 6 I=1,N
6 BRES(I)=QNO(I)*A(J)
READ(3,1020) NLW
1020 FORMAT(I4)
READ(3,1030) (XT2IN(I), I=1,NLW)
1030 FORMAT(8F10.7)
DO 2 K=1,NLW
T2IN=XT2IN(K)
WRITE(4,255) T2IN,BI,BF,NB
255 FORMAT(48R FIRST DERIVATIVE LINWIDTH(NO-EXCHANGE) P-P
=
1E12.7,6H GAUSS , /
249H INITIAL FIELD SWEEP VALUE RELATIVE TO CENTER =
3E12.5,6H GAUSS , /
447H FINAL FIELD SWEEP VALUE RELATIVE TO CENTER =
5E12.5,6H GAUSS , /
642H NUMBER OF POINTS FOR "HALF-SPECTRUM" = I4)
T2INL=T2IN*(SQRT(3.)/2.)
T2ING=T2IN/2.
DEL=(BF-BI)/FLOAT(NB-1)
RES=BI
C23456789012345678901234567890123456789012345678901234567890
123456789012
DO 261 IB=1,NB
261 GSUM=0.DO
GSUM1=0.DO
GSUM2=0.DO
DO 262 I=1,N
262 GSUM1=ETA(J)*2./PI*(BRES(I)-RES)*T2INL/(((BRES(I)-RES)*
1(BRES(I)-RES)+T2INL*T2INL)*((BRES(I)-RES)*(BRES(I)-RES)+
2T2INL*T2INL))
GSUM2=(1.-ETA(J))/SQRT(2.*PI)*(BRES(I)-
RES)/(T2ING*T2ING*T2ING)*
1EXP(-(BRES(I)-RES)*(BRES(I)-RES)/(2.*T2ING*T2ING))
GSUM=GSUM-DEG(I)/SDEG*(GSUM1+GSUM2)
DERAB(IB) = GSUM
BFLD(IB) = RES
261 RES=RES+DEL
C
GOTO 30
C
IF (ANS.EQ.'Y'.OR.ANS.EQ.'Y') THEN
MDERAB=0.DO
DO 10 IBB=1,NB
IF (DERAB(IBB).LT.MDERAB) MDERAB=DERAB(IBB)
10 CONTINUE

```

```

WRITE(4,100) MDERAB
100 FORMAT(2X,'MINIMUM INTENSITY = ',D14.8)
DO 20 JB=1,NB
DERAB(JB)=DERAB(JB)/MDERAB
20 CONTINUE
WRITE(4,3010)
3010 FORMAT(/3X,'FIELD(GAUSS)',4X,'INTENSITY',/)
WRITE(4,3020)(BFLD(IB),DERAB(IB), IB=1,NB)
3020 FORMAT(1X,F12.8,2X,D14.8)
ENDIF
C
30 IMIN=1
YMIN=DERAB(1)
DO 4000 IB=2,NB
IF(DERAB(IB).LT.YMIN) IMIN=IB
IF(DERAB(IB).LT.YMIN) YMIN=DERAB(IB)
4000 CONTINUE
FPOS=BFLD(IMIN)
WRITE(4,400) FPOS,IMIN
400 FORMAT(7H FPOS= ,E13.6,10X,7H IMIN= ,I4)
WIDTH=2.*(ABS(FPOS))
WRITE(4,300) WIDTH
300 FORMAT(29H THE OBSERVED LINewidth IS = ,E13.6,6H GAUSS
)
C23456789012345678901234567890123456789012345678901234567890
1234567890
DEL=0.5*FPOS
RES=BF
WRITE(4,499)
499 FORMAT(55H MULTIPLES OF 1/4 DEL PP FROM CENTER
REL AMPLITUDE)
DO 361 M=1,11
GSUM=0.D0
GSUM1=0.D0
GSUM2=0.D0
DO 362 I=1,N
GSUM1=ETA(J)*2./PI*(BRES(I)-RES)*T2INL/(((BRES(I)-RES)*
1(BRES(I)-RES)+T2INL*T2INL)*((BRES(I)-RES)*(BRES(I)-RES)+
2T2INL*T2INL))
GSUM2=(1.-ETA(J))/SQRT(2.*PI)*(BRES(I)-
RES)/(T2ING*T2ING*T2ING)*
1EXP(-(BRES(I)-RES)*(BRES(I)-RES)/(2.*T2ING*T2ING))
362 GSUM=GSUM-DBG(I)/SDEG*(GSUM1+GSUM2)
Y(M)=GSUM/YMIN
X(M)=RES/(0.5*FPOS)
WRITE(4,500) ABS(X(M)),ABS(Y(M))
500 FORMAT(13X,F12.8,16X,F12.8)
361 RES=RES-DEL
C WRITE(4,1060)
C1060 FORMAT(///)
2 CONTINUE
CLOSE(3,STATUS='KEEP')
CLOSE(4,STATUS='KEEP')
STOP
END

```

GSUMHP.FOR

```

C
IMPLICIT REAL*8(A-H,O-Z)
DIMENSION XT2IN(449),A(25),QNO(25),C(2),B(2),W(449),T2(449),
*H(449)
COMMON
DEG(25),BRES(25),BFLD(601),DERAB(601),SDEG,FPOS,WIDTH,
*HEIGHT,N,NB,DNB,T2INL,T2INL2,T2ING2,T2ING3,DEL,ETA
C
CHARACTER FNAME*8, EXTI*4, EXTO*4, FINAME*12,
FONAME*12
C
EXTI = '.DAT'
EXTO = '.TXT'
WRITE(*,900)
900 FORMAT(/,6X,'*** THE NAME OF THE FILE MUST BE OF THE
FORM "T22???'
1??'.dat" ***/,/,
2 2X, 'INPUT DATA FILE NAME WITHOUT THE EXTENSION .dat-
-> ',S)
READ(*,910) FNAME
910 FORMAT(A)
FINAME(1:8) = FNAME
FINAME(9:8+4) = EXTI
FONAME(1:8) = FNAME
FONAME(9:8+4) = EXTO
OPEN(UNIT = 3,FILE=FINAME, STATUS = 'OLD', FORM =
'FORMATTED',
* ACCESS = 'SEQUENTIAL')
OPEN(UNIT=4,FILE=FONAME,STATUS='NEW',FORM = 'FORMATTED',
* ACCESS = 'SEQUENTIAL')
C

```

```

1 FORMAT(I2)
8 FORMAT(I4)
3 FORMAT(I3)
4 FORMAT(8D9.5)
89FORMAT(3X,'HYDROGEN HYPERFINE SPLITTING
IS',D12.5,2X,'GAUSS',/,
*3X,'ETA = ',D12.5,/)
98 FORMAT(3X,'NO OF POINTS IS',I4/)
500 FORMAT(3X,'OBSERVED LINewidth INTRINSIC
LINewidth
* PP HEIGHT '/,8X,' (GAUSS)',22X,' (GAUSS)')
300 FORMAT(4X,D16.8,12X,D16.8,8X,D16.8)
NPTS=449
READ(3,*) N,AD,ETA
WRITE(4,98) NPTS
WRITE(4,89) AD,ETA
WRITE(4,500)
READ(3,*) (DBG(I),QNO(I),I=1,N)
SDEG=0.D0
DO 223 I=1,N
SDEG=SDEG+DBG(I)
223 READ(3,1) NSETS
DO 2 J=1,NSETS
DO 6 I=1,N
6 BRES(I)=QNO(I)*AD
READ(3,*) NB,DNB,BI,BF
READ(3,3) NLW
READ(3,*) (XT2IN(I),I=1,NLW)
DO 22 K=1,NLW
T2IN=XT2IN(K)
T2INT=T2IN
T2INL=T2IN*(DSQRT(3.D0)/2.D0)
T2INL2=T2INL*T2INL
T2ING=T2IN/2.D0
T2ING2=T2ING*T2ING
T2ING3=T2ING*T2ING*T2ING
CALL MAX(BI,BF)
BIN=FPOS-DEL
BFN=FPOS+DEL
CALL MAX(BIN,BFN)
BI2=FPOS-DEL
BF2=FPOS+DEL
CALL MAX(BI2,BF2)
W(K)=WIDTH
T2(K)=T2INT
22 H(K)=HEIGHT
WRITE(4,300) (W(I),T2(I),H(I),I=1,NLW)
2 CONTINUE
CLOSE(3,STATUS='KEEP')
CLOSE(4,STATUS='KEEP')
STOP
END
SUBROUTINE MAX(BI,BF)
IMPLICIT REAL*8(A-H,O-Z)
COMMON
DEG(25),BR(25),X(601),Y(601),SDEG,FP,W,H,N,NB,DNB,T2L,
*T2LSQ,T2GSQ,T2GCB,DEL,E
PI = 3.141592654
DEL=(BF-BI)/DNB
RES=BI
DO 200 IB=1,NB
GSUM=0.D0
GSUM1=0.D0
GSUM2=0.D0
DO 100 I=1,N
B=BR(I)-RES
BSQ=B*B
GSUM1=B*2.D0/PI*B*T2L/((BSQ+T2LSQ)*(BSQ+T2LSQ))
GSUM2=(1.D0-B)/DSQRT(2.D0*PI)*B/T2GCB*EXP(-BSQ/(2.D0*T2GSQ))
100 GSUM=GSUM-DBG(I)/SDEG*(GSUM1+GSUM2)
Y(IB)=GSUM
X(IB)=RES
200 RES=RES+DEL
IMIN=1
YMIN=Y(1)
DO 300 IB=2,NB
IF(Y(IB).LT.YMIN) IMIN=IB
IF(Y(IB).LT.YMIN) YMIN=Y(IB)
300 CONTINUE
FP=X(IMIN)
W=2.D0*(DABS(FP))
H=DSQRT(DABS(YMIN))
RETURN
END

```

INTERP.FOR

```

C THE PROGRAM INTERPOLATES BETWEEN TWO DATA POINTS.
C THE PROGRAM IS BASED ON THE CUBIC SPLINE
INTERPOLATION.

```

```

C REFERENCE: PRESS,W.E. ET AL. "NUMERICAL RECIPES,"
CAMBRIDGE
C UNIVERSITY PRESS:NY, (1987), pp. 86-89.
C
C MAIN PROGRAM
COMMON KA, YA, N, YP1, YPN, Y2A, X, Y
DIMENSION KA(500), YA(500), Y2A(500), FLD(2500), FINT(2500)
INTEGER N, NPT, NSET, NB
CHARACTER FINAME*10, FONAME*10, FNAME*6, EXTI*4, EXTO*4, EXTOO*4,
*FOONAME*10
C
EXTI = '.DAT'
EXTO = '.ASC'
EXTOO = '.TXT'
WRITE (*,40)
40 FORMAT (//,2X,'HOW MANY FILES TO PROCESS? --> ')
READ (*,*) NSET
C
WRITE (*,50)
50 FORMAT (//, 12X,'*** THE NAME OF THE FILE MUST BE OF
THE FORM
1 ??????.DAT ***,////,12X,
2**** INPUT THE NAME OF THE FILE WITHOUT THE EXTENSION
.DAT ****')
DO 4 L = 1, NSET
WRITE (*,55) L
55 FORMAT (///,2X, 'INPUT THE NAME OF FILE NO. ',I2,' -
-> ',S)
READ (*,60) FNAME
60 FORMAT(A)
FINAME(1:6) = FNAME
FINAME(7:6+4) = EXTI
FONAME(1:6) = FNAME
FONAME(7:6+4) = EXTO
FOONAME(1:6) = FNAME
FOONAME(7:6+4) = EXTOO
OPEN (3, FILE=FINAME, STATUS='OLD',
* FORM='FORMATTED',ACCESS = 'SEQUENTIAL')
OPEN (4, FILE=FOONAME, STATUS='NEW',
* FORM='FORMATTED',ACCESS = 'SEQUENTIAL')
NPT=1
READ(3,10) N
10 FORMAT(I4)
M=1024/N+1
READ(3,20) (XA(I),YA(I), I=1,N)
20 FORMAT(11X,F10.4,4X,E12.4E3)
CLOSE (3, STATUS = 'KEEP')
WRITE(4,30) NPT,XA(1),YA(1)
30 FORMAT(4X,I4,3X,F10.4,4X,E12.4E3)
NPT=NPT+1
YP1=1.E30
YPN=1.E30
CALL SPLINE(XA, YA, N, YP1, YPN, Y2A)
DO 1 I=2,N
DEL=(XA(I)-XA(I-1))/FLOAT(M)
DX=DEL
X=XA(I-1)
2 IF(X.LT.XA(I)) THEN
X=XA(I-1)+DX
CALL SPLINE(XA, YA, Y2A, N, X, Y)
WRITE(4,30) NPT,X,Y
NPT=NPT+1
DX=DX+DEL
GOTO 2
ENDIF
1 CONTINUE
NB=NPT-1
CLOSE (4, STATUS = 'KEEP')
OPEN (4, FILE=FOONAME, STATUS='OLD',
* FORM='FORMATTED',ACCESS = 'SEQUENTIAL')
READ(4,20) (FLD(IB),FINT(IB),IB=1,NB)
CLOSE(4)
MINT=0.D0
DO 11 IBB=1,NB
IF(FINT(IBB).GT.MINT) MINT=FINT(IBB)
11 CONTINUE
DO 12 JB=1,NB
FLD(JB)=FLD(JB)-XA(1)
FINT(JB)=FINT(JB)/MINT
12 CONTINUE
OPEN (5, FILE=FONAME, STATUS='NEW',
* FORM='FORMATTED',ACCESS = 'SEQUENTIAL')
WRITE(5,100) (FLD(IB),FINT(IB),IB=1,NB)
100 FORMAT(4X,F10.4,4X,E14.7)
CLOSE (5, STATUS = 'KEEP')
WRITE (*,70) FONAME, FNAME
70 FORMAT (//,2X,'THE RESULTS ARE STORED IN --> ',A,
1//,2X,'THE PROCESSED RESULTS ARE STORED IN --> ',A )
WRITE (*,80) NB
80 FORMAT (//,2X,'NO. OF DATA POINTS IS --> ',I4)
4 CONTINUE
STOP
END

```

```

C SUBROUTINE SPLINT. CALCULATES THE 2-DERIVATIVES OF THE
C INTERPOLATING FUNCTION. THE OUTPUT IS THEN USED IN
SPLINT.
C
SUBROUTINE SPLINE(XA, YA, N, YP1, YPN, Y2A)
PARAMETER (NMAX=500)
DIMENSION KA(500), YA(500), Y2A(500), U(500)
IF (YP1.GT..99E30) THEN
Y2A(1)=0.
U(1)=0.
ELSE
Y2A(1)=-0.5
U(1)=(3./(XA(2)-XA(1)))*((YA(2)-YA(1))/(XA(2)-
KA(1))-YP1)
ENDIF
DO 11 I=2,N-1
SIG=(XA(I)-XA(I-1))/(XA(I+1)-XA(I-1))
P=SIG*Y2A(I-1)+2.
Y2A(I)=(SIG-I)/P
U(I)=(6.*(YA(I+1)-YA(I))/(XA(I+1)-XA(I))-
(YA(I)-YA(I-1))
/(XA(I)-XA(I-1)))/(XA(I+1)-XA(I-1))-
SIG*U(I-1))/P
11 CONTINUE
IF (YPN.GT..99E30) THEN
QN=0.
UN=0.
ELSE
QN=0.5
UN=(3./(XA(N)-XA(N-1)))*(YPN-(YA(N)-YA(N-1))/(XA(N)-
KA(N-1)))
ENDIF
Y2A(N)=(UN-QN*U(N-1))/(QN*Y2A(N-1)+1.)
DO 12 K=N-1,1,-1
Y2A(K)=Y2A(K)*Y2A(K+1)+U(K)
12 CONTINUE
RETURN
END
C
C SUBROUTINE SPLINT. IT PERFORMS THE INTERPOLATION.
C
SUBROUTINE SPLINT(XA, YA, Y2A, N, X, Y)
DIMENSION KA(500), YA(500), Y2A(500)
KLO=1
KHI=N
1 IF (KHI-KLO.GT.1) THEN
K=(KHI+KLO)/2
IF (XA(K).GT.X) THEN
KHI=K
ELSE
KLO=K
ENDIF
GOTO 1
ENDIF
H=XA(KHI)-XA(KLO)
IF (H.EQ.0.) PAUSE 'Bad XA input.'
A=(XA(KHI)-X)/H
B=(X-XA(KLO))/H
Y=A*YA(KLO)+B*YA(KHI)+
* ((A**3-A)*Y2A(KLO)+(B**3-B)*Y2A(KHI))*(H**2)/6.
RETURN
END

```

Appendix D

D200.FOR

```

C PROGRAM TO CALCULATE ORDER PARAMETER
C
PROGRAM D200
C
CHARACTER JUNK
CHARACTER FILEID(2), NMD0(8)
CHARACTER*8 DONAME
C
DOUBLE PRECISION X, Y, Z, XF, XINC
DIMENSION ZD(5000), XL(5000)
EQUIVALENCE (NMD0, DONAME)
C
DOUBLE PRECISION DAWSON
C
DATA DONAME /'D0 .FMT'/
EXTERNAL DAWSON
WRITE(*,1000)
WRITE(*,1111)
READ(*,1112,ERR=100) FILEID
DO 2 I=1,2
NMD0(I+2) = FILEID(I)
2 CONTINUE

```

LAMBDA.FOR

```

C
101  WRITE(*,1010)
      READ(*,*,ERR=101) X
      WRITE(*,1121)
102  READ(*,*,ERR=101) XF
      WRITE(*,1113)
      READ(*,*,ERR=102) XINC
      N=1
103  IF (X.LT.0.0D0) THEN
        WRITE(*,1030)
        GOTO 100
      ELSEIF (X.EQ.0.0D0) THEN
        Z=0.0D0
      ELSE
        Y=SQRT(1.5D0*X)
        Z=Y/DAWSON(Y)
        Z=(Z-1.0D0)/(2.0D0*X)-0.5D0
      ENDIF
      XL(N) = X
      ZD(N) = Z
      X=X+XINC
      IF(X.GT.XF) THEN
OPEN(UNIT=5,FILE=DONAME,STATUS='NEW',FORM='FORMATTED')
      WRITE(5,1115) N
      WRITE(5,1114) (ZD(I),XL(I), I=1,N)
      CLOSE (UNIT = 5)
      GOTO 200
      ELSE
        N=N+1
      ENDIF
      GOTO 103
C
200  WRITE(*,1040)
      READ(*,1045,ERR=200) JUNK
      IF((JUNK.EQ.'1').OR.(JUNK.EQ.'Y').OR.(JUNK.EQ.'y'))
GOTO 100
C
      WRITE(*,1050)
      STOP
1000  FORMAT(/,2X,70('#'),/,20X,'*** <D(2,0,0)> ***')
1010  FORMAT(/,2X,'PLEASE ENTER LAMBDA (2,0) (LAMBDA > 0):',5)
C1020  FORMAT(8X,'<D(2,0,0)> = ',F8.4)
1030  FORMAT(/,5X,'*** NEGATIVE ARGUMENTS NOT ALLOWED
***')
1040  FORMAT(/,2X,'DO YOU WANT TO DO ANOTHER CALCULATION:',5)
1045  FORMAT(A1)
1050  FORMAT(/,2X,70('#'),/)
C
1111  FORMAT(2X,'PLEASE ENTER TWO CHARACTER FILE IDENTIFIER:',5)
1112  FORMAT(2A1)
1121  FORMAT(2X,'PLEASE ENTER FINAL LAMBDA(2,0): ',5)
1113  FORMAT(2X,'PLEASE ENTER INCREMENT FACTOR: ',5)
1114  FORMAT(2(G14.7,''))
1115  FORMAT(I5)
      END
C
      DAWSON'S INTEGRAL
      DOUBLE PRECISION FUNCTION DAWSON(X)
      DOUBLE PRECISION X
      INTEGER N
      DOUBLE PRECISION Z,ZZ,T1,T2,T3
      DOUBLE PRECISION A
      PARAMETER (A=0.5D0)
      Z=X*X
      ZZ=A+Z
      IF(Z.LT.0.0D0) THEN
        WRITE(*,*) '*** IMPROPER CALL TO DAWSON ***'
        WRITE(*,*) '*** NO NEGATIVE ARGUMENTS ***'
        GOTO 9999
      ELSEIF (Z.EQ.0.0D0) THEN
        DAWSON=0.0D0
      ELSE
        N=40
        T1=0.0D0
        T2=N*Z
        T3=DBLE(N)+ZZ
        T1=T2/(T3-T1)
        N=N-1
        IF(N.GT.0) GOTO 100
        DAWSON=A*X/(ZZ-T1)
      ENDIF
C
      RETURN
C
9999  STOP
      END

```

```

PROGRAM LAMBDA
INTEGER MXPT
PARAMETER (MXPT=512)
DOUBLE PRECISION ZERO, UNITY
PARAMETER (ZERO=0.0D0,UNITY=1.0D0)
LOGICAL FPRMPT
CHARACTER FILEID(2),NMDO(8),NMSO(8),NMRO(8)
CHARACTER*8 DONAME,SONAME,RONAME
INTEGER I,J,NPTS,NVAL
DIMENSION D2(2500),SOL(2500)
DOUBLE PRECISION D2CAL,TVAL,SOLORD,D2COR
DOUBLE PRECISION D2,SOL
DIMENSION TVAL(MXPT),D2CAL(MXPT)
DIMENSION SOLORD(MXPT),D2COR(MXPT)
C
EQUIVALENCE (NMDO,DONAME),(NMSO,SONAME),(NMRO,RONAME)
DATA DONAME /'DO .FMT'/
DATA SONAME /'DO .DAT'/
DATA RONAME /'DO .CSV'/
WRITE (*,1010)
WRITE (*,1000)
5  WRITE (*,1020)
   READ (*,1030,ERR=5) FILEID
   DO 10 I=1,2
     NMDO(I+2) = FILEID(I)
     NMSO(I+2) = FILEID(I)
     NMRO(I+2) = FILEID(I)
10  CONTINUE
   OPEN (UNIT=7, FILE=DONAME,STATUS='OLD')
   READ(7,*) NPTS
   READ(7,*) (D2(I),SOL(I), I=1,NPTS)
   CLOSE (UNIT = 7)
   OPEN (UNIT=8, FILE=RONAME, STATUS='OLD')
   READ (8,*) NVAL
   READ (8,*) (TVAL(I), D2CAL(I), I=1,NVAL)
   CLOSE (UNIT = 8)
   DO 400 N=1,NVAL
     DO 100 K=1,NPTS
       IF (D2(K).EQ.D2CAL(N)) GOTO 200
       IF (D2(K).GT.D2CAL(N)) GOTO 300
100  CONTINUE
200  D2COR(N) = D2(K)
     SOLORD(N) = SOL(K)
     GOTO 400
300  I2 = K
     I1 = I2-1
     P=(D2CAL(N)-D2(I1))/(D2(I2)-D2(I1))
     D2COR(N) = D2(I1)+P*(D2(I2)-D2(I1))
     SOLORD(N) = SOL(I1)+P*(SOL(I2)-SOL(I1))
400  CONTINUE
C
OPEN(UNIT=6,FILE=SONAME,STATUS='NEW',FORM='FORMATTED')
WRITE(6,1130)
WRITE(6,1120) (TVAL(I),D2CAL(I),D2COR(I),SOLORD(I),
I=1,NVAL)
CLOSE (UNIT = 6)
WRITE (*,1010)
STOP
C
1000  FORMAT(25X,'PROGRAM LAMBDA',/,25X,14('-',),/)
1010  FORMAT(/,70('#'),/)
1020  FORMAT(2X,'PLEASE ENTER TWO CHARACTERS FILE
IDENTIFIER: ',5)
1030  FORMAT(2A1)
1120  FORMAT(4(G14.7,''))
1130  FORMAT(' TEMP.(deg C) ', ' D<2,0,0>-Cal ',
D<2,0,0>-Cor ',
*'Lambda<2,0,0>',/)
      END

```